The University of Aston in Birmingham

Department of Physics

PITTING OF ROLLING AND SLIDING STEEL DISCS BY FIRE-RESISTANT FLUIDS

BY

MARK ROBERT MIDDLETON

A thesis submitted for the degree of Doctor of Philosophy, The University of Aston in Birmingham. October, 1985.

SUMMARY

In many industries lubrication by mineral oils is not possible due to the risk of ignition and fire-resistant fluids have, therefore, been developed as a substitute. A major disadvantage of the use of such fluids however, is their relatively poor performance in high-stress rolling-contact bearings where components suffer fatigue cracking and pitting at an earlier stage than would be expected with mineral oils.

In this investigation factors affecting the cracking and pitting of EN31 steel in the presence of water-glycol based fire-resistant fluids have been studied using an Amsler 2-disc machine. A stribeck curve was plotted for the system and it is shown that pitting damage is dependant on the region of the curve in which the system is operated, pitting life being a minimum in the mixed-elastohydrodynamic region. Wear rates were found to be inversely proportional to the fluid film thickness.

A good inverse correlation was found between the pitting life and initial surface roughness to lubricant film thickness, D, up to a value of D = 22. Above this value an increase in life was observed.

The introduction of decanoic antiwear additive increased pitting life between two and seven times. Other experiments are described using the Unisteel and Rolling four-ball machines in which a similar trend was observed.

Finally, based on the observations made by optical and Scanning Electron Microscopy (SEM) a mechanism for crack initiation, propagation and subsequent pit formation in aqueous lubricants is proposed.

Key words: Fatigue, Pitting, Aqueous lubricants, Fire-resistant fluids, Cracking.

ACKNOWLEDGMENTS

I would like to express my sincere thanks and appreciation to J.L. Sullivan and S.G. Rudston (BP Research Centre, Sunbury-on-Thames, Middlesex) for their guidance and advice throughout the research project. I would also like to thank A. Abbot and C.J. Chapman of the Tribology Department, and, in particular H. Arrowsmith of the Technical Workshop.

The research was carried out with the support of the Science and Engineering Research Council (SERC), Swindon in conjunction with BP Research through the Co-operative Awards in Science and Engineering scheme (CASE Award).

Finally, I am indebted to 3M United Kingdom PLC., Gorseinon Road, Swansea., for allowing me to use their word-processing facilities.

CONTENTS

CONTENTS (CONTINUED)

CONTENTS (CONTINUED)

CONTENTS (CONTINUED)

CONTENTS (CONTINUED)

TABLES

Page

Page

Chapter Four

FIGURES

Page

FIGURES (CONTINUED)

FIGURES (CONTINUED)

FIGURES (CONTINUED)

CHAPTER ONE

INTRODUCTION

1.1. Background to the Problem

1.1.1. The Hydraulic System

It has been nearly two centuries since the use of fluid as a power transfer medium was first realised (1). The earliest application was Bramah's hydraulic press, patented in 1796 which offered an unprecedented increase in power compared to conventional mechanical systems of the period. In addition to this, the unit pressure exerted by the fluid remained constant over the entire piston stroke and eliminated any lost motion or spring-back, that was often associated with the mechanical systems.

Throughout the nineteenth century the fundamental hydrostatic principles were applied to other machinery such as lifts and cranes and by 1910 hydraulic accumulators, valves and piping were regularly in use.

Working pressures were well below 7mPa but increased steadily after the Second World War. Today hydraulic pumps are commercially available up to pressures of the order of 0.1GPa and equipment working to 0.7GPa is currently being developed. Figure 1.1 shows a simplified hydraulic circuit incorporating a full flow filter in the return line.

A hydraulic circuit is basically a liquid circulation system in some part of which work is performed. The practical hydraulic circuit consists of eight components these being (i) a container or reservoir for holding and supplying the fluid

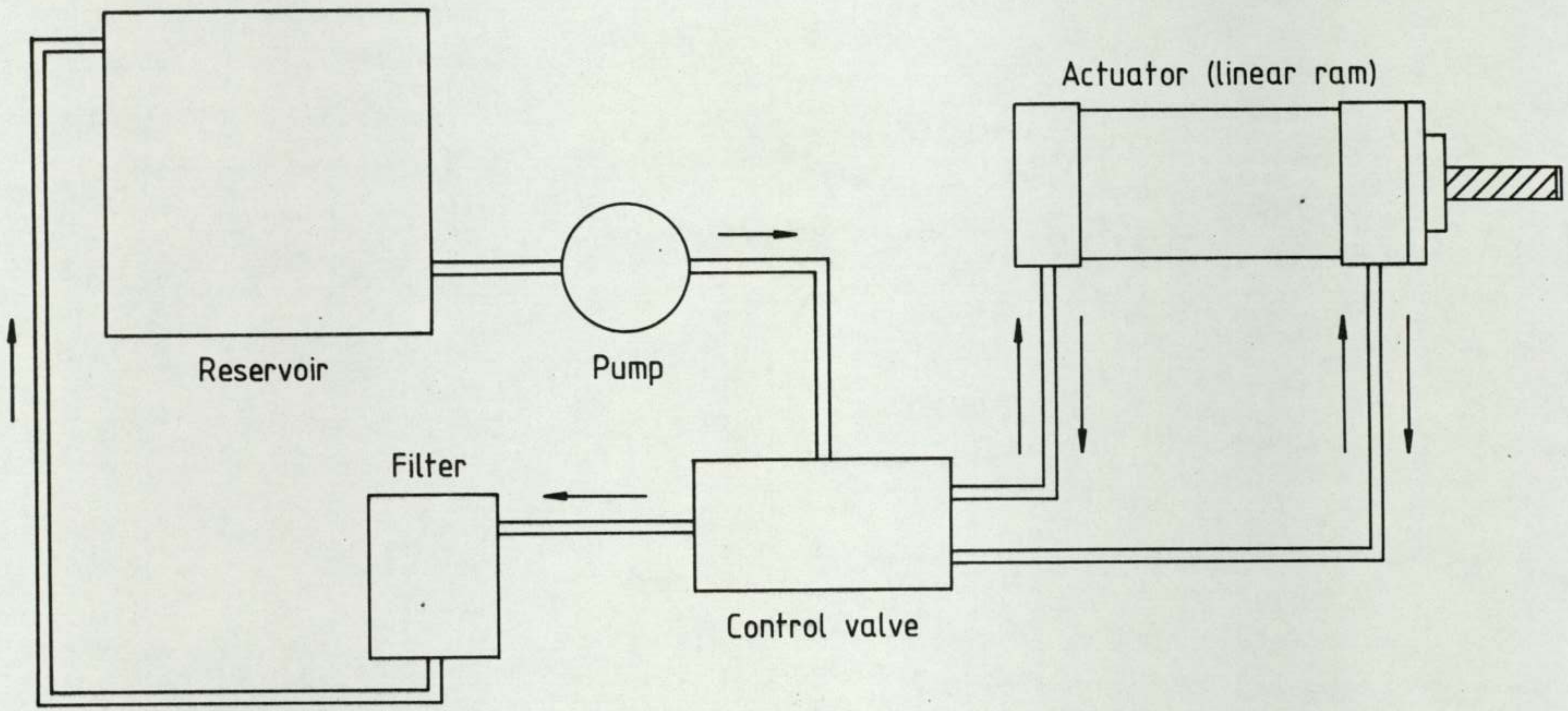

Figure 1·1. Hydraulic circuit incorporating a full flow filter in the return line.

to the working part of the system; (ii) piping to convey the fluid to and from each of the components; (iii) filter to keep the fluid clean; (iv) control valves to regulate pressure, direction of flow and flow rate; (v) accumulator to maintain constant pressure; (vi) actuator to convert hydraulic energy to mechanical energy; (vii) hydraulic pump to feed the fluid to the system and convert mechanical energy to hydraulic energy. Most hydraulic pumps used for transmission of power are of the rotary, positive displacement type, and they include the gear, vane and piston pumps (2).

The final component (viii) in a hydraulic system, is the hydraulic fluid itself. Any liquid will transmit energy but the choice of fluid will depend on the particular application. Water was the standard fluid used for the earliest hydraulic machinery and is still employed in a few modern systems, particularly in very large equipment, where there are high leakage rates or several systems are served from the same accumulator (3). The chief advantage of water as a hydraulic fluid is its cheapness and ready availability. The main disadvantages of water are its poor lubricating qualities - virtually a complete lack of lubricity resulting in the wear of moving parts, erratic motion (5),(6) and the readiness with which it promotes rusting of ferrous metals (4). It is also limited as regards the range of temperature over which it can be used. Hydraulic fluids are blends of relatively light bodied, high quality mineral oils of low pour point containing various additives such as oxidation and rust inhibitors, viscosity index improvers and anti-foam compounds. Oils are generally preferred to water for hydraulic systems because of their more favourable properties, namely, greater chemical stability, better lubrication properties and lack of corrosive tendencies towards ferrous metals.

1.1.2. The need for Non-flammable Hydraulic Fluids

Mineral oils treated with suitable additives can therefore serve as satisfactory hydraulic fluids, however, there has always been a need for a non-flammable hydraulic fluid for industrial systems where a fire risk exists, or high pressure hydraulic equipment is in close proximity to naked flames or high temperature sources. All mineral oils are flammable and in the event of a fractured line, fluid under high pressure can be ejected considerable distances in the form of a fine spray which is highly combustible, if not explosive by nature. Non-flammable hydraulic fluids must therefore be used for hydraulic equipment associated with die casting machines, foundry equipment and furnace door mechanisms as well as for many other applications where the fire risk may be less apparent, but present nevertheless.

Early disasters (7) particularly from underground fires within the mining industry (8) initiated a collaboration between selected countries, the National Coal Board (NCB) and the United Kingdom government to investigate the use of mineral hydraulic oils underground. As a result of the findings a working party was commissioned to produce draft requirements for non-flammable hydraulic fluids or Fire Resistant Fluids (FRF) as they are now known. In all cases of fluid development it was necessary that (i) the fluid should demonstrate acceptable fire resistant characteristics, (ii) that the performance and longevity of hydraulic equipment was not reduced below acceptable limits and (iii) the fire resistant fluids did not exhibit a health hazard.

Fire resistant fluids are not necessarily completely fire resistant, and some can be made to burn under certain conditions. Myers (8) who also gives details of their applications in British mines, defines the term 'Fire resistant' as "The ability of a fluid to resist ignition; its reluctance to propagate flame when a source of ignition is present and its ability to self extinguish when such a source is removed ...". Water is, of course, a perfect fire resistant fluid, but its many limitations as a satisfactory hydraulic fluid prevent its adoption in modern equipment for this class of duty.

The early research work carried out in the 1960s resulted in the NCB adopting a water-in-oil type fire resistant fluid and since then numerous fire resistant hydraulic fluids have been researched and used worldwide in underground mining equipment. Their use can be expected to grow in applications where their ability to resist ignition is considered to be paramount. Different countries have adopted different legislative philosophies towards these fluids and at the present time, usage ranges from compulsory for essentially all mining hydraulic systems as in the United Kingdom, to advisory as in the United States (9).

There are currently four main types of fire resistant fluid which have established themselves as practical, commercial fluids. The International Standards Organization (ISO) has classified the four types of fire resistant fluid as HFA, HFB, HFC and HFD representing oil-in water, water-in-oil, water glycols and non-water containing synthetic fluids respectively. These are described in more detail in Section 1.3.

1.1.3. The Problems Associated With Fire Resistant Fluids

Many of the problems associated with sliding wear and corrosion have been solved by the inclusion of suitable chemical additives, thus fire resistant fluids can be used with ferrous systems and the lubrication of plain or journal bearings can be satisfactorily achieved (10). However, a major drawback remains to be overcome, fire resistant fluids behave poorly in rolling contact bearings, the steel balls and races suffering fatigue cracking and pitting at a much earlier stage than with mineral oil lubrication (11),(12),(13),(14),(15).

It is unfortunate that the water glycol based fluids (HFC), which exhibit the most pronounced fire resistance and are hence potentially the most attractive in this respect, are, in certain applications the poorest lubricants causing rapid crack and pit formation in rolling element bearings compared to the three other types of fire resistant fluid (16),(17),(18).

Knight (10) using actual gear pumps has compared the fatigue lives of bearings run with different types of fire resistant fluid and has shown that under these particular conditions water-glycols exhibit inferior lubricating properties. The results are given in Table 1.1. However, it has been reported that dilute emulsions cause the greatest reduction in fatigue life (17). In addition to this, modified polyalkylene glycols used as synthetic coolants have been shown to yield better properties than emulsified oils (18).

Lubricant	L_{50} Life (hours)
Mineral oil*	1400
Phosphate ester (HFD)	900
Invert emulsion (HFB)	300
Dilute emulsion (HFA)	60
Water glycols (HFC)	20

Table 1.1. Comparison of fatigue lives for different types of fire resistant fluid.
*** Included for reference.**

It must be remembered, however, that caution must be maintained when comparing bearing life relationships obtained from different test methods since similar fluids could vary in performance under different test conditions (10).

It is thus of great commercial interest to study the factors affecting the pitting failure of steels in the presence of aqueous lubricants in order that systems and fluids might be developed to reduce pitting and increase life.

In this investigation the cracking and pitting of steel discs lubricated by a water-glycol based fire resistant fluid has been undertaken.

Before describing in detail the various factors which influence pitting, it is necessary to outline first the different types of lubrication associated with rolling contact fatigue.

1.2. Regimes of Lubrication

1.2.1. Friction and Lubrication

The function of a lubricant is to impose a film thickness between two contacting surfaces, thus minimising wear and when in copious supply to dissipate heat. The process of lubrication does not, however, depend entirely on the properties of the lubricant but also upon the relative speed of the bodies in motion together with the applied load the surfaces have to support.

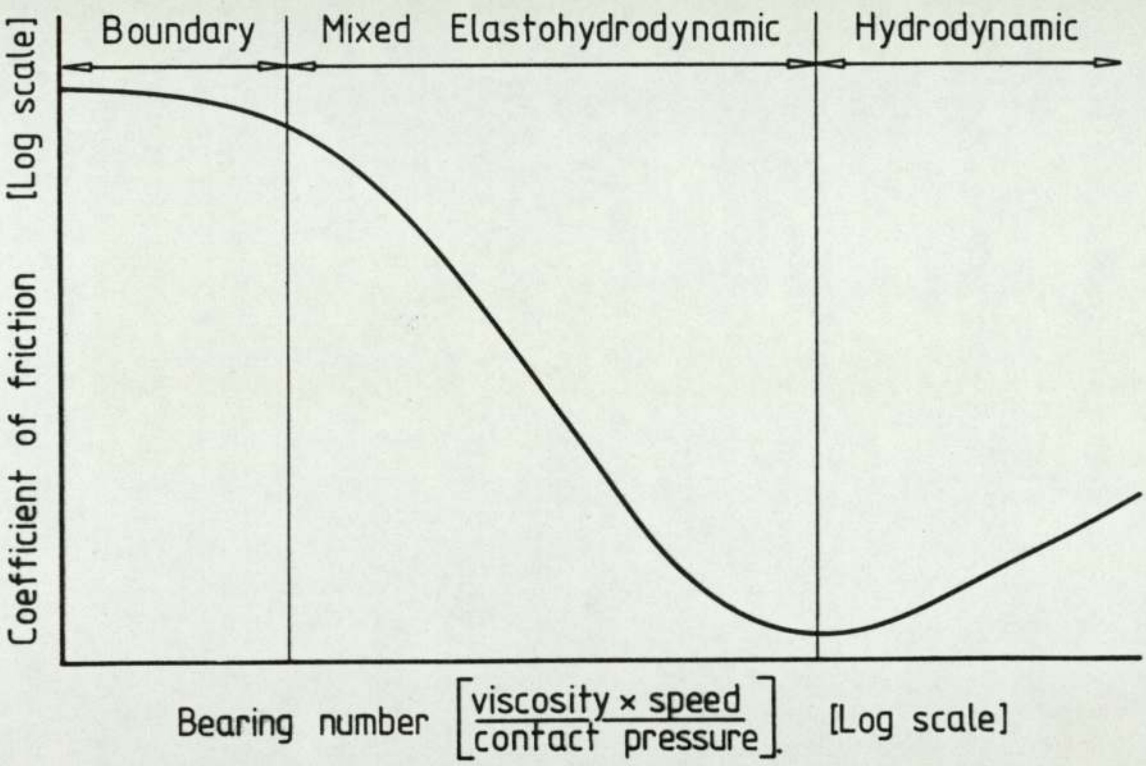

Figure 1·2. The Stribeck curve showing the boundary, mixed-elasto hydrodynamic, elastohydrodynamic and hydrodynamic regimes of lubrication.

In liquid lubrication, the combination of these parameters has led to the classification of four types of lubrication regime based on the relative separation of the surfaces. The four regimes have been named Hydrodynamic, this being characteristic of full or significant film separation; Elastohydrodynamic where surfaces are elastically deformed and the lubricant undergoes significant viscous change under pressure; Mixed-elastohydrodynamic where film breakdown occurs and Boundary lubrication. The latter representing little or no fluid film separation. The degree of surface separation in relation to the different regimes of lubrication can be observed as the classical Stribeck (20) plot of friction against bearing number shown in Figure 1.2 although it must be remembered that Stribeck did not recognise boundary lubrication.

The bearing number or duty parameter (21) as it is sometimes called is a dimensionless function incorporating the viscosity of the lubricant, the speed of the opposing surfaces and the applied load and is given by Equation 1.1.

$$\text{Bearing number} = \frac{\text{Viscosity } (\mathrm{Nsm^{-2}}) \times \text{Speed (rpm)}}{\text{Contact pressure } (\mathrm{Nm^{-2}})} \qquad 1.1$$

1.2.2. Hydrodynamic Lubrication

Hydrodynamic lubrication is based on the formation of a thick fluid film that developes automatically between opposing non-parallel surfaces in relative motion. Furthermore the films are generated at relatively low pressures that do not cause local elastic distortion of the solids.

An example of hydrodynamic lubrication can be found in the plain journal bearing having a continious liquid supply and a small radial clearance between the journal and bearing. The three diagrams of Figure 1.3 illustrate the basic sequence.

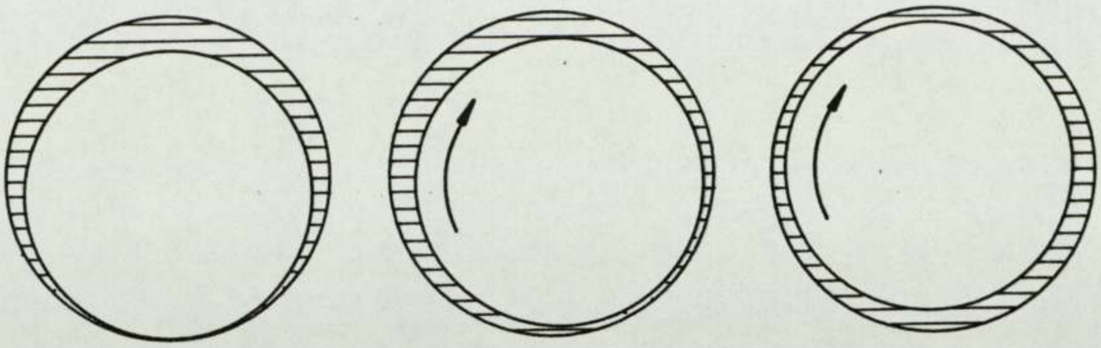

Figure 1·3. Hydrodynamic lubrication in the plain journal bearing.

The lowest level of frictional resistance is obtained when there is just sufficient speed to separate the surfaces. Increase of speed beyond this point gives rise to greater resistance due to the additional work being done in shearing the liquid film, thus friction increases with bearing number in this region (21).

Hydrodynamic lubrication is therefore the term used to cover the regime where complete separation of the moving surfaces has been attained throughout the majority of the run and its achievement depends on the geometrical design and the maintenance of adequate speed between two surfaces. Qualitatively the controlling factors for hydrodynamic conditions are (i) liquid supply - a minimum quantity of oil needed to fill the clearance and make up losses from the edge of the surfaces; (ii) sliding velocity - required to maintain sufficient liquid in the contact by viscous resistance; (iii) viscosity - the viscous attraction of the liquid will determine the thickness of film generated; (iv) attitude - surfaces must adopt a very slight taper or wedge to generate a film pressure.

The concept that a pressure develops within a lubricating oil was discovered in 1883 by Beauchamp Tower (22), who at the time was studying different methods for oiling journal bearings. His experiments involved a partial bearing located on the upper part of a journal with pressure gauges appropiately placed. He also showed that maximum pressure occurred at a point in the middle of the bearing, tappering off to zero at each side. Three years later Osborne Reynolds (23) demonstrated mathematically that the pressure profile developed in Tower's experiments was the result of hydrodynamic action and thus founded the principles underlying hydrodynamic lubrication. By assuming an incompressible fluid of constant viscosity Reynold's showed that the wedge-shaped oil film possess a load carrying capacity directly proportional to viscosity and speed but inversely proportional to the thickness of the oil film.

1.2.3. Elastohydrodynamic Lubrication

Classical hydrodynamic lubrication is characterised by very low friction and wear and is dependant on a simple function of viscosity, speed and load. Elastohydrodynamic lubrication, however, is a condition in which the elastic deformation of the bounding solids and the pressure-viscosity relationship of the lubricant play a significant role in the lubrication process.

Pressures experienced at elastohydrodynamic conditions are higher than those at hydrodynamic conditions but are not so high as to cause fluid film breakdown by surface penetration and interaction.

Elastohydrodynamic theory was developed in order to explain the phenomenon associated with the relatively low friction and wear rates occurring under extremely high pressures, which could not be supported theoretically using the classical hydrodynamic derivation of fluid film thickness. The essential difference between elastohydrodynamic and hydrodynamic lubrication is that for elastohydrodynamic lubrication two further properties of the system are recognised. Firstly, the surface of the materials in contact deform elastically under pressure, a consequence of which, is that load is spread over a greater area. When two identical discs are brought tangentially together they deform to support the load as shown in Figure 1.4.

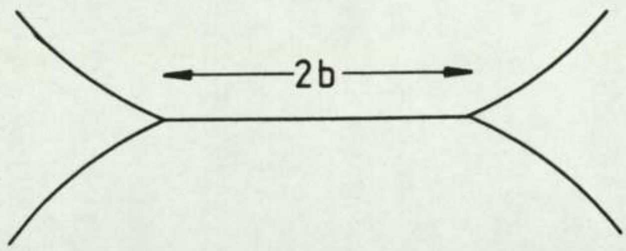

Figure 1·4. Hertzian deformation for two discs in contact.

The area of contact, often called the Hertzian contact (after the work by Hertz (24) on elastic deformation) forms a narrow rectangle in which the Hertzian area is given by the equation:

$$\text{Hertzian contact area } (m^2) = 2bw \qquad 1.2$$

Where w is the disc track width of the disc (m) and b is the rectangular half width given by the equation (25):

$$b = (4P'kR)^{0.5} \qquad 1.3$$

Where P' is the applied force per unit length (Nm^{-1})

k is given by: $(1 - \sigma^2) / \pi E$

where σ is Poisson's ratio of the material and

E is Young's modulus of the material (Pa).

R is the radius of the discs (m).

The pressure profile accross the Hertzian contact varies elliptically with maximum pressure occurring at the centre of the contact. The maximum Hertzian pressure for two discs in contact is given by the equation:

$$\text{Maximum Hertzian Pressure (Pa)} = (2P')/(\pi b) \qquad 1.4$$

where the symbols have their usual meaning.

For two identical balls in contact the Hertzian contact area deforms cirularly, the contact radius (a) given by the equation:

$$a = (\tfrac{3}{4}\pi PkR)^{\frac{1}{3}} \qquad 1.5$$

where P is the applied force between the two bodies (N) and

R is the radius of the balls (m).

The maximum Hertzian pressure (varying hemispherically) for two identical balls in contact is given by the equation:

$$\text{Maximum Hertzian Pressure (Pa)} = 3P/(2\pi a^2) \qquad 1.6$$

For a ball-on-flat configuration the Hertzian contact radius a is given by the equation:

$$a = (1.5\pi PkR)^{\frac{1}{3}} \qquad 1.7$$

where R is the radius of the ball (m).

The maximum Hertzian pressure is then found on substitution of the radius a in Equation 1.6.

The Hertzian theory of contact between elastic bodies is based on the assumption that their surfaces are topographically smooth, thus the roughness effects must be considered when scaling down experimental apparatus. For this reason Greenwood et al (26) have developed a non-dimensional roughness parameter based upon surface roughness and the Hertzian contact radius for two spheres in contact. Using this scaling parameter it was shown that the effects of roughness could be compared between large and small scale apparatus. However, provided that the scaling parameter was less than 0.05 it was reported that errors incorporated by the application of the Hertzian theory due to surface roughness could not exceed 7%.

The second property which must be taken into account in elastohydrodynamic lubrication is the effect of pressure on lubricant viscosity. At very high pressures developed within the contact zone the viscosity of the lubricant increases dramatically thus increasing the load carrying ability of the lubricant. The relationship between viscosity and pressure is dependant on both temperature and the chemical structure of the fluid making it difficult to generalise, however, a relationship that is widely used to approximate the pressure effect is given by (27):

$$\eta p = \eta o \exp(\alpha p) \qquad 1.8$$

where ηp is the absolute viscosity at pressure p,

ηo is the absolute viscosity at atmospheric pressure and

α an empirical constant termed the pressure coefficient of viscosity dependant on temperature and is a characteristic of the fluid being considered.

Equation 1.8 is in reasonable agreement with measurements over a moderate range of pressures but gives too great a change in viscosity with pressure at higher pressures. Other mathematical descriptions for the viscosity-pressure relationship have been proposed that include the dependence of temperature (28),(29).

The pressure coefficient of viscosity is determined from a plot of the logarithm of the viscosity measured at various pressures versus the corresponding pressure for a fluid at constant temperature, with the slope of the best fitted curve giving α. However, a method to calculate α from more accessible and easily measured properties of the fluid has been proposed by Johnston (30). The compressibility of the lubricant is also required, but this can be obtained by the method of Wright (31). The difference between the calculated pressure coefficient of viscosity and the experimental values is not perfect, and is limited to a maximum pressure of 0.14GPa above which the actual vicosity-pressure function changes. Johnston (30) has shown that a relationship does exist between the pressure coefficient of viscosity of a hydrocarbon lubricant and its density at different temperatures, without the need for empirical constants.

The calculation of a lubricant film thickness at elastohydrodynamic conditions requires a simultaneous solution of elasticity, hydrodynamics and lubricant viscosity-pressure characteristics. An approximation of film thickness was developed for the case of two discs in contact by Grubin and Vinogradova (32) who assumed a Hertzian deformation of the contacting solids (Figure 1.4) and a viscosity-pressure relationship to that given in Equation 1.8. A more detailed account on Grubin and Vinogradova's formula in elastohydrodynamic lubrication has been given by Terrill (33).

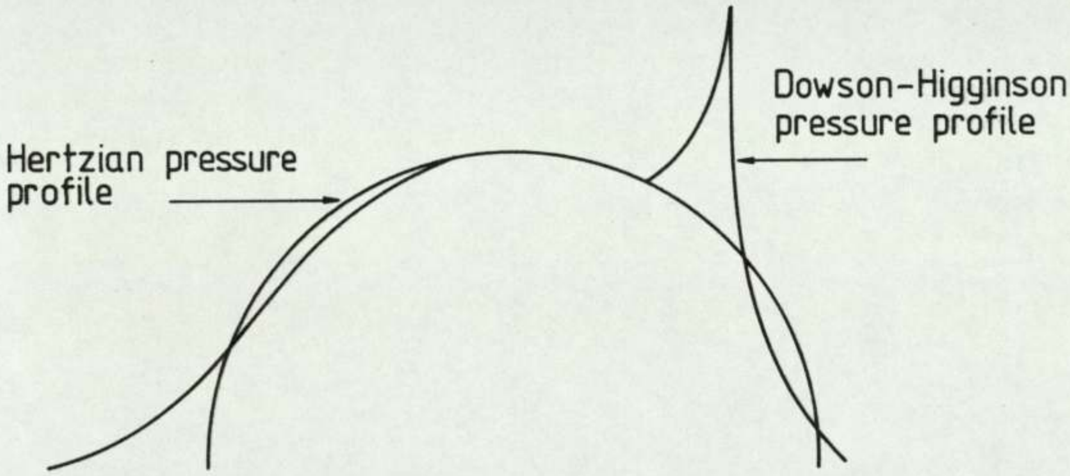

Figure 1·5. Hertzian and Dowson-Higginson pressure profiles for two discs in contact.

Grubin and Vinogradova's analysis provided film thickness predictions, but more complete solutions giving details of the film shape and pressure distribution were provided by Dowson and Higginson (34). By adopting an iterative technique they were able to show that the elastohydrodynamic pressure distribution was very similar to the

Hertzian semi-elliptical stress pattern of dry contact over most of the Hertzian zone (Grubin and Vinogradova's hypothesis), with the exception of a sharp pressure peak which occurs toward the outlet end of the zone. A typical theoretical solution showing details of the elastohydrodynamic pressure distribution and film shape is presented in Figure 1.5 and Figure 1.6 respectively.

The high loacal pressure peak and local constriction at the outlet are necessary in order to maintain a continious flow of lubricant. If there were no constriction, the sudden drop in pressure would force more fluid out than was coming in, thus the surfaces are required to deform according to the Reynolds equation to restrict the outgoing flow (35).

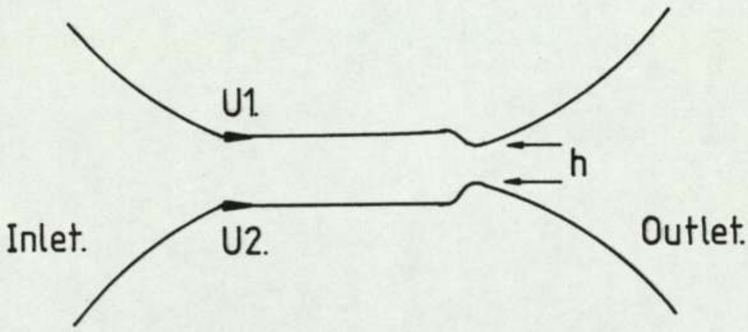

Figure 1·6. Film shape for two discs in contact [rotating with lubricant].

In addition to this the lubricant film is of almost constant thickness over most of the Hertzian zone, the minimum film thickness (h) being typically about 80 or 90% of the central film thickness.

By varying parameters such as load, speed and material properties (36) it was shown that the film thickness varied hardly at all with load, significantly with material properties and greatly with speed and viscosity. The Dowson and Higginson film thickness equation (37) is given as:

$$h\ (m) = 1.6\ (\eta u)^{0.7}\ \alpha^{0.6}\ R^{0.43}\ E'^{0.03}\ W^{-0.13} \qquad 1.9$$

where h is the minimum film thickness (m),

η is the viscosity of the fluid at the inlet (Nsm^{-2}),

u is given as: $0.5(u_1 + u_2)$. Where u_1 and u_2 are the respective speeds of the two surfaces (ms^{-1}).

α is the pressure coefficient of viscosity determined from Equation 1.8 $(Pa)^{-1}$,

R is given as $R_1 R_2 / (R_1 + R_2)$. Where R_1 and R_2 are the radii of the two discs (m).

E' is given by: $E / (1 - \sigma^2)$. Where E is Young's modulus (Pa) and σ is Poisson's ratio of the two identical discs.

W is the applied force (Nm^{-1}).

The minimum film thickness equation above assumes an isothermal condition, that is, the effects of the change in viscosity of the fluid with temperature and the thermal expansion of the lubricant and rollers, are neglected. An incompressible Newtonian fluid was also assumed.

Further work by Dowson et al (38) investigated the effect of both lubricant compressibility and speed. When compressibility was considered they showed that it had little effect on the film thickness but did reduce the magnitude of the pressure peak, especially at high speeds. Speed, on the other hand, affected the actual position of the pressure peak, such that at very high speeds the peak tended to adjust itself towards the inlet region. They concluded that at very low speeds the film shape settled towards the Hertzian conditions of dry contact.

Most of the initial work in elastohydrodynamic lubrication was restricted to isothermal conditions, and the solutions were therefore valid for only pure rolling or conditions of very small slip or sliding. However, to obtain a better understanding of the failure mechanisms in machine elements, the next generation of elastohydrodynamic lubrication analysis should incorporate such effects as non-Newtonian lubricants, surface roughness and temperature effects (39).

Cheng and Sternlicht (40) and Dowson and Whitaker (41) took into account the thermal effects associated with sliding in a theoretical model. They showed that sliding had little effect upon the film thickness calculation but had a marked effect upon surface traction.

Trachman and Cheng (42), using a large disc machine and two synthesised hydrocarbon lubricants, have investigated the traction in elastohydrodynamic contacts. They showed that the traction coefficient increased with increasing load but decreased with higher rolling speeds and temperature. They also found that the coefficient rose to a maximum value with increasing sliding speed and then decreased with further increase in the sliding speed.

Krause and Poll (43) have demonstrated that the effect of surface tangential traction can influence stresses in contacting bodies. It was shown that for rolling-sliding conditions the stresses were governed by four parameters, these being: (i) sliding friction, (ii) maximum Hertzian pressure (iii), the ratio of the coefficients of traction to sliding friction and (iv) the knowledge of whether the body was driving or being driven (direction of tangential load).

Crook (44) investigated the effects of friction produced in pure rolling and rolling with sliding and showed that at high speeds of sliding the consequent reduction in viscosity due to frictional temperature increases was more dominant than the relationship to the viscosity increase and the influence of pressure.

An accurate elastohydrodynamic film thickness equation for radial rolling element bearings, requiring only geometrical data available in bearing catalogues has been derived by Jackson (45). The equation, based on Cheng's (46) elliptical contact equation was found to be accurate to within a few percent for the majority of bearings. An additional equation was also given for roller thrust bearings for which a simple equation was not applicable.

Sibley and Orcutt (47) used an X-ray transmission technique to measure the thickness and shape of oil films formed between rolling and rolling-sliding surfaces. Good agreement was obtained between theory and experiment and accuracy was reported to be of the order of 0.05μm.

Dyson et al (48) used a capacitance technique to experimentally verify Dowson and Higginson's elastohydrodynamic equation. It was shown that for both rolling and rolling with sliding theoretical and measured values were in close agreement for most of the fluids tested over the range 0.025 to 1μm. For fluid film thicknesses greater than 1μm the predicted film thickness was much greater than the corresponding measured value, this being more apparent when sliding conditions prevailed. They concluded that the discrepancy in thick films was caused by a reduction in viscosity, due to a temperature increase of the lubricant by shear effects within the inlet region. For synthetic non-Newtonian silicone fluids (49) these discrepancies were found to be considerably greater especially at higher viscosities (> 100,000 cSt).

By assuming conditions of pure rolling and a Hertzian pressure profile Archard and Cowking (50) have shown that due to elastohydrodynamic lubrication, significant fluid film thickness can occur in nominal point contacts. This has also been predicted theoretically and experimentally by Cameron and Gohar (51) who used an optical interference technique to provide direct observation of the lubricant film under various conditions.

1.2.4. Mixed-elastohydrodynamic Lubrication

Point contact conditions often lead to lubrication regimes intermediate between elastohydrodynamic and boundary conditions. The transition from elastohydrodynamic to mixed-elastohydrodynamic lubrication occurs when either load is increased or the speed is reduced and is marked by an increase in friction for only a small change in bearing number. The mixed-elastohydrodynamic region therefore represents the begining of surface interaction and is influenced jointly by boundary and elastohydrodynamic actions.

The Stribeck curve in Figure 1.2 shows the loacation of the mixed (mixed-elastohydrodynamic) and elastohydrodynamic regions in relation to the two other regimes of lubrication. The transition between the mixed and elastohydrodynamic regions is not easily located and hence has not been introduced.

To understand the mechanism of mixed lubrication and subsequently boundary lubrication an appreciation of the nature of nominally flat surfaces is required on a microscopic scale. The surfaces of all engineering metals, regardless of their finish, consist of a series of asperities of finite dimension. The size of such asperities governs surface roughness which, in turn is a function of the machining process (52).

Finishing Procedure	CLA Roughness (μm)
Turning (rough)	2 - 25
Boring, Reaming	2.5 - 6
Grinding (commercial)	0.25 - 2.5
Honing, Lapping	0.05 - 1
Polishing (mirror)	0.025 - 0.12

Table 1.2. Roughness values for some industrial finishes.

Surface roughness can be quantified by the use of stylus profilometry and more recently by interferometry (57) to yield a numerical 'Centre Line Average' (CLA) roughness value. Table 1.2 shows some typical CLA roughness values for various industrial finishing procedures.

The apparent increase in friction, characteristic of the mixed regime of lubrication is therefore attributed to progressive increase in metallic contact through the lubricant film by asperity - asperity interaction. The mixed lubrication regime presents difficulties from both the theoretical and experimental points of view, since two entirely different phenomena namely hydraulic effects and direct metallic contact (if there is no boundary lubricant) between the surfaces interact. In addition, contact between the surface asperities will cause wear to take place. This wear, however, may not always be detrimental to the surfaces and for example, "running in" may have a directly beneficial influence on later working characteristics of the surfaces through the production of conforming surfaces. However, wear usually leads to destruction and seizure and it is normally the primary purpose of lubricant additives to ensure that this does not occur.

To investigate the effects of metallic interaction Chrisensen (53) has devised an experimental method utilizing a two disc machine for studying mixed lubrication regimes under rolling or rolling with sliding conditions. Electrical resistance was used as the main criterion to quantify asperity - asperity interaction. It was shown that the number of metallic contacts depends largely upon load, viscosity, speed and sliding.

Furey (54) has also used an electrical resistance method for studying the effects of metallic contact with nominal point contacts in pure sliding. It was found that appreciable metallic contact of an intermittent nature can occur even under light loads, and that metallic contact could be more prevalent in elastohydrodynamic or even hydrodynamic regimes of lubrication, than first expected.

Tallian et al (55) used a four-ball machine to study point contacts in pure rolling and attempted to correlate the amount of wear with direct metallic contact. They also attempted to correlate surface roughness with the number of actual metallic contacts that were found with their experimental system.

1.2.5. Boundary Lubrication

If the load is increased, the running speed too low or the surface roughness too great direct asperity interaction will take place over an area comparable to that found in dry contacts (see Figure 1.7). As the running conditions are made more severe increased contact occurs subsequently increasing friction and wear until finally, the system seizes.

To reduce friction and wear boundary additives are employed in the base lubricant to limit asperity contact by low shear strength reaction products formed as films in the critical contact areas. The type of lubrication provided by these surface films is known as boundary lubrication, a term first used by Hardy (56).

The chemical mechanisms which operate in these conditions are still incompletely understood and in general, practical lubricants must be found by trial an error. It is fortunate that at these conditions of lubrication, additives in the basic lubricant are extremely responsive and the choice of additive will be determinant. Thus the control of friction and wear is provided by the properties of the lubricant other than its viscosity.

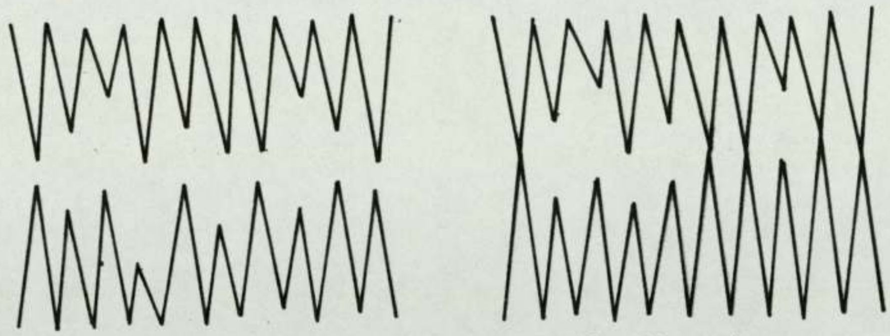

Figure 1·7 The degree of asperity contact for hydrodynamic and boundary conditions of lubrication.

1.3. Aqueous Lubricants

To meet the demands placed on lubricants by the progress of technology it is sometimes necessary to supplement the established mineral oils. It is also necessary to develop new kinds of lubricant when the products of petroleum crudes cannot be considered. In the case of supplements, hydraulic fluids exposed to ignitable environments must be fire resistant as a safety precaution. The different types of fire resistant fluid as briefly mentioned in Section 1.1.2 are now discribed.

Firstly the ISO designated HFA. This is an oil-in-water dilute emulsion, consisting of about 95% water. In this case the oil represents the disperse phase and the water, the dispersion medium. These fluids have a low viscosity requiring that the surface finish and flatness of the machined parts are made to tighter tolerances. Some limited use is made of oil-in-water dilute emulsions for hydraulic systems but the majority of emulsion type fluids are water-in-oil

(HFB), or invert emulsions as they contain more oil than water. A typical mixture is 60% oil (dispersion medium) and 40% water (disperse phase). Additives are included to prevent oxidation and protect against the growth of bacteria. Metal dithiophosphates are also added to improve wear characteristics.

Pure oil and pure water do not mix with each other, that is they will form a temporary emulsion when shaken but will immediately separate when turbulence ceases, with the lighter density oil rising to the top. A third ingrediant, known as an emulsifier is therefore required to give a more permanent emulsion. The emulsifier acts as a wetting agent resulting in one of the substances becoming microscopic droplets within the other. Whether the oil or water becomes the droplet depends on the type of emulsifier and the proportions of the fluid components.

Invert emulsions are used to protect the rubbing surfaces of pneumatic cylinders and for the lubrication of steam cylinders, particularly in high-pressure super heat systems. They are also used as oiliness agents in lubricants for worm gears.

Oil and water emulsions are non-Newtonian, that is, at low shear rates their viscosity will agree with the figure obtained in a conventional viscometer. As the shear rate increases the viscosity falls but will never drop below that of its oil phase. Non-Newtonian flow may be advantageous in that the greater body at low shear rate reduces leakage.

The third type of fire resistant fluid is known as HFC or water glycol and it is with these that the present work is concerned. Unlike HFA or HFB, water glycols are true stable solutions containing about 45% water blended into selected glycols and polyglycols with additional additives including corrosion inhibitors capable of preventing rust.

A glycol may be defined as a compound having intermediate properties between those of glycerin and alcohol. There are two important basic glycols, the simplest being ethylene glycol and the other propylene glycol. Polymers of ethylene and propylene glycols are termed polyglycols. The reaction of an alcohol and propylene oxide produces a series of polyglycols that are insoluble in water. By the addition of ethylene oxide in the reaction, a series of water-soluble polyglycols result. The water soluble polyglycols are commonly refered to as fire resistant water-based fluids and are used extensively as hydraulic fluids in vane-type and in-line axial piston pumps.

Since water is the fire resistant ingrediant in this type of fluid, it must be maintained at a specific volume level of the fluid to maintain correct viscosity and effective fire resistance qualities (58). The viscosity of water-based glycols varies inversely with water content. The loss of water by evaporation at temperatures greater than 70 °C increases the viscosity of the fluid and also decreases the fire resistive effectivness.

The final class of fire resistant fluid is those of HFD or non-water containing synthetic fluids and can be further divided according to the nature of the synthetic products. Most of the synthetic products pose some fire or toxicological risk (16) and so only phosphate ester based fluids have been accepted by the NCB. Phosphate esters are inherently fire resistant but are not non-flammable and remain stable up to working temperatures of about 150 °C. Phosphate esters have found applications as hydraulic fluids rather than lubricants, though the phosphates are, due to their excellent lubrication properties, used in a wide variety of products as additives. However, they cause deterioration of certain materials used for seals and gaskets. The physical properties of phosphate esters have been surveyed, and their chemical stability and anti-corrosion properties determined (59).

No overall method exist for assessing fire-resistance, which has been defined previously as the ability to resist ignition by a heated surface or hot flame and the inability to support combustion or propagate a flame. Various types of flammability test have, however, been introduced both in military specifications for fire resistant aircraft hydraulic fluids (60) and by individual manufacturers as a standard for the development of their own products for industrial application. The NCB has developed particular tests to determine how resistant some fluids are to fire (8). Generally these embrace flash point tests, dropping fluid onto a heated surface or a molten metal, spraying fluid onto a heated surface, investigating the ignition properties of a high pressure spray with a suitable flame and combining the fluid with known combustible substances such as coal.

Flash point tests are of a class which do not significantly designate the potential flammability of a fluid since standard flash points are conducted under controlled conditions unique to the test method.

Many of the synthetic fluids have flash points similar to mineral oils, although in practice they may be essentially non-flammable. Water-base fluids, have no conventional flash point but water-in-oil invert emulsions may exhibit apparent flash points on test due to separation of the oil content or evaporation of the water content.

The Autogenous Ignition Temperature (AIT) of a fluid is the minimum temperature at which ignition of the fluid can occur in a specified standard test apparatus without an external ignition source.

No specific rules can be laid down for the choice of the most suitable fire resistant fluid for a specific application (61). Viscosity, although remaining a most important factor from the performance point of view, is no longer a major criterion for selection. The flammability characteristics of hydraulic fluids indicate that in most cases, the most fire resistant fluid for one application may not be the best fluid for another, this being due to the sensitivity of the various test methods to differences in chemical and physical properties of the fluids. Cost is another major factor. Fire resistant fluids can cost up to five times that of standard mineral oils and their introduction will call for higher standards of maintenance. Compatability is another factor which must be considered when a system is changed to, or designed for, a fire resistant fluid. Primarily this affects the choice of materials for seals, although it may extend to paint finishes and various materials used in the fabrication of the system. Table 1.3 gives some general properties of industrial fire resistant fluids.

Property	Mineral Oil	Water-oil Emulsions	Water Glycol	Phosphate Esters
Relative cost	1	1.5	4	5
AIT	350°C	450°C	450°C	>600°C
Roller lubriaction	V.Good	Good	Poor	V.Good
Metals attacked	None	None	Zn/Cu	Al
Max sevice temperature	100°C	70°C	70°C	150°C
Effect on rubber	None	Fair	Fair	Severe
Boundary lubrication	V.Good	Poor	Good	V.Good
Flame test (No. Passes)	2	50	66	80
Approx pour point (°C)	-50	0	-32/-57	-6/-32

Table 1.3. General properties of industrial fire resistant fluids.

In the previous sections the need for a non-flammable hydraulic lubricant has been established. Four main types of fire resistant fluid have been described from which it was apparent that the aqueous based fluids, in particular the water-glycols cause early fatigue cracking and pitting and thus cannot adequately protect the surfaces of rolling element bearings. To understand this it is necessary to examine the mechanisms of crack and pit formation under rolling contact fatigue conditions and in particular the stress incurred within the bearing elements.

1.4. Rolling Contact Fatigue

1.4.1. Contact Stresses

One of the important considerations in the design of an engineering component or structure is that it shall not deform excessively or break under the loads or forces to which it will be subject to during its working life. For any particular design a stress system at any point in a solid can be defined by three mutually perpendicular planes on which only normal stresses exist. The normal stresses on these planes on which no shearing stresses occur are called principle stresses. From these stresses the maximum shear stress, which acts on a plane 45° to the surface and the octahedral shear stress, the resultant of shear stresses acting on planes parallel and perpendicular to the surface can be found (62). It was shown in Section 1.2.3 that for two discs in contact, held by forces normal to the area of contact, the maximum Hertzian pressure occurred on the surface and at the centre of the contact.

The positions of the maximum shear and octahedral shear, however, occur at a distance of 0.786b below the surface, where b is the rectangular half width of the Hertzian contact zone. The maximum shear stress occurs on a centre-line directly below the contact area and has a value 0.3 of the maximum Hertzian pressure (see Appendix I). The octahedral shear stress acts on either side of the centre-line and undertakes a full reversal of sign, its maximum value being (depending on Poisson's ratio) 0.26 of the maximum Hertzian pressure (see Appendix I).

Frequently the normal force is accompanied by a tangential frictional force in the contact area which results from sliding contact. The presence of the frictional force causes the maximum values of the shear and octahedral stresses in the two discs to become substantially larger than those produced by the normal force alone (62). For example, when the coefficient of friction is 0.3, the maximum shearing stress and octahedral shearing stress will be 0.44 and 0.37 of the maximum Hertzian pressure respectively. In addition to the increase in magnitude with friction the actual position of the maximum shear and octhedral stress will move from beneath the surface of contact towards the contact area (see Appendix II). When the coefficient of friction exceeds 0.24, however, the positions will be on the contact surface and the principle stresses must be determined by a different technique (63).

A similar phenomenon was observed by Dowson et al (64) in a theoretical analysis for isothermal rolling contact conditions. Under thin film conditions it was shown that the pressure profile departed from Hertzian and that the locations of the maximum shear stresses were drawn toward the surface. However, when the pressure profile was near Hertzian the positions and magnitudes of the shear stresses were similar to the dry contact case. A similar result was also obtained by Czyzewski (65).

Under light cyclic loading plastic deformation takes place in the vicinity of the maximum shear stress below the surface. Continued rolling introduces residual elastic compressive stresses running parallel to the surface region of the discs which act to reduce the maximum shear stress, thus inhibiting further plastic deformation (66). At higher loads a steady pattern of plastic action is repeated with each passage of the load and is restricted to a much thinner layer centred closer to the surface. The significant component of plastic strain is now one of shear parallel to the surface and a cumulative process exists whereby the surface of each disc is progressively displaced in the forward direction of rotation. This phenomenon was first observed by Crook (67) and later by Hamilton (68), using disc machines to simulate gear tooth contacts.

Stresses can therefore reside in rolling element bearings, their magnitude and location being dependant on the immediate contact conditions. The fatigue cracking and subsequent pitting of rolling element bearings is now reviewed by examining the fatigue mechanisms associated with contact stress.

1.4.2. Fatigue Mechanisms

When a number of fatigue tests are performed under similar conditions the lives obtained are scattered, due mainly to the nature of the fatigue process. For roller bearings it is necessary to express the properties of the material, environment and operating conditions as a statistical probability of failure (69). Investigations of lives of rolling element bearings (70) have shown that the results can be represented by a positively skewed distribution of the Weibull type (71). The cumulative distribution:

$$F = 1 - \exp(-(\lambda x)^{\alpha}) \qquad 1.10$$

where F is the cumulative propability of failure up to life x, λ is a scale parameter and α is a shape parameter can be rearranged so that a plot of: $\ln \ln (1 / (1 - F))$ against $\ln x$ will produce a straight line of slope α. By fitting fatigue life data to the Weibull distribution, estimates of the L_{10} and L_{50} lives (the times in which 10% and 50% of the bearings will be expected to fail) can be obtained. Manufacturers of bearings characterise their bearings with the L_{10} life, the reason being that the catalogue lives used by design engineers to select a bearing for a given application must represent a life value during which most bearings (90%) would not fail.

The basic mechanism of fatigue failure consists of three stages: crack nucleation or crack initiation; propagation of the crack; and failure by fracture or some other limiting factor. It is generally accepted that the initiation and subsequent propagation of fatigue cracks are the result of cyclic stresses which are locally intensified by the shape, size and distribution of non-metallic inclusions that occur within the vicinity of the two main shear stresses (72),(73).

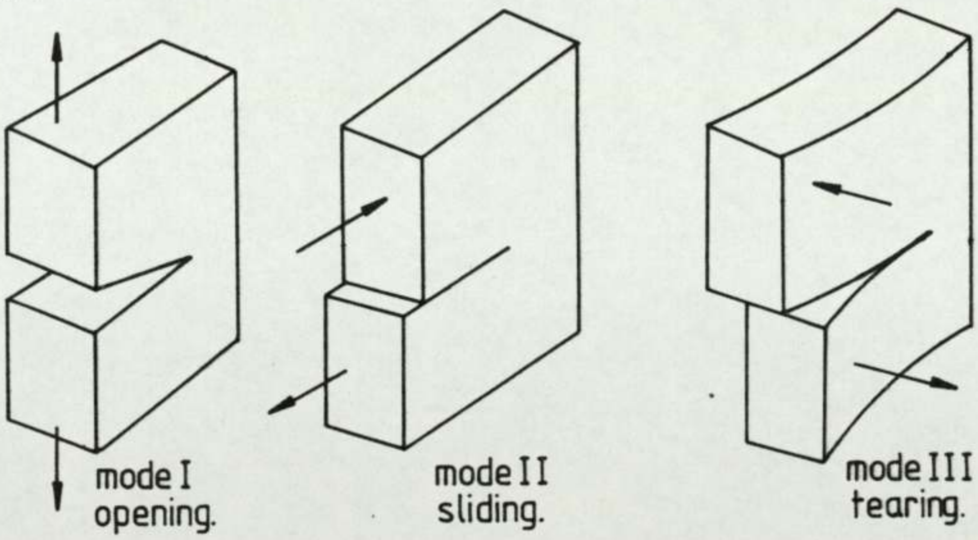

Figure 1·8. The three modes of cracking.

Cracks formed in solid machine components can be stressed in three different modes, as illustrated in Figure 1.8. In Figure 1.8a) the crack is opened by a tensile force and in

Figure 1.8b) is sheared by a force acting in the plane to the crack edge. In Figure 1.8c) the crack is sheared in a direction parallel to the crack edge. The superposition of the three modes describes the general case of cracking.

Griffith (74) was the first to appreciate that fracture was governed by an energy criterion. Griffith supposed that a macroscopically homogeneous test sample might contain small defects which enabled the stress to be concentrated sufficiently for the ideal fracture stress to be attained in small localised regions of the sample. Surface or internal cracks act as stress concentrators, so that at the tip of the crack the stress is above the fracture stress. For a crack to grow a minimum fatigue stress is necessary (75) but is safe until it reaches a critical length (76) at which point fast fracture occurs. The major problem is to distinguish between the number of cycles which cause initiation of cracks and those which cause the cracks to propagate to the critical length and hence to complete fracture (77),(78). However, a method has been described in which the crack initiation and propagation stages of notched beam specimens can be seperated (79).

Once a fatigue crack is formed, early macroscopic propagation takes on a characteristic pattern with additional subsurface cracks forming around the inclusion, propagation being rapid perpendicular to the rolling direction. The resulting surface pit is elliptical in shape and is typical of inclusion fatigue on many bearing components. Another mode of propagation can occur from subsurface origins known as hydraulic pressure propagation (80). Branching cracks that reach the surface early on in life are further propagated by the action of fluid ingress of lubricant into the part of the surface crack that leaves the contact zone last. Propagation is then controlled mainly by the action of lubricant under pressure (81). Subsurface initiated cracks are therfore unaffected by the lubricant and the environment until they reach the surface whereafter, the propagation rate will be determined by lubricant chemistry (82).

Littmann (83) reported that in addition to the subsurface inclusion mode of failure, other modes can be classified according to their appearance and the factors which promote their initiation and propagation. These are (i) Geometric stress concentration; (ii) Peeling; (iii) Subcase; and (iv) Point surface origin failures.

The Geometric stress concentration mode of failure occurs due to misalignment of the contact geometry or at the end of line contacts (84). Fatigue will be apparent within the narrow band in which the contact stresses are more severe.

Peeling is characterised by the limited depth of fatigue cracks and the propagation over areas rather than propagation in depth (85). It is mainly caused by frequent asperity interaction under lightly loaded conditions.

Subcase failure is the result of subsurface cracking below the effective case depth and occurs mainly in heavily loaded bearings. Bearings with thin cases relative to the radius of curvature and low hardness cores will tend to accelerate this type of failure (86).

Point surface origin represents the second most important mode of crack initation for pitting failure and identifies those cracks which initiate or nucleate at the surface. Way (87), in his pioneering work with rolling steel discs, demonstrated that highly polished surfaces gave an increased pitting life compared to rough-machined surfaces. He concluded that the pits originate from cracks formed on the surface. He also showed that for pitting to occur it was necessary for a lubricant below a certain viscosity to be present, however, cracks running almost parallel to the surface have been observed in discs run under unlubricated conditions (88). On the introduction of lubricant pits were generated from the formation of primary cracks penetrating the subsurface at an angle between 10 and 30°.

The major features which characterise this mode of failure are (i) arrow shaped pits with the arrow pointing in the direction from which the loaded contact area approaches the contact zone and (ii) early stages of cracking open to the surface. Since the fatigue cracks start at the surface, the lubricant and the environment can influence initiation and propagation (89). Surface cracks are generally formed by local surface stress raisers such as (79): surface flaws or inclusions; debris dents from wear particles in the lubricant; peeling; corrosion pits (91) and asperity-asperity interaction.

The mechanism responsible for the propagation of surface cracks is similar to that of the hydraulic pressure propagation described earlier, except that only thoses cracks which are suitably orientated with respect to the rolling direction will propagate. Cracks that are orientated, such that the crack mouth passes beneath the contact zone after the crack tip cannot propagate by this mechanism, since any lubricant that enters the crack will be rolled out as the crack passes through the contact.

Dawson (92), (93), (94) repeated Way's experiments, and confirmed his crack propagation mechanism. He also noted that pitting occurring between two discs rotating at different speeds was always present on the slower, softer disc and that above a certain slip ratio (95) pitting did not occur.

Using a disc machine, Dawson also introduced the concept of the D-ratio defined as:

$$D = \frac{\text{Combined initial surface roughness of the discs}}{\text{Fluid film thickness}} \quad 1.11$$

where the combined initial roughness is the sum of the CLA roughness values taken for each disc. On inspection, the D-ratio is in fact the inverse of the film thickness ratio λ, (96) except that the surface roughness term is calculated in a slightly different way. The use of the film thickness ratio, however, appears to have found more acceptance than the D-ratio mainly beacuse larger values of λ represent greater film thicknesses and hence better lubricating conditions.

Dawson demonstrated that the life to first pit was inversely proportional to the D-ratio and explained this in terms of intermetallic contact or asperity interaction. The greater the D-ratio the greater the degree of asperity interaction and hence shorter the life. For D-ratios less than 0.1, pitting did not occur due to the absence of asperity interaction.

Onions and Archard (97) extended the work of Dawson and confirmed the value of the concept of a D-ratio as a significant factor in determining the pitting life of both discs and gears. It was shown that the pitting life of gears was much shorter than the pitting life of discs.

The L_{10} lives of rolling element bearings were also found to be influenced by the film thickness to surface roughness ratio, when run under constant load (98).

By varying surface finish, shaft speed and lubricant viscosity on both tapered and cylindrical roller bearings, Skurka (99) has also demonstrated the relationship between bearing life and film thickness ratio. An empirical equation to predict the effect of varying lubricant and surface finish conditions on fatigue life was given. It was shown that between a film thickness ratio (λ) of 1 and 2.5 bearing life increased dramatically with λ, whereafter it remained independent of λ.

Fatigue cracks that originate at the surface have been observed on discs, under both rolling and rolling with sliding (87),(92),(100), gear teeth (101),(102) and rolling bearings (90).

As indicated above, the initiation of cracks can either start at, or below the surface thus, it is a matter of conjecture as to which type of fatigue will predominate. However, as a general rule it would appear that at low film thickness ratio and conditions of sliding are more likely to influence crack initiation at the surface, whereas a high film thickness ratio together with pure rolling will result in deep subsurface crack initation.

Soda and Yamamoto (103) using a disc machine, have shown that microscopic cracks leading to rolling contact fatigue initiate at the surface or in a thin subsurface layer. They concluded that the initiation of cracks during the early stages of life is more strongly influenced by the surface roughness, and that the propagation of the cracks in the latter stages was affected by tangential traction.

Polk and Rowe (104) have used an optical technique to determine crack growth rates under conditions of rolling contact. It was shown that a relationship exists between fatigue life and the rate at which cracks branch and propagate. Chemical factors were also observed to affect the fatigue lives through the crack branching rate.

Keer and Bryant (105) have developed a pitting model, based upon the work of Way (87) and Yamamoto (106) to simulate the process of crack propagation in rolling contact fatigue. They showed that the calculated pitting life values agree in order of magnitude to the experimentally observed lifetimes. It was believed that this slight discrepancy was brought about by estimating certain parameters and considering the mechanism as a two dimensional case. It is interesting to note that the model used a fatigue crack initially inclined at 25° to the surface, although no attempt was made to discuss this.

A technique for studying crack growth under repeated rolling contact has been proposed by Yoshimuna et al (107). The method involves indenting the surface of a disc below which a small hole has been drilled. The disc is then turned down and heat treated leaving a crack like (collapsed hole) defect below the disc rim. Preliminary work has shown that the induced cracks are subject to mode II type crack growth (Figure 1.8b)) although systematic measurements of crack growth rates have yet to be reported.

Eisenstadt and Fuller (108) have reported a method for generating crack propagation rate data to evaluate the material properties of rotating beam specimens by means of an interrupted stressing technique. In addition, the technique allowed the direct calculation of crack propagation rates together with the stress intensity factor - a parameter particularily useful for the analysis of fatigue crack growth (75).

Earlier it had been stated that the presence of a lubricant was necessary for pitting to occur and that the mechanism for crack propagation was governed purely by the physical nature of the lubricant. However, considerable work has been carried out which show that chemical effects can also influence pitting fatigue lives.

1.4.3. The Influence of Additives on Fatigue Life

Petroleum oils, synthetic lubricants and fuels often require modification by the inclusion of additives to meet certain demands imposed on them by modern equipment.

Rust inhibitors are used to protect ferrous metals from moisture by the formation of thin surface films. Antiwear additives are employed when boundary conditions are likely to prevail and are used to reduce friction and wear. They generally consist of long chain molecules with an active end group, typically fatty acids, alcohols and amines. Being polar molecules they reduce friction by adsorbing onto metal oxide surfaces forming a close packed, low shear strength surface film. However, under conditions of increased contact pressure and consequently higher temperatures the antiwear additive film breaks down and metal-to-metal contact occurs resulting in an increase in friction accompanied by rapid wear. Under these circumstances extreme pressure (EP) additives must be used. These are sulphur or chlorine additives which decompose locally to form free sulphur or active chlorine in response to flash temperatures at asperity-asperity interactions. These then react with metal yielding an iron sulphide or iron chloride coating that will sustain the load or prevent contacting surfaces welding together.

Phillips and Quinn (109) using a disc machine have reported that for D-ratios less than 1.5 the effect of a sulphur-phosphorus type extreme pressure additive was to decrease the pitting life, whereas above this ratio the EP additive tended to increase life. They explained this phenomenon by considering crack initation and propagation. For low D-ratios the additive promoted crack initation and propagation but for higher D-ratios the additive inhibited crack propagation by a corrosive wear process.

Rowson and Wu (110), using elemental sulphur as an EP additive have found that temperature effects were significant in the pitting process. For experiments conducted at a D-ratio of 7 it was shown that the pitting life increased at 100°C but decreased at 30°C. Analysis of the wear debris revealed that different reaction products had formed at the two temperature conditions.

Kelley (111) has shown that some EP additives can reduce the contact fatigue life under combined rolling-sliding conditions. The reduction in life was accompanied by an increase in the Weibull slope, indicating that there was less scatter in the fatigue life, compared to the results obtained with mineral oil. A similar observation was made by Littmann et al (112) on the effect of adding 1% of a zinc dialkyldithiophosphate (Zddp) to a low viscosity mineral oil, on the other hand Rounds (113) has shown that 2.5% Zddp can increase the fatigue life by a factor of 30.

In a more recent study Can et al (114) have demonstrated that Zddp's form stable, thick chemical films during lubrication which can survive pure rolling. The formation and stability of the films, however, was found to be dependant upon purity. At higher concentrations, Zddp's increased wear and friction and became unstable at temperatures greater than 240°C.

Scott (115), in an extensive study on the effects of EP type additives on fatigue life, found that when normal concentrations of additive were blended into a paraffinic mineral oil, no significant effect on fatigue life was observed. Elemental sulphur and elemental sulphur with lead naphthenate appeared to increase life, whereas particularly at high concentrations, chlorinated wax and dibutylphosphite caused a severe reduction in fatigue life. From examination of the test specimens it was found that chlorinated wax increased surface roughness with concentration.

Mould and Silver (116), on the other hand, have shown that the acidity of the lubricant can also affect fatigue life. By adding small concentrations of dibutyl phosphate and dichloroacetic acid, to liquid paraffin produced large reductions in fatigue life. With a weak myristic acid a larger concentration was required before any noticable reduction in fatigue life was detected.

Rounds (117), using a Rolling four-ball fatigue tester observed that the presence of aromatic or naphthenic rings in the lubricant molecule increased fatigue life but reaction or polar groups were generally found to be detrimental. Later work by Rounds (118) showed that the choice of steel can affect additive performance. Each additive tested produced different tribological effects on the various steels when compared to the base oil, however, almost all of the additives tested improved fatigue life with case hardened steels but reduced life when used in conjunction with through-hardened materials.

Collectively the work on additive performance has highlighted the complex interaction that takes place between lubricant additives and materials. Such interactions are strongly dependant upon the specific material, base stock and additive combination.

1.4.4. The Influence of Water on Fatigue Life

The influence of water contamination has been extensively studied in both high stress fatigue test machines and full scale bearing tests. Work undertaken in previous years and more recently by Cantley (119) has shown that even a small concentration of water in a mineral oil can have a detrimental effect on fatigue life.

Grunberg and Scott (120) were amongst the first to observe that pitting failure was accelerated by the presence of water in the lubricant. Using a conventional four-ball machine they demonstrated a reduction in fatigue life of up to three times when 6% by weight of water was added to the lubricant. Crack propagation rates were also shown to be governed by the water content, although when stainless steel bearing balls were substituted, water contamination had no effect.

Schatzberg and Felsen (121),(122) used a planetry type four-ball machine to compare the fatigue lives of bearing balls run with both a 'dry' refined paraffinic hydrocarbon lubricant (squalane) and a 'wet' lubricant, containing 0.01% water. The squalane was considered to act as an inert lubricant serving as a carrier for the water. Compared to the dry lubricant, the additional water content reduced the fatigue life by between 32 and 48%. An increase in wear during rolling contact was also observed, due to the presence of water, and was identified by both surface profile and weight-loss measurements.

Felsen et al (123) investigated the effects of seawater on the fatigue life and failure distributions of flood-lubricated angular contact ball bearings. Reductions in fatigue life as high as 80% were observed when 1% by volume of seawater was added to various lubricants. Significant life reductions were also obtained when tests were conducted at elstohydrodynamic conditions of lubrication.

Mantel et al (124) using a rotating beam fatigue tester, has shown that even atmosphere moisture can influence the fatigue life of steel. He concluded, by emphasising the critical importance attached to controlling the specimen environment during fatigue testing.

The wear of lightly loaded sliding contacts has been studied by Vaessen and De Gee (125) as a function of load and relative humidity. For experiments conducted under relatively low loads a characteristic zero wear period occurred until a critical humidity value was reached, characterised by a sudden increase in wear. The critical humidity values for Ag-Au-Cu sliding on Cu, Cu-Zn, Cu-Sn and Cu-Ni-Zn were 30%, 35%, 45% and 55% respectively. They suggested that the critical values were determined by the water adsorption properties of the different surface oxides and therefore a function of alloy composition.

Beagley and Pritchard (126), using both small and full-scale tribometers, have investigated the effects of rain water on the adhesion of railway wheels and steels. It was shown that water had an overriding influence upon the magnitude of the friction developed between rail and tyre steels. Water was found to mix with wear debris yielding a lubricant paste which subsequently reduced friction.

While the overall mechanism by which water in a lubricant reduces fatigue life is still in doubt, there is convincing evidence that the formation of atomic hydrogen, and subsequent hydrogen embrittlement (127),(128),(129) can account for the low fatigue lives inherent in water contaminated lubricants. The precise mechanism by which the water decomposes to produce atomic hydrogen is not clear, however, the formation of hydrogen peroxide by the interaction of water and oxygen on newly formed metal surfaces (128),(130),(131) and electrochemical corrosion (120),(132) are suggested mechanisms. The formation of hydrogen by electrochemical corrosion occurs when dissolved water in the lubricant condenses to form a water rich phase at the propagating crack tip. Along the crack are both anodic and cathodic regions, the fresh metal surface at the crack tip being anodic. Atomic hydrogen is then produced in the cathodic regions of the crack by the reduction of hydrogen ions, formed in the ensuing corrosive reaction. Attempts have been made to negate the deleterious effect of water by the inclusion of suitable additives.

Grunberg and Scott (130) and Scott (133) found iso-amyl alcohol and a commercially available de-watering agent (an imidazoline derivative) to be particularly successfull. The average fatigue life of the water saturated mineral oil was increased to that of the dry oil by the addition of 2% de-watering agent. Detergent and water soluble anti-corrosive additives had no beneficial action, whereas long chain alcohols, oleic acid and triethanolamine were only partially successfull.

Grunberg and Scott (130) proposed that the surface active additives formed a hydrophobic film on the metal surface, thus preventing water-metal interactions.

Schatzberg (132) demonstrated that isopropylamino-ethanol (IPAE) at 0.1% concentration was an extremely effective additive for counteracting the effect of 1% added seawater in a mineral based hyraulic fluid. An alternative mechanism to that of Grunberg and Scott (130) was proposed, whereby the IPAE additive neutralised protons formed by the electochemical corrosion process, previously described.

Murphy et al (134) tested fourteen potential additives using a rotating beam fatigue tester. The results were expressed according to a percentage relative "effectiveness parameter", reflecting the ability of 0.1% additive in overcoming the deleterious effect of 0.05% water in a mineral oil. Diisopropylaminoethenol (DPAE) mixed with morpholine and IPAE were amongst the better additives, having a rating of 92% and 78% respectively. This did not compare to eicosene which had a rating of only 16%.

The influence of relatively low concentrations of water within mineral oil lubricants can therefore be partially counteracted by the inclusion of certain additives. Aqueous fire resistant fluids, contain a very much higher concentration of water than that employed in these contamination studies and thus appear to pose a much more serious problem, although it is not clear from the literature as to the exact relationship between fatigue life and water concentration.

Invert emulsions and water glycol based fire resistant fluids typically contain between 40% and 45% water and dilute emulsions can have as much as 95% water. It is well known that when fire resistant fluids are substituted for conventional mineral oil in hydraulic systems a considerable reduction in fatigue life is observed as was shown in the early work of Cordiano et al (12),(13), Hobbs and Mullet (11) and Hobbs (15). Other additional problems associated with the use of fire resistant fluids have also been encountered (135), (136).

Scott (137) has demonstrated that hydraulic machinery designed around a particular fire resistant fluid would be more beneficial than designing oversize components or de-rating units originally designed for operation with mineral oils.

The assessment of the performance of fire resistant fluids as roller bearing lubricants, has over a number of years, been persued using in-service gear pumps (10). However, it is both time consuming and expensive to conduct experiments with such machinery, hence for a fundamental investigation, accelerated tests must be devised. A number of wear test machines have been used in such investigations.

Scott and Blackwell (138) have used a Rolling four-ball machine and have claimed that results correlated well with full-scale tests from in-service machinery run in the presence of fire resistant fluids. Scott (139) has shown that the Rolling four-ball machine can be used to compare lubricants and materials for rolling contact applications. Hardness was shown to be an important factor in determining fatigue life and the repeatability of the results was reported to be good.

Zaretsky et al (140), using a five-ball tester, showed that in order to maximise fatigue life, a small difference in hardness should exist between the rolling-element and the race-way.

Kenny and Yardley (14) used a Unisteel machine for their study of three different types of fire resistant fluid. By comparing the L_{10} lives they showed that water glycols had the worst effect on fatigue life viz. Mineral oil (for comparison) > phosphate ester > invert emulsion > water glycol, however, when the L_{50} lives were compared the positions of the water glycol and invert emulsion were reversed. They concluded by demonstrating that the Unisteel offered a useful means to compare the effect of different fire resistant fluids but emphasised the importance of steel specimen quality and hardness. Surface finish appeared to have no overall effect.

Yardley et al (141) have combined rolling contact fatigue test data accumulated from both Rolling four-ball and Unisteel experiments to provide a much more comprehensive picture of lubricant performance over a wide range of loading conditions. They showed that by plotting the bearing L_{10} life against a ratio of dynamic load rating C to dynamic bearing load P, a relationship of the form given in Equation 1.12 could be used to accurately predict bearing life.

$$L_{10} \text{ life (revs)} = (C/(DP))^{B} \times 10^{6} \qquad 1.12$$

Bearings could then be denoted according to particular values of B and D.

For the lubrication of rolling elements, mineral oils had the values B = 3 and D = 1, whereas for fire resistant fluids (142) B = 3.37 and D = 1.18 for phosphate esters; B = 2.71 and D = 1.43 for invert emulsions; B = 2.51 and D = 2.02 for dilute emulsions and for water glycols B = 2.46 and D = 2.01.

One reason why water-based fire resistant fluids behave poorly in rolling contact bearings is the formation of a relatively low elstohydrodynamic film thickness within the contact zone.

Dalmaz and Godet (143) used an optical film measurement technique to investigate the elastohydrodynamic properties of several types of fire resistant fluid. Results obtained with water glycols were in good agreement with theory, even though the pressure-viscosity coefficient was small. With invert emulsions, experimental results were very much lower than those predicted by theory, however, good correlation was obtained when the viscosity of the oil was considered as opposed to the viscosity of the emulsion. They explained this by noting that the size of the water droplets were larger than the film thickness, thus under the conditions of high shear only base oil could pass through the contact zone. This confirmed the work of Hamaguchi et al (144) who suggested that the elastohydrodynamic film thickness developed with an invert emulsion was governed mainly by the properties of the base oil.

Wan and Spikes (145) used point contact interferometry to extensively study the elastohydrodynamic lubricant properties of water-polyglycol based fire resistant fluids. They showed that elastohydrodynamic film thicknesses were generally two to three times lower than those obtained with conventional mineral oils of similar viscosity. By combining different proportions of polyglycol, monoglycol and water they demonstrated that the reduction in film thickness was attributed to the pressue-viscosity coefficient, which in turn was governed by the water and monoglycol content in the polyglycol.

Wan et al (17), using a rotating glass plate and steel ball together with optical interferometry have studied the elastohydrodynamic properties of three water based fire resistant fluids. It was shown that invert emulsions gave elastohydrodynamic film thicknesses similar to their component base oils, however, for very fine particle size emulsions a thicker film was observed. Dilute emulsions were found to give no measureable elastohydrodynamic film thickness, although elastohydrodynamic films were produced by destabilizing the emulsion. High speed photography revealed an accumulation of oil in the inlet zone capable of forming an elastohydrodynamic film. Polyglycol-water solutions gave low elastohydrodynamic film thicknesses this being determined by the low pressure-viscosity coefficient of the solution.

1.5. Surface Analytical Techniques

The preceding sections were an attempt to illustrate the various complex interactions that occur between surfaces in relative motion. To understand such complex interactions it is necessary to employ analytical techniques either during or after experimental runs. As techniques become more refined and readily available complex chemical interactions of those previously described can be studied and the information gathered used to ultimately explain their mechanisms.
One of the most commonly used analytical tools used in tribological applications is the Scanning Electron Microscope (SEM). Its main advantage is the ease with which one can obtain direct electron micrographs of bulk surfaces. Furthermore, it can be combined with an energy dispersive X-ray detector to give elemental information regarding the composition of the bulk material. For information about the structure of these elements X-ray diffraction or X-ray Photoelectron Spectroscopy (XPS) can be used.

Syniuta and Corrow (146) have used scanning electron microscopy to undertake a fractographic study of rolling contact fatigue. Using high magnifications they were able to examine both the spall cavity (pit) and fragment associated with the pitting of a steel bearing ball. By showing that the spall fragment comprised two topographical areas they concluded that the rolling contact fatigue pit process involved two fracture mechanisms.

In order to obtain very high magnification and high resolution it is necessary to turn to the Transmission Electron Microscope (TEM). Thin foil specimens or replicas are necessary and this means a substantial amount of specimen preparation is involved.

O'Brien and King (147) have used the TEM to identify the white-etching structure alterations that occur around non-metallic inclusions in cyclically stressed bearing steels, otherwise known as 'buterflies'. By preparing thin foil samples across the alteration they found that the alteration was due to the formation of celluar grains, their size being between 0.05 and 0.1 micron. The cell formation was similar to that previously seen in fatigued iron but they could not relate its presence to the fatigue process.

Although the SEM is generally used to examine surface features after the event, it has been shown that direct observations of wear processes can be made if experiments are conducted in the chamber of the SEM (148). It would then be possible to examine the surface during a sliding process say, at high magnifications with little loss of field. The propagation of surface micro-cracks could then be followed. However, if a particular wear process relied on the formation of thick oxide films or moisture, then this particular experimental method would not be suitable, since such conditions are not provided for in the chamber. Experiments would also be required to run at slow speeds in order to be able to make sensible observations at high magnifications. Such an experimental arrangement appears to have considerable potential, but the need for high vacuum conditions prevent this type of dynamic analysis.

For both quantitative and qualitative analysis, Auger Electron Spectroscopy (AES) can be used (149). AES is often complemented with ion milling, enabling the identification of elements below the surface to be made.

Phillips et al (150) have shown that AES is a valuable technique in examining the surface films formed by additives in lubricant processes. Using a 'one ball-on-three flats' configuration to generate sliding wear specimens they reported that a significant difference occurred in the relative proportions of various elements according to whether or not 1% zinc dibutyldithio-phosphate (ZDP) was used in the lubricant.

Dynamic experiments conducted in the vacuum environment of an Auger spectrometer have also been undertaken. Pepper (151) has used AES to assess the transfer characteristics of various halogenated polymers in sliding contact with metal. The 'in situ' technique showed that a continuous film could be established by sliding, of two to four layers thick.

There are indeed many more analytical techniques available to the user all offering particular advantages and disadvantages in their use. New techniques are also being developed. The choice of which technique to use, however, will undoubtly depend upon the particular application at hand (152).

1.6. Programme of Work Carried out in this Investigation

Past research has shown the contact fatigue problem to be dependant upon a complex interaction involving the choice of material used, the physical and chemical actions between lubricant and environment, the type of additive blended with the lubricant and the stress induced within contact zones. Most of this work was based on experiments conducted with conventional mineral oils and their additives. However, a few studies have been undedrtaken where particular emphasis has been given to the effects of aqueous lubricants or where water contamination plays and important role in the fatigue process. Most of this research was based on a "comparison-type" study where the effects of various water-based lubricants were assessed relative to a mineral oil. To do this experiments were conducted at particular, constant regimes of lubrication. No investigation, however, has been explicitly carried out to ascertain the effects of an aqueous lubricant in different lubrication regimes. The aim, therefore, of this investigation was to partially fill this gap.

The influence of a water-glycol based fire resistant fluid, varying in viscosity both with and without the addition of an antiwear additive has been studied using the Rolling four-ball machine, the Unisteel rolling contact machine and the Amsler 2-disc machine. As will be described in Chapter Two, the Rolling four-ball and Unisteel machines were used to initially assess the lubricating performance of the fluids. The Amsler 2-disc machine was chosen to allow the continuous monitoring of wear, friction and crack initiation and propagation to be made at different lubrication regimes. Also described in Chapter Two is the application of magnetic crack detection to the examination of water induced fatigue cracking and pitting. Optical and Scanning Electron Microscopy together with Auger Electron Spectroscopy and X-ray diffraction are also described.

The results obtained from the three different fatigue tests together with the results from the analysis are presented in Chapter Three. Finally, in Chapter Four, the overall results are compared and discussed with previous investigations in order that the mechanism of pitting failure in this important range of lubricants can be identified.

CHAPTER TWO

EXPERIMENTAL APPARATUS AND PROCEDURES

2.1. Introduction

This chapter describes the apparatus, material and chemicals used, together with the various experimental procedures adopted for the three fatigue testing machines. Failed test specimens were then analysed using different techniques and procedures, which are described towards the end of the chapter.

2.2. The Unisteel Machine

2.2.1. Introduction

The Unisteel test machine was originally designed for assessing the fatigue properties of steel billets intended for roller bearing manufacture but has subsequently been applied to the evaluation of mineral oil lubricants and more recently to fire resistant fluids. Many authors (14),(153) have shown that the Unisteel machine is a reliable and effective machine for studying the influence of fire resistant fluids on rolling contact bearing fatigue life, as has the author of this work. Figure 2.1a) shows an overall view of one of the Unisteel machines used in the programme.

2.2.2. The Unisteel Machine

Test lubricant is supplied via a closed reciprocating pump system to an axial thrust bearing assembly made up from two steel races consisting of one flat washer (the test specimen), one grooved lower race and one cage containing

a) Overall view.

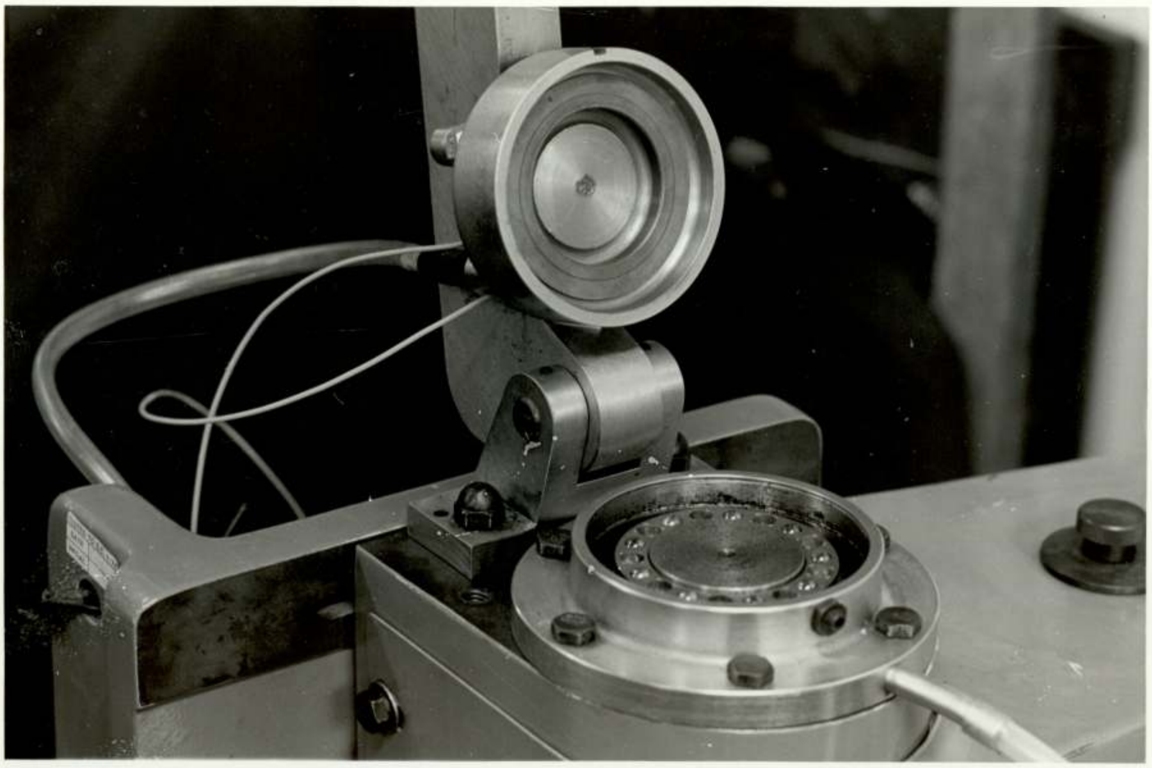

b) Close-up of the bearing assembly.

Figure 2·1. The Unisteel Rolling Contact Machine nine steel balls as shown in Figure 2.1b). A schematic diagram of the bearing assembly is given in Figure 2.2.

The cage used was that of standard configuration having eighteen sockets for the inclusion of bearing balls. Only nine sockets were required for the test and these were filled alternately by bearing balls of diameter 7.9mm. The balls were initially weighed and sorted so that they would give an evenly balanced cage, thus eliminating uneven load distribution between balls.

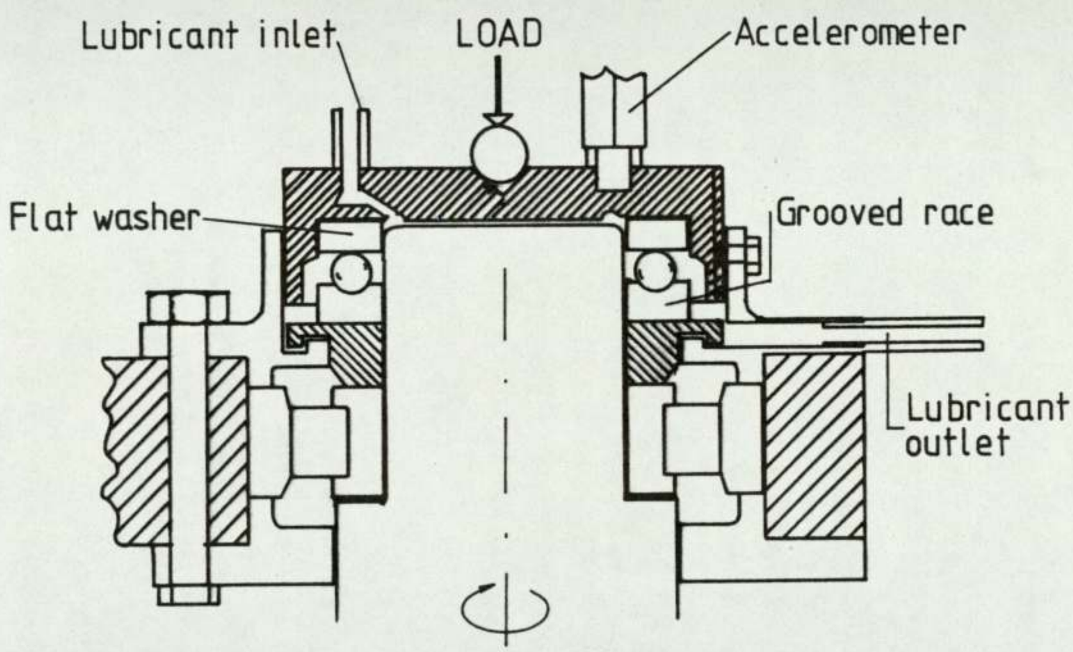

Figure 2·2. Schematic diagram of the Unisteel machine.

The test specimen was held stationary in the bearing housing while the grooved race was rotated at a speed of 1500rpm, driven by a 0.75Hp three phase electric motor. Test lubricant was supplied at the rate of 0.54×10^{-3} litres per minute. The thrust bearing assembly was run under constant load until a crack or pit forms on the flat washer and grows sufficiently to trigger one of the two accelerometers located on the housing, thus stopping the motor and associated timer. The load was obtained by attaching weights to a vertical rod connected to a horizontal arm, as shown in Figure 2.1a).

2.2.3. Test Specimens

The test specimens had the dimensions 75mm outside diameter, 50mm inside diameter and thickness 6mm. They were made from hardened BS EN31 steel having a hardness of 830 VPN and a surface average finish of $0.17\mu m$ CLA. These measurements were taken directly on the flat surface of the washer well away from the running track yielded by the balls. The flat washer was also given an identification number and a mark to distinguish the two sides by spark errosion.

2.3. The Rolling Four-ball Machine

2.3.1. Introduction

The Rolling four-ball machine represents a particularly severe fatigue test for any lubricant and indeed the high pressures developed tend to yield results at a much quicker rate that with the Unisteel machine. Nevertheless, it has been shown (138) that the Rolling four-ball machine can give useful information regarding the lubricating properties of various lubricants when results must be obtained rapidly. In addition, the cost of the ball bearing specimens is relatively cheap compared to the thrust races and cages of the Unisteel machine.

2.3.2. The Rolling Four-ball Machine

The Rolling four-ball fatigue machine differs from the conventional four-ball machine in that a steel bearing ball is held in a chuck and rotated at 1500 rpm against a triangular configuration of three similar balls able to rotate freely in a special ball cup housing of test lubricant. Figure 2.3 shows an overall view of the Rolling four-ball machine together with a close-up view of the ball configuration. A schematic diagram showing the positioning of the bearing balls is given in Figure 2.4. A series of weights are then attached to a horizontal arm arrangement such that a force develops between the top and bottom balls.

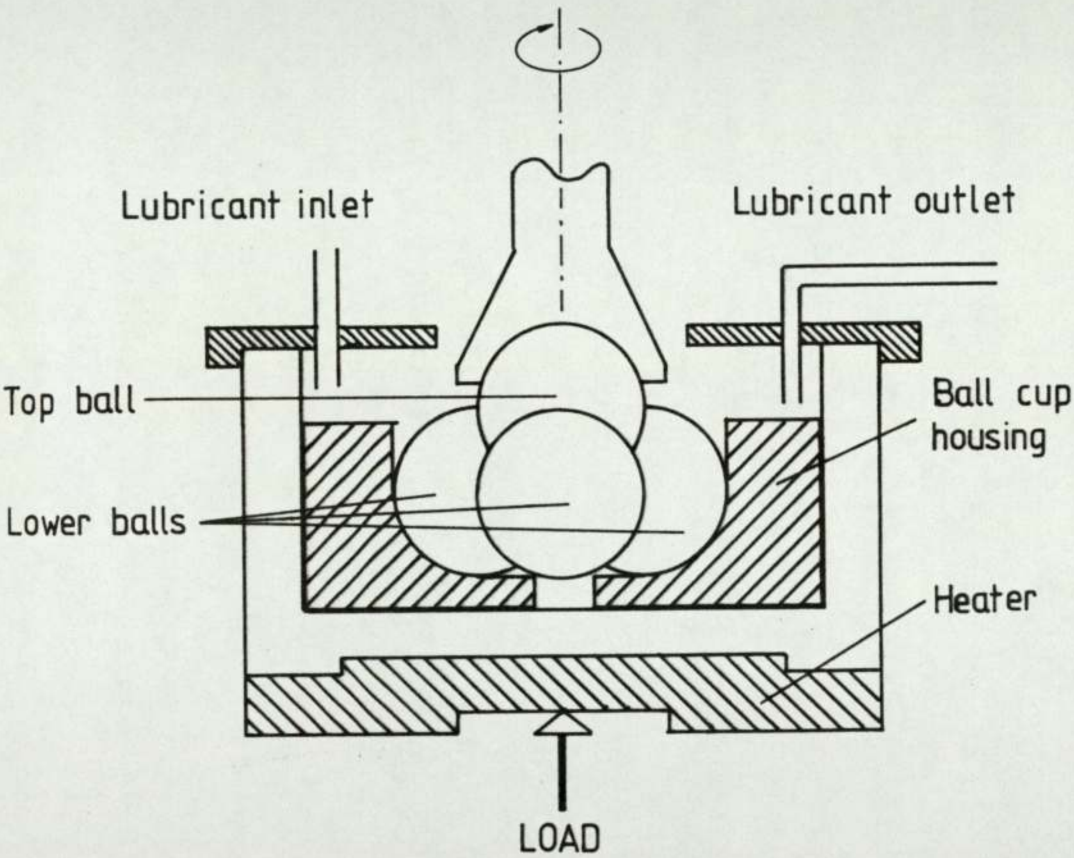

Figure 2·4. Schematic diagram of the Rolling four-ball machine.

The test lubricant was continuously cycled between the ball cup housing and a one litre resevoir bottle at a rate of 0.25 litres per minute, by means of a peristallic pump.

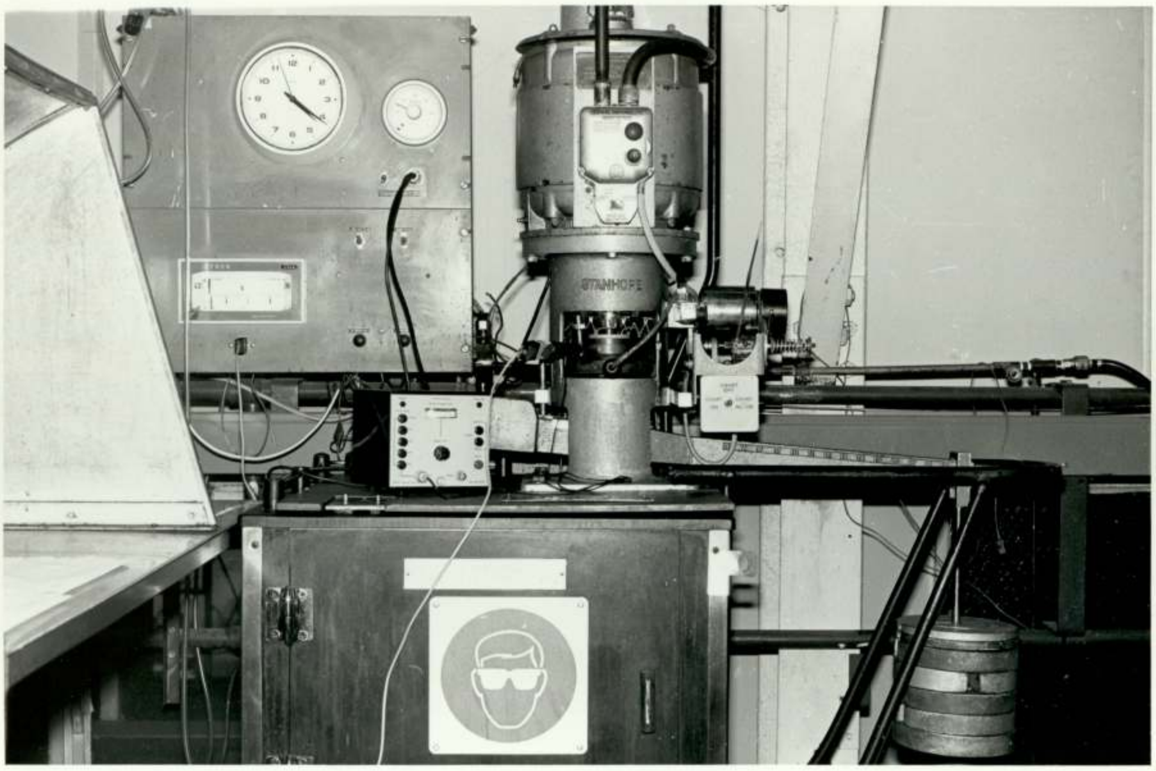

a) Overall view.

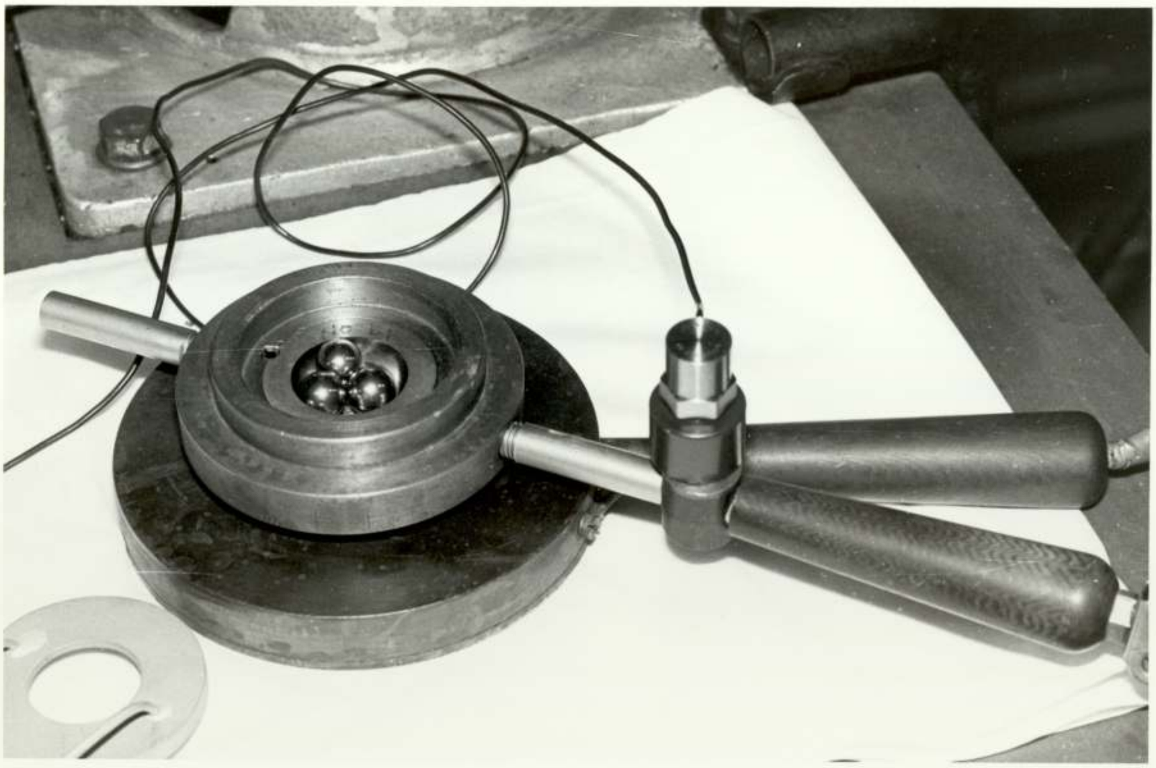

b) Close-up of the ball cup housing.

Figure 2·3. The Rolling Four Ball Fatigue Machine

The temperature of the test lubricant could be held at a constant value in the range 20 to 80°C ±1 °C by the means of a thermostatically controlled heater plate held in position under the ball cup housing.

The rig and associated timer were run until switched off by a vibration sensor which detects pit formation. The electrical signal from the sensor was continuously monitored throughout each experiment and its amplitude plotted against time on a chart recorder.

2.3.3. Test Specimens

Special BS EN31 steel bearing balls supplied by SKF of diameter 12.7mm were used. They have a surface roughness of 0.04μm CLA and a hardness of between 746 and 832 VPN.

2.4. The Amsler 2-disc Machine

2.4.1 Introduction

Disc machines have been used extensively since the pioneering work of Way in 1935 (87) for the analysis of the various phenomena associated with pitting fatigue.

Because it is a relatively simple operation to alter the individual velocity of the discs, so introducing a known amount of slip, disc machines can be used for simulating and subsequently investigating the damage suffered by meshing gear teeth along the various regions of each tooth (154).

The use of the Unisteel and Rolling four-ball machines as described in the previous sections are inherently limited in tribological applications since they both suffer from the disadvantage that the continuous monitoring of wear, friction and crack initiation and propagation is not possible, and examination of wear processes and of crack and pit formation must be postponed until after the event.

In an investigation of this type it is essential to examine all of the above parameters continuously and for these reasons a 2-disc machine was employed for the major part of the study.

2.4.2. The Amsler 2-disc Machine

The 2-disc machine chosen was an Amsler fatigue test machine and is shown in Figure 2.5a). This had the further advantage in that disc specimens of equal diameter were rotated with a constant slip, or difference in velocity, of 10%. This slip is necessary in order that pitting damage could be obtained at a sensible rate.

The machine can accommodate disc specimens of diameters between 30 and 70mm and these are locked onto the ends of their respective shafts by nuts. The rotational directions of each of the discs can be altered independently by the inclusion of a reversing gear in the main drive unit or if desired, one disc can remain stationary held by a locking pin. The speed of the faster disc can be varied between 14 and 400 rpm. Discs were driven by a 1.2 kW rated three phase electric motor. The applied load could be adjusted between 20 and 200 Newtons by means of a compressible spring.

Attached to the Amsler 2-disc machine was a load dynamometer and diagram recorder for monitoring the changes in torque during experimental runs. The maximum torque that could be read from the pointer and scale was 150 kgcm.

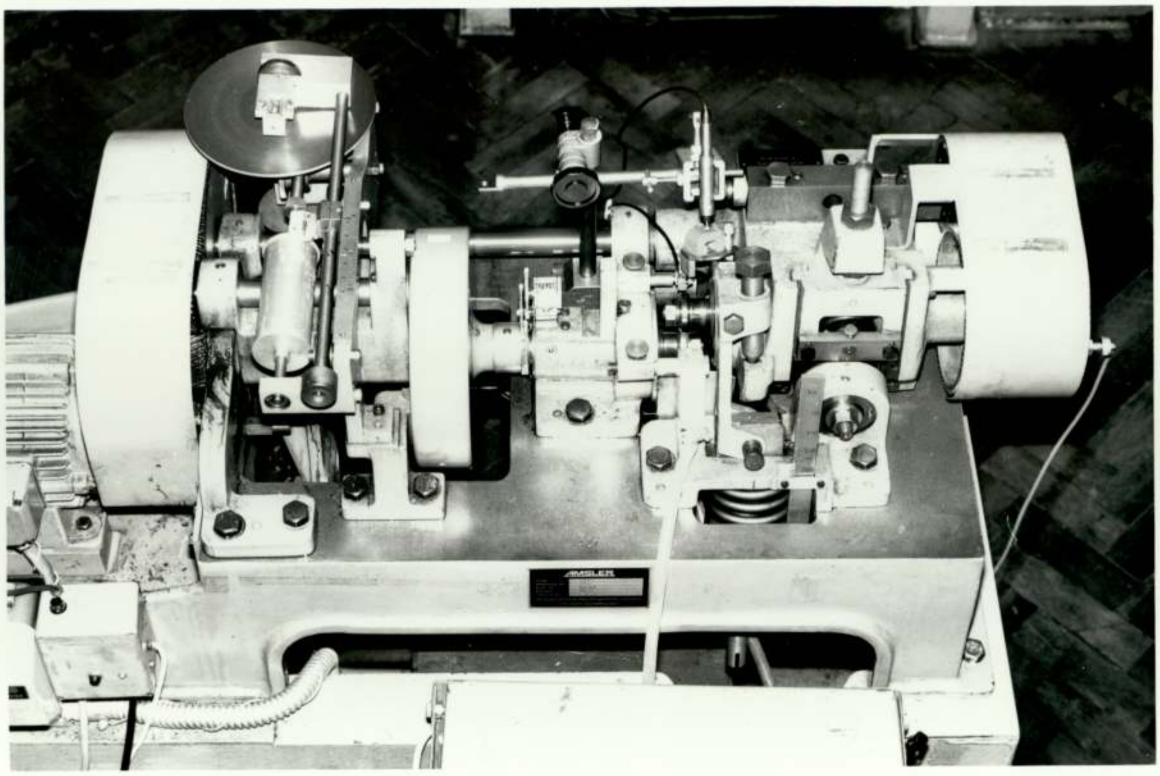

a) Overall view.

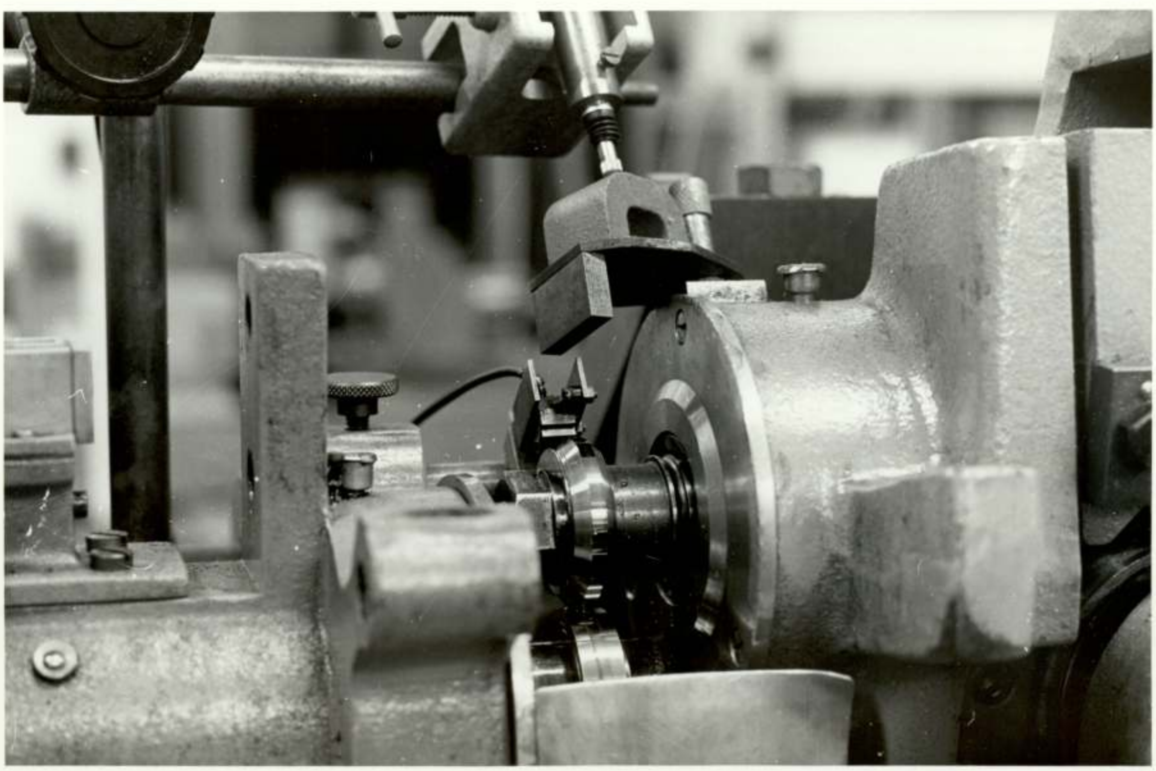

b) Close-up of the disc configuration, L.V.D.T. transducer and the magnetic crack detector pick-up head.

Figure 2·5. The Amsler 2-Disc Machine

Test lubricant was supplied at the rate of 0.24 litres per minute to the disc conjunction and recirculated through a glass wool filter system by means of a peristallic pump.

2.4.3. Test specimens

For the slower rotating shaft, disc specimens were machined from a solid bar of BS EN31 steel. They had outside diameter 40mm, bore 16mm and width 10mm. The track surface was further machined to about 3mm in width by two 45° chamfer cuts on either edge of the disc, as indicated in Figure 2.5b) and Figure 2.6.

The measured hardness of these discs varied between 203 and 232 VPN. The average surface finish was about 0.25μm CLA, but for experiments designed to investigate the effects of initial surface roughness on pitting life, roughnesses of between 0.05 and 0.5μm CLA were produced by a combination of surface grinding and polishing.

All pitting discs were numbered and each had a 'start' mark on one chamfered side for alignment of the crack detector pick-up head.

The disc specimens intended for the faster shaft had hardness values between 763 and 856 VPN, a surface average finish of 0.07μm CLA and were formed from original BS EN31 steel inner bearing races. These bearings were supplied by Torrington and had 40mm outside diameter, 35mm inside diameter and width 25mm. Preparation required circumferential sectioning of the bearing in two and further grinding of the sides to give a bearing ring width of 10mm. These were then

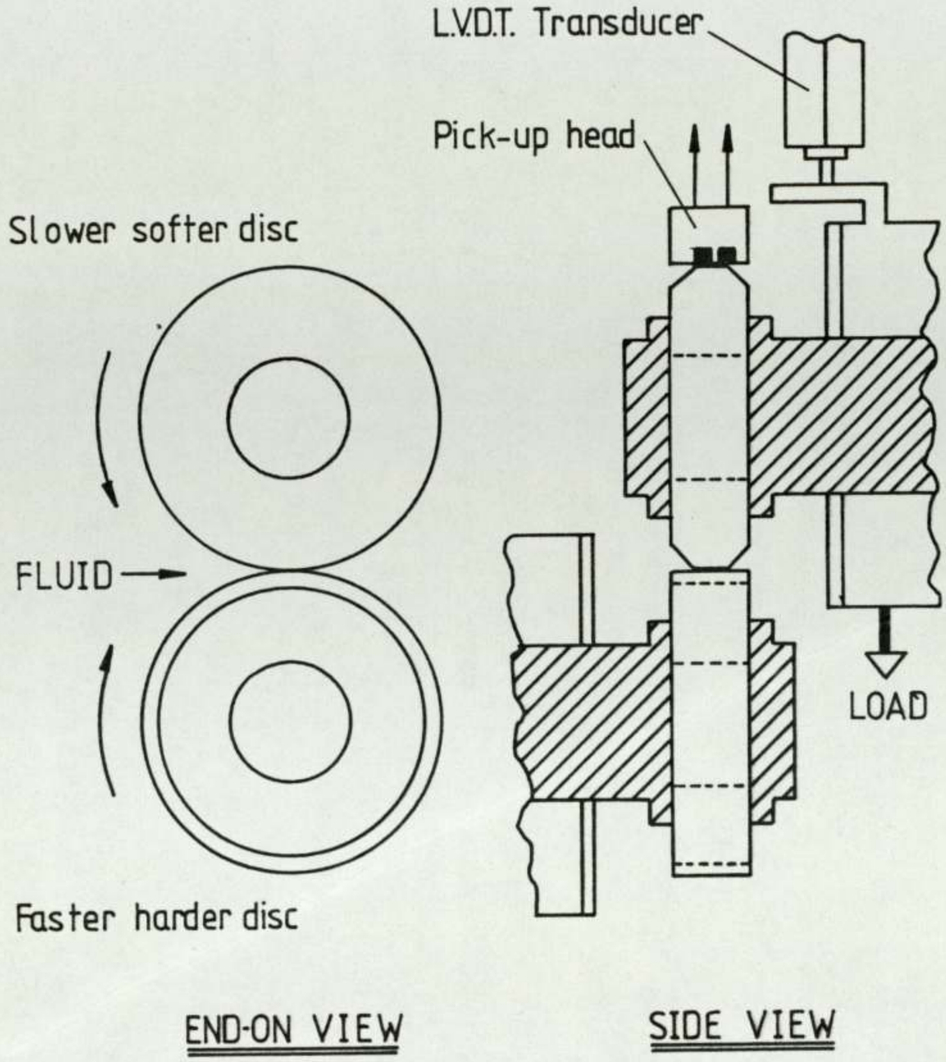

Figure 2·6. Schematic diagram of the Amsler 2-disc machine.

push fitted onto a steel disc having outside diameter 35.02mm, width 10mm and bore diameter 16mm as shown in the schematic diagram given in Figure 2.6. This method provided a relatively inexpensive supply of hardened discs.

The slower disc (designated the "pitting disc") and the faster ring (designated the "driving disc") were weighed before and after each experiment. In addition, because of the technique of crack detection used, the discs were demagnetised in an AC field, before each run.

2.5. Material Specification and Test Specimen Preparation

2.5.1. Material Specification

All test specimens for the three fatigue testing machines were made from BS EN31 steel, whose composition is given in Table 2.1 and material specification in Table 2.2. The steel, which is used mainly in the hardened and lightly tempered condition, is used extensively in applications that require a relatively cheap, wear resistant surface, which makes it ideal for ball and roller bearings, lathe centres, collets and bullet cores.

EN31 has been found to offer excellent fatigue and corrosion resistant properties together with high thermal conductivity and the ability to withstand high pressures and seizure during normal modes of operation. It is for these reasons that EN31 is chosen for the production of bearings. The American equivalent to EN31 is SAE52100.

Chemical Composition		
Element	Min	Max
Carbon	0.9	1.20
Silicon	0.1	0.35
Manganese	0.3	0.75
Sulphur	-	0.05
Phosphorus	-	0.05
Chromium	1.0	1.60

Table 2.1. EN31 One per cent carbon - chromium steel.

2.5.2. Test Specimen Preparation

All test specimens were ultrasonically washed in petroleum ether to remove any grease and oil contamination and further washed in acetone immediately prior to use. Surface roughness and bulk hardness were then recorded before the start of each experiment apart from the ball bearing specimens required for the Rolling four-ball machine. The properties of these were taken from the manufacturer's specification. In all, up to three different positions were chosen at random for testing, and the respective measurements averaged.

Density ρ:	7800 kgm^{-3}
Young's Modulus E:	200 Gpa
Poisson's ratio σ:	0.295

Table 2.2. EN31 Specification.

2.5.3. Surface Roughness Measurements

These were obtained on a Rank Taylor Hobson Talysurf machine. The Talysurf consists of a stylus having a tip diameter of 0.0025mm in slow horizontal motion along the surface of the specimen. The surface roughness is then proportional to the mean vertical motion of the stylus tip given in the units micrometers Centre Line Average or CLA.

2.5.4. Bulk Hardness Measurements

Hardness measurments were taken using a Vickers hardness tester. The hardness tester was equipped with a pyramid shaped diamond indentor which was brought into contact with the specimen for a short period under a load of 30kg. The hardness number is then based on the relative diagonal length of the indentation and is given in the units Vickers Pyramidal Number or VPN.

2.6. Aqueous Lubricants

The Fire Resistant Fluids (FRF) used in the experiments were the water glycol based lubricants or ISO designated HFC aqueous glycols. These were blended from the individual chemical constituents given in Table 2.3 and all of the test lubricants contained a similar amount of amine rust inhibitor. This was found necessary to prevent the development of rust on the fatigue machines due to the high water content of the lubricants. Apart from Test Lubricant A (see Table 2.3), all fluids contained the same percentage weight of de-ionized water and the remainder of each solution was a mixture of propylene glycol and polyalkylene glycol thickener, a co-polymer of ethylene and propylene oxide, the relative proportions of which determined the viscosity.

For a second series of experiments two fluids, namely F and G (see Table 2.3), contained a fatty acid antiwear additive and were similar in viscosity to fluids B and E respectively. The empirical formulae and structure of the various chemicals are given in Figure 2.7.

In order to introduce the antiwear additive to a test lubricant solution, it was necessary to heat the additive above its melting point of 31°C and to combine this with an excess of rust inhibitor. The solution formed was water soluble and could subsequently be added to the solution of water and glycol.

Test Lubricant	De-ionised Water	Propylene Glycol	Glycol Thickener	Rust Inhibitor	Anti-Wear	Viscosity @ 40°C
A	98.75	0	0	1.25	0	0.6
B	43.00	55.75	0	1.25	0	3.7
C	43.00	48.75	7	1.25	0	8.9
D	43.00	41.75	14	1.25	0	14.0
E	43.00	22.75	33	1.25	0	46.0
F	43.00	54.95	0	1.25	0.8	3.7
G	43.00	21.95	33	1.25	0.8	46.0
H	43.00	33.75	22	1.25	0	24.3
I	43.00	27.75	28	1.25	0	33.8

Table 2.3. Chemical Composition and Viscosity of the Test Lubricants.

All percentages were determined by weight and test lubricants made in batches of 1kg. The kinematic viscosity, measured in cSt or m^2s^{-1} for each lubricant was determined using a U-tube viscometer placed in a temperature-controlled water bath at various selected temperatures between 30 and 70°C. Since all calculations involving viscosity required the coefficient or absolute viscosity, measured in Nsm^{-2}, the density of the lubricants was also required.

Density was determined by measuring the relative displacement of test lubricants within a fine capillary tube at selected temperatures. Because the weight of test lubricant will remain constant, any change in volume will be proportional to a corresponding change in density.

Propylene glycol [Propane 1,2-diol]

$CH_3CH(OH)CH_2OH$

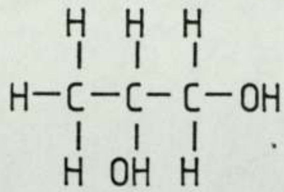

Rust inhibitor [N,N-Dimethylaminoethanol]

$(CH_3)_2NCH_2CH_2OH$

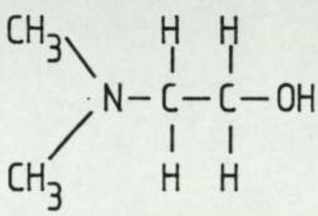

Anti wear agent [Capric acid]

$CH_3(CH_2)_8COOH$

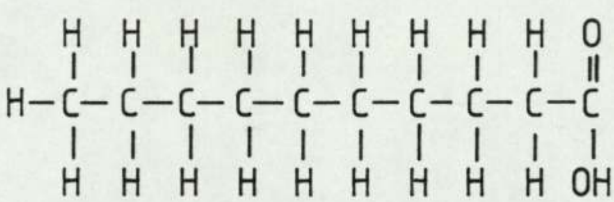

Thickener [Polyalkylene glycol type]

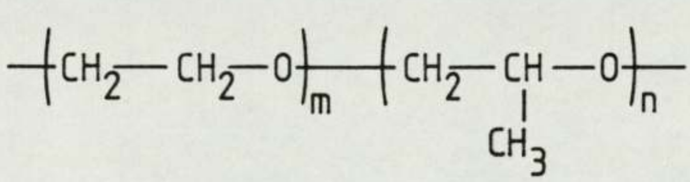

Figure 2·7. Empirical formulae and structure of the chemicals used in the test lubricants.

The coefficient of viscosity could therefore be calculated from the product of kinematic viscosity and density and plotted as a function of temperature, as shown in Figure 2.8. From this the actual viscosity of the lubricant could be determined at the working temperature of the machine.

The pressure viscosity coefficient could not be measured directly and a value of 4.5 $(GPa)^{-1}$ (155) was used in all calculations.

2.7. Friction and Wear Measurements

Friction and wear measurements were taken for the Amsler 2-disc machine only and were not implemented in the Unisteel or Rolling four-ball experiments.

Friction was measured using the load dynamometer attached to the Amsler 2-disc machine. This displayed the torque developed between the pitting and driving discs during any particular run and could also be recorded as a function of time on an endless loop of paper attached to a rotating drum. The coefficient of friction is calculated from:

$$\text{Coefficient of friction} = \frac{\text{Torque (kgcm)}}{\text{Load (kg) x Disc radius (cm)}} \qquad 2.1$$

Wear was determined by two independent methods the first of which made use of a weight-loss technique. This involved separately weighing the two discs before and after each run and calculating the weight of metal removed. Wear was then expressed as the volume of metal removed per unit distance rotated in the units m^3m^{-1}.

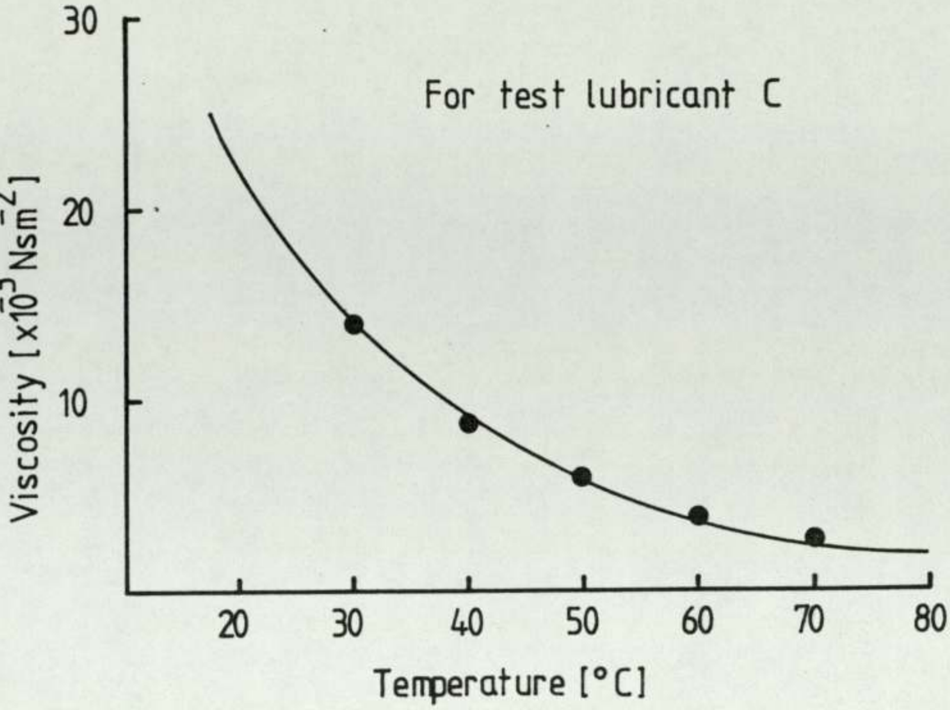

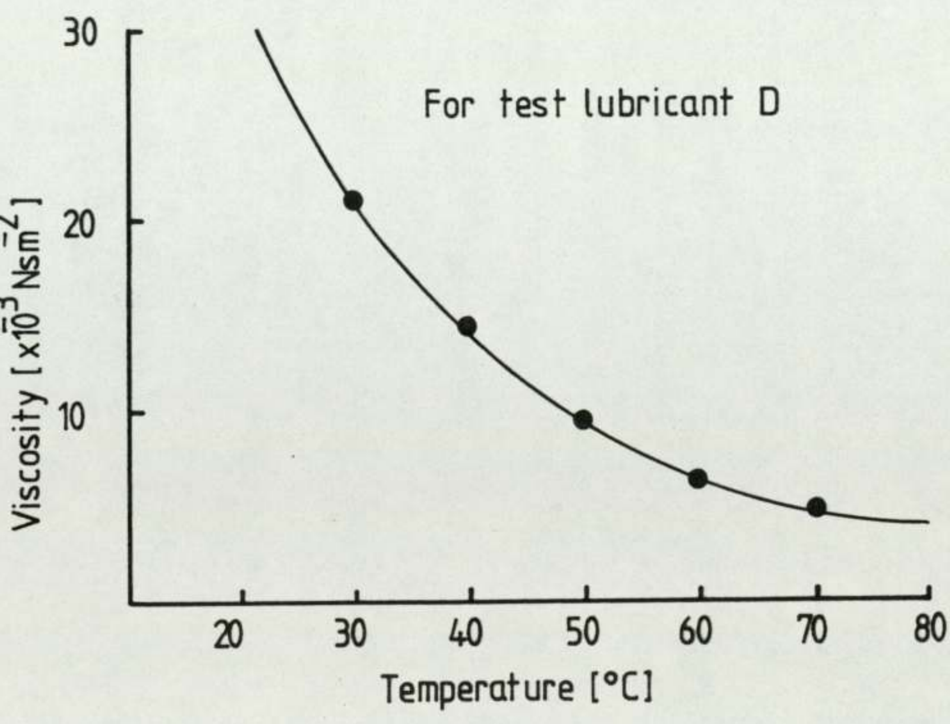

Figure 2·8. Viscosity against temperature for the test lubricants.

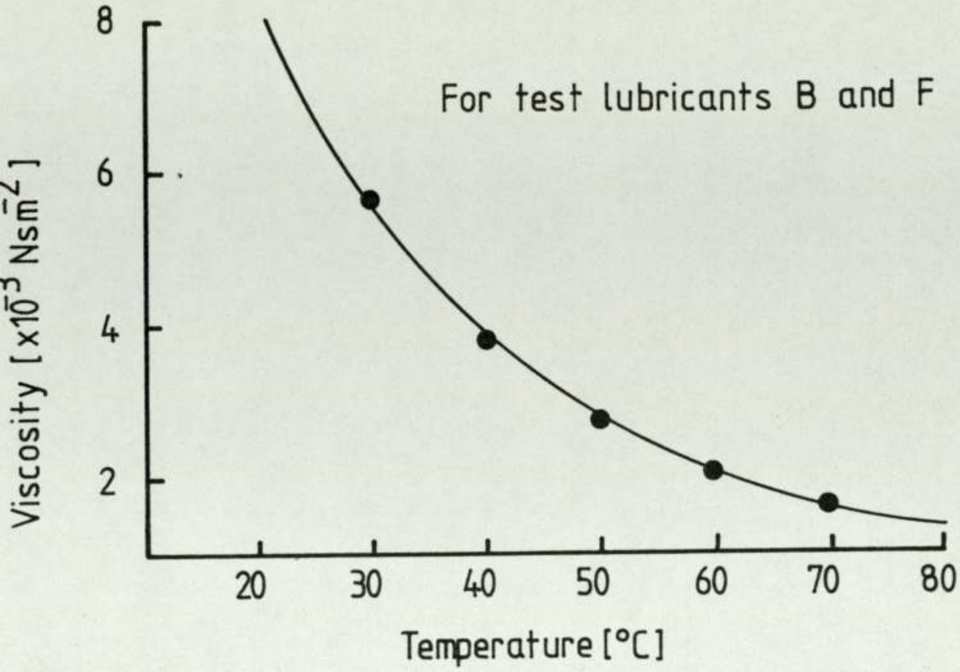

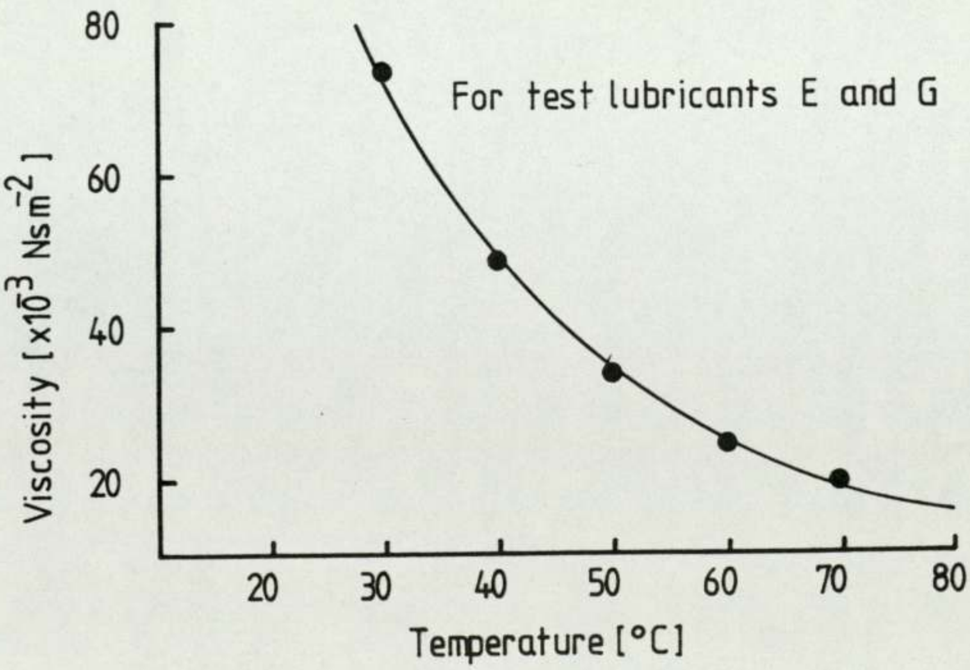

Figure 2·8(cont). Viscosity against temperature for the test lubricants.

The second method required a Linear Variable Differential Transformer (LVDT) transducer placed normally on the pitting disc housing as shown in Figure 2.5b) and 2.6.

From preliminary experiments, the amount of wear determined from the weight-loss method for the harder driving disc was found to be negligible compared to the amount of wear that had taken place on the softer pitting disc. It was therefore reasonable to assume that any pitting disc wear would be proportional to the relative displacement of the housing, as measured by the LVDT transducer.

The electrical signal from the transducer was subsequently fed into a chart recorder through an adjustable gain amplifier. The amplifier was calibrated such that for every 1mm of pen movement the pitting disc would have been displaced by 2.108×10^{-3}mm. The trace obtained was therefore a plot of pitting disc displacement against time.

The use of an LVDT transducer allowed the displacement of the pitting disc to be continuously checked throughout each experimental run and any damage occurring at localised areas on the surface would not have an effect on the overall mean displacement of the transducer. Wear rates were expressed in the same units as before (m^3m^{-1}).

2.8. The Magnetic Crack Detector

2.8.1. Introduction

To understand fully the fatigue mechanisms involved during the pitting failure of steel, it was necessary to adopt a system that would readily detect initial surface cracks or subsurface inclusions.

One method would be to stop the machine at predetermined intervals and visually inspect the surface of the pitting disc for crack damage. Alternatively, many of the non-destructive tests such as fluorescent dye penetrants, magnetic particle methods and eddy currents could be employed to locate such damage, while large subsurface inclusions could be detected by either X-ray and gamma ray or ultrasonic echo sounding techniques.

All of these methods, however, suffer from the disadvantage that the fatigue machine would require constant attention and numerous checking operations via the removal and replacement of the disc throughout each experimental run. Also, the measurement of crack propagation would be difficult to quantify, since it would be impossible to monitor crack progress, especially with the penetrant type tests.

A much better method was to incorporate the magnetic crack detector originally designed by Phillips and Chapman (156). This technique involved the detection and measurement of the rate of change of magnetic flux leakage brought about by cracks in and under the surface of a rotating metal disc. One important aspect of this method of detection, was that the amount of flux leakage was found to be dependant to the crack length, a feature which was utilised extensively throughout this work.

2.8.2. Modifications Made to the Original Crack Detector

The magnetic crack detector has undergone several development modifications, including the addition of new features, since the original design was first published.

Amongst the improvements was a high gain amplifier offering a much better signal to noise ratio, thus allowing the onset of pit formation to be detected at a much earlier stage. New features included an infra red trigger source, digital frequency counter and a facility to prevent premature shut down of the apparatus caused by freak signals. A schematic diagram showing the various electronic circuits incorporated in the crack detector is shown in Figure 2.9.

The entire circuit can be divided into three main groups namely, crack signal handling circuits, automatic shut down circuits and external trigger circuits which are now described.

2.8.3. Crack Signal Handling Circuits

This particular group of circuits handles the initial detection of the cracks through to the visual display on the oscilloscope and to the quantification of the cracks by the digital frequency counter.

A commercially available cassette tape recorder head having a pole gap width of 0.04mm and length 2.2mm, was allowed to rest on the pitting disc surface sandwiching a thin film of test lubricant. The positioning of the pick-up head relative to the pitting disc can be seen in Figure 2.5b). The electrical signal from the pick-up head was then amplified according to a preset gain and subsequently displayed on an oscilloscope. Amplifier gains ranging from 400 to 2000 could be selected. At this stage the entire signal was run through a precision full wave rectifier changing all negative signals into positive ones before

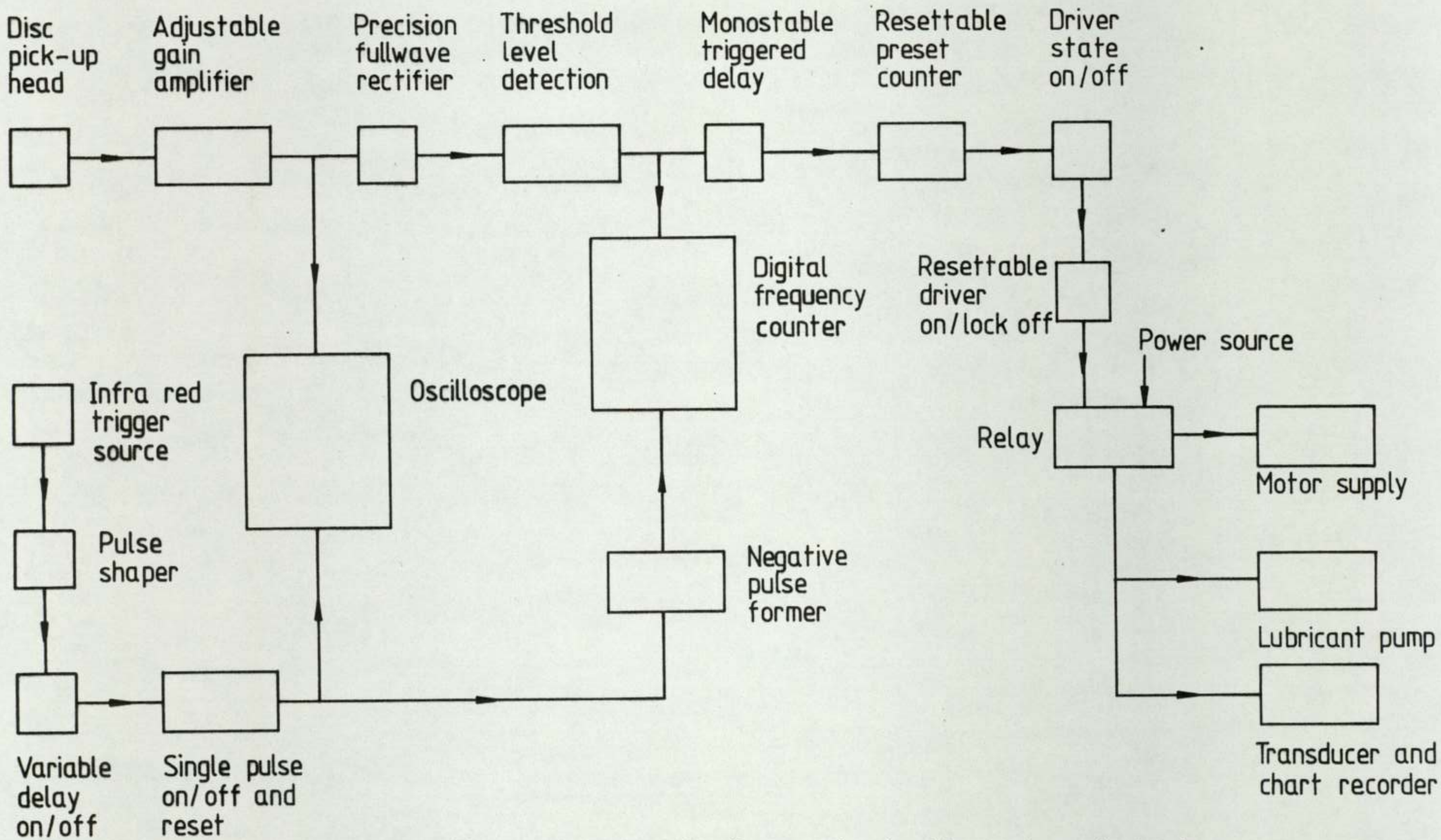

Figure 2·9. Schematic diagram showing the various electronic circuits incorporated in the crack detector.

entering the threshold level detection circuits. Here, all individual signals were filtered according to signal height, such that only those signals exceeding a pretetermined signal level or threshold level were allowed through. Altogether, ten threshold levels could be preset ranging from Threshold Level 1 corresponding to the first detectable crack, continuing up to Threshold Level 10. Table 2.4 gives the non-amplified and respective amplified peak-to-peak voltages corresponding to the ten threshold levels. At this stage the number of selected signals were quantified by the digital frequency counter.

Crack Detector Threshold Level	Input P to P Voltage (mV)	Oscilloscope P to P Voltage (V) ±0.2V
1	2.32	2.6
2	4.84	5.0
3	7.30	8.0
4	9.79	10.0
5	12.30	13.0
6	14.79	15.0
7	17.28	18.0
8	19.77	20.0
9	21.61	22.0
10	21.84	24.0

Table 2.4. Crack detector threshold levels. (Gain = 1050. See section 2.8.6.)

2.8.4. Automatic Shut Down Procedure Circuits

After threshold level detection the selected, rectified signals continue to the automatic shut down circuits. This section handles the operating procedure required to successfully turn off the rig and associated equipment. Once a crack has grown sufficiently to exceed a preset threshold level, it passes to a monostable triggered delay circuit, which differentiates between an 'event' and a group of pulses. Thus additional pulses arising from one crack location are not registered by the counter circuit.

The counter incorporated could be preset to count a maximum of 2^{10} pulses before activation of the relay driver circuits. When a finite number of pulses have been recorded the driver is activated and will remain in its present state until the driver is reset manually. During this time the relay is triggered, thus turning off the power supply to the motor, lubricant pump, transducer and chart recorder. Figure 2.10 illustrates the effects of the previously described electrical circuits on a hypothetical signal.

2.8.5. External Trigger Circuits

To count the selected signals between successive cycles and to display a complete signal trace on the oscilloscope over a wide range of speeds, an external method of triggering was required.

An infra red source and detector was interrupted once every revolution by the pitting disc shaft. The subsequent pulse was then shaped into a positive 15 volt square wave, lasting about 1μs which externally triggered the oscilloscope and digital frequency counter. (The digital frequency counter required a negative 3 volt pulse produced by the negative

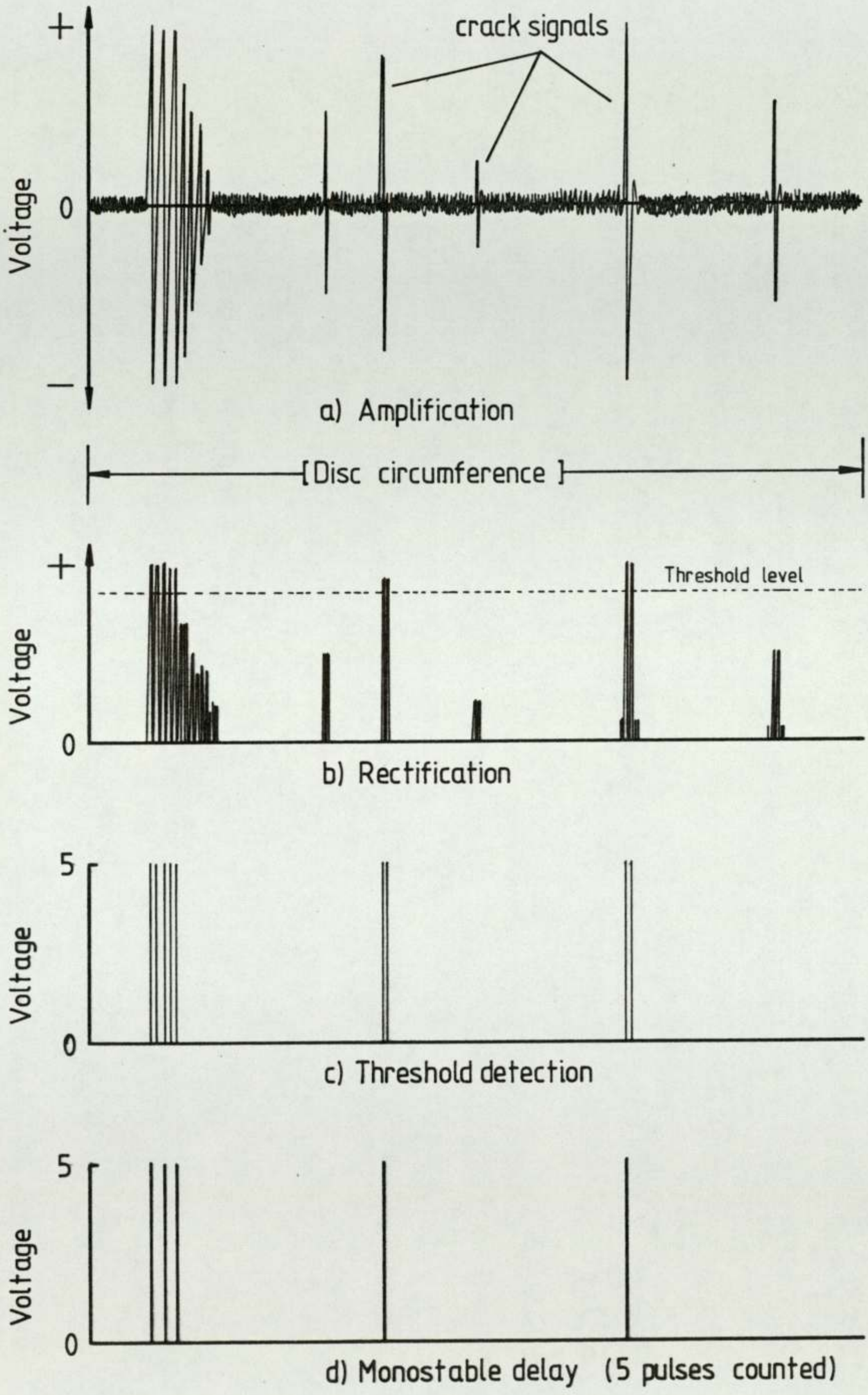

Figure 2·10. Threshold detection on a hypothetical signal.

pulse former circuit).

By delaying the trigger pulse for a brief period via the variable delay and in conjunction with an expanded time base, individual signals arising from particular crack locations could be studied. A single pulse option was also included for photographically recording the oscilloscope display.

2.8.6. Initial Set-up Procedure

Before any long term experiments could be conducted using the Amsler 2-disc machine it was necessary to adjust the pick-up head for optimum sensitivity. It was found that the sensitivity was greatly effected by the thickness of test lubricant between the head and disc surface. In order that signals arising from different lubrication conditions could be compared, it was necessary to apply a small, but constant load of 110gm to the pick-up head. In addition to this the sensitivity was effected by the relative positioning of the pick-up to that of this disc surface. Subsequently a 'standard disc' was made with a 1mm diameter hole drilled centrally into the surface to a depth of 3mm. By carefully moving the pick-up head, a position was found whereby a maximum signal for the hole could be obtained.

The magnetic field required in the operation of the crack detector could be induced by either placing a permanent magnet above the pick-up head or by passing a direct current through it. Both methods were found to have advantages and disadvantages but the most sensitive method for the initial detection of cracks coupled with crack propagation measurements was obtained using the permanent magnet arrangement.

An amplifier gain of 1050 was chosen from trial experimental runs. It was found that using a gain of this magnitude, the signal arising from the appearance of the first crack could be detected and that the signal corresponding to final pit formation would not be too large so as to cause amplifier saturation or clipping. In addition to this, the majority of crack to pit propagation sequences would occur within the ten pre-defined threshold levels.

The resettable preset counter was adjusted to allow automatic shut down after 2^7 pulses had been registered. This figure prevented spurious signals accidentally shuting down the machine and was sufficiently low to limit further crack development once the crack had exceeded the crack threshold level.

To count the number of crack locations on the disc surface it was necessary to inhibit the driver state temporarily. By adjusting the detector threshold level to the most sensitive position (Threshold Level 1), the digital frequency counter would display the current number of crack locations on the disc surface. Increasing the threshold level to a higher value would ultimately yield the number of cracks sustaining to that particular level.

For photographic purposes, the oscilloscope time base was adjusted such that the signals arising from the entire circumference of the pitting disc were represented in one trace. An identification mark was etched onto the pitting shaft to facilitate the re-alignment of discs after they had been removed for inspection. The position of the etch mark corresponded to the start of the trace and allowed the location of cracks to be identified by there relative positions along the trace. From measurements, it was found that 1cm of horizontal trace represented 1.4cm of disc circumference.

2.9. Fatigue Test Procedures

2.9.1. The Unisteel Experiment

The following describes the test procedure adopted and is similar to that of the IP305 test method (157).
Four Unisteel test machines were used altogether which gave eight experimental results for each test lubricant from four double sided test washers.

A clean test washer was inserted into the housing of each machine thus forming the completed thrust bearing assembly. To prevent any excess initial strain to the balls and test washer, weights were added in increments while the bearing was in motion. A dead weight load of 3.34kN was reached after one minute resulting in a maximum Hertzian stress of 3.2GPa being developed between each ball and the flat washer.

The machines were left running until a pit had formed, whereby the motor would automatically shut down. At this stage the flat washer was examined for pitting and the total time noted before the washer was turned over for a second run. If any machine shut down for no apparent reason such that no crack or pit was visible in the track, the cage and balls were replaced and the run continued. Sometimes there was no pit on either the flat washer or the balls and so the lower grooved race was replaced. A new cage/balls combination was always used when a new fluid was introduced.

When a test washer had successfully provided two results, the machine and pump was then cleaned in acetone and petroleum ether, and the procedure repeated for a new test lubricant. This method ensured that no test machine could be used more than once for the analysis of each lubricant thus eliminating any individual characteristics of the machines that could influence the results.

Interpretation of the results required ranking them in ascending order and plotting them as a Weibull distribution on probability graph paper. With eight experimental results the cumulative percentage failed value for the shortest duration commences at 11% and increases to 88% in incremental steps of 11%. From this, the best straight line was fitted and the 50% or L_{50} life obtained.

2.9.2. The Rolling Four-ball Experiment

The experimental procedure adopted for the Rolling four-ball machine is similar to that of the IP300 test method (158).

Three cleaned bearing balls were placed in the special ball cup housing containing a small reservoir of test lubricant. A fourth ball was then fitted to the chuck and allowed to come into contact with the lower balls. The test lubricant was circulated through the system at a temperature of 40°C. This was to allow for any machine dependant temperature rises caused mainly by the high loads encountered.

The prevention of any initial stress and deformation to the balls was achieved by applying the load, as a series of smaller weights, while the balls were rotating. The full load of 500kg was applied after one minute, resulting in a maximum Hertzian stress of 7.24GPa between the top and each of the lower balls.

The machine was then left running until a pit had grown sufficiently to trigger the accelerometer sensor, located near the ball cup housing. The total time taken to pit was then noted.

Pitting was generally confined to the top ball and this signified a successfull test. Sometimes pitting would be apparent either on one of the balls or the inside of the ball cup housing and when this occurred the test was repeated with a set of new balls and the ball cup housing replaced if this was damaged. Altogether, ten individual experiments were conducted for each test lubricant, after which the machine was washed with acetone and petroleum ether and a new fluid evaluated.

The ten life values were plotted in ascending order, as a Weibull distribution on propability graph paper and the 50% or L_{50} life interpolated from a best fitting straight line. Individual points were plotted in increments of 9%, starting at 9% for the shortest duration and finishing at 90% for the longest duration.

2.9.3. The Amsler 2-disc Experiment

Prior to any long term experimental tests a Stribeck curve was plotted for the system in order that the different lubrication regimes associated with these tests could be identified. Two discs were attached to the respective shafts and allowed to rotate under a low load of 20kg for a settling period of 24 hours. Test Lubricant B was circulated through the system for a similar time, after which the temperature was taken and the viscosity determined from Figure 2.8.

Five different load settings namely, 20, 50, 100, 150 and 200kg were applied in turn to the discs during which the speed was varied between 14 and 400 rpm. At each speed increment all the relevant parameters were measured together with the resultant torque as read directly from the scale and pointer of the load dynamometer. The whole test procedure, including the settling period, was then repeated with the thicker Test Lubricant E.

The coefficient of friction was calculated from the torque using Equation 2.1 and the bearing number obtained from Equation 1.1.

It was now possible to run experiments in any desired lubrication regime by altering either the speed of the discs or the viscosity of the lubricant. Although the load could also be varied it was decided to keep this constant throughout the majority of experiments in the pitting test programme. This would keep the stress developed within the discs constant, and allow direct comparisons to be made between experiments conducted at different lubrication regions.

A load was determined from trial experimental runs in order that (i) pitting would occur at a reasonable rate and (ii) the surfaces of the pitting discs would not widen too much under the applied load and subsequently reduce stress.

All experiments, unless otherwise stated, were therfore run at a load of 90kg resulting in a maximum Hertzian stress of 1.01Gpa.

From the Stribeck curve, nine main lubrication regions were chosen for investigation and an average of ten individual experiments conducted at each region. The machine operating conditions for these regions are given in Table 2.5 together with the particular test lubricant. Lubrication regions are numbered chronologically in order of increasing fluid film thickness. For experiments conducted with loads greater than 90kg, decimal point notation is used. Lubrication Region 4 was of particular interest as it could be obtained by two different lubricant viscosity and speed conditions. These are distinguished by the letters a) and b). Lubrication Region 9 was conducted at a load of 20kg.

Each experiment consisted of attaching a pair of clean discs to the respective shafts and adjusting the speed to suit the particular test lubricant under investigation, so obtaining the desired operating region. The 90kg load was applied after the discs were in motion.

Throughout the experiment the pitting disc was continuously monitored for crack initiation, wear and any changes in friction that might occur during the test. The magnetic crack detector was adjusted to Threshold Level 1 such that on the formation of the first crack, the machine and associated equipment would automatically shut down. At this stage, the number of cycles was noted and the pitting disc removed so that the crack could be photographed through an optical microscope. A photograph of the oscilloscope trace was also taken. The threshold level of the crack detector was

Lubrication Region	Film Thickness (μm)	Bearing Number $x10^{-11}$	Speeds (rpm)	Load (N)	Contact Pressure (GPa)	Working Temperature (^{o}C)	Viscosity at Working Temp ($x10^{-3}$ Nsm^{-2})	Test Lubricant Antiwear Additive		Maximum Hertzian (GPa)
								Without	With	
1	0.0035	0.38	30	900	0.8	28	6.0	B	F	1.01
1.1	0.0078	1.00	100	1500	1.0	28	6.0	-	F	1.37
2	0.0083	1.30	100	900	0.8	28	6.0	B	F	1.01
2.1	0.0122	1.69	200	2000	1.2	28	6.0	-	F	1.51
2.2	0.0125	1.87	200	1500	1.0	28	6.0	-	F	1.37
2.3	0.0130	2.17	200	1200	0.9	28	6.0	-	F	1.18
3	0.0136	2.50	200	900	0.8	28	6.0	B	F	1.01
4a	0.0220	5.30	100	900	0.8	28	23.5	D	-	1.01
4b	0.0225	5.50	400	900	0.8	28	6.0	B	F	1.01
5	0.0260	6.70	200	900	0.8	28	15.0	C	-	1.01
6	0.0475	15.00	100	900	0.8	30	70.2	E	G	1.01
7	0.0580	21.00	400	900	0.8	28	23.5	D	-	1.01
8	0.0780	31.00	200	900	0.8	30	70.2	E	G	1.01
9	0.1540	130.00	400	200	0.4	30	70.2	E	G	0.45

Table 2.5. Machine operating conditions and test lubricants used for the lubrication regimes.

increased to level 2 and the experiment allowed to continue until the original crack, or additional new cracks had grown sufficiently to trigger the current threshold level. During this and subsequent stages, all the cracks at their various degrees of development were quantified using the digital frequency counter and the increased number of cycles noted.

The above procedure was repeated until a pit had formed on the disc whereby the current threshold level was noted in addition to the number of cycles elapsed. Both the pitting and driving discs were washed in acetone and petroleum ether before they were weighed and prepared for metallurgical examination.

2.10. Metallography

2.10.1. Introduction

Any work involved with the fatigue cracking and pitting of materials naturally leads on to the science of metallography. Here information is obtained from the test specimen by examination after the cracking or pitting event and therefore adds to the overall amount of data accumulated during the investigation.

2.10.2. Specimen Preparation (For examination)

Preparation required a cross sectional cut through the relevant damage by the careful alignment and minipulation of a slowly rotating abrasive wheel. The various types of sectional cut for the different specimens are given in Figure 2.11. Once sectioned, the pit or crack was mounted within electrically conductive Bakelite, after which it was polished to a surface finish of 0.025μm CLA using a progressive series

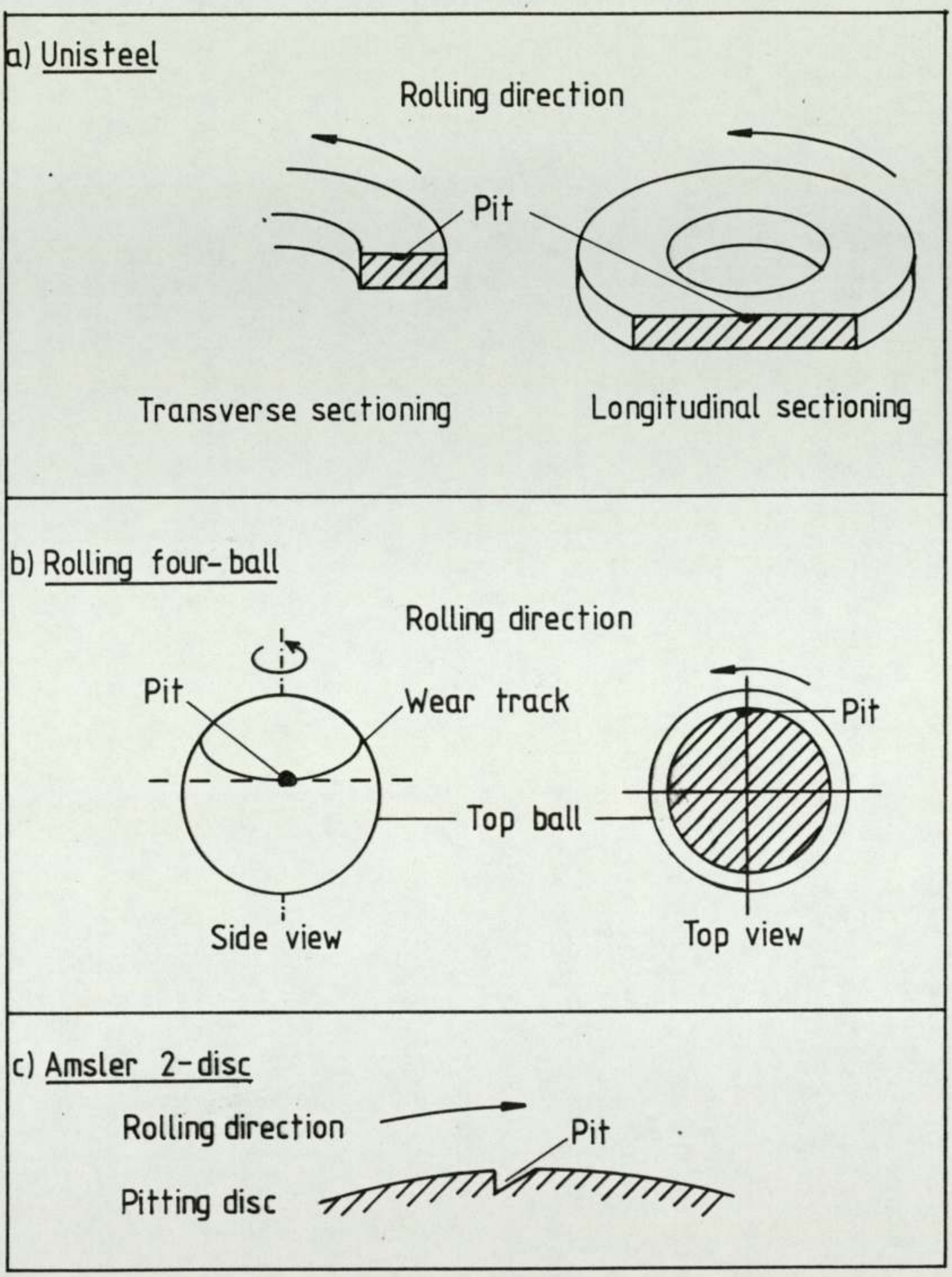

Figure 2·11. Sectional cuts for the three types of test specimen.

of grit and diamond polishing wheels. The mounted specimens 30mm in diameter and 10mm in height were then studied using the Scanning Electron Microscope (SEM), and microhardness measurements were taken at selected areas.

It has been suggested (159) that such an examination technique could give rise to the introduction of further cracks due to the preparation method. To check this an unused disc was subsequently sectioned and prepared as in the above procedure. Scanning Electron Microscopy revealed no subsurface damage and microhardness depth measurements showed no work hardening had occurred.

All failed test specimens from the Amsler 2-disc machine were sectioned and examined, but only selected test specimens from the Unisteel and Rolling four-ball machines were analysed.

2.10.3. Scanning Electron Microscopy (SEM)

The SEM (160) can offer much better resolution than the optical microscope, resulting in greater overall magnification. In addition, because of the relatively small electron beam diameter or spot size, a higher depth of field is possible making it ideal for the examination of rough surfaces.

The failed test specimens were examined in a Cambridge Stereoscan 150 SEM, having a standard size specimen chamber which required that the specimen should not exceed 30mm in diameter and 10mm in height. For general surface topography, the microscope was operated in the secondary electron mode with an accelerating voltage of 20kV. Particular attention was given to the overall cross sectional profile of the pit and to the depth of branching cracks in the bulk of the specimen. Scanning electron micrographs were taken as necessary.

2.10.4. Microhardness Testing

The principle of the microhardness testing machine is similar to that of the Vickers hardness machine described in Section 2.5.4. except that the indentor and applied load are very much smaller than those employed in the larger machine. Subsequently, microhardness depth profiles could be obtained from the mounted test specimen by making a series of measurements starting at the surface and leading into the bulk of the cross section. Failed Amsler pitting discs were examined by taking hardness readings every 20 to 25μm, up to a subsurface depth of 500μm. A graph of microhardness against subsurface depth was then plotted for the specimen.

2.11. Auger Electron Spectroscopy (AES)

2.11.1. Introduction

The use of Auger Electron Spectroscopy has become a valuable analytical technique for the characterisation of solid surfaces, such that information regarding the elemental composition of the outer most atomic layer of a solid can be obtained.

AES is a relatively new technique for surface analysis, although the discovery of the Auger electron after Pierre Auger (161) dates back to 1925. AES has only recently been made aware of (162) with the advent of commercially available equipment and often includes an ion source for sputter removal of surface layers, allowing AES to carry out composition depth profiling.

2.11.2. The Auger Process

Auger electrons are produced by bombarding a sample with a focused beam of electrons accelerated by a potential of between 1 and 10kV. Core electrons are subsequently ejected from the sample within a depth of about 50Å. The process of Auger emission in a solid is represented by a schematic energy level diagram given in Figure 2.12.

The first illustration shows the initial ground state of the solid before electron bombardment has taken place. Binding energies are measured downwards from zero with respect to the Fermi level (E_F).

The second illustration shows the sequence of events following the ionisation of a K shell core electron by an incident electron of energy E_P. The hole in the K shell is filled by an electron from L_1, releasing an amount of excess kinetic energy (E_K - E_{L1}) which can either appear as a photon of energy h = (E_K - E_{L1}) or can be given to another electron either in the same level or in a more shallow level, whereupon the second electron, termed the Auger electron is ejected. The probability of relaxation by Auger or photon emission is governed by the atomic number of the element. In the lighter elements ($Z < 11$), photon or X-ray fluorescence is virtually nonexistant whereas Auger emission occurs with a probability of about 1.0. Above atomic number 11, the probability of Auger emission decreases as that for X-ray fluorescence increases, the 50% probability point being about atomic number

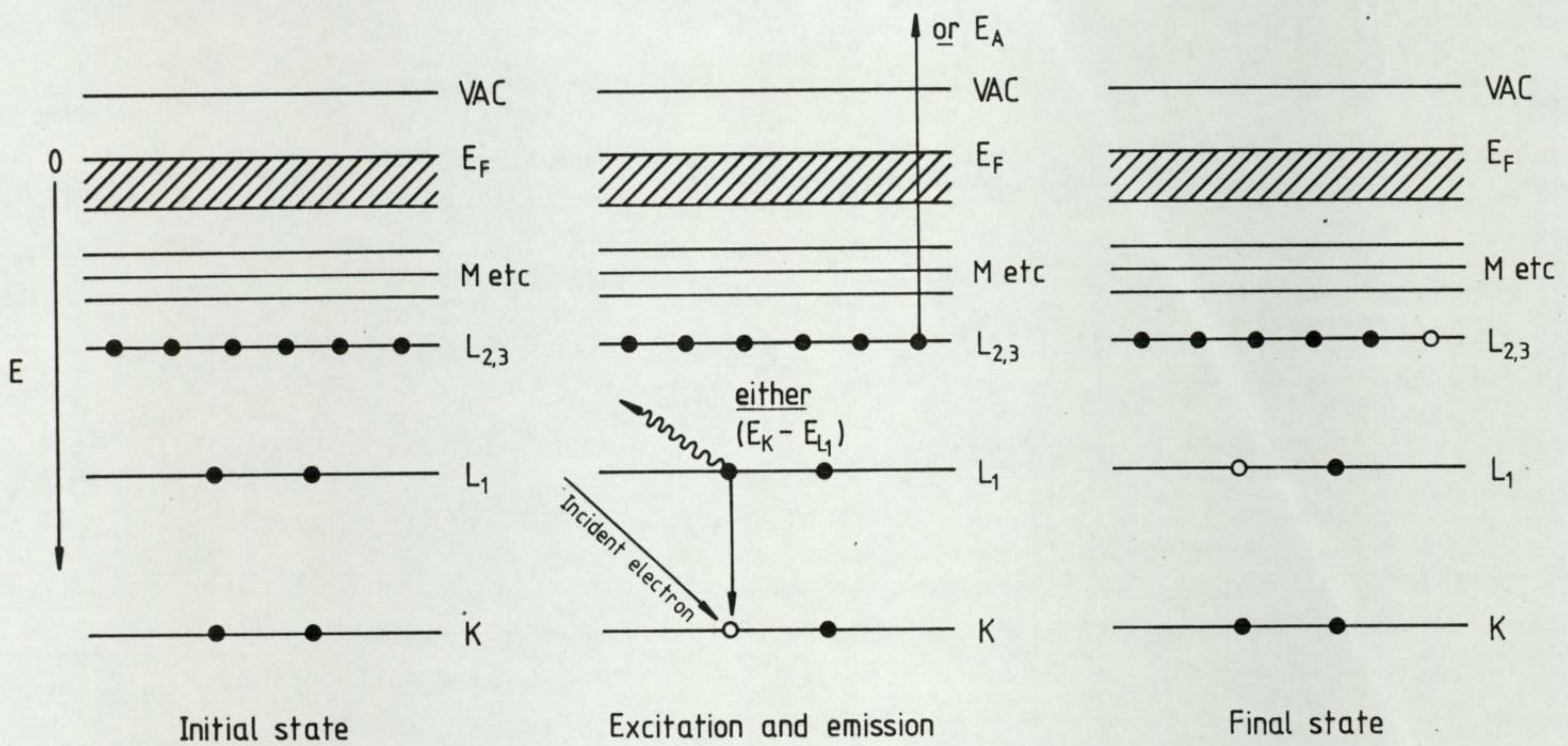

Figure 2·12. Schematic diagram showing the process of Auger emission in a solid.

33 (Arsenic).

In this particular example an electron from core level $L_{2,3}$ is ejected with energy $E_A = (E_K - E_{L1} - E_{L2,3})$ where $E_{L2,3}$ is the energy of level $L_{2,3}$ in the presence of the hole at core level L_1. The doubly ionised final state is shown on the right.

The Auger electrons thus have energies unique to each atom, allowing the identification of elements. All elements except Hydrogen and Helium yield Auger electrons within the 0 to 2000eV range. Low energy Auger electrons occurring with 0 to 1000eV range are especially important, as they escape only from the first few atomic layers, giving the Auger technique its unique surface sensitivity.

AES data can be interpreted by plotting the number of Auger electrons (N) against the kinetic energy (E), but because the Auger peaks are superimposed on a large continuous background and are difficult to detect, it is necessary to differentiate the energy distribution function N(E). Thus the more common informative plot of dN(E)/dE against (E) is obtained.

The relative positions of the peaks will then give the qualitative information required, whereas the actual peak-to-peak height of the Auger peaks will be related to the surface concentration of the elements they represent, but require the inclusion of sensitivity factors (163) characteristic to each element.

2.11.3. Depth Profiling

Depth profiles of chemical compositions can be obtained by use of ion milling. This is accomplished by bombarding the surface with ions accelerated in an ion gun to an energy greater than 200eV. A small fraction of the energy is transferred to surface atoms which cause them to be sputtered away.

The most frequently used ion guns are electrostatic devices where Argon gas ions are generated by collisional excitation with electrons from a hot filament. Argon ions are generally used beacuse they do not react with the bombardment surface and with hot filaments in the vacuum system. The positive ions are then accelerated and focused on the sample, creating a sputtering spot diameter of about 1 to 5mm diameter.

Sputtering is therefore a destructive method leaving the sample decomposed in an abraded part for subsurface elemental identification by AES. Sputtering can also be used to remove unwanted surface contaminants before examination.

2.11.4. AES Analysis of Amsler Test Specimens

Selected Amsler pitting disc specimens were examined using a Kratos XSAM 800 spectrometer incorporating a Hemispherical Analyser (HSA). A small surface area about 3 x 2 x 2mm was sectioned from the failed discs and ultrasonically cleaned in acetone, petroleum ether and again in acetone before it was placed in the specimen chamber and pumped down to a pressure of 10^{-9} Torr. The surface was then subject to an alternate AES and ion milling procedure to obtain an elemental concentration depth profile. Table 2.6 gives the machine operating conditions for AES and ion milling.

Depth profiling was carried out using Argon ions at cumulative etch times of 0; 1; 5; 15; 30; 60; 120; 180 and 240 minutes. Argon gas was introduced continuously throughout the analysis.

	Auger	Ion milling
Source voltage	5kV	2kV
Current in Specimen	0.4μA	20μA
Spot Size (diameter)	15μm	-
Mode (FRR)	5	-
Magnification	Hi	-
Region Scanned	100 - 1100eV	-
Increment	1eV	-
Scan Time	1000s	-

Table 2.6. Xsam machine operating conditions.

2.12. Analysis of Wear Debris

During some experimental runs it was noticed that the colour of the test lubricant had darkened to a much greater degree than normal. Collected debris was then analysed using powder X-ray diffraction (164). The method described is the one developed by Debye and Scherrer (165).

To separate the debris from the test lubricant, it was necessary first to centrifuge the solution and then evaporate the remainder by heating. After grinding, the debris was placed in a fine glass capillary tube and carefully fitted to the rotating spindle of a Phillips cylinderical powder camera designed for X-ray diffraction. Exposure of the film was 45 minutes using 40kV, 20mA cobolt Kα radiation, after which the film was developed and the subsequent diffraction pattern analysed.

CHAPTER THREE

RESULTS

3.1. Introduction

The results obtained from the work have been divided into seven sections, the first of which contains the data from the Unisteel and Rolling four-ball experiments. Results obtained from the experiments conducted using the Amsler 2-disc machine are given in the second section and the third and subsequent sections contain the information associated with the final analysis of the various failed test specimens.

3.2. Rolling Contact Fatigue Tests

3.2.1. Introduction and Interpretation of Results

Bearing lives, when subject to similar environmental conditions can differ by a great amount due mainly to the non-uniform structure between different steel specimens. This results in randomly distributed stress locations which ultimately lead to an inherent scatter of results obtained in such fatigue experiments. The standard analysis for such a spread of data is the Weibull (166),(167) statistical interpretation giving the bearing life as a cumulative percentage probability against time or cycles. From Equation 1.10 the probability of failure may be obtained by plotting the results on linear coordinates, however, Weibull coordinates (71) are available and are used to give a more direct analysis. The respective results obtained from each experiment are first sorted into ascending order and the plotting positions found from the following equation:

$$\text{Plotting Position} = \frac{i}{(n + 1)} \times 100\% \qquad 3.1$$

Where i is the number of the result in the sequence and n is the total number of results.

This equation has been found to give a better estimation for the population distribution when small samples are used (158).

Test lubricants in the rolling contact fatigue tests were evaluated by the L_{50} life, this being the life expected to be taken before 50% of the bearings fail.

3.2.2. Unisteel Results

In the Unisteel machine experiment eight results were obtained for each test lubricant and collated in ascending order. The respective plotting position for each of the eight results was determined by Equation 3.1 by substituting $i = 1...8$ and $n = 8$. Thus the plotting positions fall at: 11%, 22%, 33%, 44%, 55%, 66%, 77% and 88%. The results are given in Figure 3.1 and for clarity, the individual plotting positions are included in the first graph.

The L_{50} lives, extrapolated from individual Weibull graphs together with the fluid references are summarised in Table 3.1.

No L_{50} life value was obtained when the test lubricant consisted of deionised water with a trace of rust inhibitor (Test Lubricant A). It is believed that in this case the track suffers rapid wear which roughens it to the point at which the vibration cut-out is triggered at once.

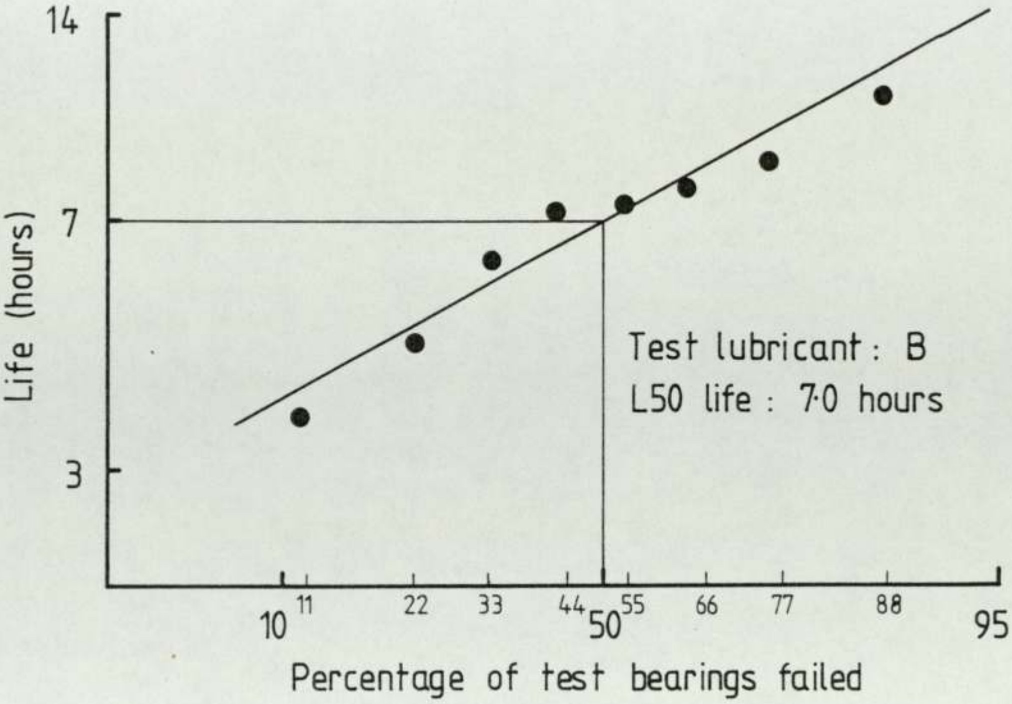

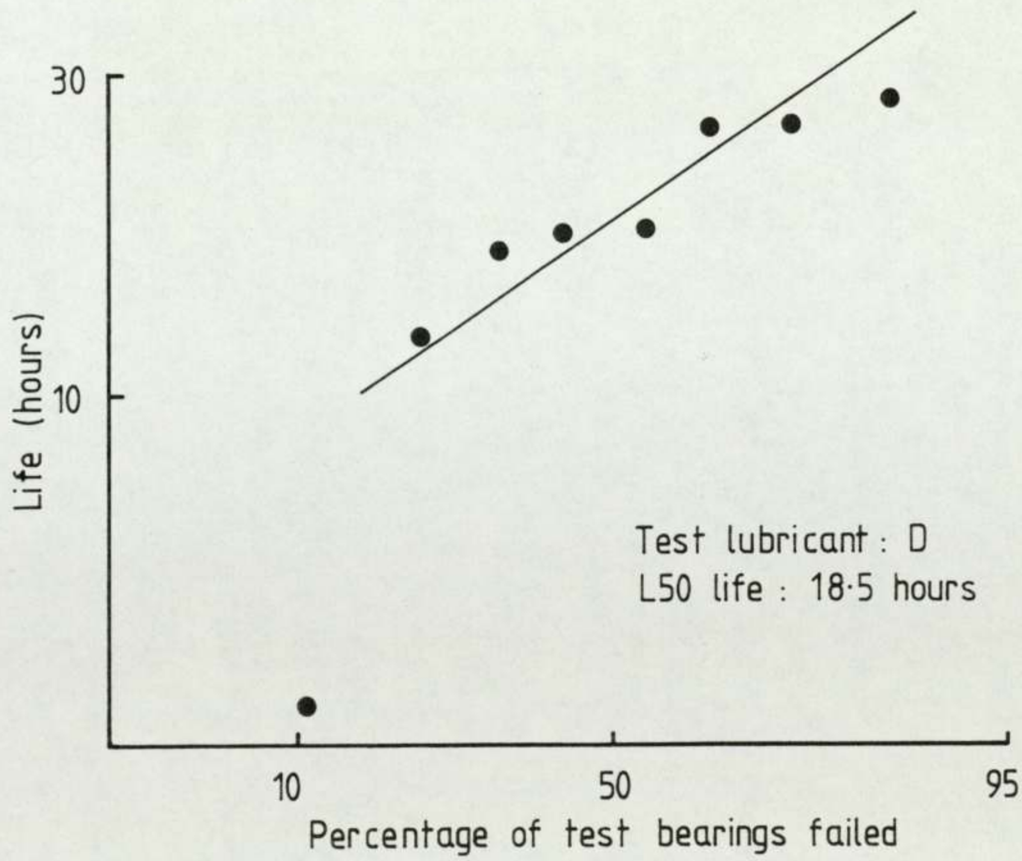

Figure 3·1. Results obtained from the Unisteel experiments.

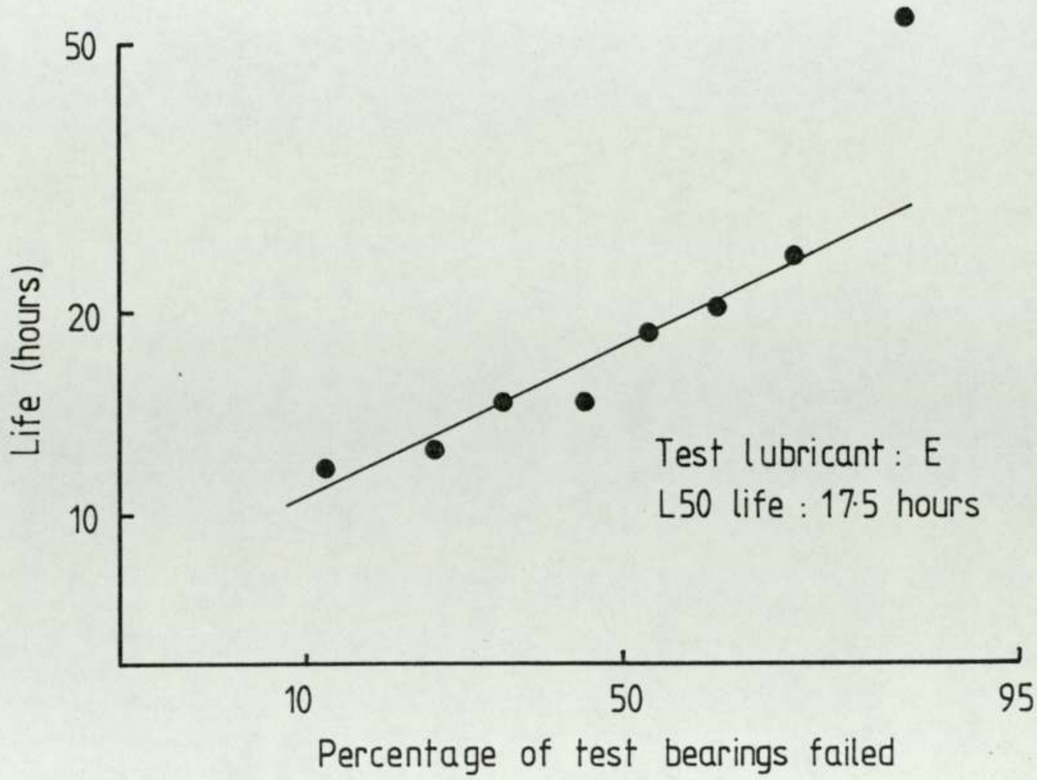

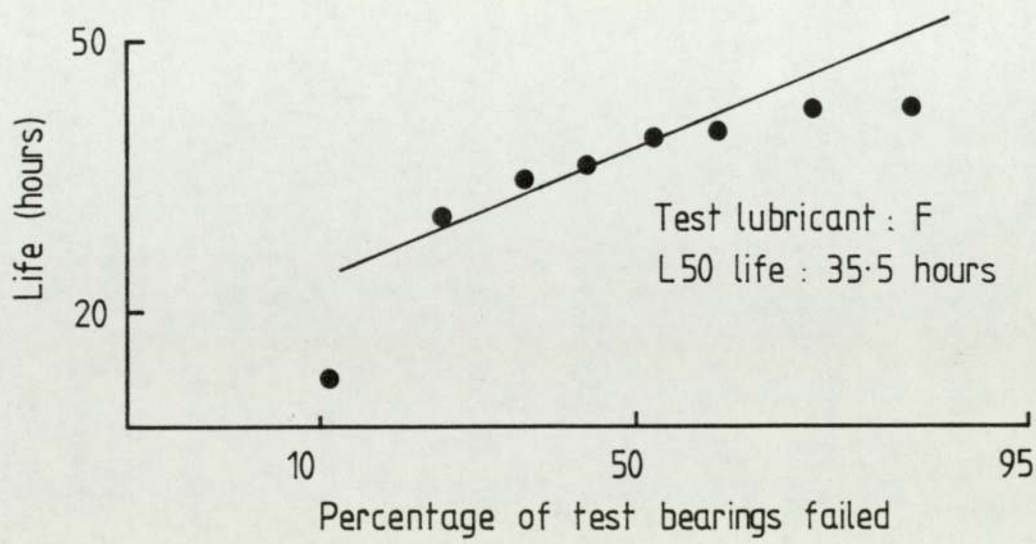

Figure 3·1(cont). Results obtained from the Unisteel experiments.

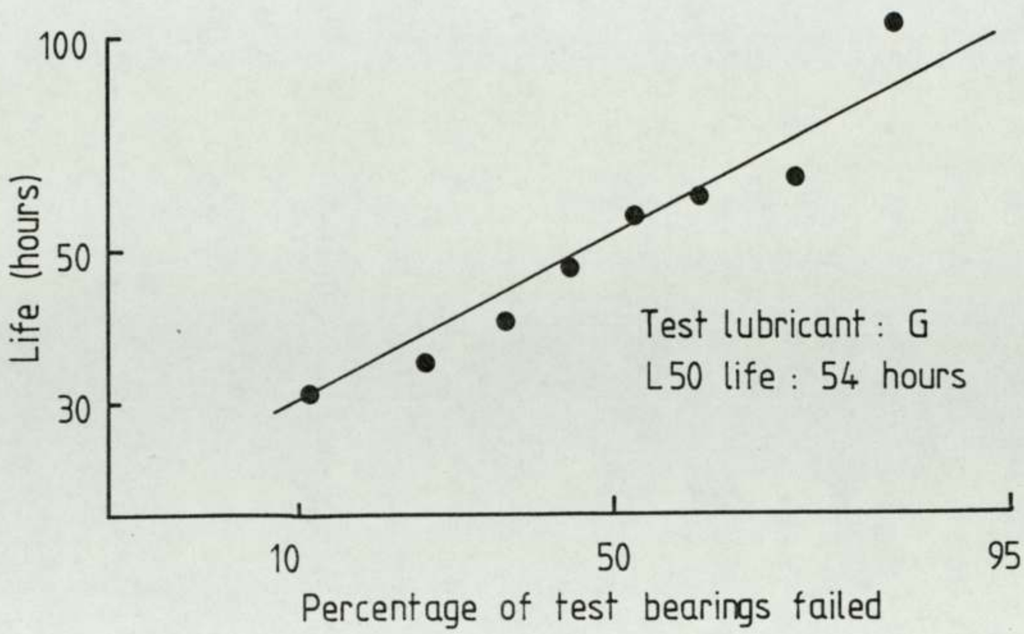

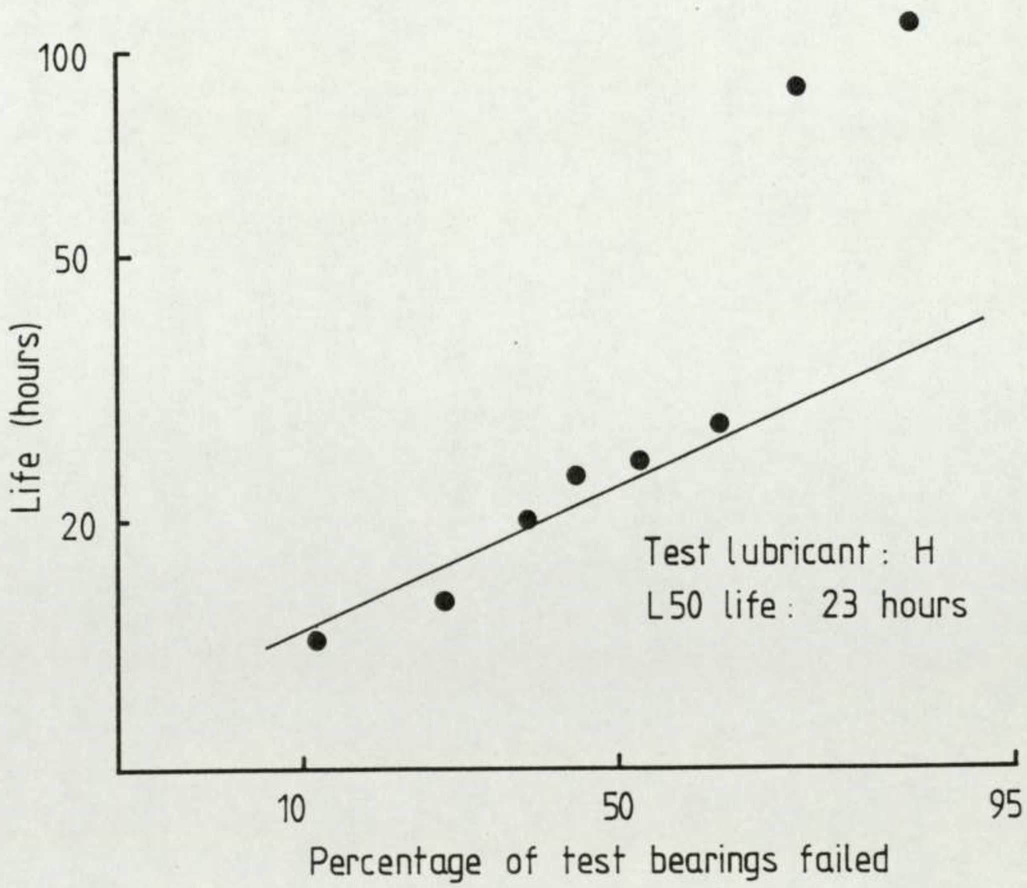

Figure 3·1(cont). Results obtained from the Unisteel experiments.

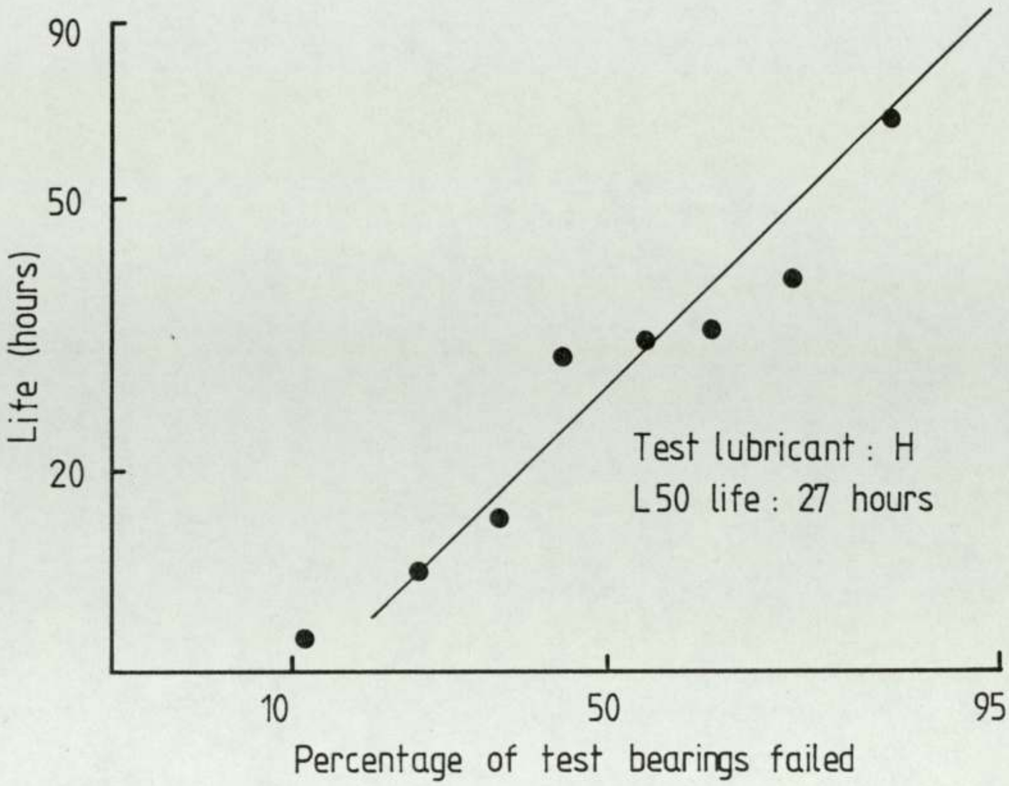

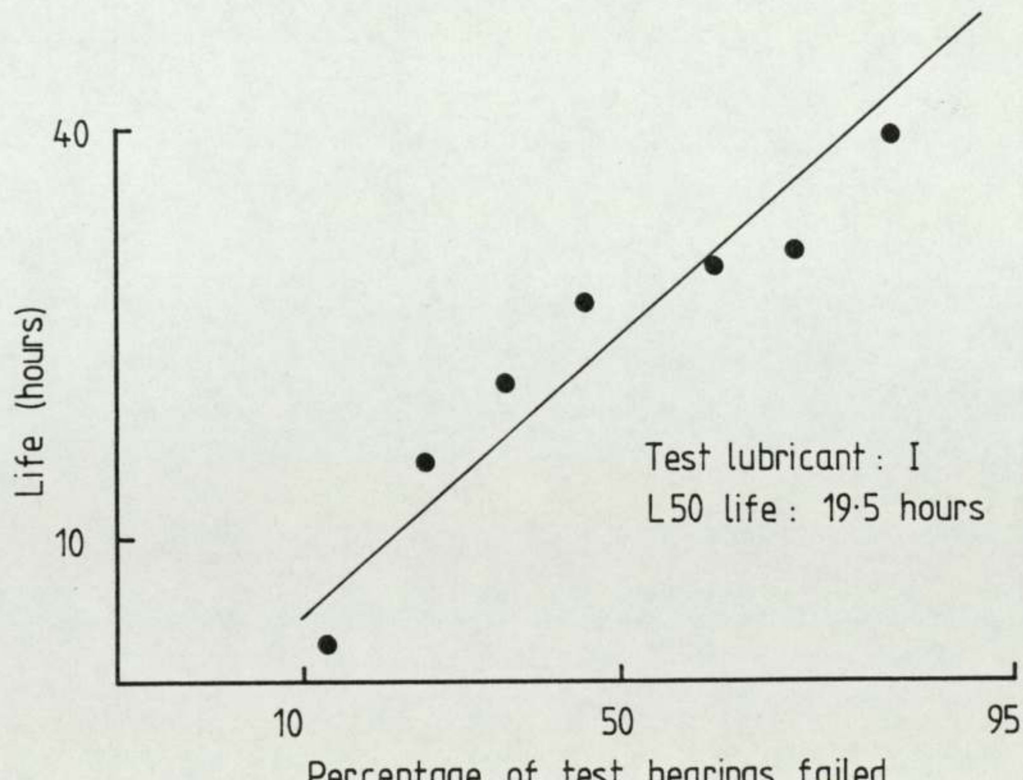

Figure 3·1(cont). Results obtained from the Unisteel experiments.

Test lubricant	L_{50} LIfe - Hours	
Viscosity @ 40°C	Without Additive	With Additive
0.6	- (A)	35.5 (F)
3.7	7.0 (B)	-
14.0	18.5 (D)	-
24.0	25.0 (H)	-
33.0	19.5 (I)	-
46.0	17.5 (E)	54.0 (G)

Table 3.1. Summary of the Unisteel L_{50} lives

Test Lubricant B containing propylene glycol allowed the experiment to be run giving an L_{50} life of 7 hours. It seems likely that the improvement in performance was due to the increase in viscosity from 0.6 to 3.7cSt. Further increase in viscosity was obtained by the addition of polymeric thickening agent with Test Lubricants D, I, H and E which gave L_{50} lives of 18.5, 19.5, 25 and 17.5 hours respectively. Thus there appears to be an optimum viscosity for bearing life as shown in Figure 3.2.

When decanoic acid antiwear additive was present in the aqueous mixture (Test Lubricant F) the effect was to raise the L_{50} life to 35.5 hours despite the low viscosity of 3.7cSt. This contrasts with the 7 hour life (Test Lubricant B) found when the antiwear additive was absent. When antiwear and viscosity additives were used together (Test Lubricant G) a double benefit was seen and the L_{50} life of 54 hours was the highest observed in the programme.

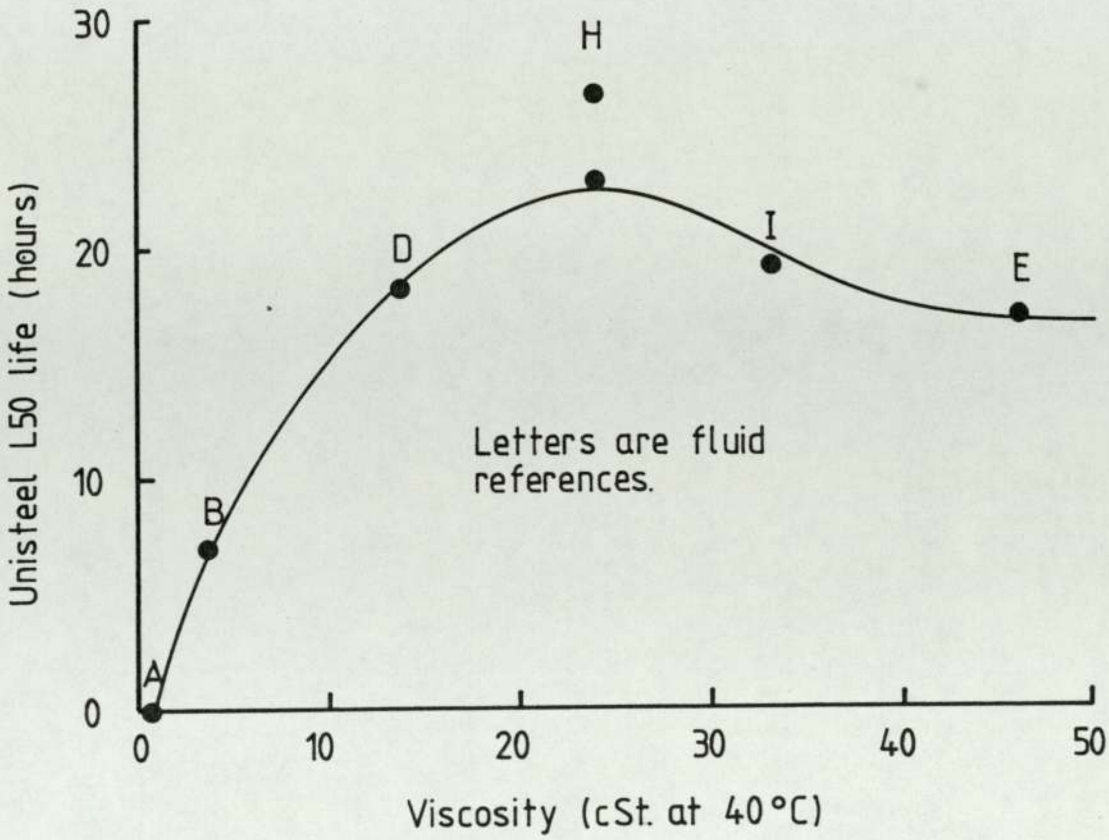

Figure 3·2. Unisteel L50 life against test lubricant viscosity.

3.2.3. Rolling Four-ball Results

In the Rolling four-ball test, ten results for each test lubricant were obtained and collated into ascending order. As before, the respective positions for each of the ten results were determined from Equation 3.1 on substitution of i = 1...10 and n = 10. Thus the plotting positions fall at: 9%, 18%, 27%, 36%, 45%, 54%, 63%, 72%, 81% and 90% and have been included in the first graph of the results in Figure 3.3. From Figure 3.3 a summary of the L_{50} lives together with the fluid references is given in Table 3.2.

The results form a well graduated series apart from the first test on deionised water. Thus Test Lubricant B (L_{50}

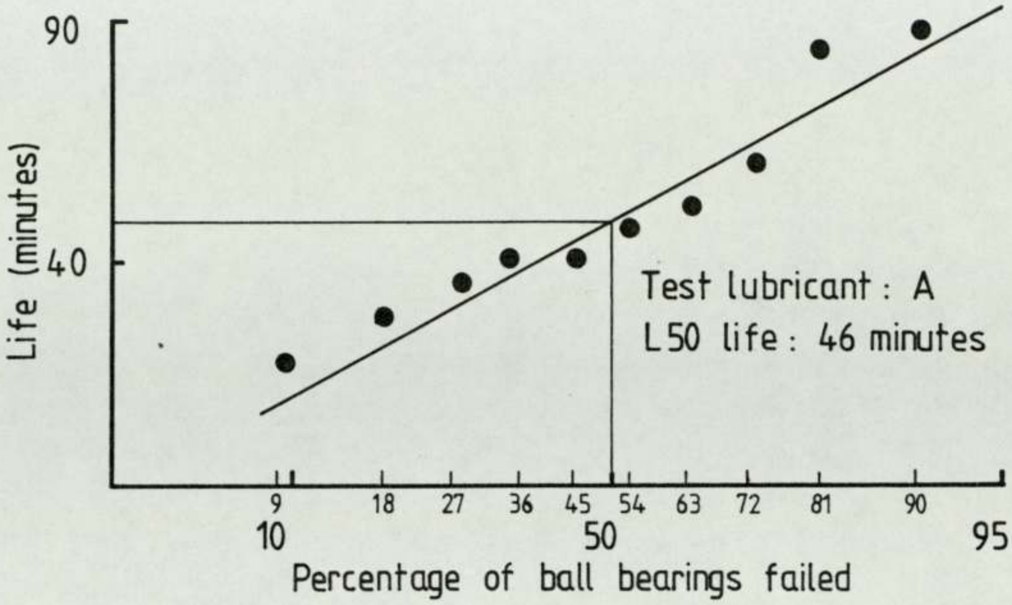

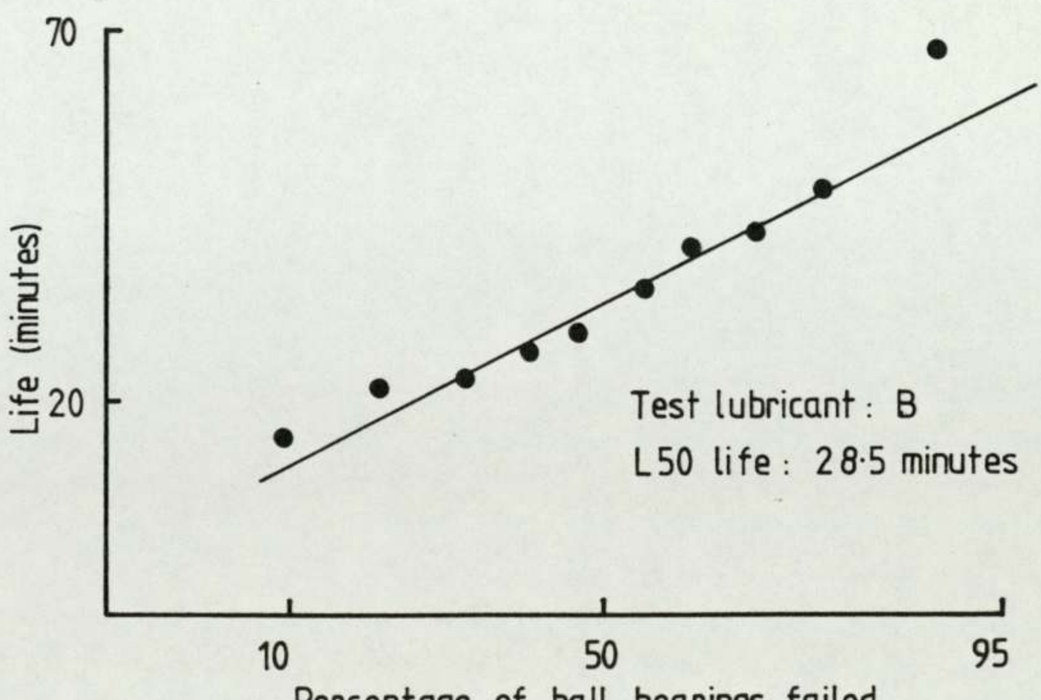

Figure 3·3. Results obtained from the Rolling Four Ball experiments.

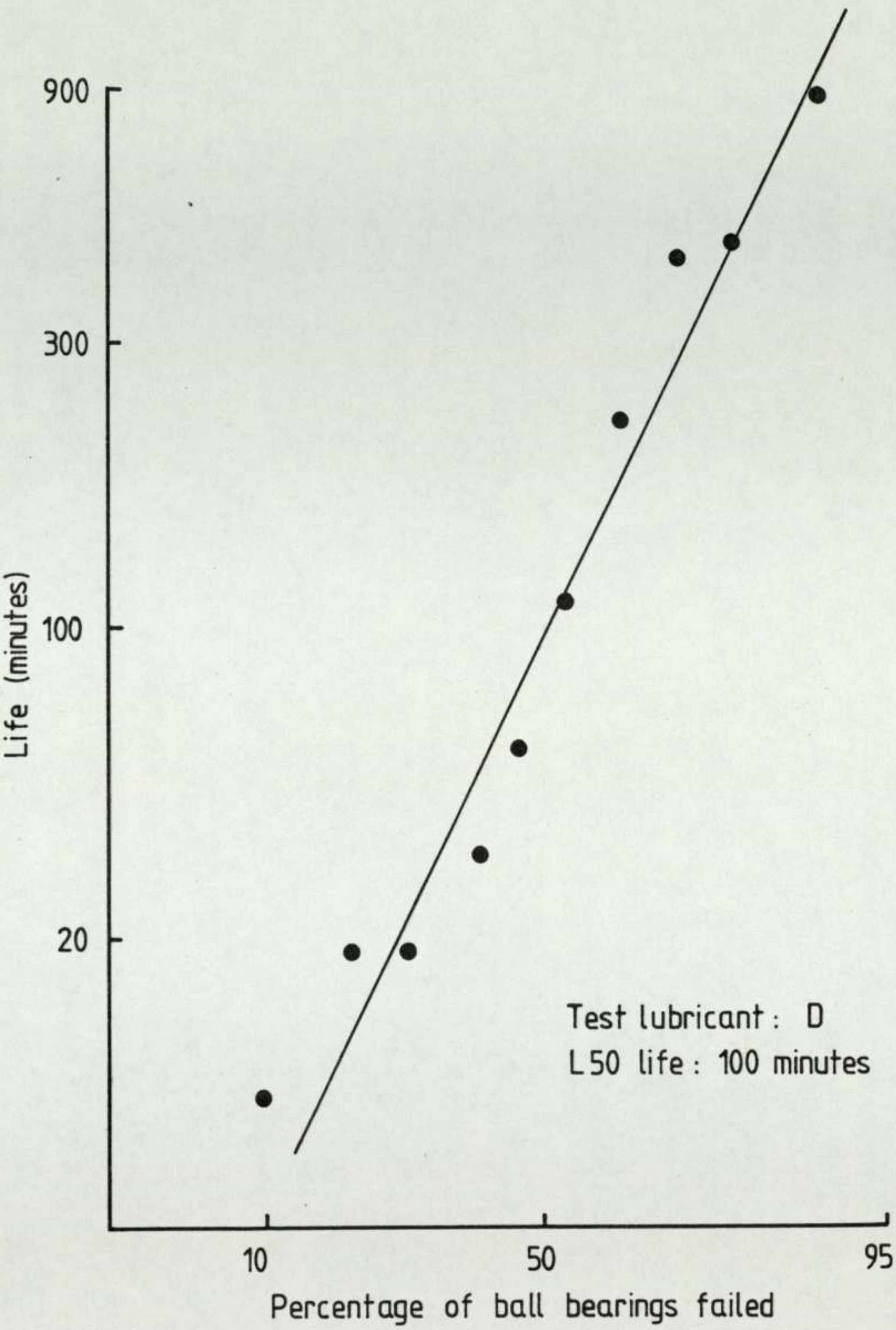

Figure 3·3(cont). Results obtained from the Rolling Four Ball experiments.

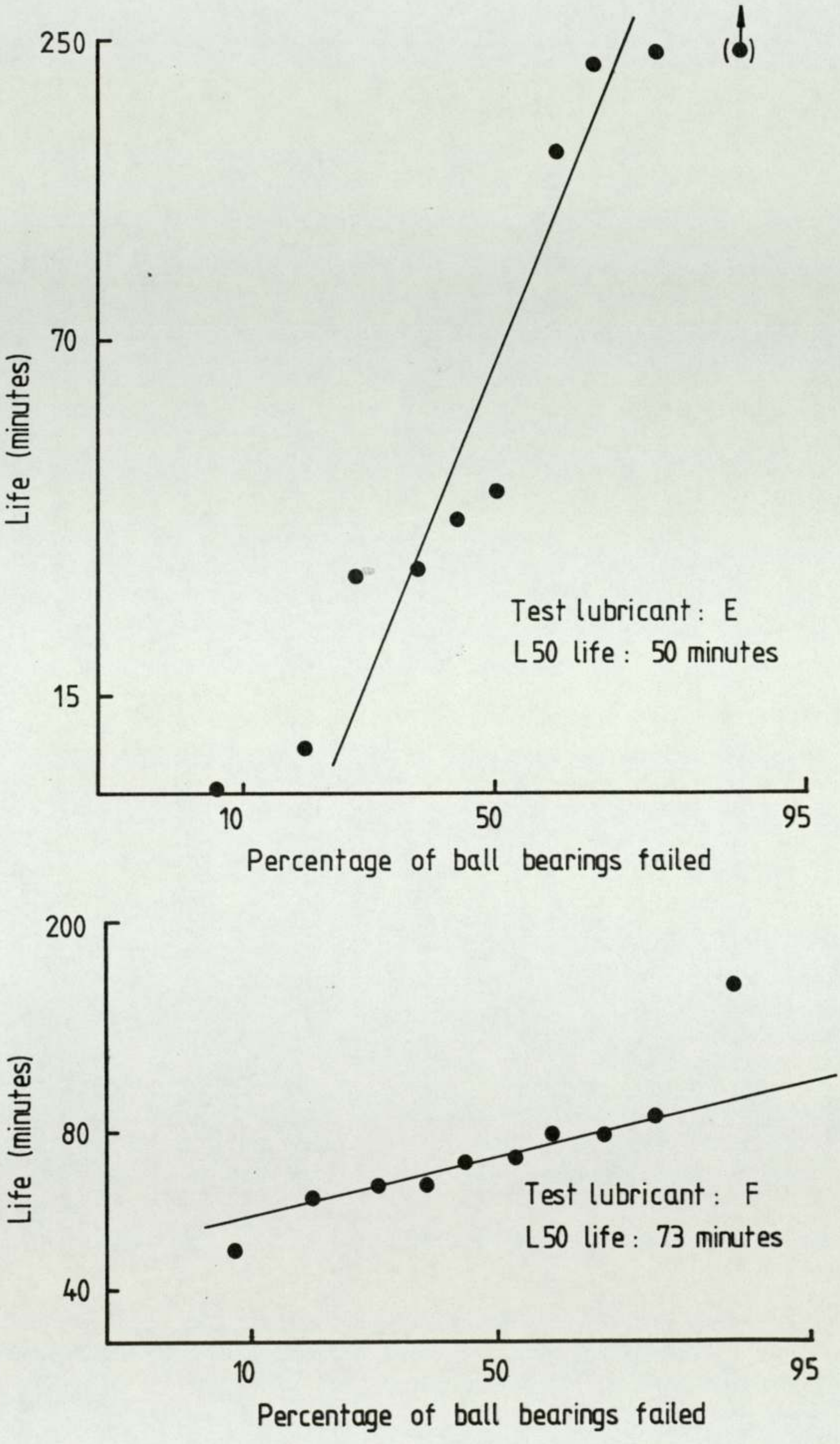

Figure 3·3(cont). Results obtained from the Rolling Four Ball experiments.

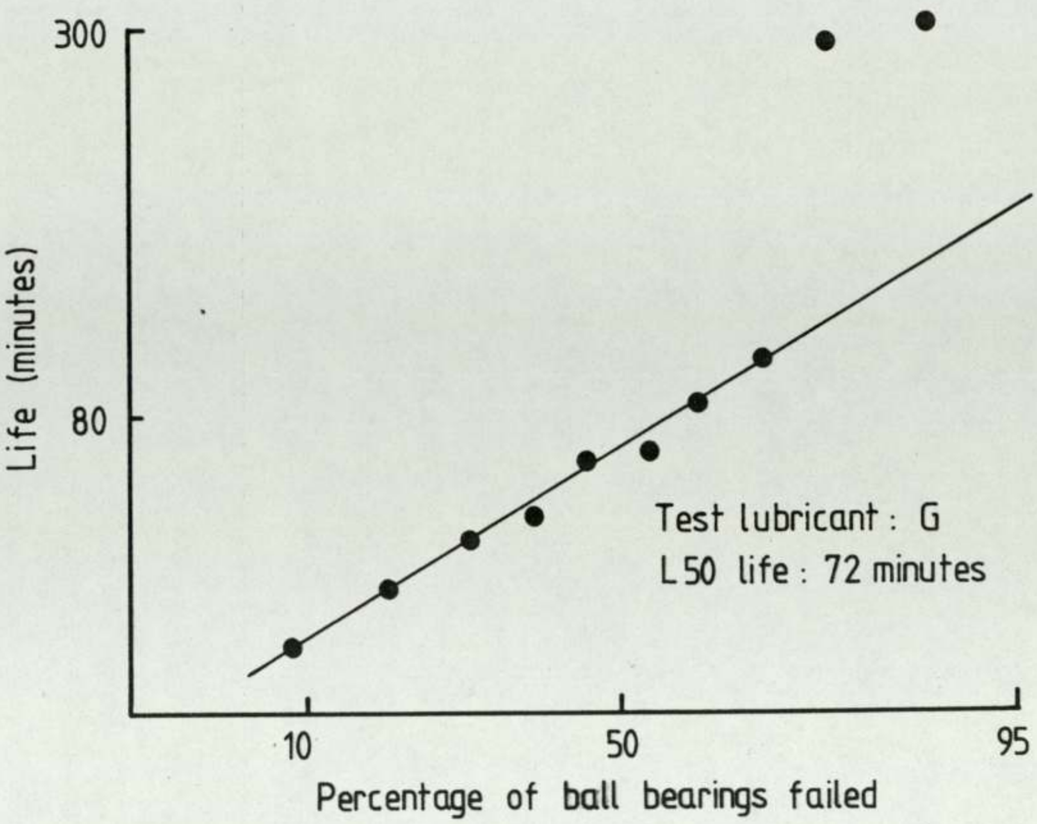

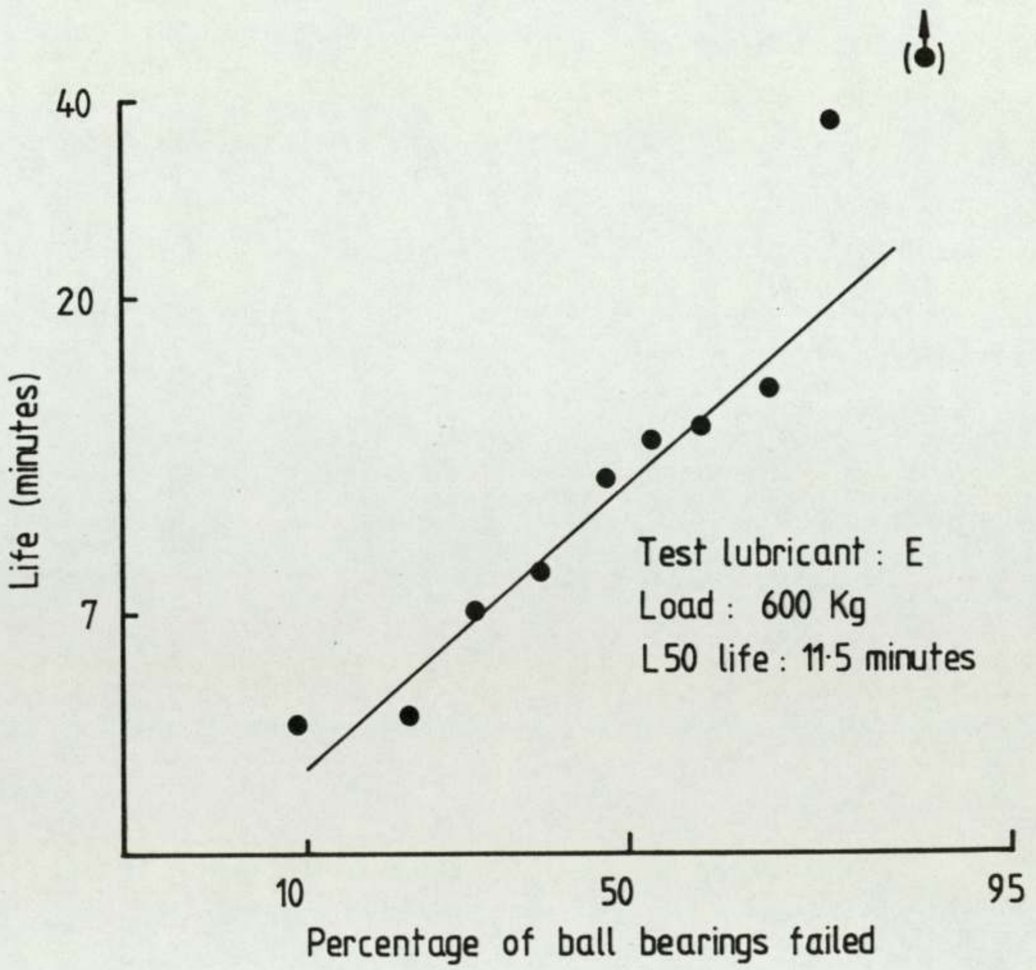

Figure 3·3(cont). Results obtained from the Rolling Four Ball experiments.

life 28.5 minutes) can be improved to 50 minutes by the addition of polymeric thickener (Test Lubricant E). However,

Test Lubricant	L_{50} Life - Minutes	
Viscosity @ 40°C	Without Additive	With Additive
0.6	46.0 (A)	-
3.7	28.5 (B)	73.0 (F)
14.0	100.0 (D)	-
46.0	50.0 (E)	72.0 (G)
46.0	11.5 (E) 600kg	-

Table 3.2. Summary of the Rolling four-ball L_{50} lives

the addition of the antiwear additive to Test Lubricant B was even more effective and the L_{50} life rose to 73 minutes (Test Lubricant F). When both antiwear and thickening additives were present (Test Lubricant G) the effect of the antiwear additive was dominant and the L_{50} life (72 minutes) was similar to that found for the low viscosity blend containing this additive (Test Lubricant F).

The Rolling four-ball result with deionised water was anomalous. Test Lubricant A gave an L_{50} life of 46 minutes which is greater than that observed for Test Lubricant B containing propylene glycol.

Test Lubricant E was evaluated again using a 600kg applied load which gave an L_{50} life of 11.5 minutes resulting in a 77% reduction in life for a 20% increase in load.

3.3. Amsler 2-disc Tests

3.3.1. The Stribeck Curve

To understand the various lubrication regimes associated with such a series of experiments it was necessary to plot a Stribeck curve. The subsequent plot of coefficient of friction against Bearing number is given in Figure 3.4 and clearly shows the main characteristic regions of lubrication. By convention the dimensionless parameter known as the Bearing number is used in Stribeck curves but in this investigation it was felt to be more informative to use calculated minimum fluid film thickness values in all subsequent plots (see Equation 1.9). Therefore the various phenomena associated with lubrication were expressed in terms of this parameter.

Since the load throughout the majority of the experiments was kept constant (90kg) it was possible to plot a graph of Bearing number against calculated fluid film thickness, and this is given in Figure 3.5. A best fit line was drawn, allowing the relationship between Bearing number and fluid film thickness to be obtained, and is described by the equation:

$$\text{Film thickness}(\mu m) = 3.68 \times 10^{-5}(\text{Bearing number})^{0.7} \qquad 3.2$$

with a correlation coefficient of 0.99.

Equation 3.2 was then used to enable a direct comparison between the Bearing number of the Stribeck curve and that of the fluid film thickness developed between the discs for the Amsler 2-disc system when run under constant pressure.

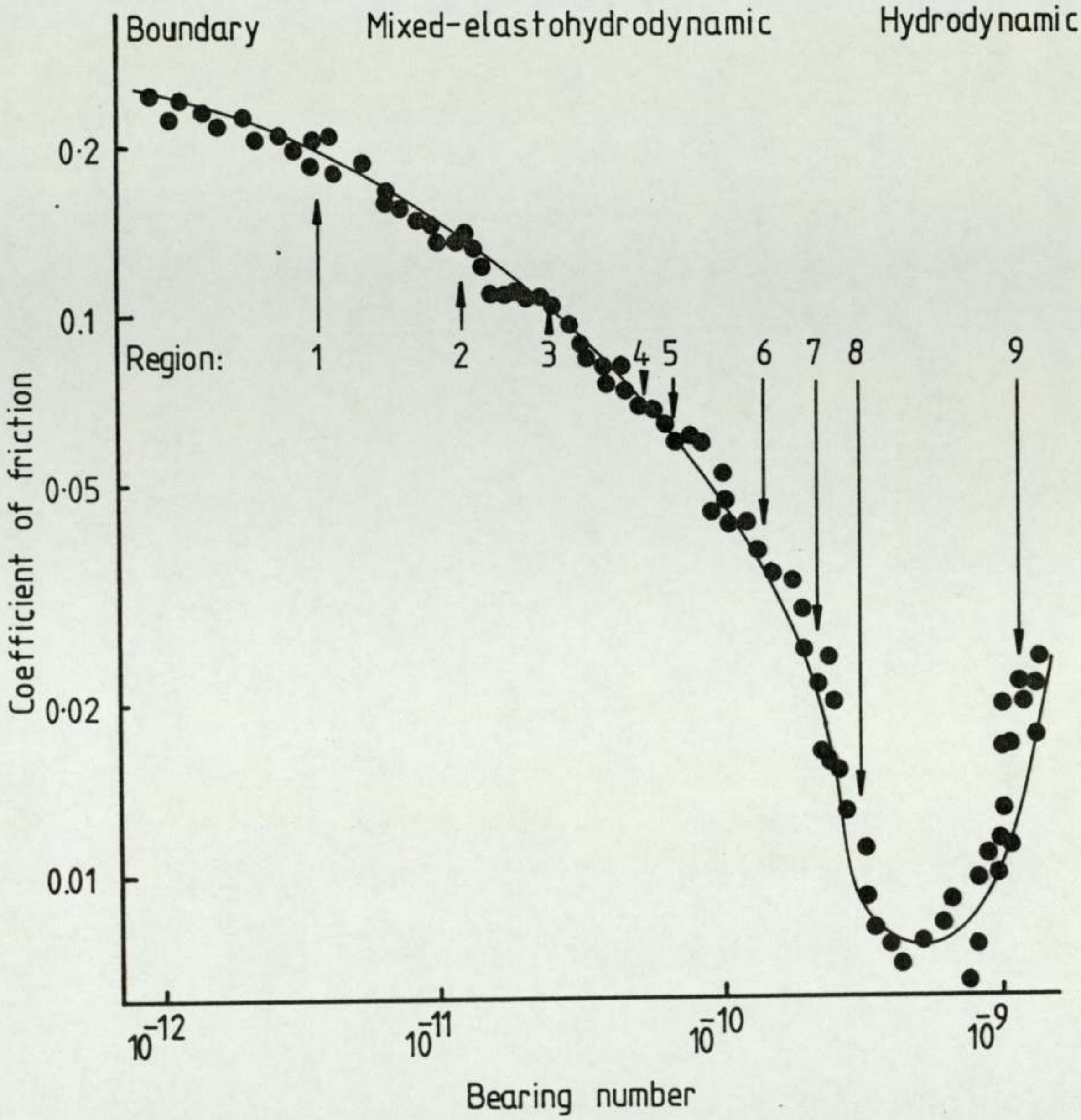

Figure 3·4. Stribeck curve plotted for the Amsler 2-disc experiments.

3.3.2. Friction and Torque

Torque and indirectly friction (Equation 2.1) was monitored continuously throughout each experiment by a load dynamometer and diagram recorder. Figure 3.6 shows torque profiles taken at lubrication regions 1, 4a and 8 respectively. The torque profiles presented are

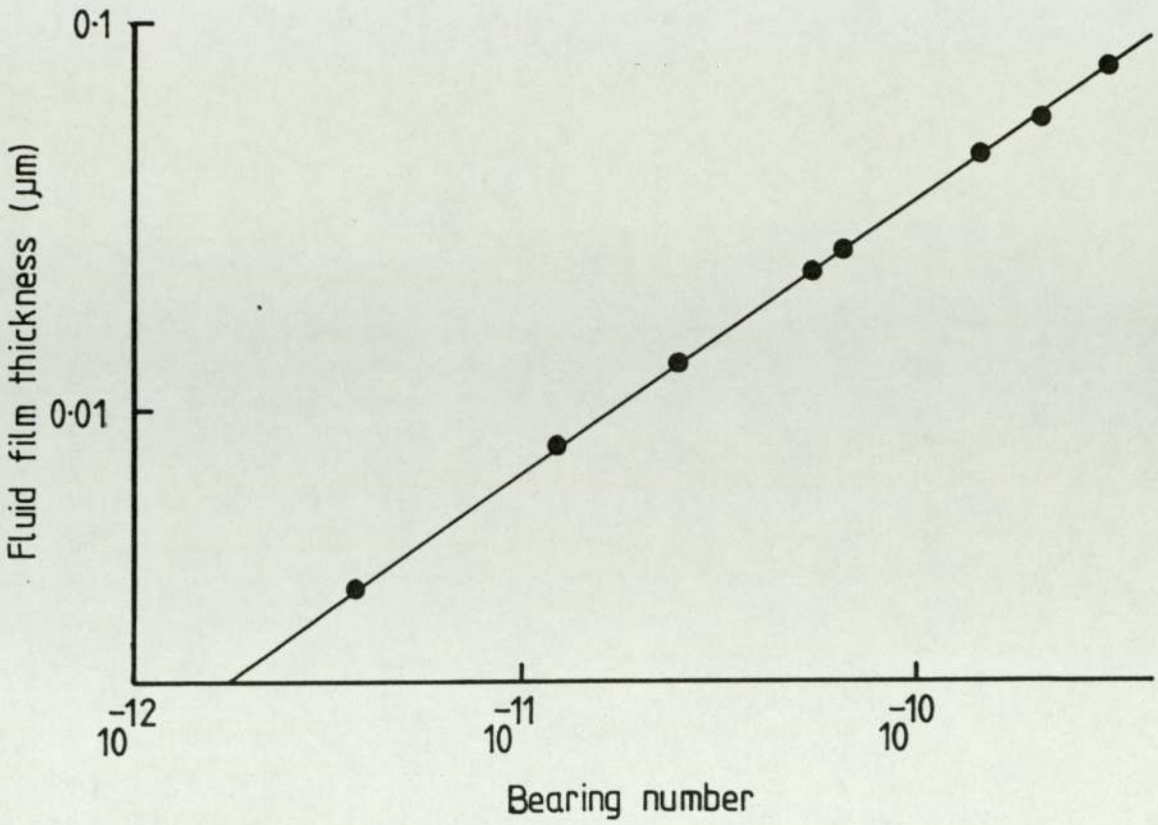

Figure 3·5. Fluid film thickness against bearing number.

representative of the three different types obtained.

Figure 3.6a) was typiacl of experiments conducted at boundary region 1 and hydrodynamic region 9 in that the torque remained constant throughout the duration of the test. The actual value of torque, however, was very much less for experiments conducted in the hydrodynamic region. Figure 3.6b) was typical of experiments conducted at Lubrication Regions 2, 3, 4 and 5 while Figure 3.6c) was typical of Lubrication Regions 6, 7 and 8.

For discs run near the boundary region (2 to 5) an initial steady state was observed, but diminished to a lower value after a certain period. Discs run near the hydrodynamic

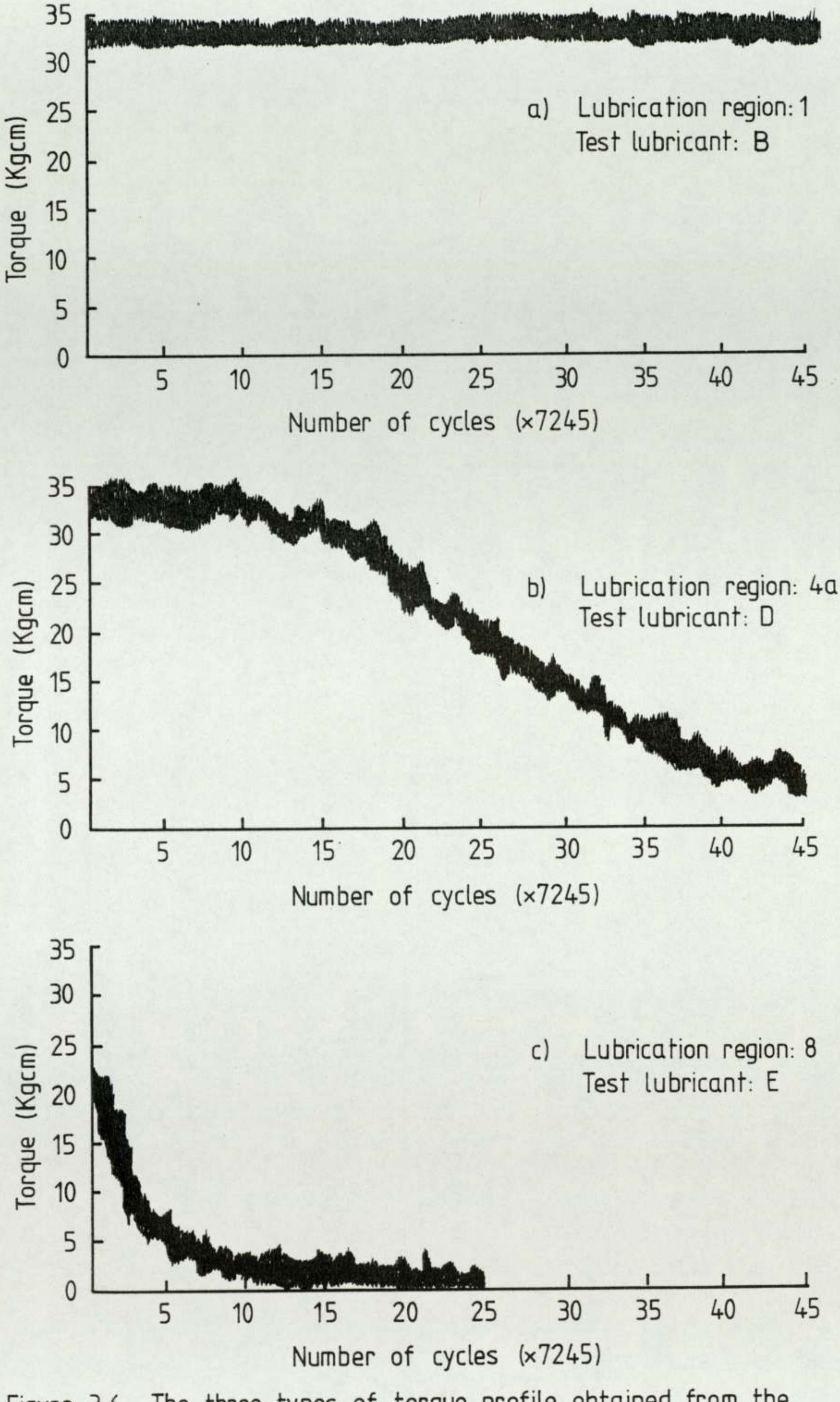

Figure 3·6. The three types of torque profile obtained from the Amsler 2-Disc experiments.

region (6 to 8) did not posses this initial steady state period and immediately decreased to a lower value. When experiments were conducted using the antiwear additive, no change to the general trend of torque profiles was observed, however, the additive did have an effect such that the initial torque value remained constant for longer in the second type of profile (Figure 3.6b)) and yielded a smoother slope in the last type of profile (Figure 3.6c)). It is believed that some asperity protection was taking place.

The minimum or final torque value, termed Nt, taken when the disc first pits, has been plotted against fluid film thickness. Figure 3.7 gives the resultant plot of Nt for test lubricants not containing the antiwear additive. The equation for the line is described by:

$$\text{Torque(kgcm)} = -21.41 \times \log(\text{Film thickness}(\mu\text{m})) - 24.63 \qquad 3.3$$

with a correlation coefficient of -0.98.

It can be seen that final torque decreases with increase in fluid film thickness and can be related to asperity contact and surface smoothing. For test lubricants containing the antiwear additive a different relationship was observed as shown in Figure 3.8. Apart from those experiments conducted under boundary conditions of lubrication, the final torque remained independent of fluid film thickness. Again, this shows the protective nature of the antiwear additive.

3.3.3. Wear Rates - Calculated by LVDT Transducer

Wear rates were carefully monitored at each of the lubrication regions by two independent methods. The first

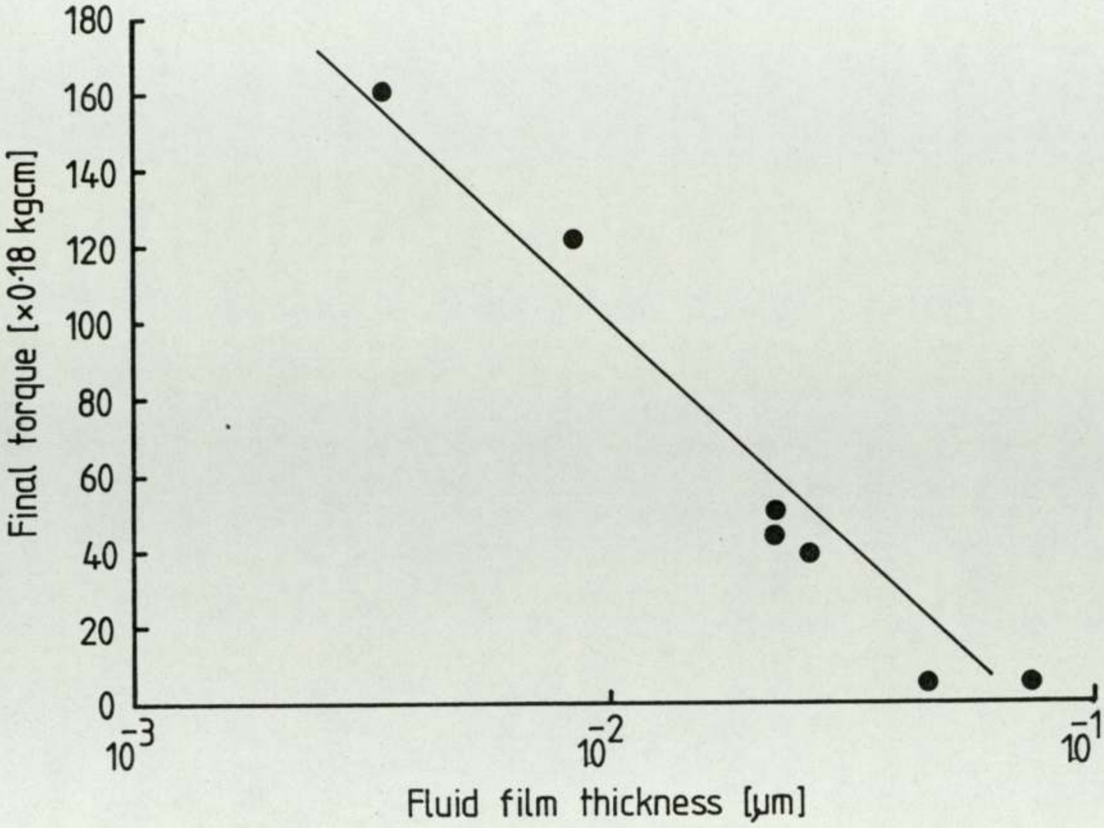

Figure 3·7. Final torque [Nt] against fluid film thickness for lubricants without the antiwear additive.

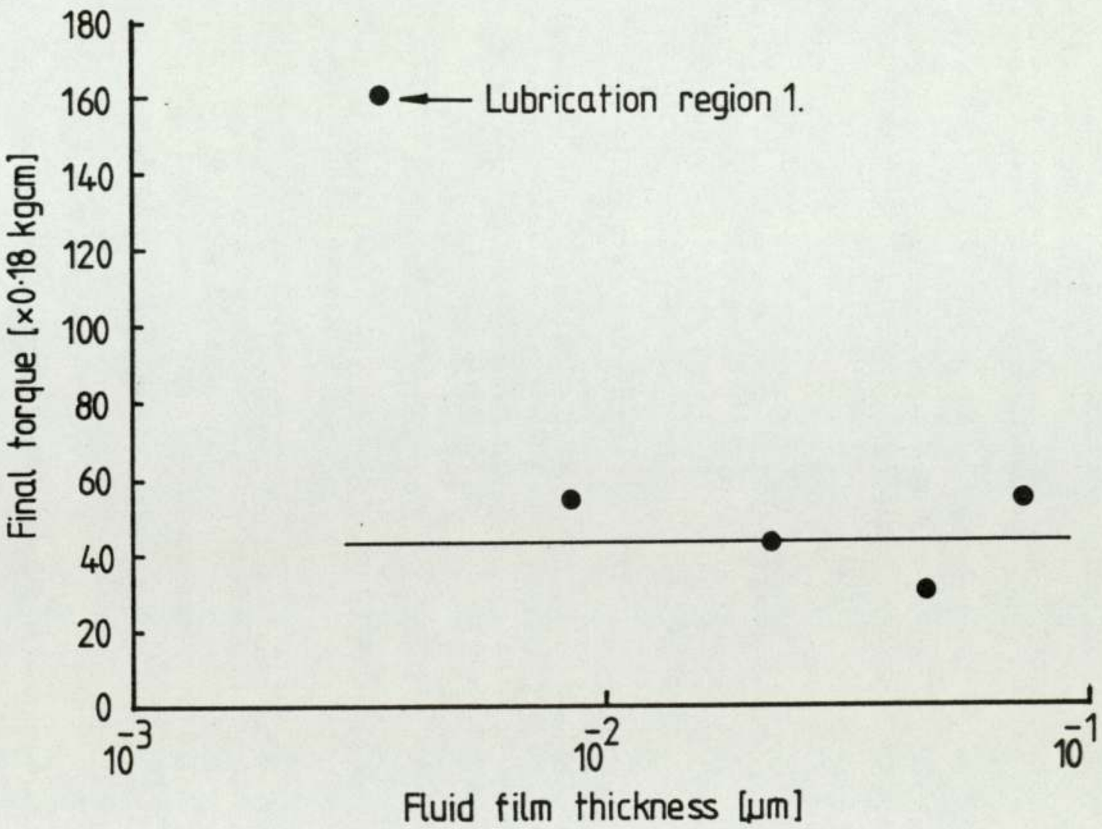

Figure 3·8. Final torque [Nt] against fluid film thickness for lubricants with the antiwear additive.

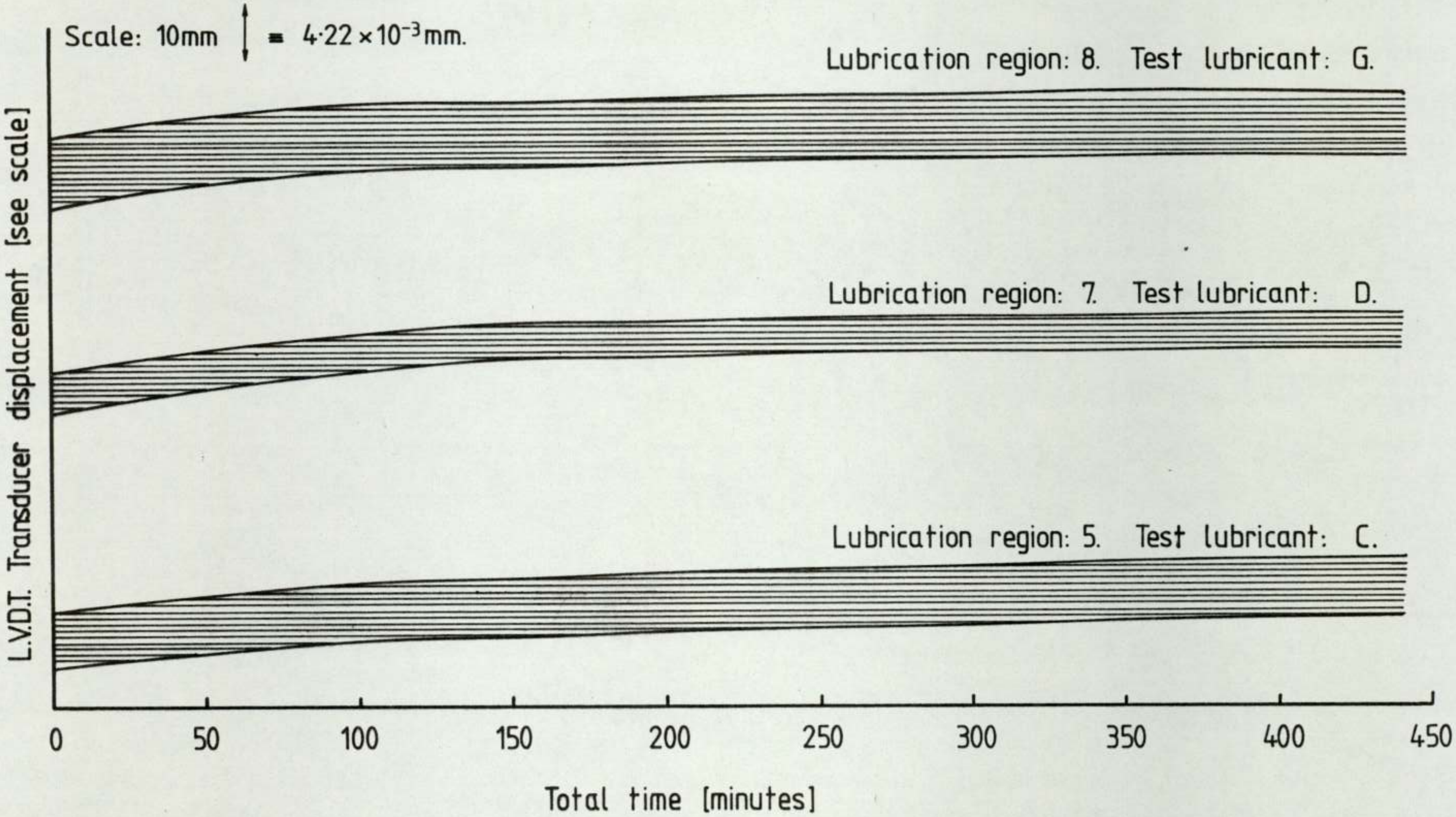

Figure 3·9 Typical examples of L.V.D.T. transducer displacement traces taken from three regions of lubrication.

made use of an LVDT transducer placed tangentially on the upper pitting discs housing. Three typical LVDT displacement traces taken from Lubrication Regions 5, 7 and 8 are shown in Figure 3.9.

All wear displacement traces apart from those obtained from experiments conducted in the hydrodynamic region 9 exhibited an initial sharp increase in displacement, termed the "settle period" after which a gradual increase in displacement was observed. For experiments run in the hydrodynamic region no initial settle period was present.

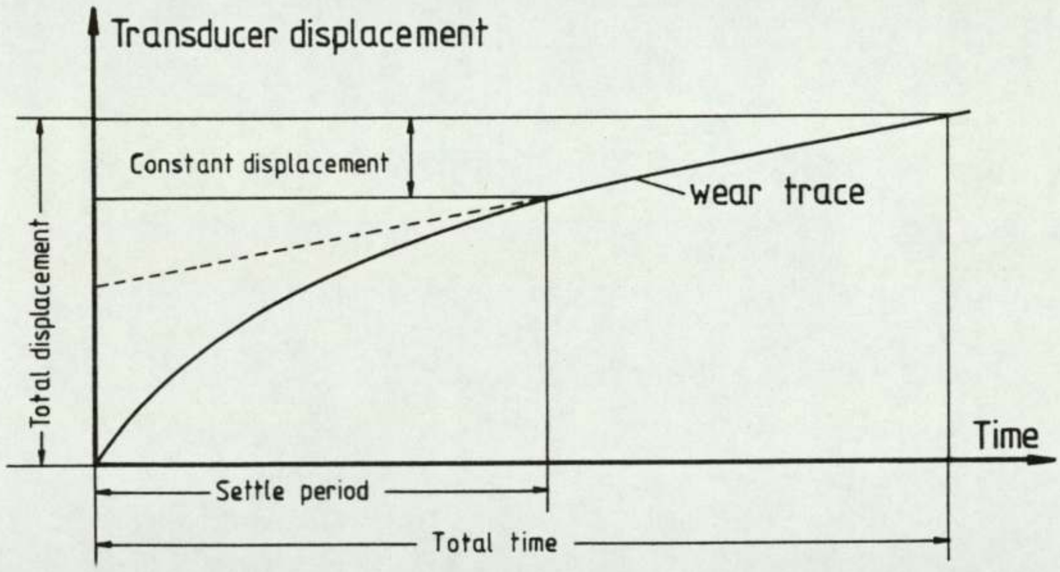

Figure 3·10. Interpretation of the L.V.D.T. transducer displacement traces.

Since no additional information could be gained by the re-alignment of the recorder pen after the successive shut down procedures of the machine, displacement traces were monitored up to the formation of the first detectable crack. The total displacement was then calculated by first determining the total time taken for both (i) the settle period as defined in Figure 3.10 and (ii) a constant transducer displacement of 2.53×10^{-2}mm, which was achieved by nearly all of the discs. For those few experiments which had very short crack initiation periods and hence could not obtain the full constant displacement, an estimated time was used.

The volume of material removed by the wear process (taking into consideration the 45° chamfer on the pitting disc) is given by:

$$\text{Volume removed } (m^3) = 4\pi \int_B^A Y(Y_0 - Y)\, dY \qquad 3.4$$

where A is the original radius of the disc in metres,
B is the new radius after the experiment in metres (B = A - Total displacement) and
Y_0 = A + (Initial track width x Tan 45°)/2.

The total distance rotated was calculated from:

$$\text{Total distance(m)} = \text{Speed(rpm)} \times \text{Total time(mins)} \times 2\pi R \qquad 3.5$$

where R is the average radius of the disc in metres
(R = A - (Total displacement)/2.

The LVDT transducer measures the relative displacement of the upper pitting disc housing which is twice the value required in Equation 3.4.

The wear rates (expressed as the volume of material removed per unit distance rotated m^3m^{-1}) for all experiments conducted at each lubrication region were averaged and plotted against fluid film thickness as shown in Figure 3.11.

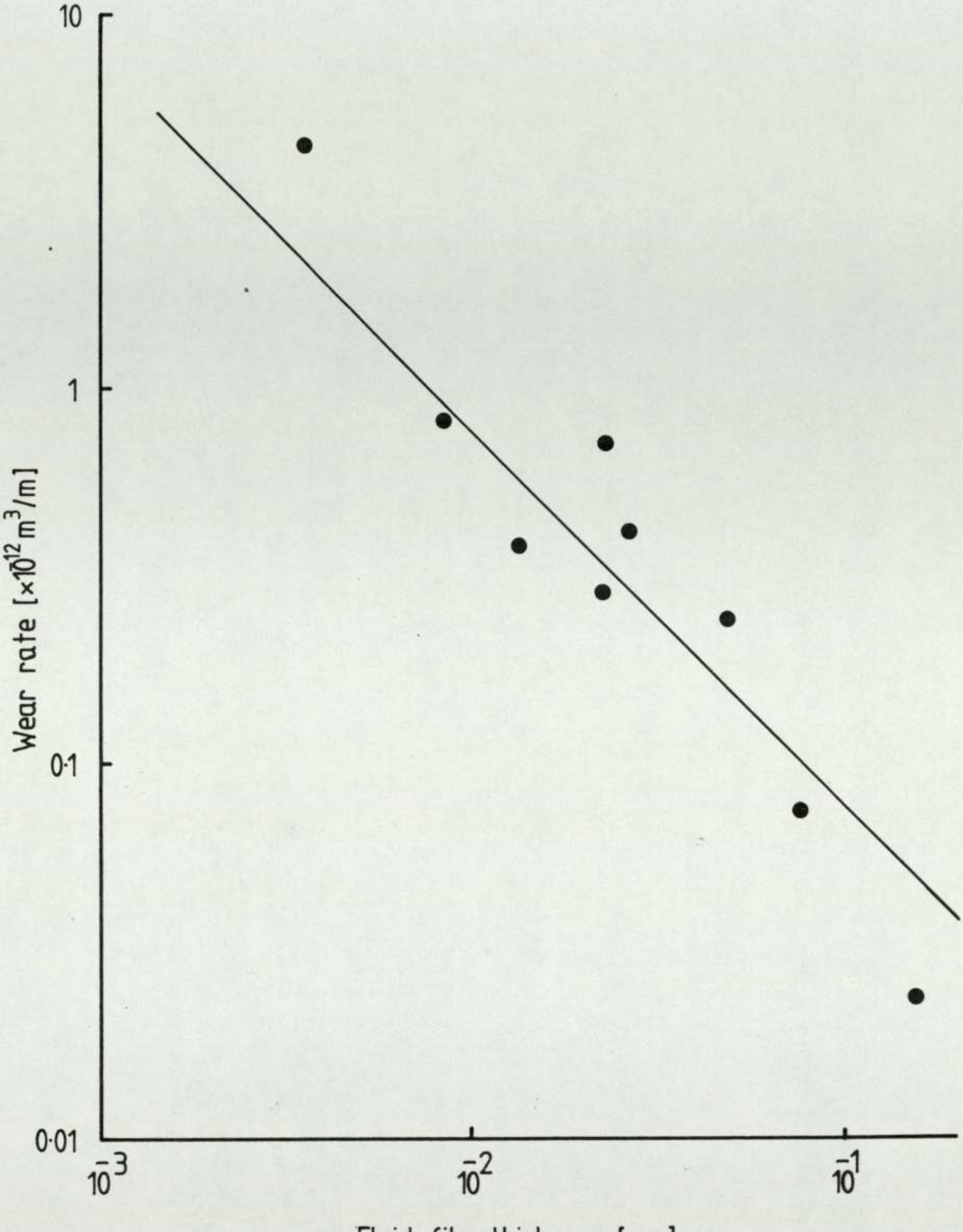

Figure 3·11. Pitting disc wear rate against fluid film thickness for test lubricants without the antiwear additive (calculated by L.V.D.T. transducer).

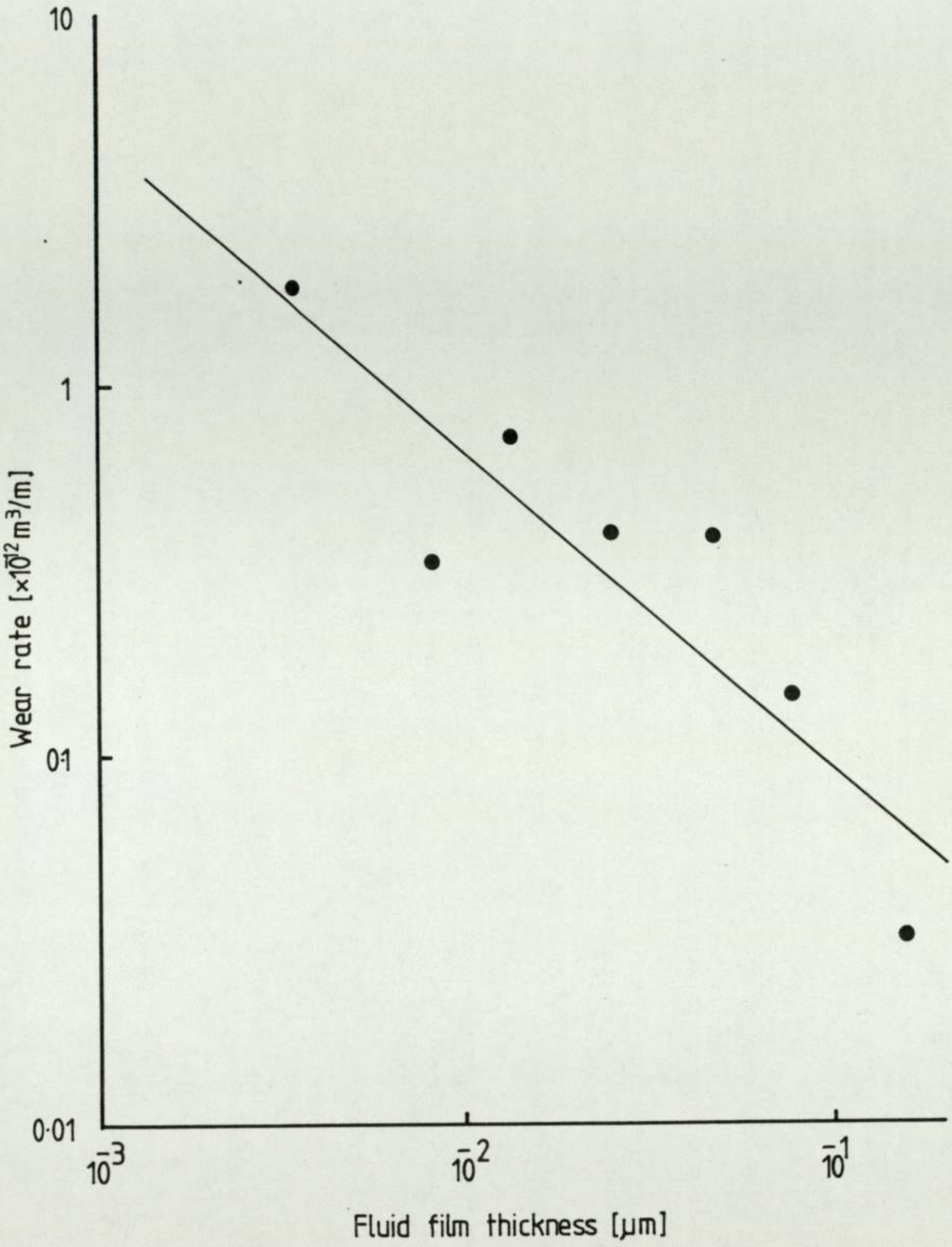

Figure 3·12. Pitting disc wear rate against fluid film thickness for test lubricants with the antiwear additive (calculated by L.V.D.T. transducer).

The equation of this line is described by:

$$\text{Wear rate}(m^3m^{-1}) = 7.5 \times 10^{-15}(\text{Film thickness } \mu m)^{-1} \quad 3.6$$

for test lubricants without the antiwear additive.

Figure 3.12 gives the plot of wear rate against fluid film thickness for experiments conducted with the antiwear additive. The equation of this line is described by:

$$\text{Wear rate}(m^3m^{-1}) = 1.3 \times 10^{-14}(\text{Film thickness } \mu m)^{-0.86} \quad 3.7$$

This relationship might be expected since the degree of asperity interaction will increase with decrease in fluid film thickness. It is interesting to note that the additive appears to be pro-wear under less severe conditions of lubrication, and only begins to exhibit its antiwear effect in the mixed region, tending towards boundary lubrication.

3.3.4. Wear rates - Calculated by Weight Loss

The amount of wear was obtained for both the pitting and driving discs by measuring the change in weight of the respective discs before and after each run. Wear rate, expressed as the volume of material per unit distance rotated was calculated from the equation:

$$\text{Wear rate}(m^3m^{-1}) = Wl/(\pi DN\rho) \quad 3.8$$

where Wl is the weight lost (kg),

D the diameter of the disc (m),

N the number of cycles rotated and

ρ the density of the material (kgm^{-3}).

Individual wear rates obtained at each lubrication

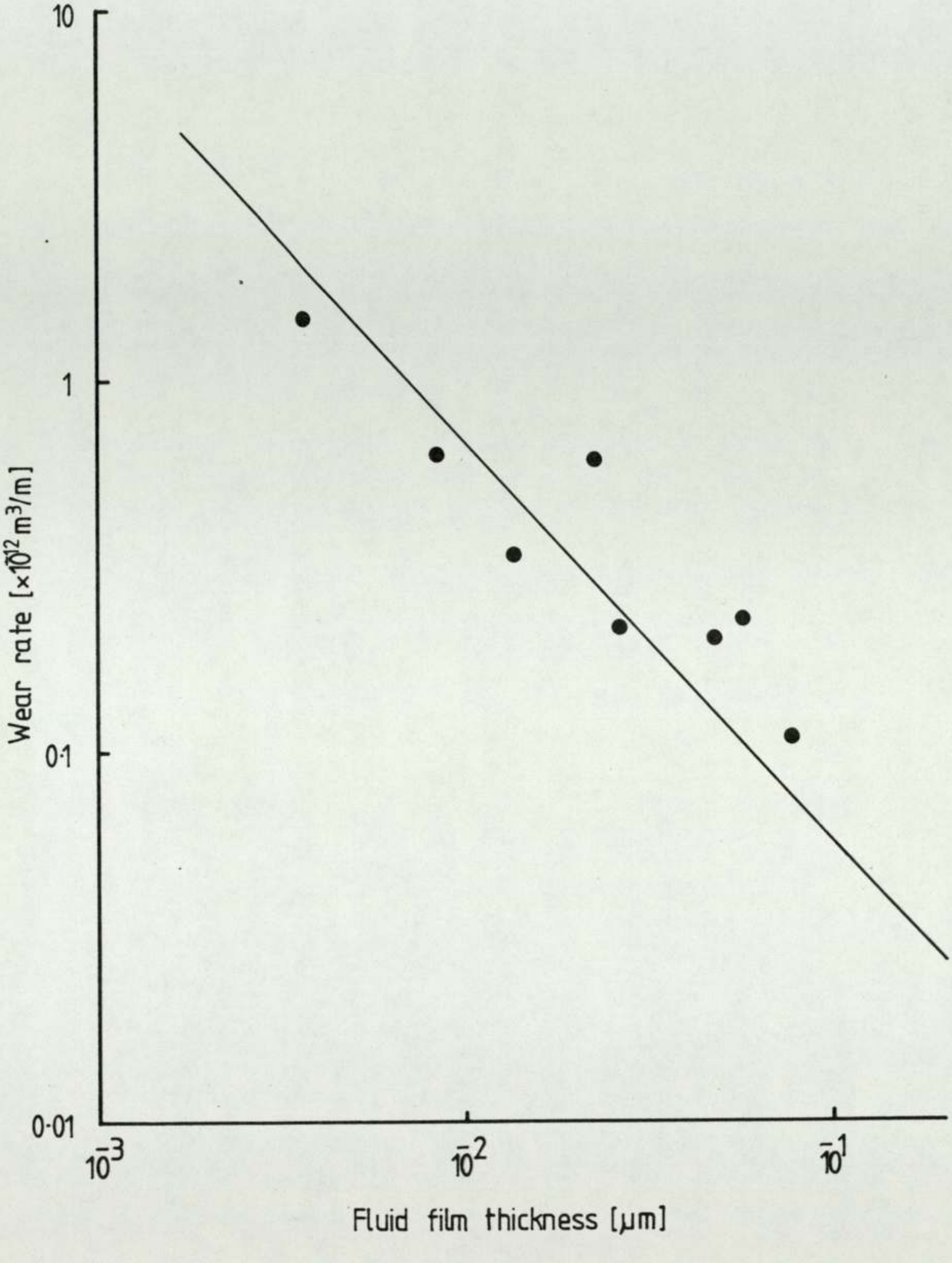

Figure 3·13. Pitting disc wear rate against fluid film thickness for test lubricants without the antiwear additive (calculated by weight loss).

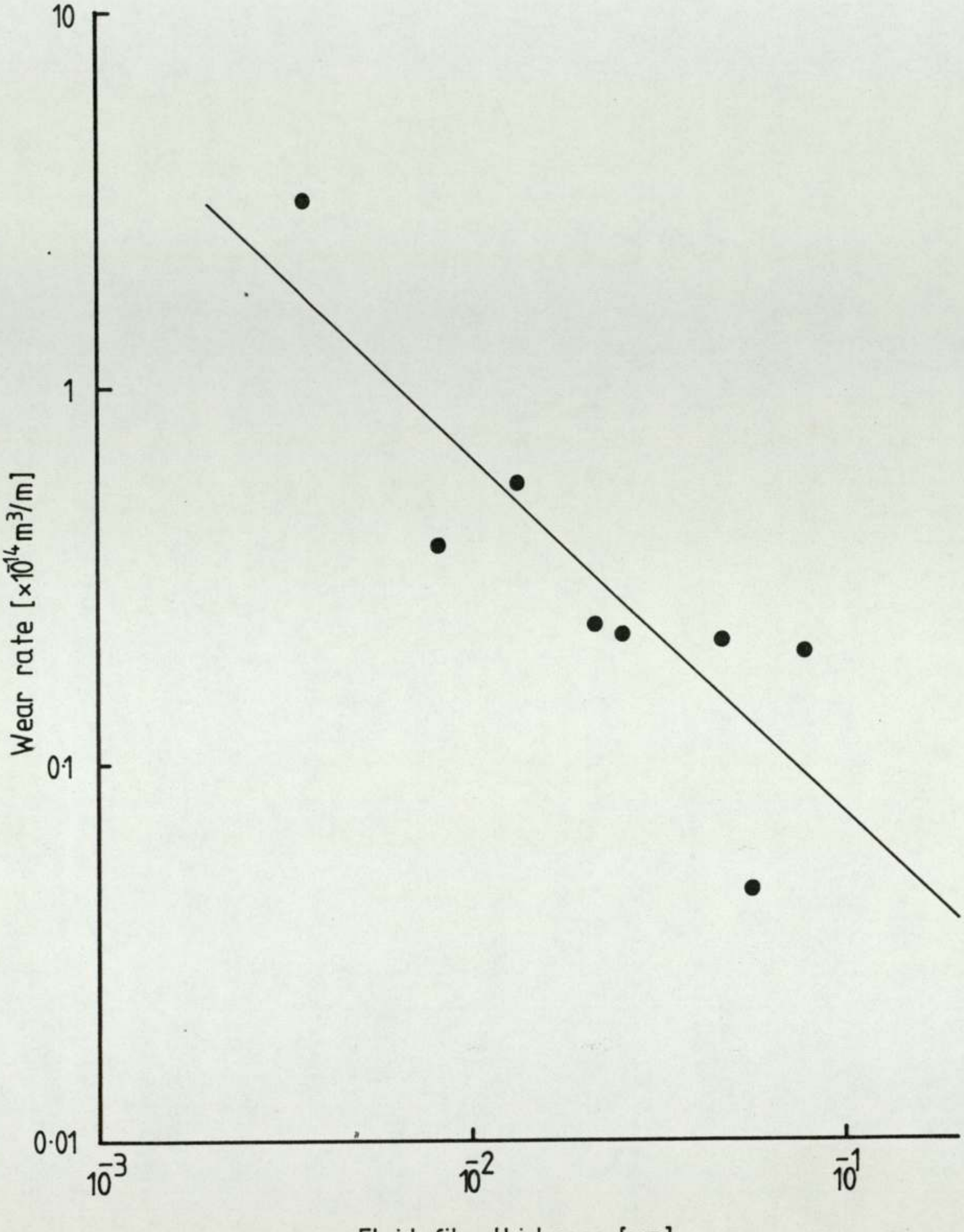

Figure 3·14. Driving disc wear rate against fluid film thickness for test lubricants without the antiwear additive (calculated by weight loss) region were averaged and plotted against fluid film thickness. Figure 3.13 and 3.14 give the resultant plot of wear rate against fluid film thickness for both pitting and driving discs respectively when run with test lubricants not containing the antiwear additive. The respective equations are described by:

$$\text{Wear rate}(m^3m^{-1}) = 4.76 \times 10^{-15}(\text{Film thickness } \mu m)^{-1.08} \quad 3.9$$

for the pitting disc and:

$$\text{Wear rate}(m^3m^{-1}) = 7.96 \times 10^{-17}(\text{Film thickness } \mu m)^{-0.96} \quad 3.10$$

for the driving disc.

The correlation coefficients being -0.88 and -0.84 respectively. Equation 3.10 indicates that wear on the driving disc is negligible.

When experiments were conducted using the test lubricants containing the antiwear additive a greater scatter of results was observed leading to a lower correlation coefficient of -0.44 for both the pitting and driving discs.

A comparison between the wear rate equation of the pitting disc, by weight loss (Equation 3.9) to the wear rate equation independently formed from the LVDT transducer measurements (Equation 3.6) reveals a degree of similarity. Figure 3.15 gives a graphic comparison of these two equations where the wear rates calculated from the transducer measurement and the weight loss method are plotted against each other. The line drawn subsequently represents the exact correlation between the two equations and it can be seen that the points converge towards this line as the fluid film thickness decreases, indicating a better correlation between the two equations at lower film thicknesses.

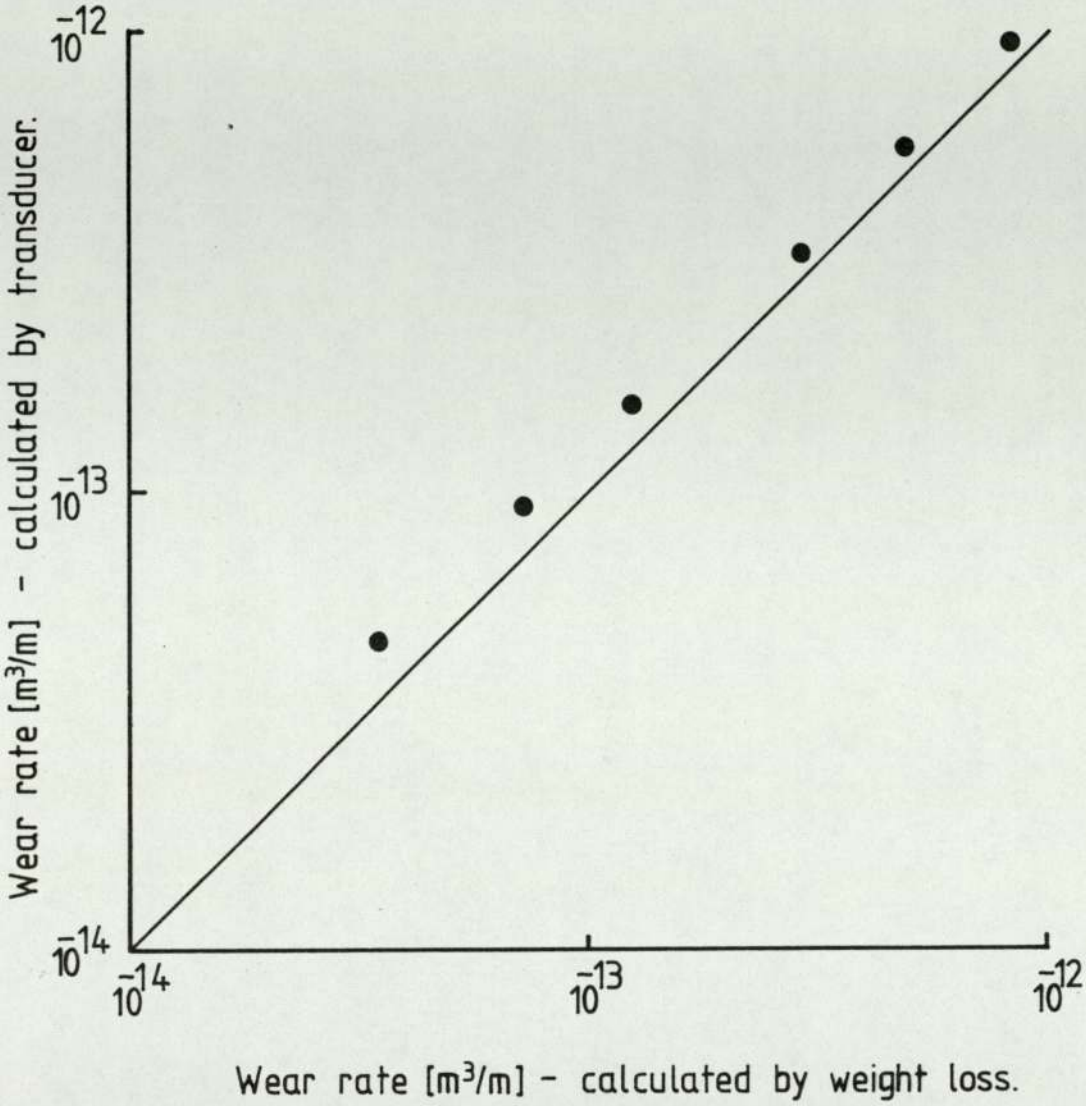

Figure 3·15. Comparison of wear rates between L.V.D.T. transducer and weight loss methods.

3.3.5. Cracking and Pitting of Disc Specimens

Damage in the form of pitting and cracking was always confined to the slower rotating softer disc, previously termed the pitting disc. The pitting life of the disc was defined as the number of cycles taken to obtain one detectable pit and was used as a means of quantifying each lubrication region. All pitting life values were averaged at each lubrication region and plotted against fluid film thickness. Figure 3.16a) shows the variation in life to first pit, expressed as the number of contact cycles N, with fluid film thickness for the mixed-elastohydrodynamic region using test lubricants without the antiwear additive. Figure 3.16b) gives the corresponding relationship of mean pitting life against fluid film thickness for test lubricants with the antiwear additive.

From these graphs it can be seen that the inclusion of the antiwear additive results in a significant increase in the mean recorded pitting life, the effect being even greater for experiments conducted near to the boundary region. In addition to this, both curves exhibit a minimum life at the centre of the mixed-elasthydrodynamic region as defined by the Stribeck curve given in Figure 3.4. As the fluid film thickness decreases in this region and hence the degree of metallic contact increases, there is the expected fall in the value of average life. However, a further decrease below a value of about 0.035μm results in an increase in average life.

The curve showing the variation in life to first pit with initial D-ratio (see Equation 1.11), that is the ratio of initial surface roughness to fluid film thickness, shown in Figure 3.17 for experiments without the antiwear additive indicates similar trends. The curve exhibits the familiar fall in life with D-ratio up to a value of D = 22 where the best fit line gives the relationship:

$$\log(\text{cycles}) = -0.42 \log(D) + 5.95 \qquad 3.11$$

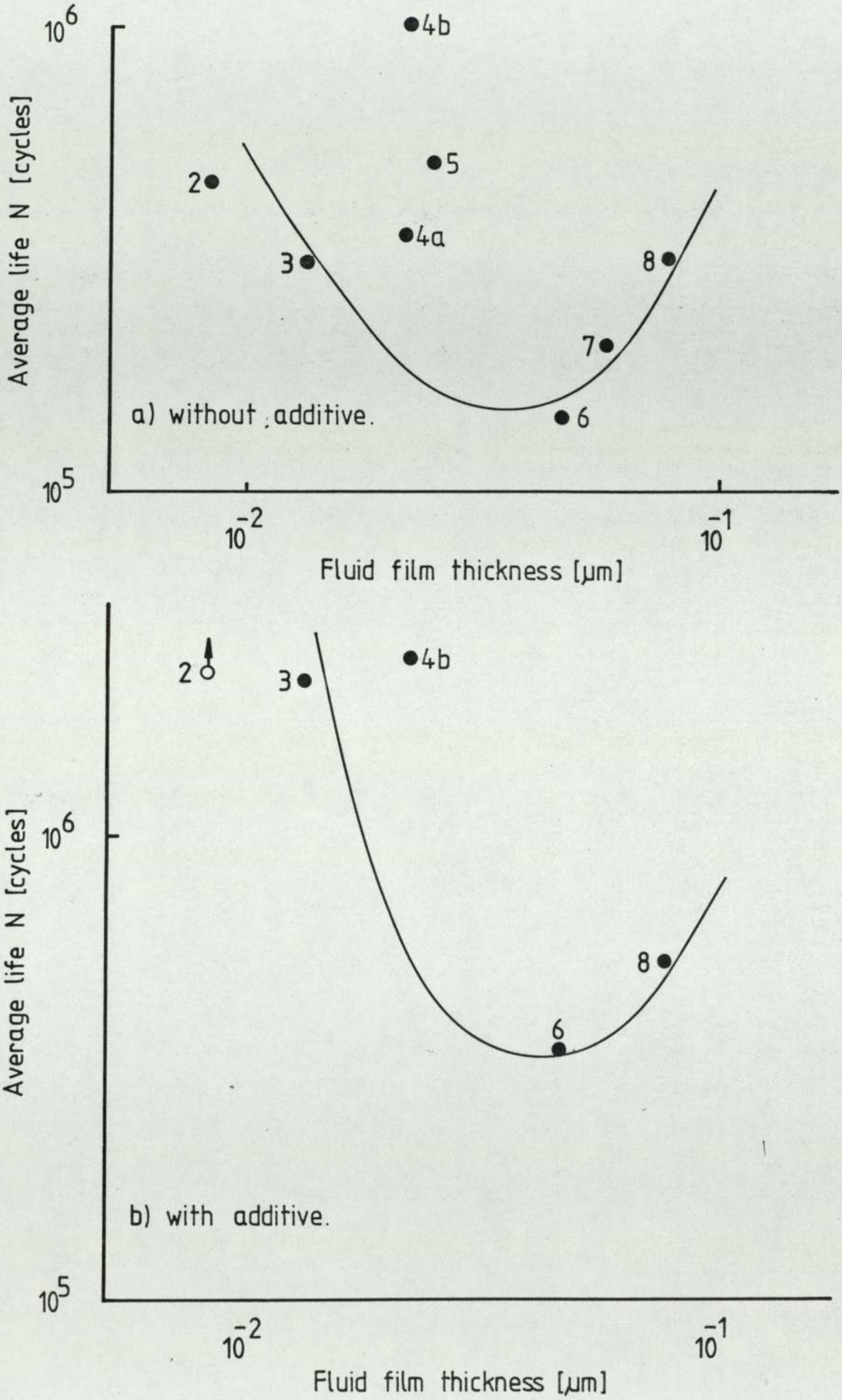

Figure 3·16. Average life to first pit [N] against fluid film thickness a) without antiwear additive b) with antiwear additive.

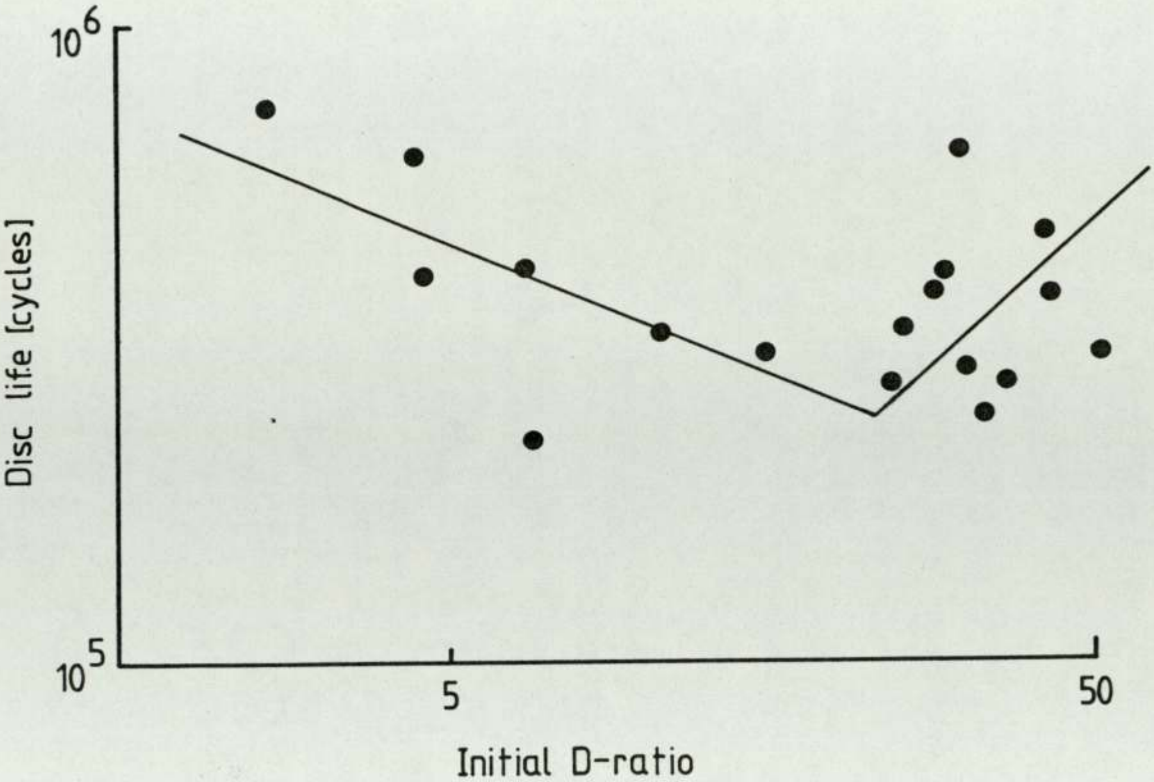

Figure 3·17. Disc life to first pit against initial D-ratio for experiments conducted without the antiwear additive.

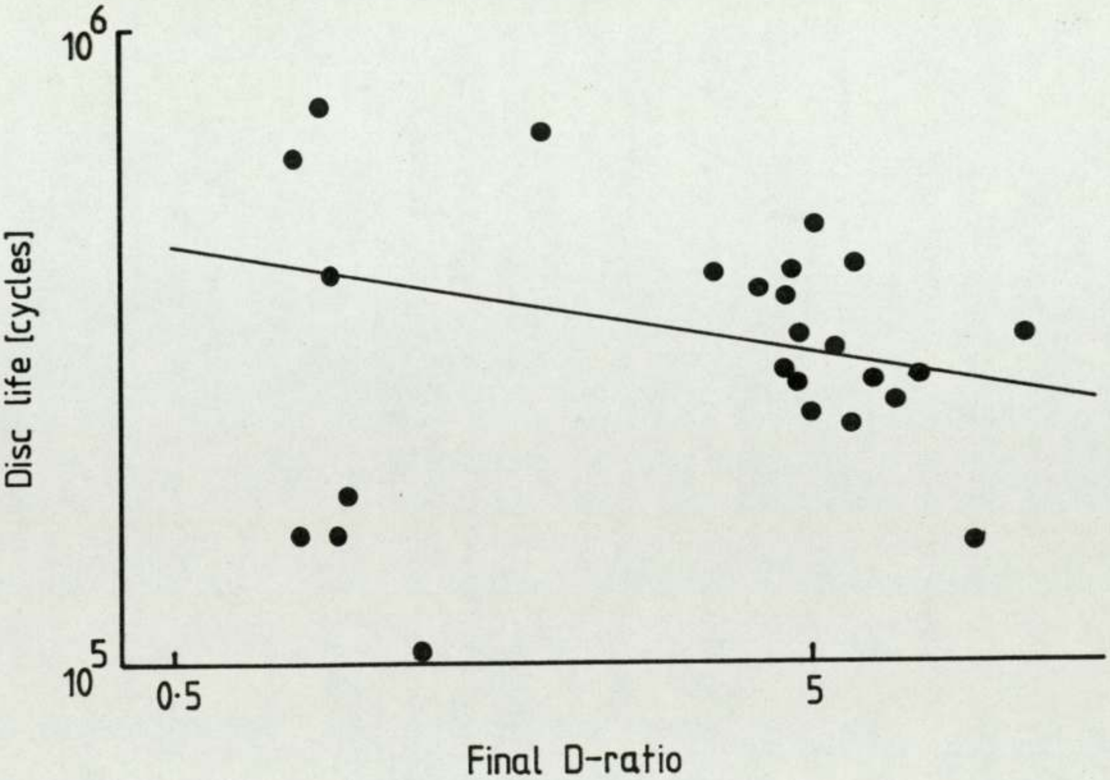

Figure 3·18. Disc life to first pit against final D-ratio for experiments conducted without the antiwear additive.

with -0.74 correlation coefficient.

Above this value of D there is a rapid increase in life with D-ratio. A curve plotted for D-ratios calculated from final surface roughnesses and track widths produced a set of points with a greater scatter, and subsequently the above trend could not be obtained. The best fit line for this graph, given as Figure 3.18, is described by the equation:

$$\log(\text{cycles}) = -0.20 \log(D) + 5.61 \qquad 3.12$$

with a correlation coefficient of only -0.24.

When the antiwear additive was included in similar experiments, even worse correlation between the mean pitting life and that of the D-ratio was obtained.

Pitting did not occur in either the boundary or hydrodynamic regions of lubrication (1 and 9) with experiments conducted with both the respective antiwear and non-antiwear lubricants.

Crack propagation (Np) has been plotted against fluid film thickness as shown in Figure 3.19. Np has been defined as the total number of cycles taken by the pitting disc between the onset of the first detectable crack and that of the appearance of the first pit. In contrast to the previous wear rate graphs (Figures 3.11 to 3.14) and pitting life graphs (Figure 3.16) there appears to be little difference in Np whether the antiwear additive is present or not as all points lie about a line described by the equation:

$$Np(\text{cycles}) = 7.26 \times 10^3 (\text{Film thickness } \mu\text{m})^{-0.5} \qquad 3.13$$

By comparing Figure 3.19 with that of mean pitting life against fluid film thickness (Figure 3.16) it can be seen that Np does not follow the variation in mean pitting life N and no minima in the value of Np occurs. In all experiments the magnitude of Np was never greater than 20% of the mean pitting life N.

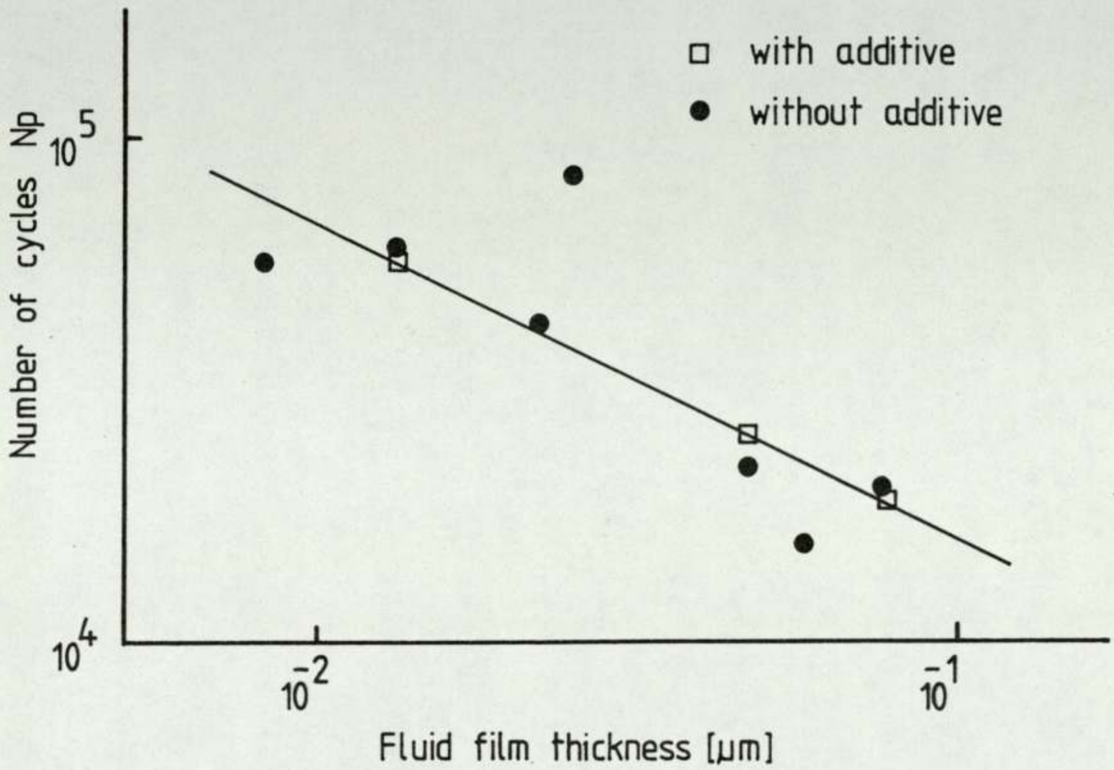

Figure 3·19. Average number of cycles [Np] against fluid film thickness with and without the antiwear additive.

Additional experiments to investigate the effect of load on pitting life were conducted with Test Lubricant F. Discs were run at a constant speed (200rpm) under different loads, ranging between 90 and 200kg until the formation of the first pit. Figure 3.20 gives the relationship between pitting life and applied load for experiments conducted at lubrication regions 2.1, 2.2, 2.3 and 3. It can be seen that there is a tendency for pitting life to increase with decreasing applied load and hence with increasing fluid film thickness. This is contrary to those experiments run with similar fluid film thicknesses but under constant load, however, stress can also effect subsurface initation and propagation (168) hence these results are to be expected.

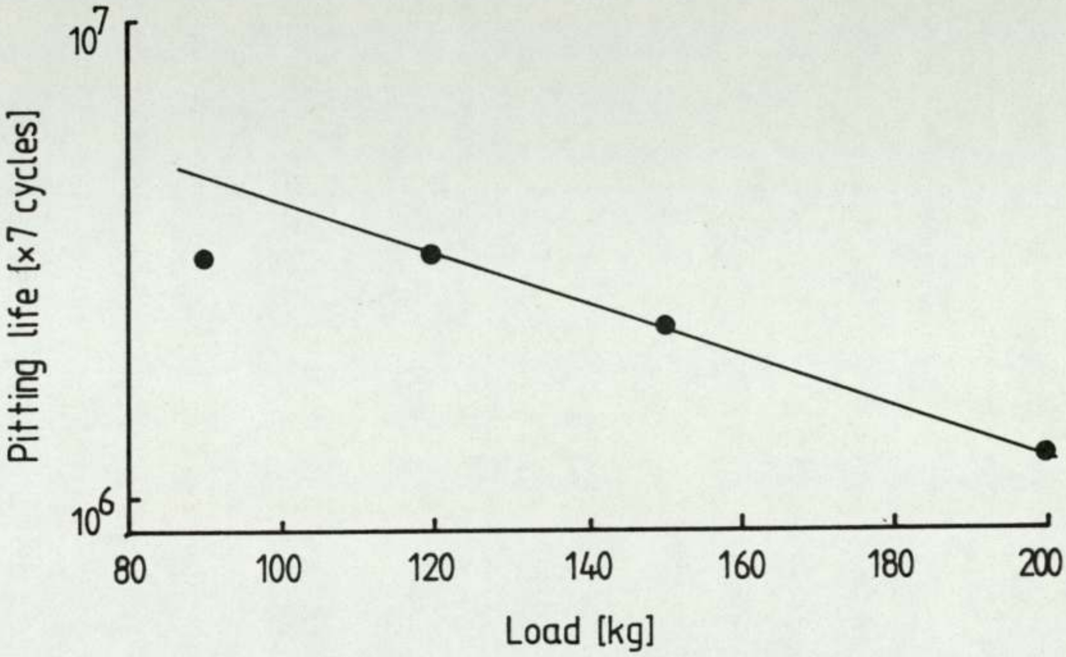

Figure 3·20. Pitting life against applied load for experiments conducted at lubrication regions 2·1, 2·2, 2·3 and 3.

Throughout each experimental run the surface of the pitting disc was carefully monitored using the continuous technique of the magnetic crack detector. As previously described in Section 2.8, discs were run until a crack had grown sufficiently to trigger a cut-out set at a pretetermined threshold level, after which they were re-run with a higher threshold setting. Altogether, ten threshold levels were used each progressively higher than the previous, thus enabling a full crack propagation to final pit formation sequence to be observed.

Averages were taken for the respective number of cycles taken to reach each threshold level and plotted as a function of threshold level. Figure 3.21 gives the respective plots for discs run with test lubricants not containing the antiwear additive. The corresponding plot of the average number of cycles taken against threshold level, for the test lubricants with the antiwear additive is shown in Figure 3.22. No correlation between the slopes of the various graphs could be obtained when run at the different regimes of lubrication, although there does appear to be a relationship between disc speed and final threshold level as shown in Table 3.3.

Table 3.3 gives the average threshold level at which the first pit occurred against lubrication region. This effectively gives an indication of crack magnitude at pit formation.

Lubrication Region		Without Additive		With Additive	
	Speed(rpm)	Fluid	Threshold	Fluid	Threshold
2	100	B	6	F	Not pitted
3	200	B	10	F	6
4a	100	D	6	-	-
4b	400	B	>10	F	6
5	200	C	9	-	-
6	100	E	3	G	3
7	400	D	10	-	-
8	200	E	4	G	6

Table 3.3. Average threshold levels at which pitting occurred.

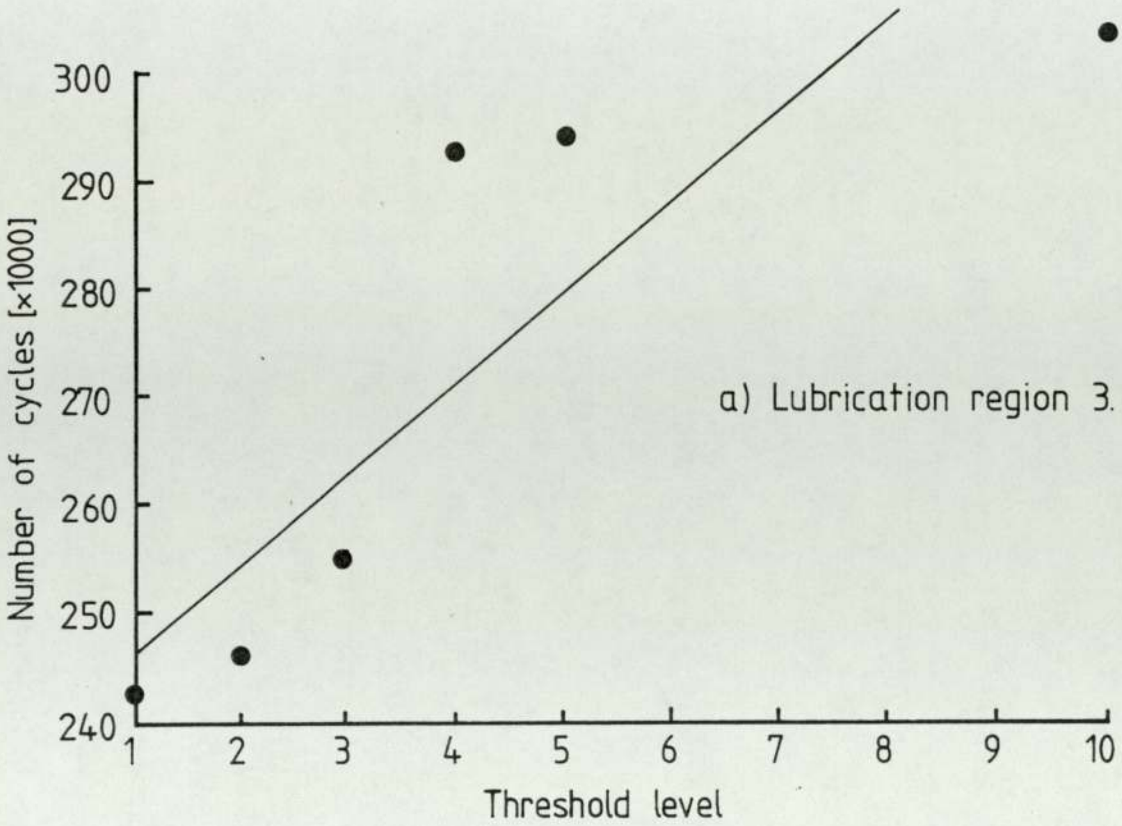

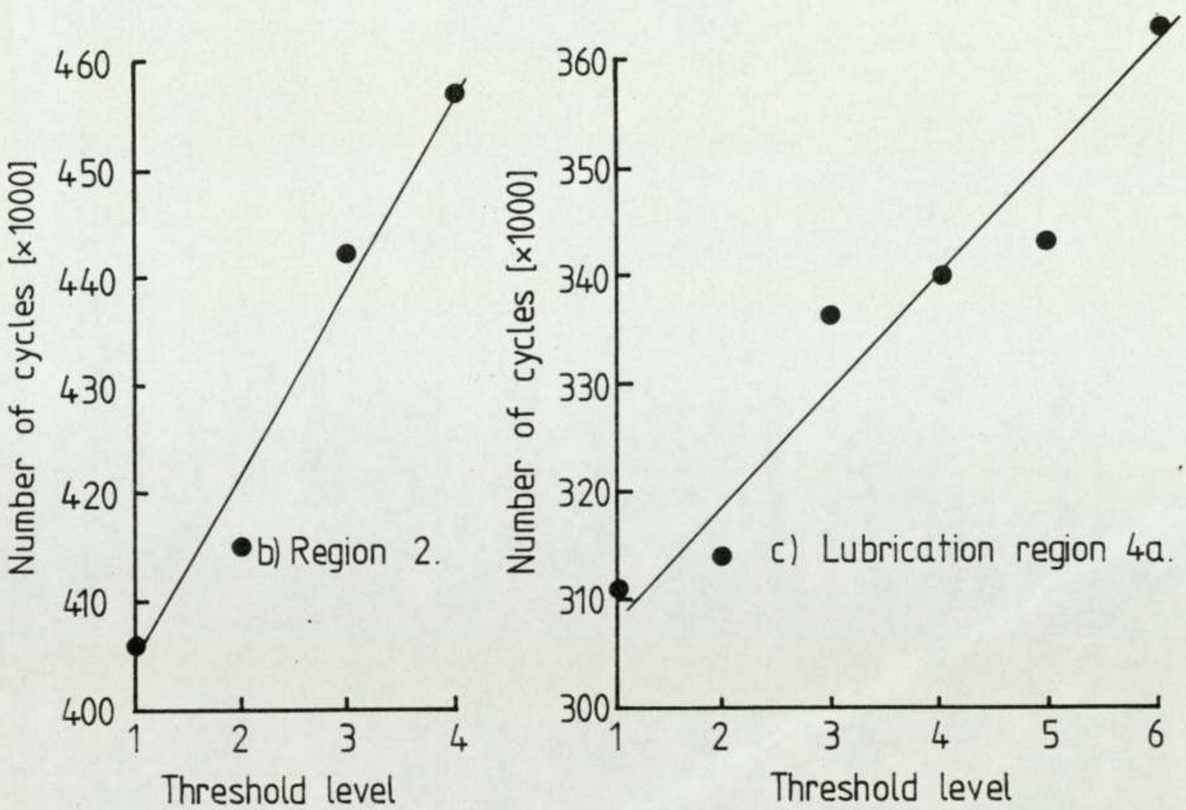

Figure 3·21. Average number of cycles against crack detector threshold level for test lubricants not containing the antiwear additive.

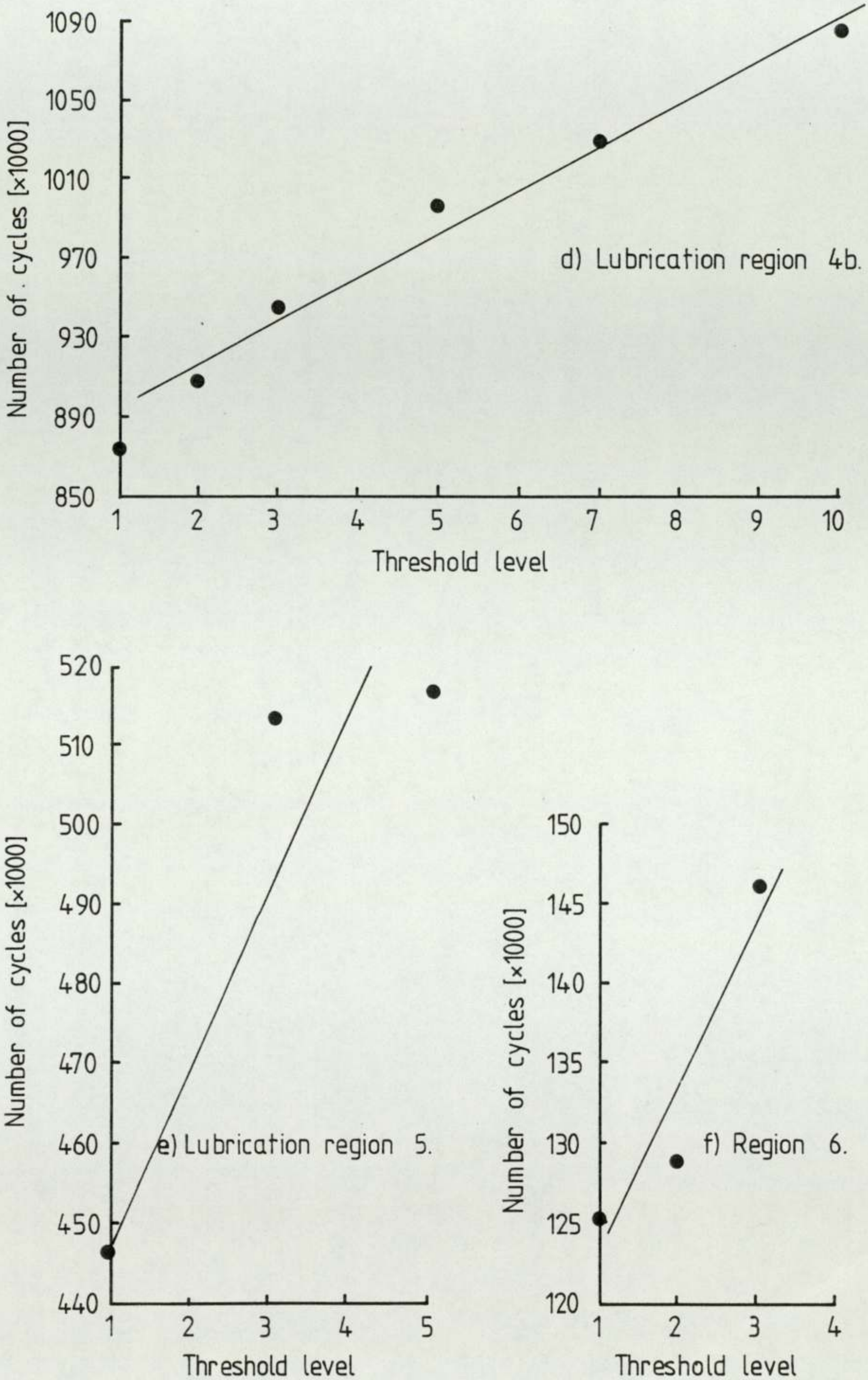

Figure 3·21(cont). Average number of cycles against crack detector threshold level for test lubricants not containing the antiwear additive.

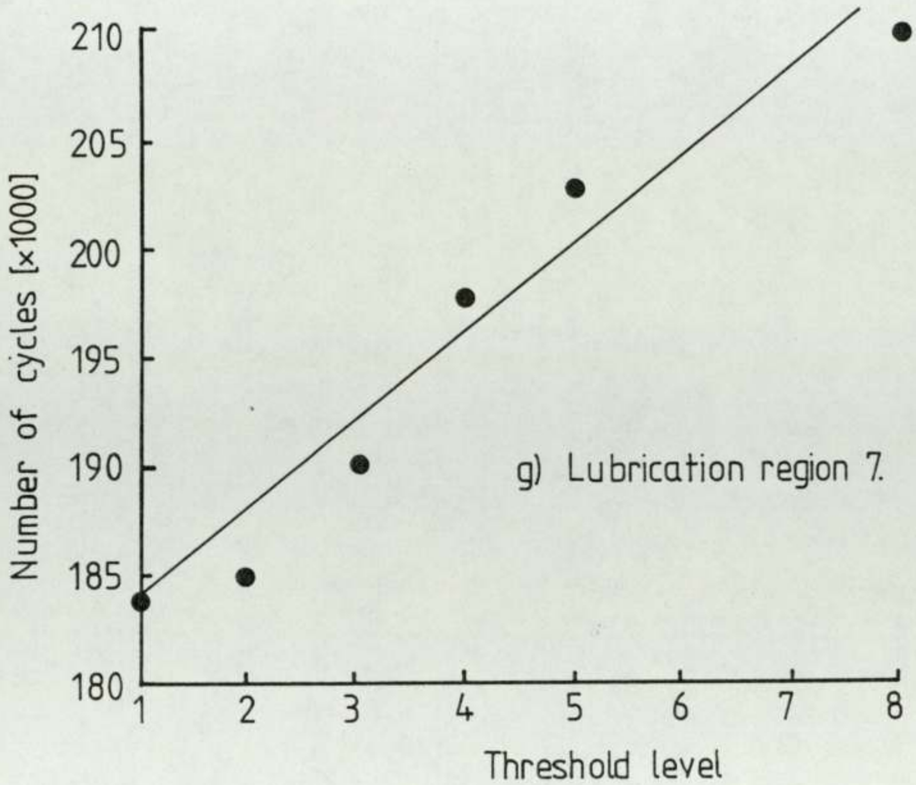

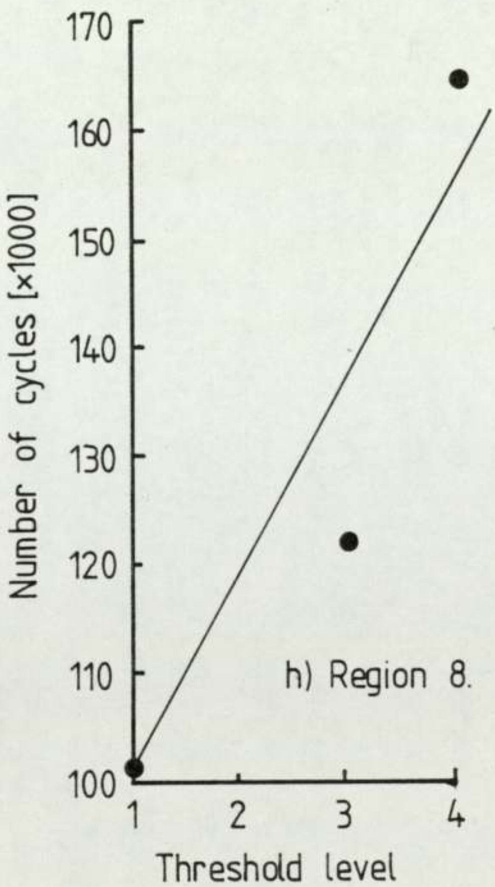

Figure 3·21(cont). Average number of cycles against crack detector threshold level for test lubricants not containing the antiwear additive.

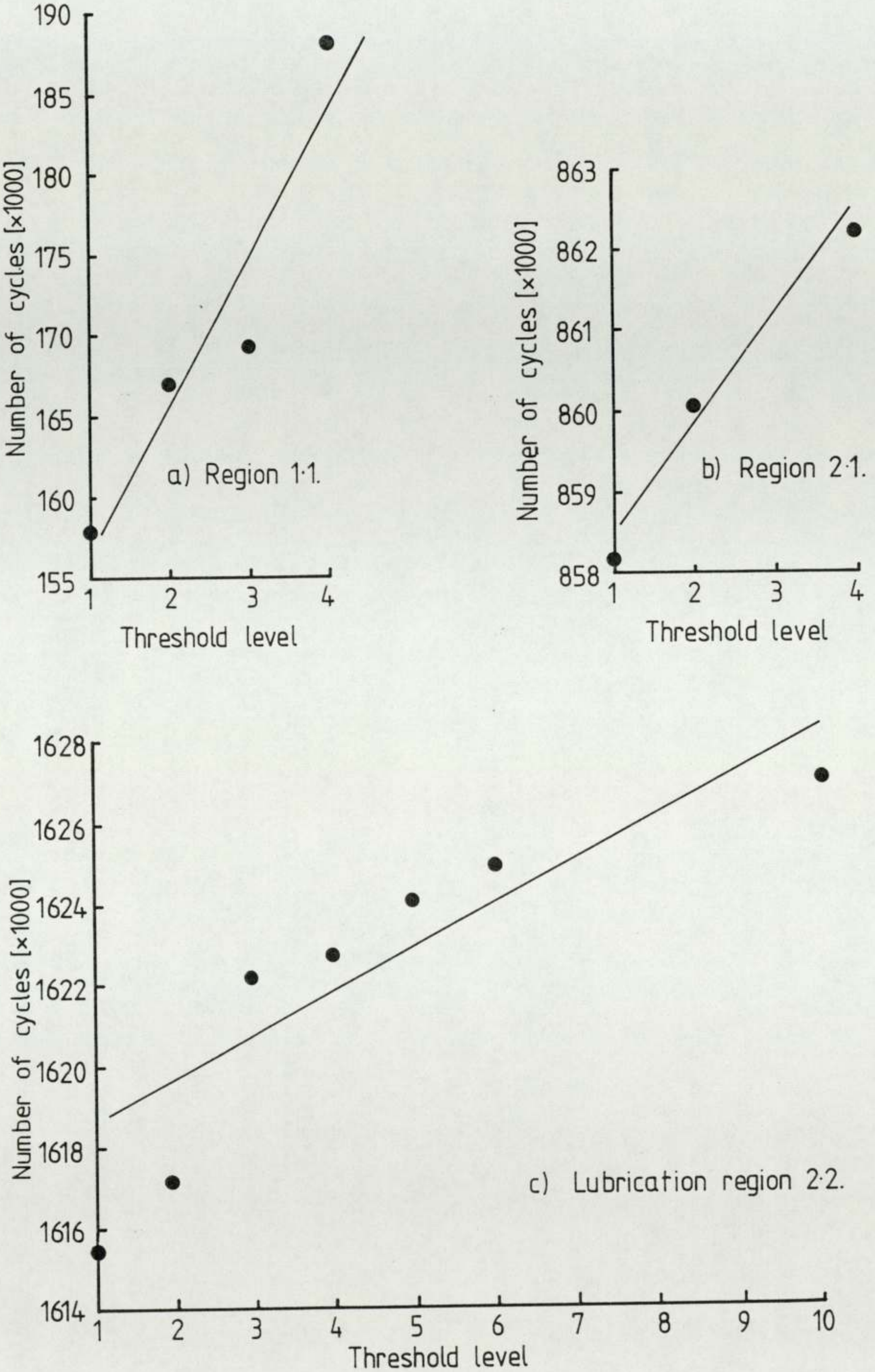

Figure 3·22. Average number of cycles against crack detector threshold level for test lubricants containing the antiwear additive.

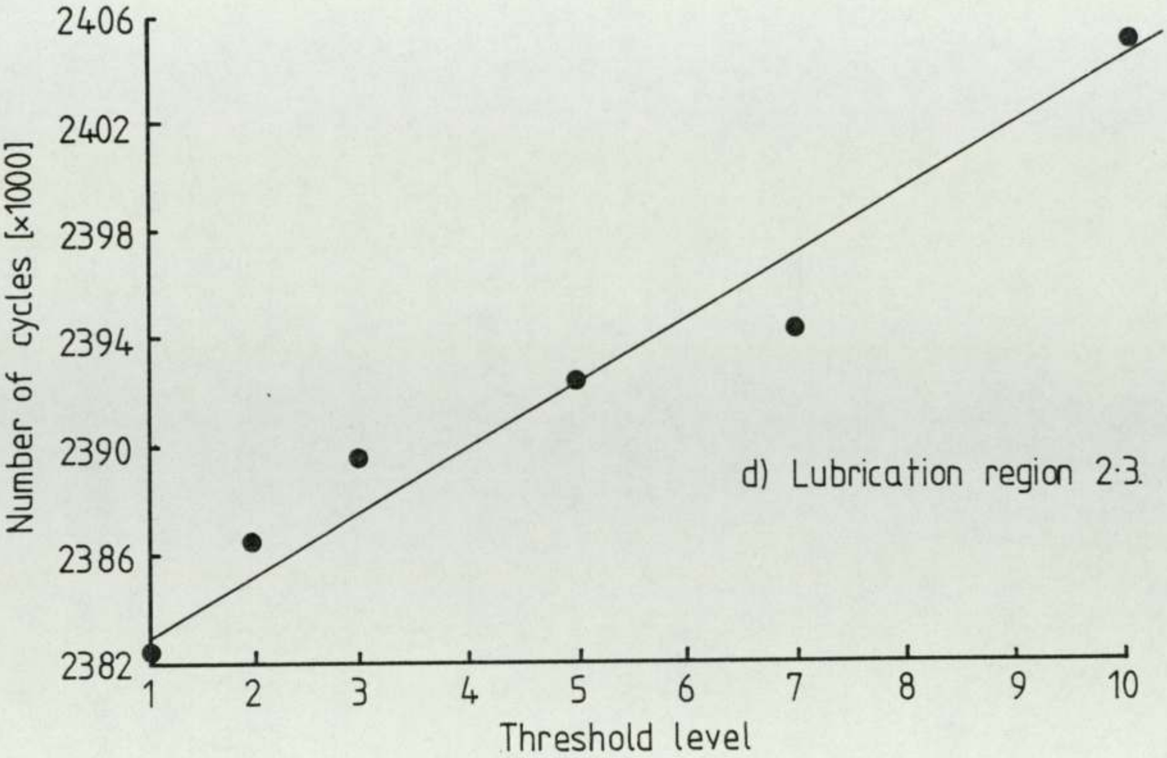

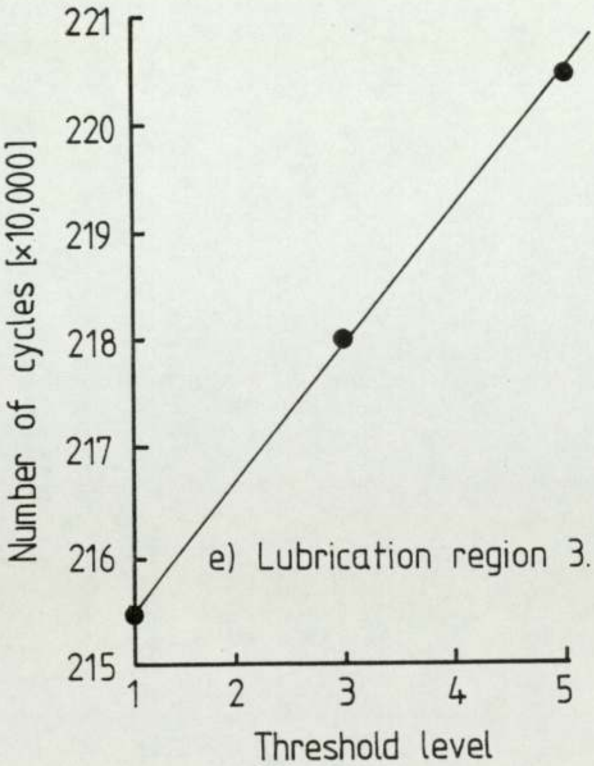

Figure 3·22(cont). Average number of cycles against crack detector threshold level for test lubricants containing the antiwear additive.

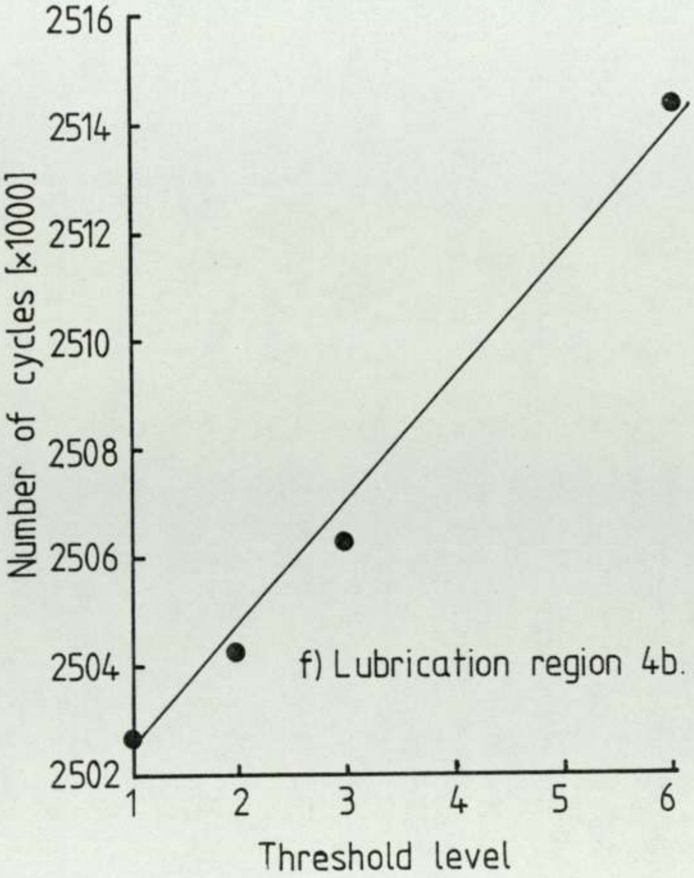

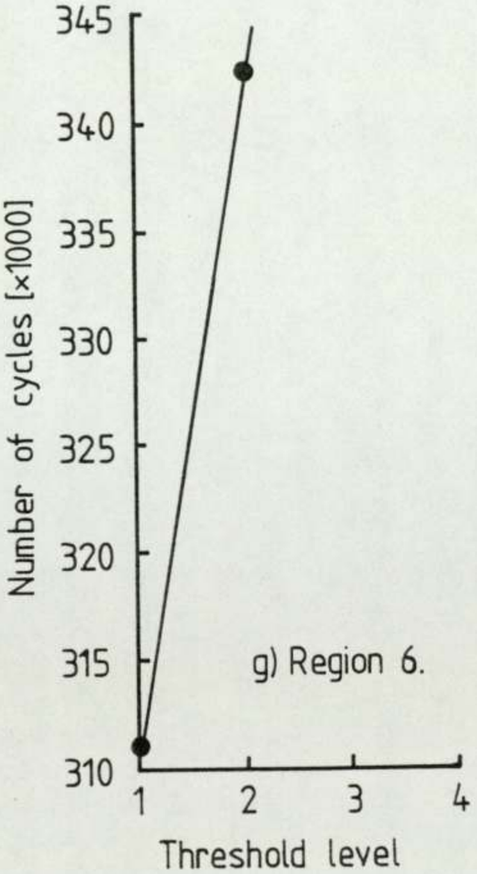

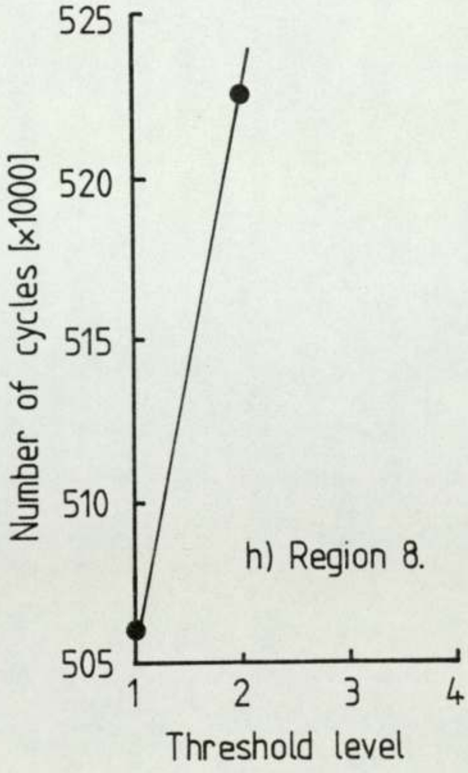

Figure 3·22(cont). Average number of cycles against crack detector threshold level for test lubricants containing the antiwear additive.

From Table 3.3 it can be seen that the threshold level at which pitting occurs is not very sensitive to change in fluid film thickness for test lubricants containing the antiwear additive. Experiments conducted without the antiwear additive, appear to show no correlation between the final threshold level and fluid film thickness, but upon a closer inspection there does seem to be a relationship between the pitting threshold level and speed for each test lubricant, irrespective of the lubrication region. For Test Lubricant B, at regions 2 (100rpm), 3 (200rpm) and 4b (400rpm) the final threshold levels are 6, 10 and >10 respectively. There are also similar increases in final threshold level with speed for Test Lubricants D and E.

After each threshold level had been reached, the crack detector output signal was run through the frequency counter, pre-calibrated to count the number of crack locations situated around the circumference of the disc. Cracks were quantifed at each level and plotted against threshold level as shown in Figure 3.23. It can be seen that the amount of damage associated with the pitting process increases during the life of the disc, the actual amount depending upon the lubrication region run in. With experiments conducted using the antiwear additive a similar increase with threshold level was observed but only for a short period, as pitting tended to occur at lower overall threshold levels.

The amount of damage at the end of each run, that is the number of crack locations present on the disc surface when the first pit had formed, were averaged and plotted against fluid film thickness as shown in Figure 3.24. The amount of

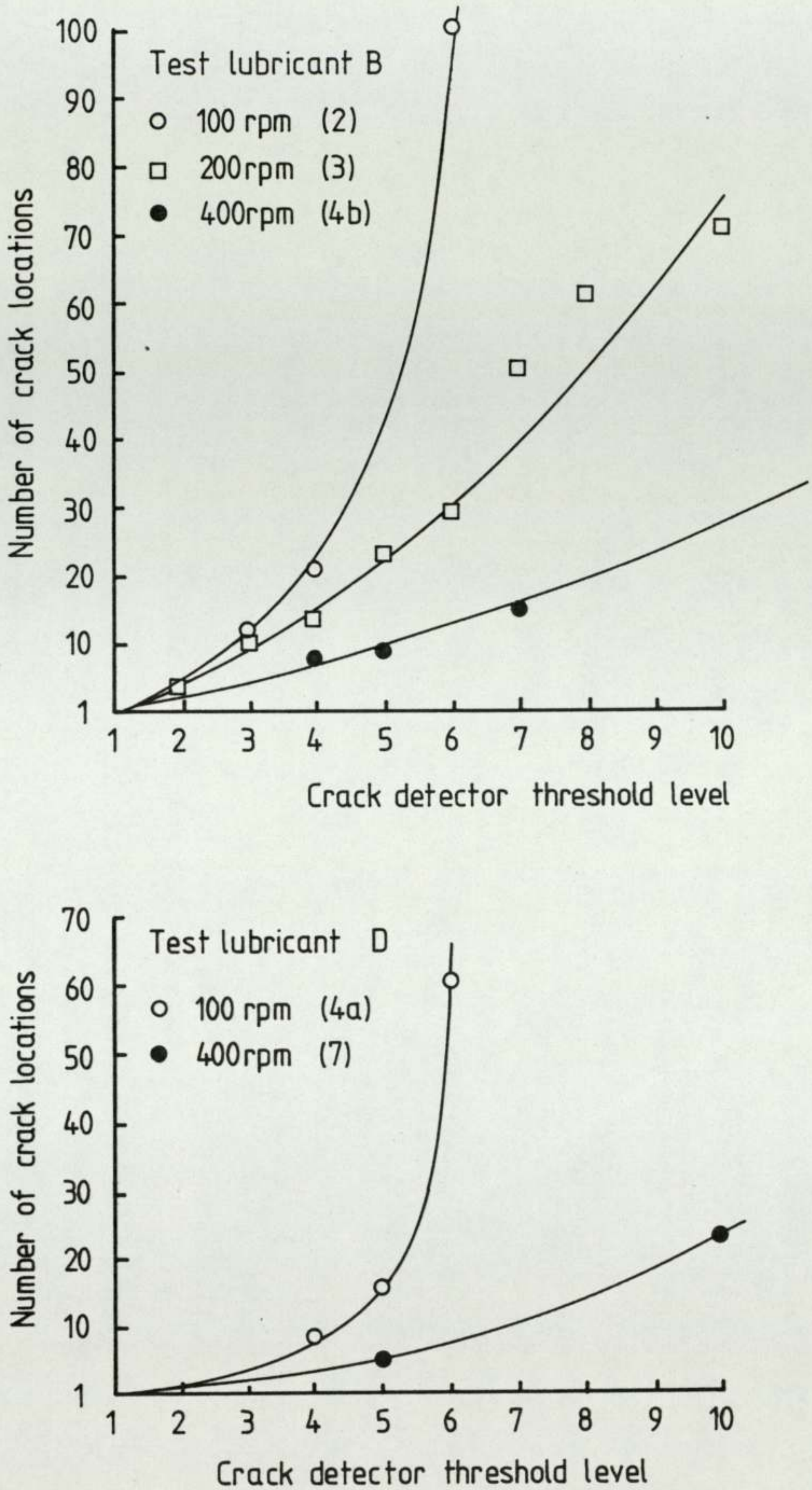

Figure 3·23. Number of crack locations against crack detector threshold level for various test lubricants. (Lubrication regions in brackets).

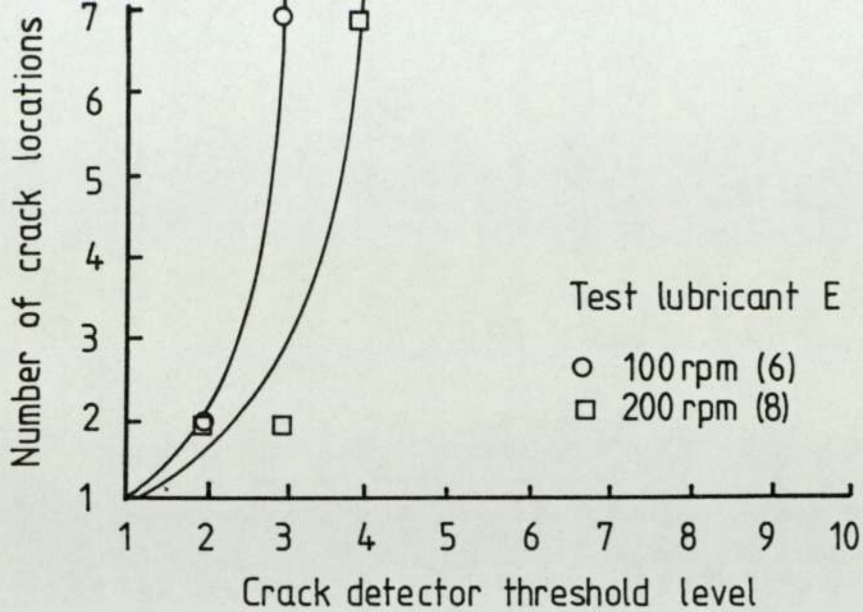

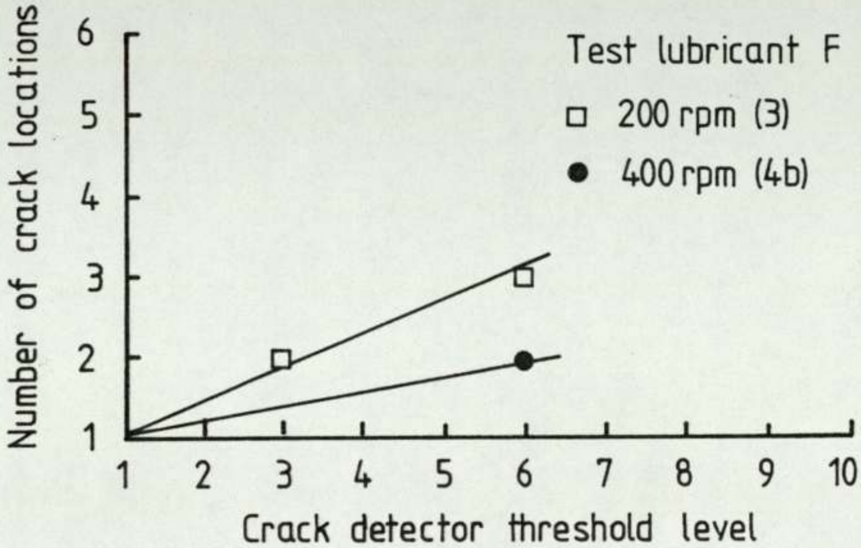

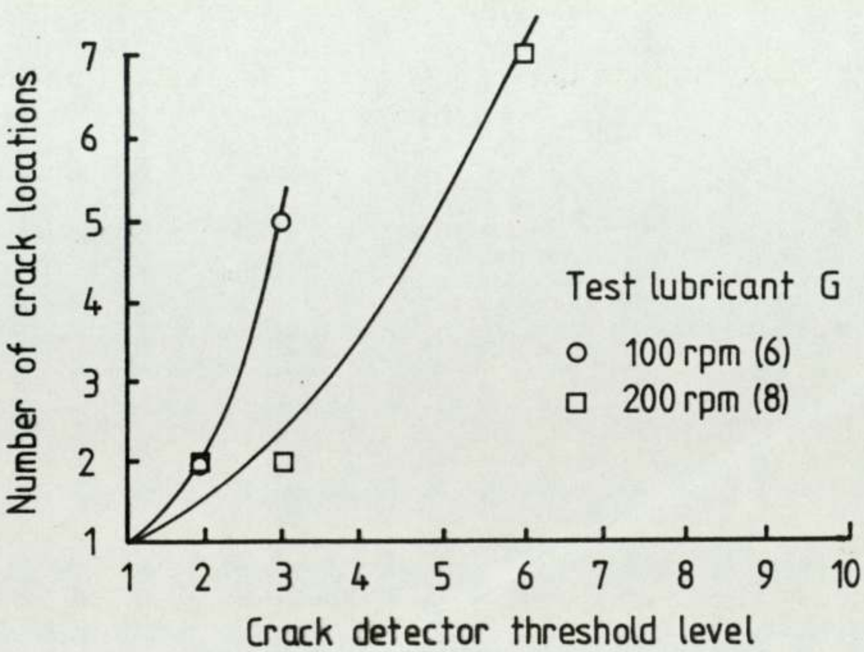

Figure 3·23(cont). Number of crack locations against crack detector threshold level for various test lubricants. (Lubrication regions in brackets).

damage can be seen to increase with decreasing fluid film thickness for test lubricants not containing the antiwear additive. However, when test lubricants with the antiwear additive were employed no significant difference between the number of crack locations and that of fluid film thickness was observed as also shown in Figure 3.24.

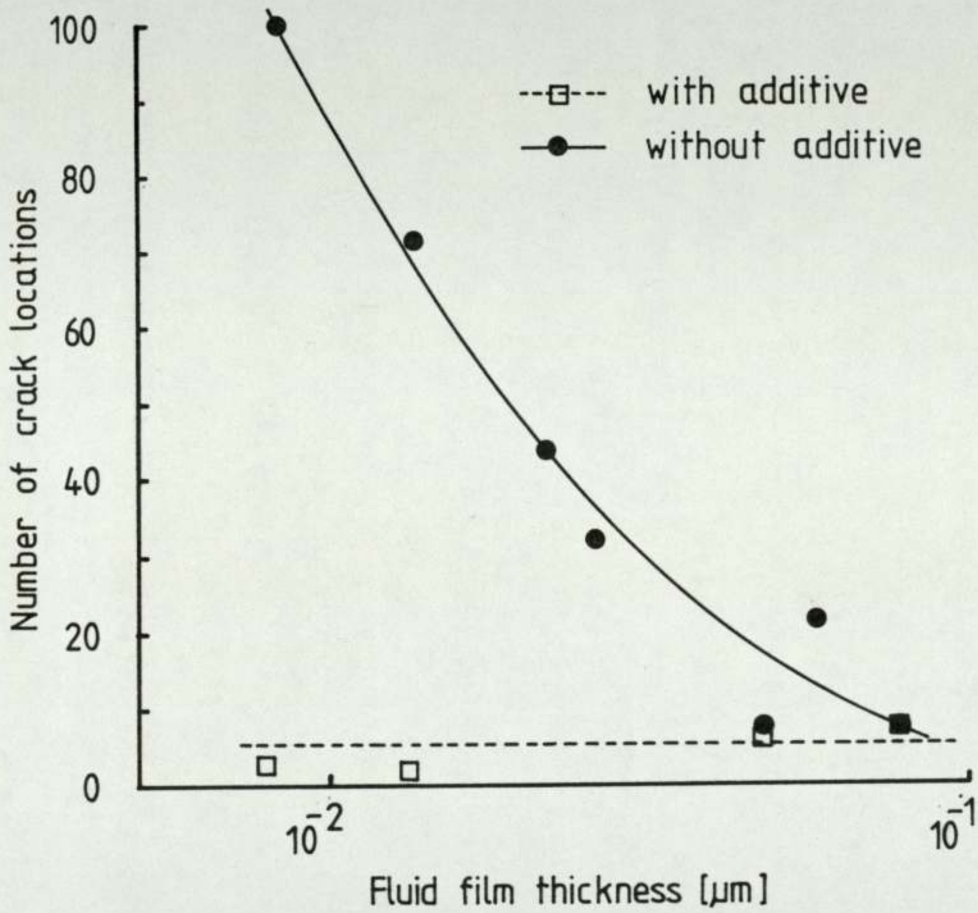

Figure 3·24 Final number of crack locations against fluid film thickness with and without antiwear additive.

3.3.6. X-ray Powder Analysis of Wear Debris

Debris retrieved from Test Lubricant B was analysed after 33 hours of circulation at Lubrication Region 3. Altogether, 49 damage locations were formed of which eight were identified as pits. The appearance of the test lubricant was very dark indicating that considerable contamination had taken place. This was in contrast to the relatively clear lubricant obtained from the experiments conducted at the other lubrication regions. Table 3.4 gives the measured diffraction angles (2θ), obtained directly from the photograpic film, together with the respective lattice plane spacings (d) calculated from the equation:

$$d = \lambda/(2\sin\theta) \qquad 3.14$$

where λ is the wavelength of the Co$k\alpha$ radiation (1.789Å).

2θ	d(Å)	α - Fe		Fe_3O_4		α - Fe_2O_3	
		d(Å)	I/I_0	d(Å)	I/I_0	d(Å)	I/I_0
35.0	2.976	-	-	2.97	30	-	-
29.0	2.680	-	-	-	-	2.69	100
41.5	2.525	-	-	2.53	100	-	-
51.0	2.071	-	-	-	-	-	-
52.3	2.030	2.03	100	-	-	-	-
59.0	1.816	-	-	-	-	-	-
63.5	1.700	-	-	-	-	1.69	60
67.5	1.610	-	-	1.62	30	-	-
74.0	1.486	-	-	-	-	1.48	35
77.4	1.431	1.43	20	-	-	-	-
99.7	1.170	1.17	30	-	-	-	-
110.0	1.092	-	-	1.09	12	-	-

Table 3.4. X-ray powder diffraction analysis.

Interpretation of the d values required the use of the Hanawalt Numerical Index and associated Powder Diffraction

Files (169). Analysis revealed that iron (α- Fe), heamatite (α- Fe_2O_3) and magnetite (Fe_3O_4) were present in the test lubricant and their respective d values and corresponding intensities (I/I_0) are included in Table 3.4.

It is unfortunate that time did not permit a more complete investigation especially at the other lubrication regions, however, this priliminary analysis has shown that several iron oxides are present in the lubricant.

3.4. Optical microscopy

3.4.1. Unisteel Test Specimens

Inspection of the test pieces revealed that they all had a circular track of approximate diameter 62mm worn by the balls. The minimum and maximum values of width were 0.415mm and 0.490 respectively, resulting in an average taken from all the test pieces of 0.45mm. The track was coated with a thin surface film giving it a characteristic brown colour. The indentation of this track over the surface of the test piece is small, but with maximum depression at the mid-point of the track corresponding with the maximum rolling diameter of the thrust balls as shown in Figure 3.25.

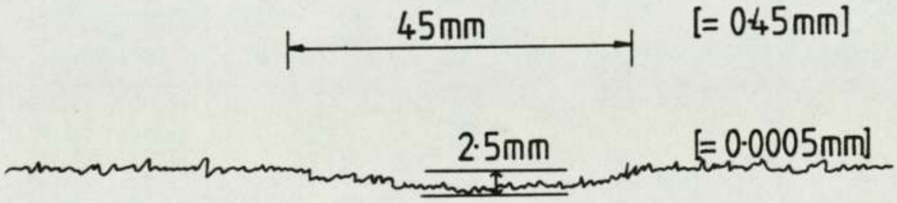

Magnification: ×5000 vertical. ×100 horizontal.

Figure 3·25. Talysurf profile taken across the wear track of a Unisteel specimen.

Damage in the form of a pit or crack, or both was nearly always concentrated at a single point on the track, but occasionally damage occurred at two or even three places around the track. The shape of the pit varied between circular (Figure 3.26a)) and elliptical (Figure 3.26b)). Geometric measurements such as pit width, length and depth have been recorded using the optical microscope and are presented against increasing test lubricant viscosity in Table 3.5.

Test Lubricant	Depth (mm)	Width (mm)	Length (mm)	Surface Area (mm^2)
B	0.48	0.35	0.27	0.024
D	0.59	0.42	0.41	0.135
H	0.83	0.43	0.44	0.149
I	0.86	0.42	0.49	0.162
E	0.73	0.40	0.51	0.160

Table 3.5. Unisteel pit geometries.

Inspection of Table 3.5 reveals an apparent trend of increasing pit surface area with that of test lubricant viscosity, calculated by assuming an eliptical pit profile. This will also take into account circular pit profiles which seem to occur with the mid-viscosity range of test lubricants. Pit depths, apart from those experiments conducted with Test Lubricant E, also show an increase with viscosity.

Figure 3.26c) shows the outline of a potential pit taking the form of a circle by the crack markings. A more

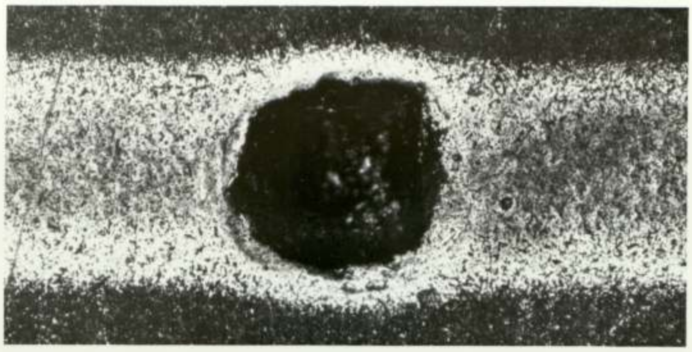

a) Circular pit.

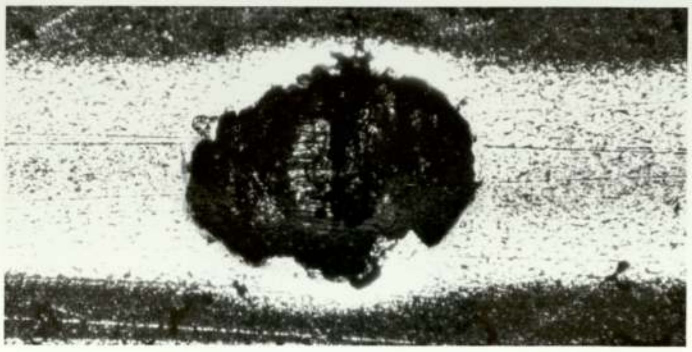

b) Elliptical pit.

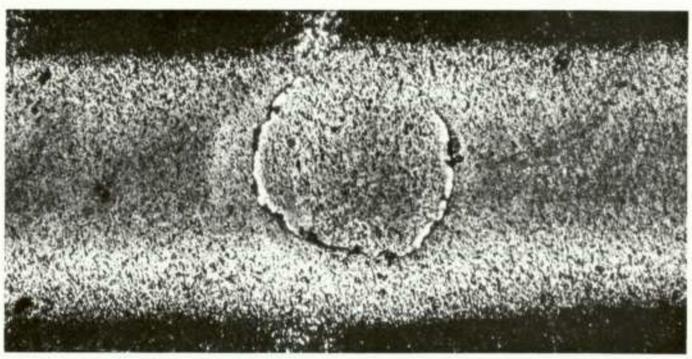

c) Crack formation prior to pitting.

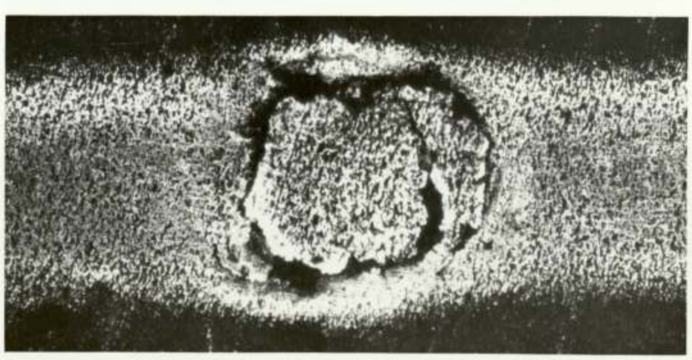

d) A more advanced stage of c).

[Rolling direction: ⟶ Magnification: ×60]

Figure 3·26. Typical damage associated with the Unisteel Machine experiment advanced stage can be seen in Figure 3.26d). Further running would probably result in the metal surrounded by the crack markings being removed, leaving the familiar pit profile.

3.4.2. Non-destructive Examination of Unisteel Test Specimens

To try to determine where and when a pit is formed new and used thrust washers were inspected for any surface cracks by the means of two non-destructive methods. Firstly by magnetic particle tracers and secondly by dye penetrant. It was found that on both new and used thrust washers there were no cracks detectable by either method thus indicating that there was an initial period followed by rapid crack and pit formation in the time it takes for a specimen to fail. However, both the above methods are unlikely to reveal either small features or subsurface flaws.

3.4.3. Rolling Four-ball Test Specimens

The top ball was inspected for damage since it experienced more load cycles within a given area of track than the freely rolling lower balls. Inspection of the top ball after each test revealed a circular track of width 1.3mm to 1.5mm and internal diameter 7.2mm as shown in Figure 3.27a). The track is deeply cut due to the high pressure encountered with the lower balls, and had maximum depth around the midpoint of the track width. The track usually contained a single pit of irregular shape which was very rough inside. Around the pit there was a tendency for the metal to flake and form scales which were also compressed into the track. The pit covered most of the track and often broke the inner boundary. For experiments conducted with water (Test

a) Normal pit.

b) Extreme widening of the track.

c) Top ball fracture.

d) Complete loss of cap.

Figure 3·27. Typical damage associated with the Rolling Four Ball Machine experiment

Lubricant A) a much deeper, wider track was observed, an example of which is given in Figure 3.27b).

More often than not a crack could be seen propagating from the edge of a pit through the metal often resulting in the enclosed metal being lost as shown in Figure 3.27c). Signs of the original pit were often seen at the edge of the track. Figure 3.27d) shows the damage associated with the top ball when occasionally a crack propagated through the entire ball resulting in a complete loss of its "cap" or top section. This cap was always removed from above the circular track. Sometimes a lower ball would split into two; being a lower ball its failure does not contribute numerically to the final result, though it illustrates the damaging nature of fatigue forces on steel in the presence of aqueous lubricants.

When a ball had been running for some time much debris, formed from the metal track and test lubricant, collected along the boundary of the track but this did not effect the development of pits or crack growth.

3.4.4. Amsler 2-disc Test Specimens

To study the development and progression of surface cracks into pits, series of optical photomicrographs were recorded for disc surfaces stopped at various stages of crack propagation defined by the ten threshold levels initially set using the crack detector. It was found that the majority of discs would pit at a Threshold Level of 10 or below, however, for experiments conducted at Lubrication Region 4b with Test Lubricant B, the average threshold level exceeded 10 and required periodic visual inspection of the disc to obtain the pitting life. Because of the large amount of data accumulated in the tests only one typical photomicrograph series has been included from each lubrication region. Further restrictions imposed by space made it necessary to limit each series to four photomicrographs, however, each series includes the first detectable crack and that of final pit formation.

Such a series of photomicrographs, taken at each lubrication region for test lubricants not containing the antiwear additive, are given in Figures 3.28 to 3.35 together with the corresponding magnetic crack detector traces.

The size of the first detectable crack varied with orientation but was generally about 1mm long across the disc, perpendicular to the rolling direction and 0.025mm wide. For experiments conducted near the boundary region at fluid film thicknesses less than 0.014μm, initial cracks were slightly longer. As the run progressed new cracks appeared and grew especially for those experiments conducted near to the boundary regions of lubrication depicted in Figures 3.28, 3.29, 3.30 and 3.31 and are represented by the additional signals appearing on the corresponding detector traces. It is important to note that for these particular conditions of lubrication, more cracks were present at the end of the run compared to the relatively few cracks present on discs run at Lubrication Regions 6, 7 and 8, as shown in Figures 3.33, 3.34 and 3.35. Eventually the crack grows or merges with a neighbouring crack to form the pit, thus terminating the run. On inspection of the pit it was seen that the overall size was dependant upon the region of lubrication. For experiments conducted with fluid film thicknesses between 0.008μm and

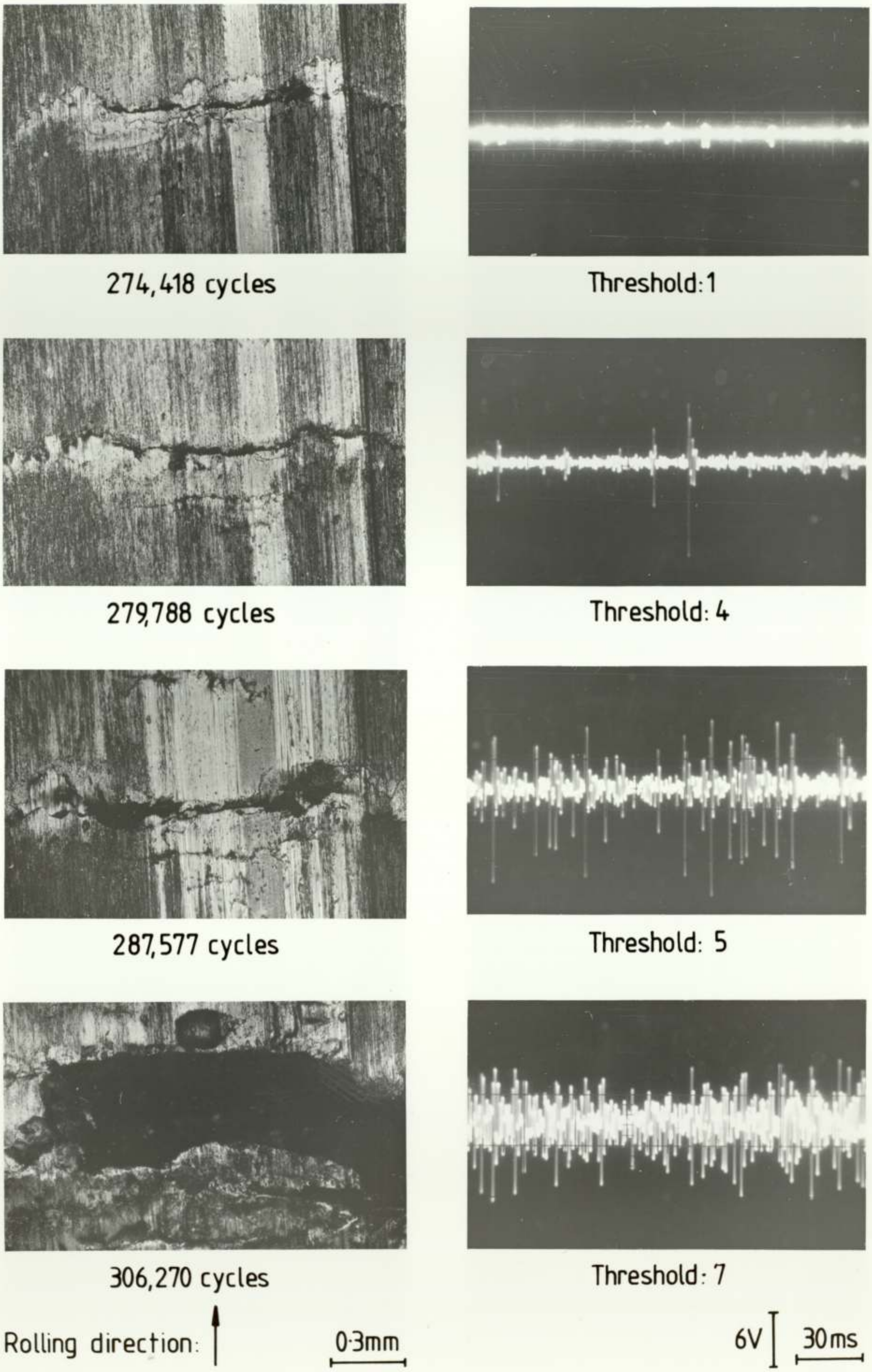

Figure 3·28. Crack propagation sequence at lubrication region 2. (test lubricant B)

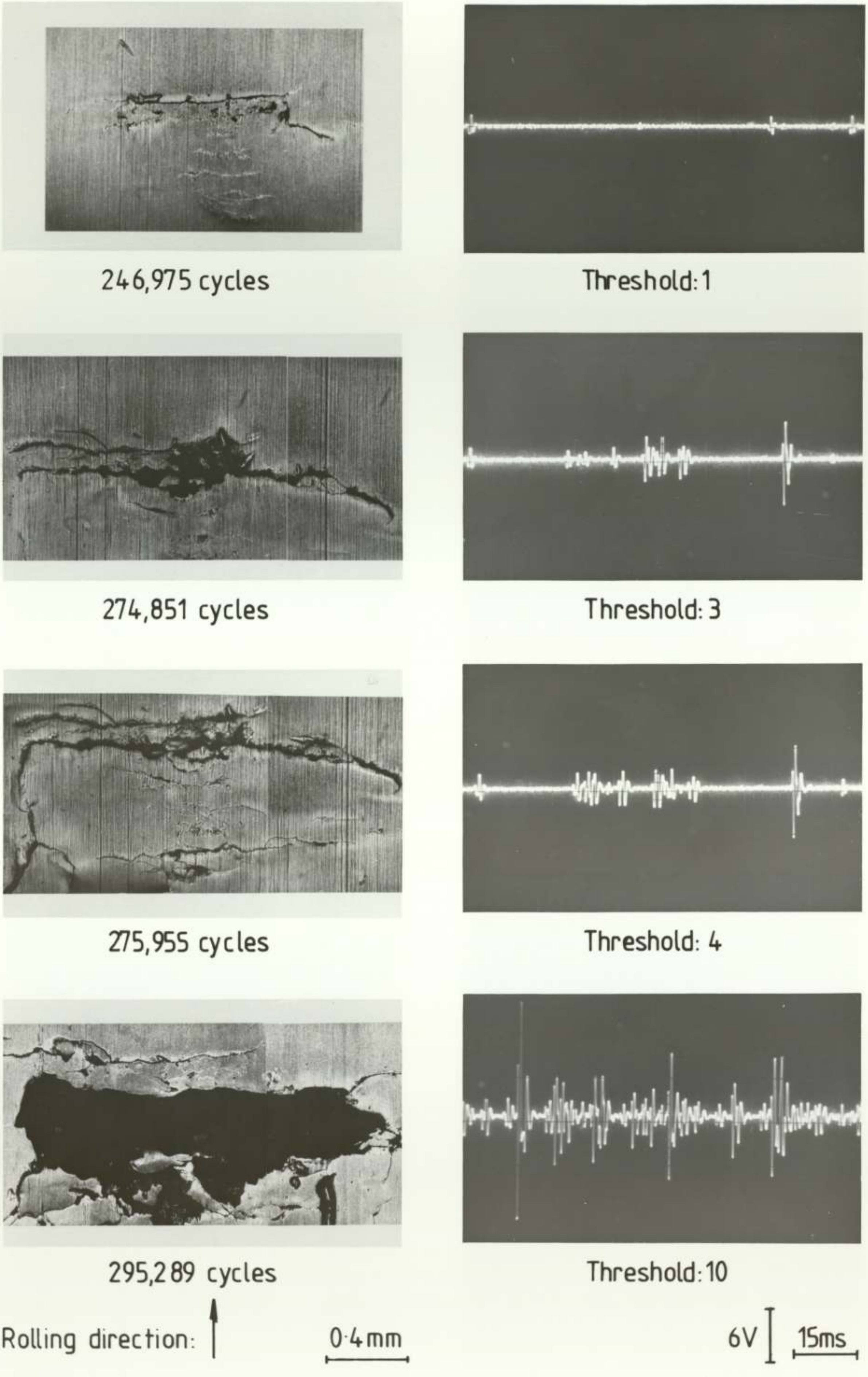

Figure 3·29. Crack propagation sequence at lubrication region: 3. (test lubricant B)

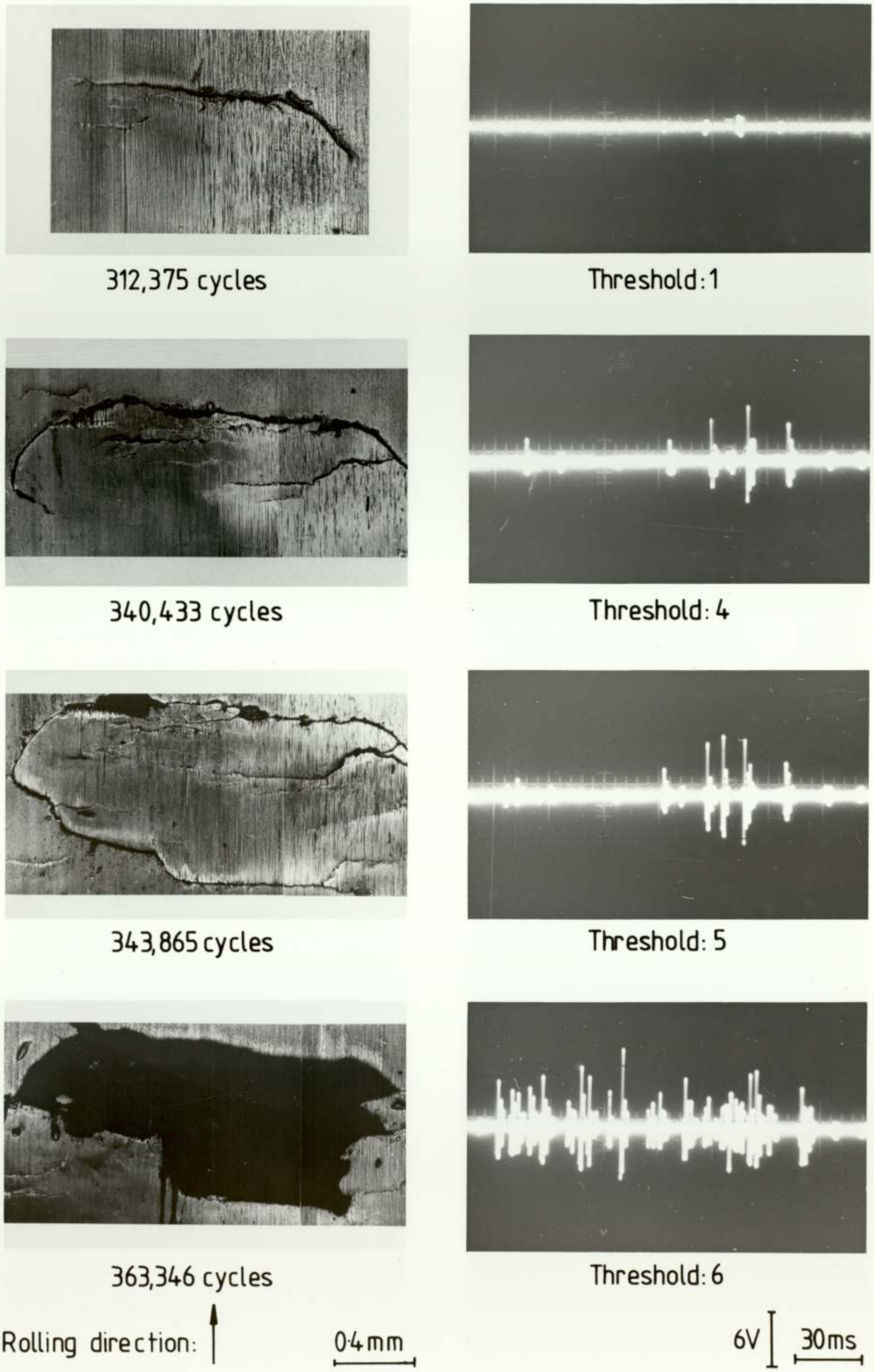

Figure 3·30. Crack propagation sequence at lubrication region 4a. (test lubricant D)

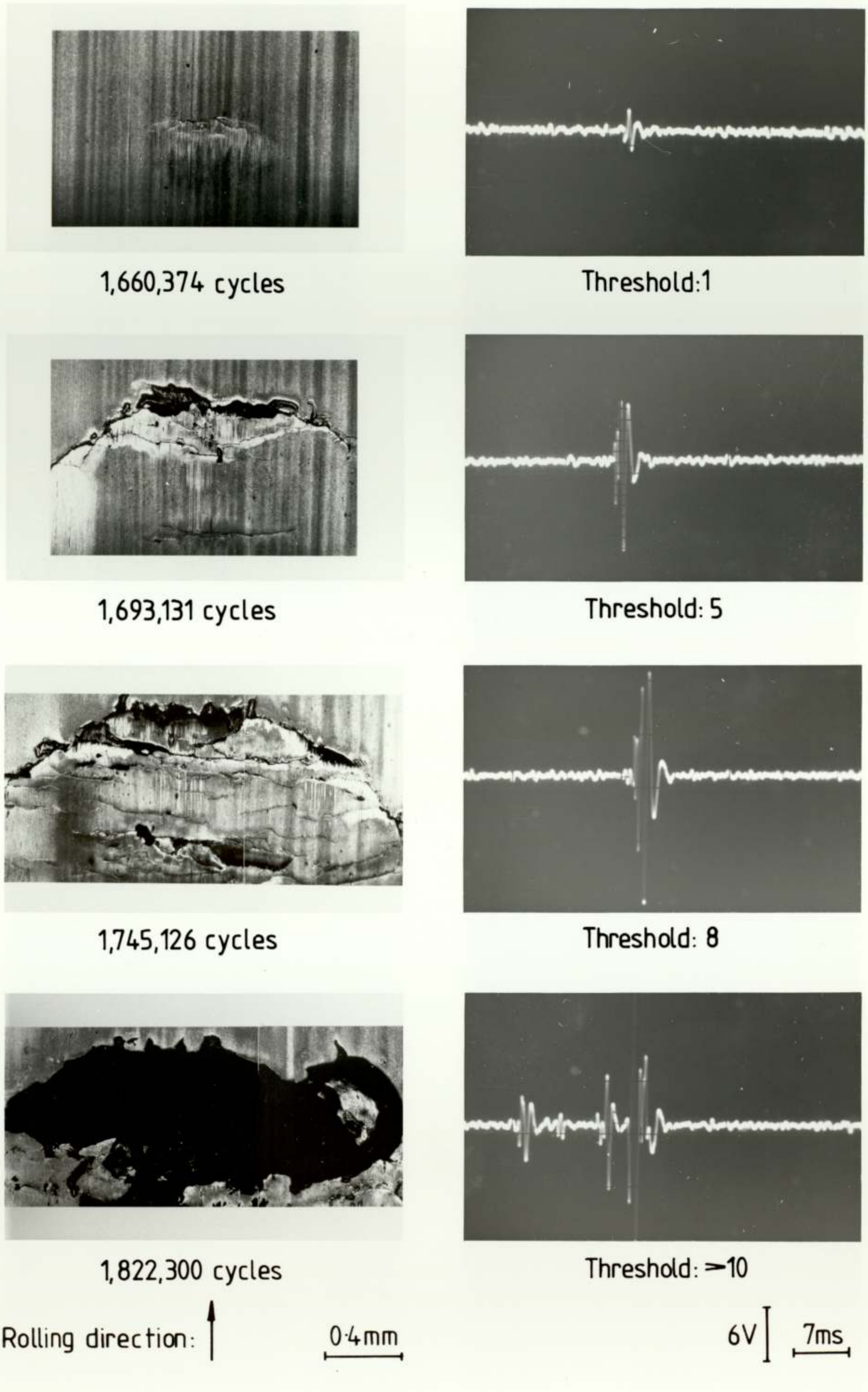

Figure 3·31. Crack propagation sequence at lubrication region 4b. (test lubricant B)

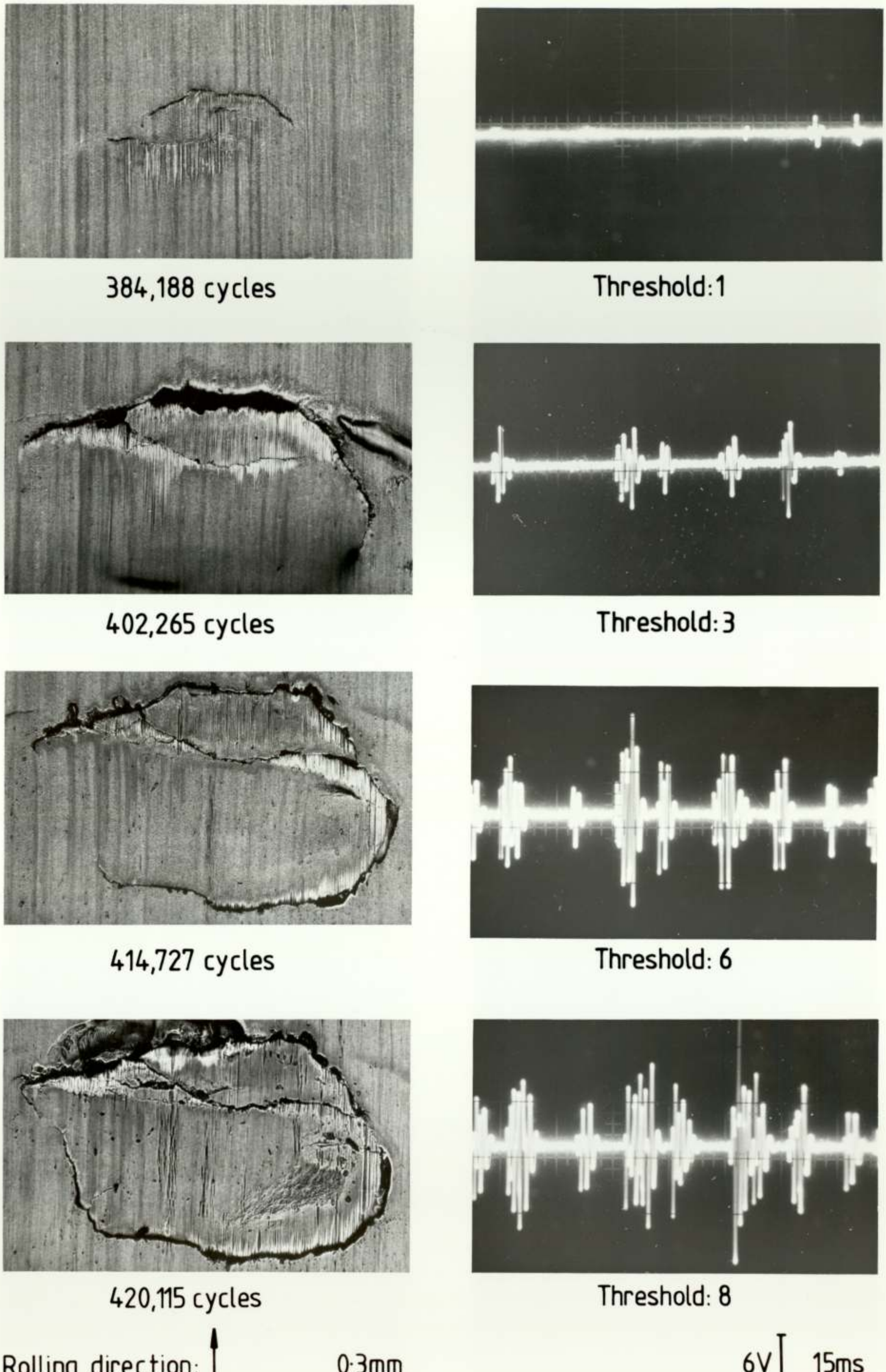

Figure 3·32. Crack propagation sequence at lubrication region 5. (test lubricant C)

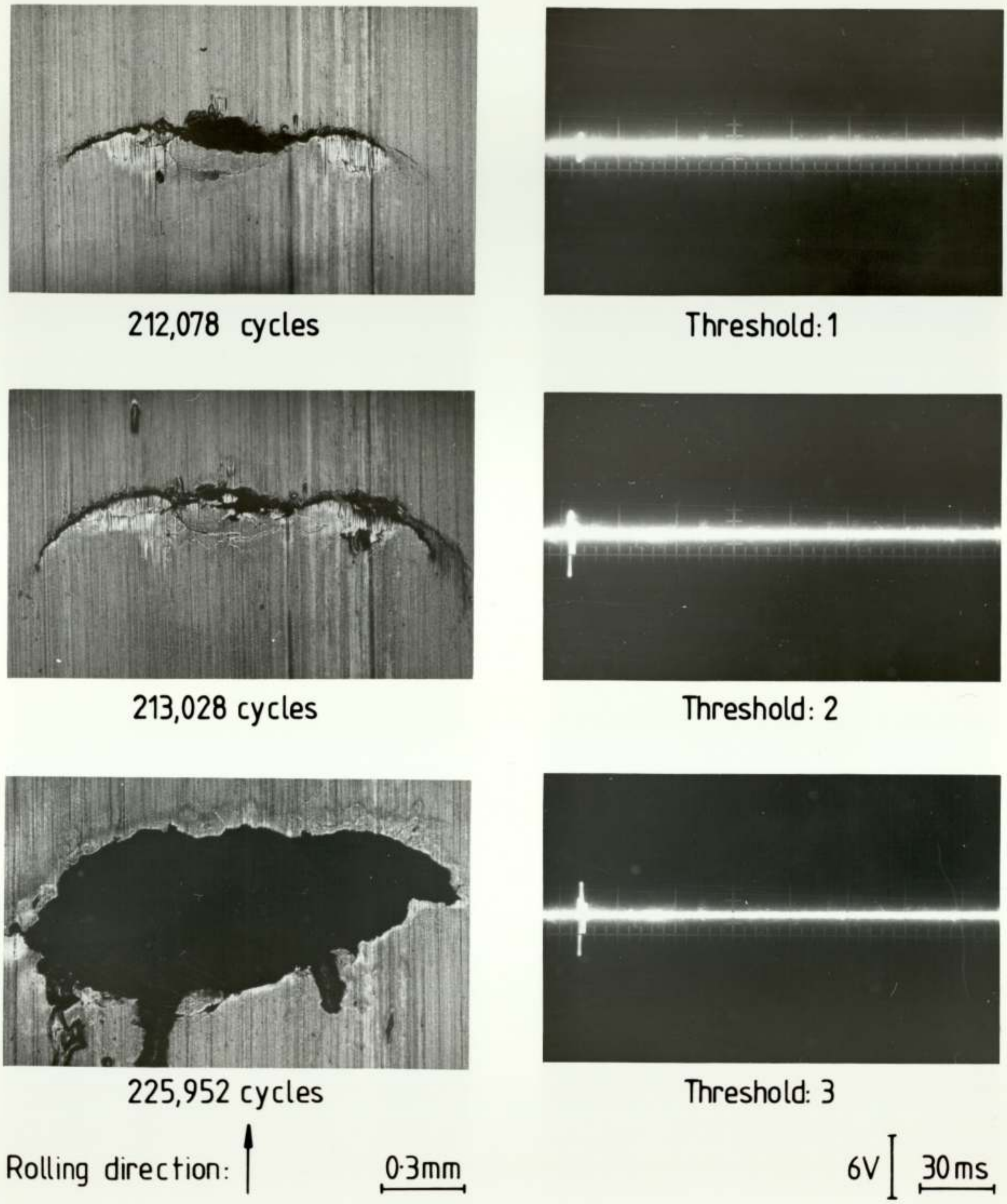

Figure 3·33. Crack propagation sequence at lubrication region 6. (test lubricant E)

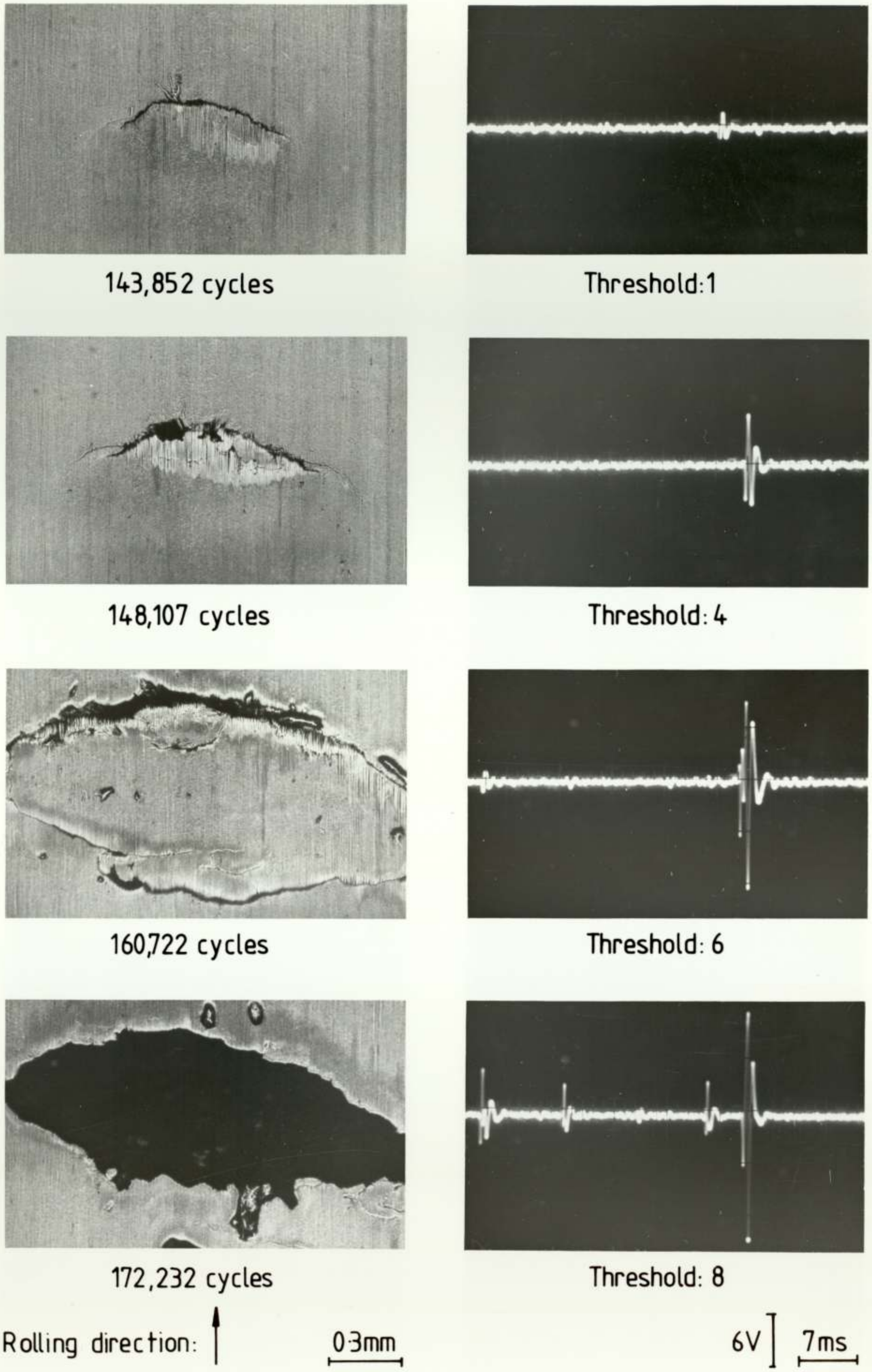

Figure 3·34. Crack propagation sequence at lubrication region 7. (test lubricant D)

391,914 cycles

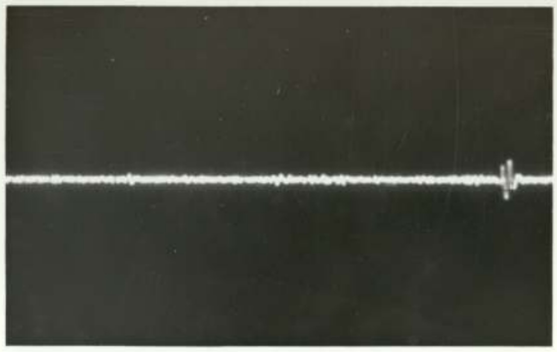

Threshold: 1

401,487 cycles

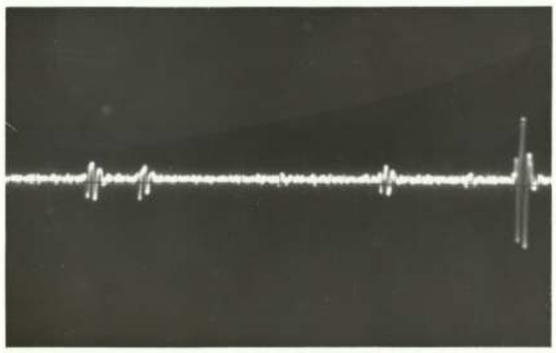

Threshold: 2

Rolling direction: ↑ 0·3mm

3V 15ms

Figure 3·35. Crack propagation sequence at lubrication region 8. (test lubricant E)

$0.03\mu m$ (Figures 3.28 to 3.32) a very large, randomly shaped pit was produced often exceeding 2.5mm in length and sometimes covering the complete width of the disc surface. There was a significant reduction in size when pits were produced under less severe conditions of lubrication. Pits formed in these regions (Figures 3.33 to 3.35) tended to be more uniform and exhibit a characteristic oval shape, never exceeding 1.5mm in length. Table 3.6 gives the average dimensions for the pit profiles taken at the respective regions of lubrication.

Lubrication Region	Without Additive		With Additive	
	Length(mm)	Width(mm)	Length(mm)	Width(mm)
2	1.60	0.72	-	-
3	1.92	0.88	0.47	0.63
4a	1.90	0.83	-	-
4b	2.06	1.04	0.95	0.95
5	1.63	0.88	-	-
6	1.39	0.50	0.90	0.55
7	1.43	0.74	-	-
8	0.92	0.62	1.31	0.82

Table 3.6. Average Amsler 2-disc pit geometries.

For test lubricants containing the antiwear additive a similar series of photomicrographs is given in Figures 3.36, 3.37, 3.38 and 3.39. Again, pits were formed by the propagation of the crack, but more important than this was the fact that the overall pit shape and size was independent of the lubrication conditions and was generally much smaller than

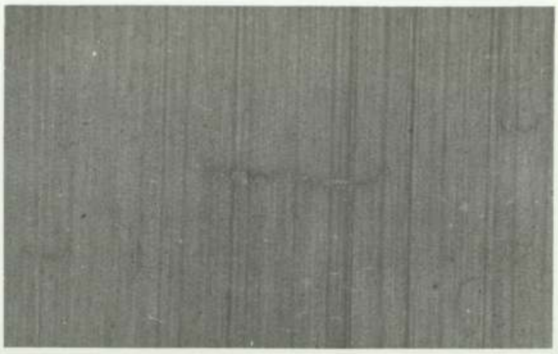

565,781 cycles

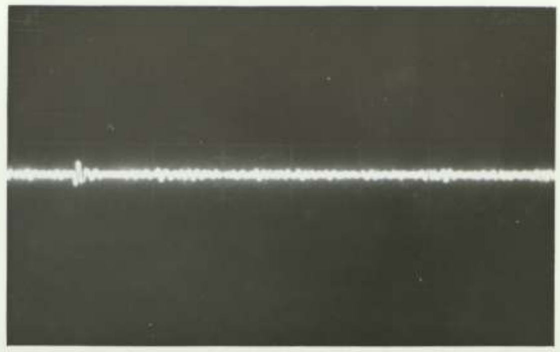

Threshold: 1

602,316 cycles

Threshold: 3

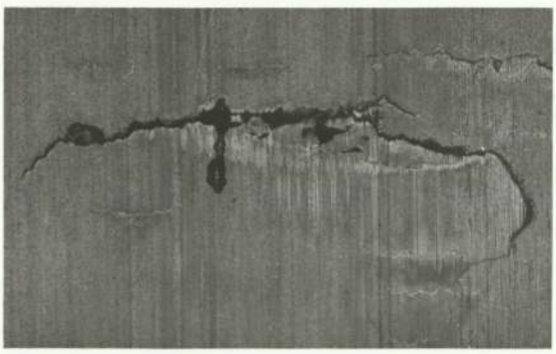

625,284 cycles

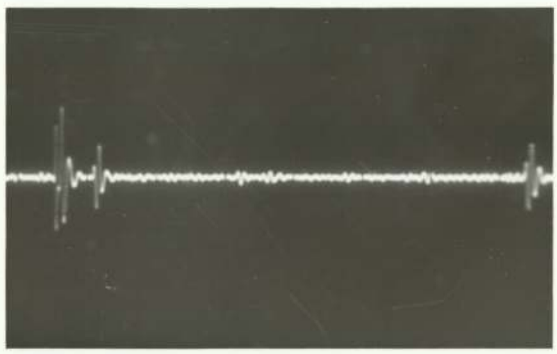

Threshold: 4

656,284 cycles

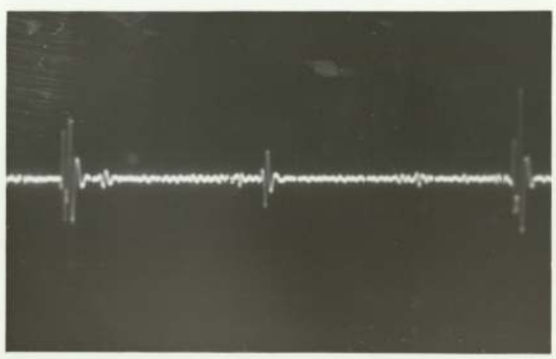

Threshold: 8

Rolling direction: ↑ 0·3mm 6V 15ms

Figure 3·36. Crack propagation sequence at lubrication region 3. (test lubricant F)

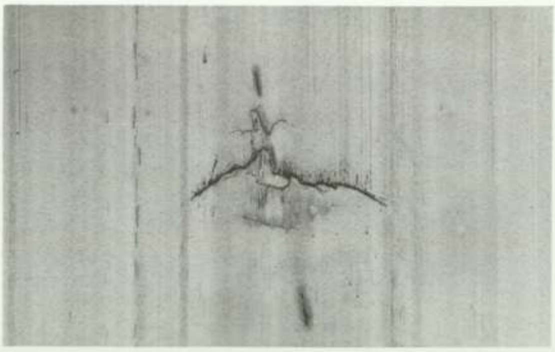

2,502,820 cycles

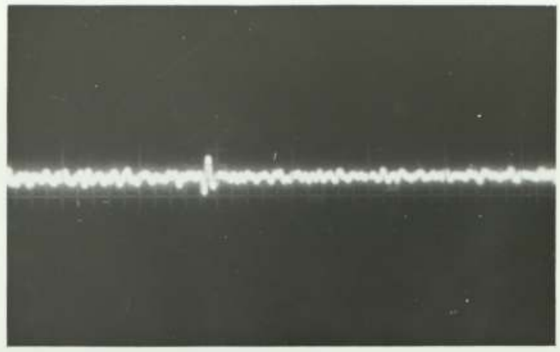

Threshold: 1

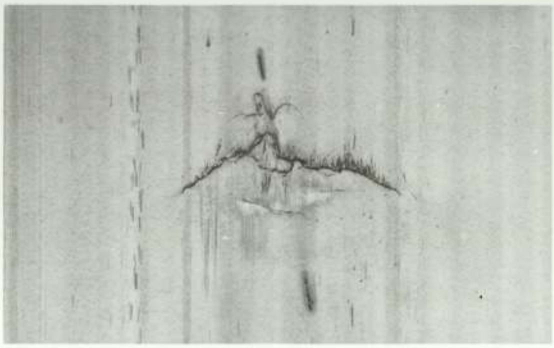

2,504,423 cycles

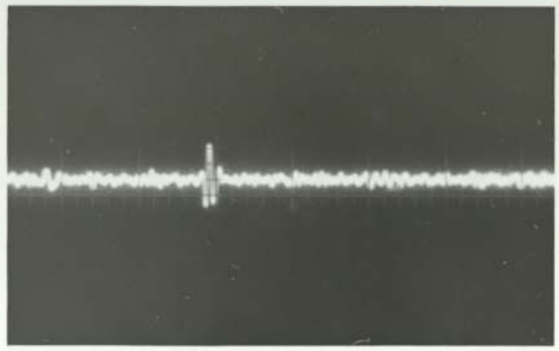

Threshold: 2

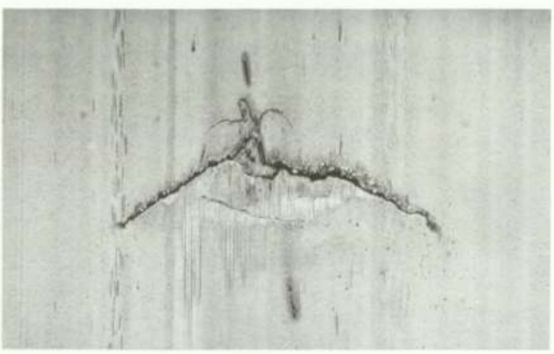

2,506,850 cycles

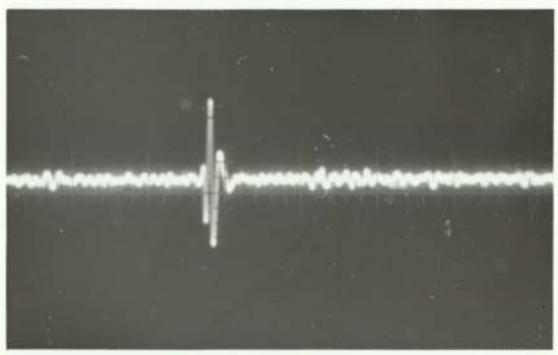

Threshold: 4

2,514,485 cycles

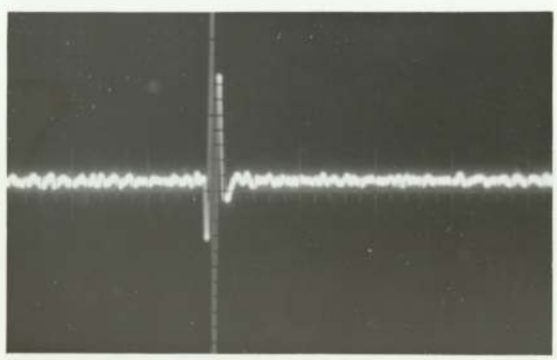

Threshold: 6

Rolling direction: ↑ 0·3mm 6V 7ms

Figure 3·37. Crack propagation sequence at lubrication region 4b. (test lubricant F)

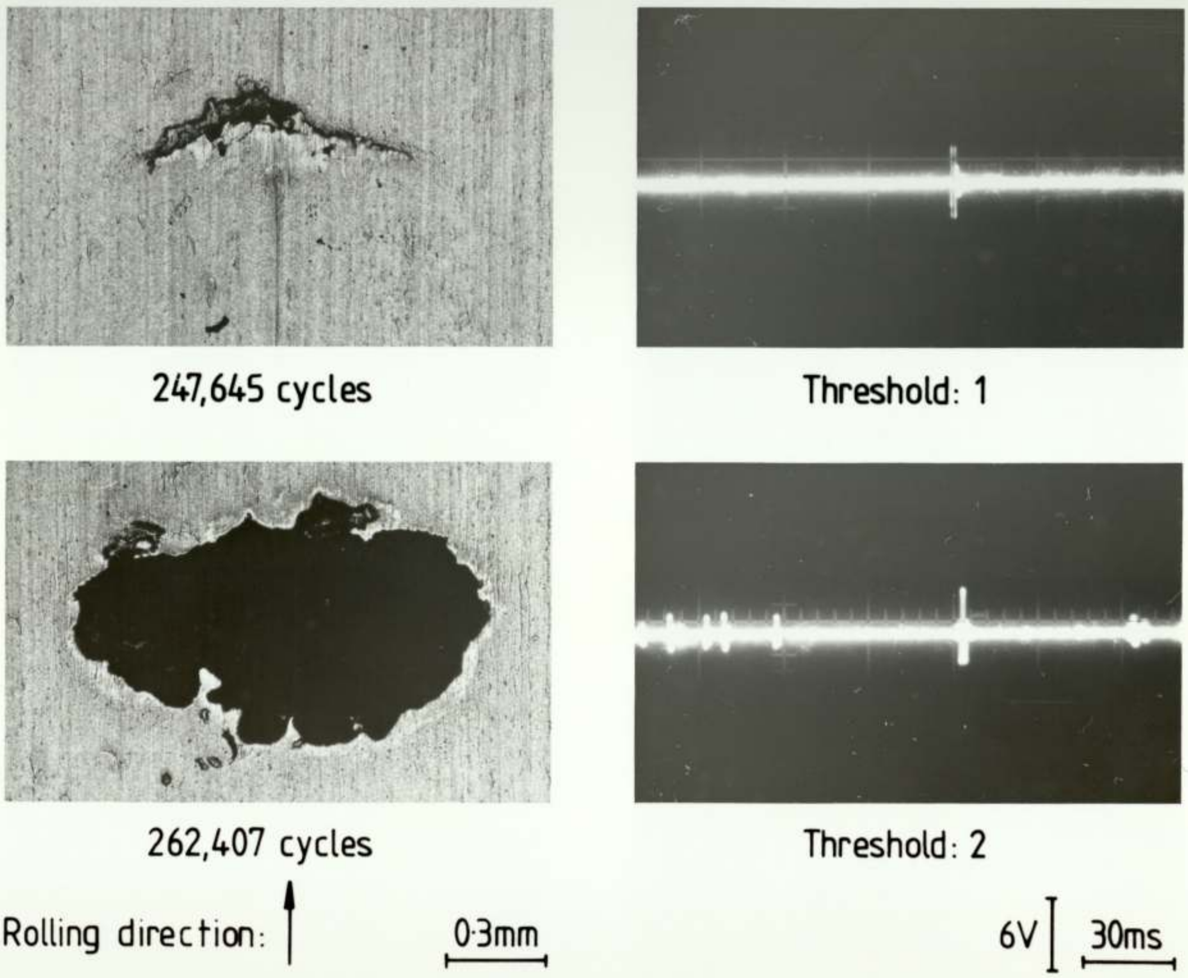

Figure 3·38. Crack propagation sequence at lubrication region 6. (test lubricant G)

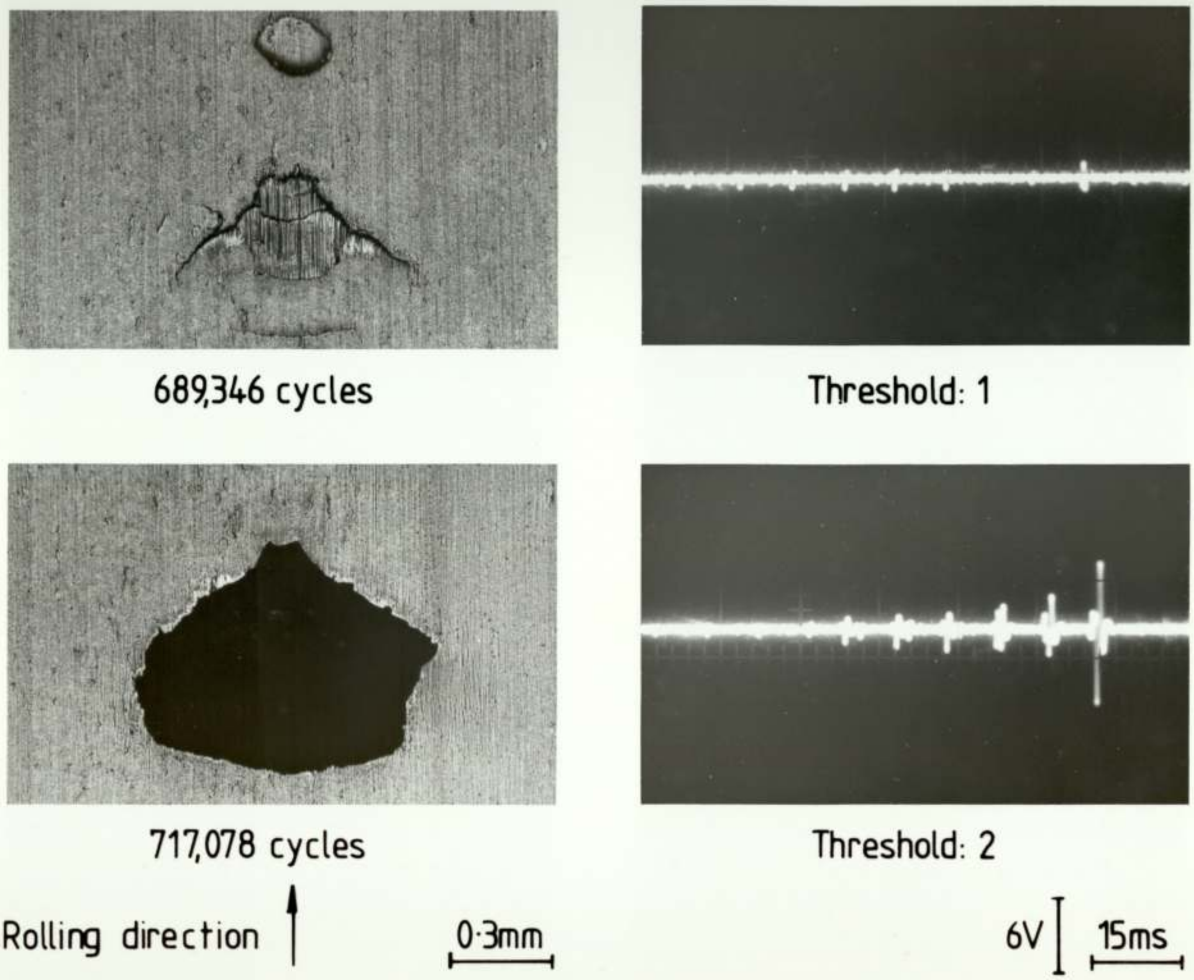

Figure 3·39. Crack propagation sequence at lubrication region 8. (test lubricant G) the corresponding pit formed with test lubricants not containing the additive. The overall amount of additional damage associated with the final pit formation was extremely low and was essentially independent of fluid film thickness. The respective pit dimensions for these experiments have also been included in Table 3.6.

Upon inspection of the discs, the additional crack detector signals could quite often be related to indentations caused by the momentary trapping of the pit fragment at the conjuction. This phenomenon can obviously occur at any lubrication region but was more difficult to detect at severe conditions when test lubricants not containg the antiwear additive were employed. Cracks forming at independent locations around the disc can be inadvertantly accelerated into pits by the severe rupture of an original pit fragment often resulting in the simultaneous appearance of two or even three pits.

Not all original cracks propagated to form pits as can be seen in Figure 3.32. Here a crack has been detected and is progressing in the regular manner, however, at Threshold Level 6 the machine was automatically shut down by a signal arising from another crack situated in the first half of the disc. Because the crack detector could not distinguish between particular cracks but only the maximum signal, the automatic shutdown procedure between threshold levels 6 and 7 was dominated by the second crack. Final pit formation was due to yet another crack as can be seen by the large amplitude of the relevant signal.

Pitting did not occur in either the boundary region 1 or in the hydrodynamic region 9 although tests were run for a substantial period. Figure 3.40 shows disc surfaces taken from region 1 and 9 after being run with Test Lubricants B and E respectively. The corresponding detector traces are shown in Figure 3.40.5.

The surfaces are of course quite different, those taken from experiments conducted in the boundary region 1 appear to be very rough and detector traces indicate many small cracks. The cracks were, in the main, quite shallow and never resulted in the formation of a pit. Final surface roughness values were of the order of 0.07μm CLA, indicating an overall smoothing of the surface from the initial surface roughness of 0.25μm CLA. In contrast, the surfaces from the hydrodynamic region 9, were much smoother in appearance with a correspondingly smooth detector trace indicating that no surface or subsurface cracks were present. The final surface roughness measurement was 0.025μm CLA.

Figure 3.41 gives a general surface view of discs run with the antiwear additive at Lubrication Regions 1 and 9. Again, there was a difference in surface topography between the two regions. Under boundary conditions there was an increase in surface roughness to 0.25μm CLA compared to the initial value of 0.20μm CLA. This differs from the reduction in surface roughness experienced for similar conditions with Test Lubricant B (not containing the antiwear additive).

Final surface roughness values and overall appearance of the surfaces taken at hydrodynamic region 9 were similar to those obtained with test lubricants containing no antiwear additive.

Lubrication region 1

Rolling direction: ↑ 0·3mm

Lubrication region 9

Rolling direction: ↑ 0·3mm

Figure 3·40. Surface view of the non-pitted discs after running at the two extreme regions of lubrication without the antiwear additive.

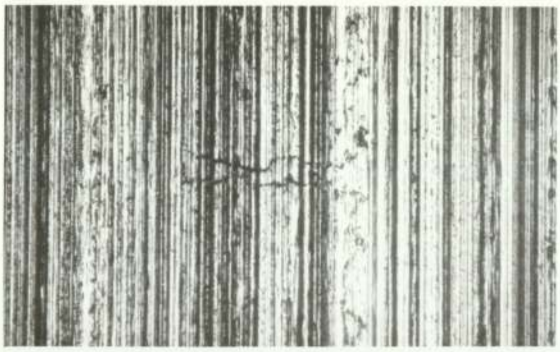

Lubrication region 1

Rolling direction: ↑ 0·3mm

Lubrication region 9

Rolling direction: ↑ 0·3mm

Figure 3·41. Surface view of the non-pitted discs after running at the two extreme regions of lubrication with the antiwear additive.

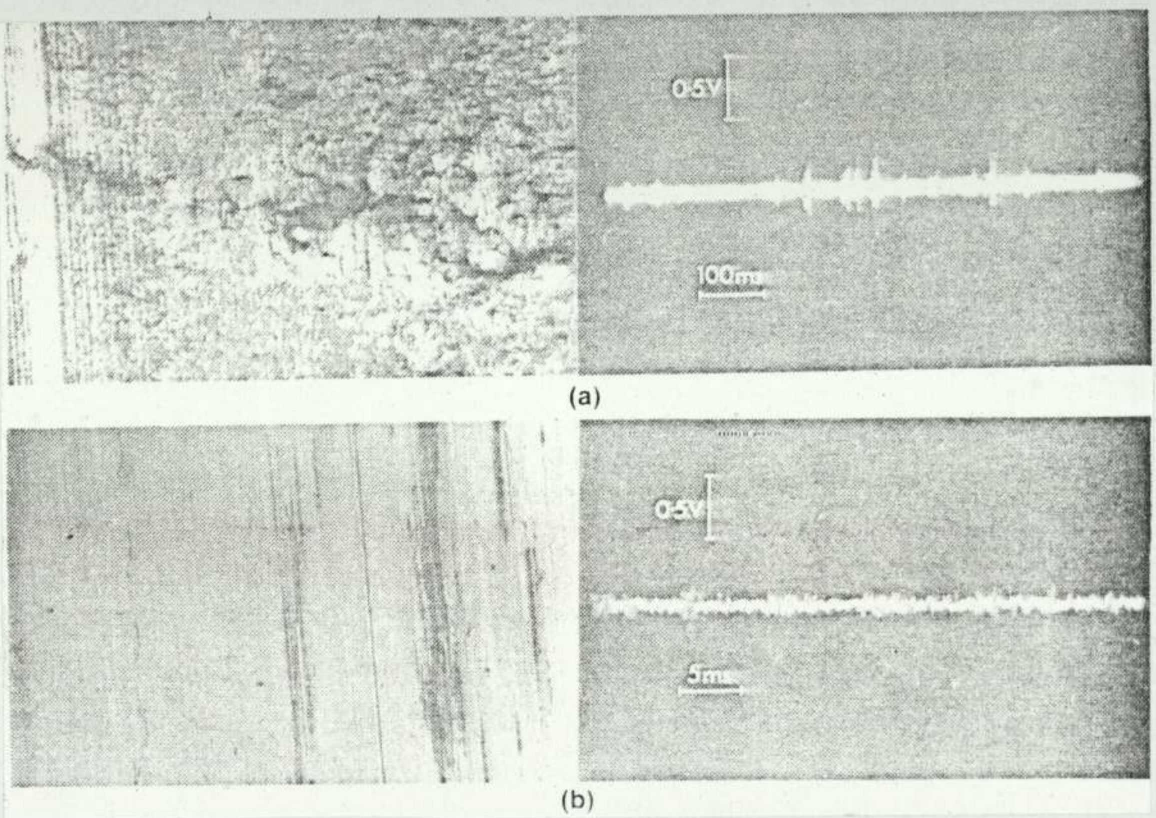

FIGURE 3.40.5. Surface view of the nonpitted surfaces after running at Lubrication Regions 1 (a) and 9 (b) with the corresponding detector traces.

The only other region where pitting did not occur was that of Lubrication Region 2 conducted with Test Lubricant F containg the antiwear additive. Runs were conducted in excess of 11 x 10^6 cycles before being terminated. The overall appearance of the disc surface was similar to that shown in Figure 3.41 but with a final surface roughness of 0.04μm CLA.

3.5. Metallography and Scanning Electron Microscopy

3.5.1. Unisteel Test Specimens

Selected used specimens were cut according to Figure 2.11a). Figure 3.42a) shows the transverse section of the wear trace with cracks running from the bottom of the pit downwards into the bulk of the used thrust washer. cracks are also propagating from the left hand side of the pit. Figure 3.42b) has cracks propagating from either side of the pit indicating an evenly distributed load. Pit depths were 80μm and 50μm respectively. Longitudinal sections can be seen in Figures 3.42c) and 3.42d), here both sections show complex crack patterns. The branching crack in Figure 3.42c) has spread downwards whereas the crack propagating from the pit in Figure 3.42d) has turned back on itself. The slope is also very interesting as it shows a distinction between the two sides and consequently, the rolling direction may be determined. It must be remembered, however, that the rolling direction in this case refers to the motion of the race and is opposite to that of ball rotation when in contact with the thrust washer.

3.5.2. Rolling Four-ball Test Specimens

Figure 3.43 shows a sectioned failed top ball cut

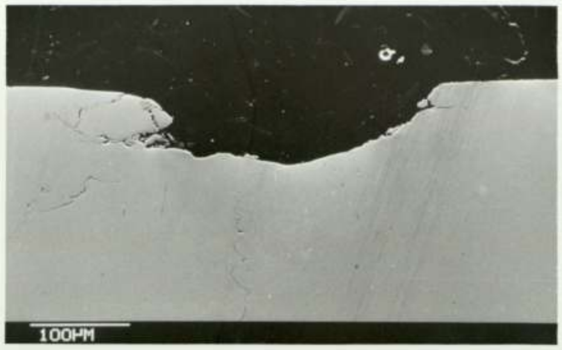

a) Transverse section (pit formed after 12·6 hours)

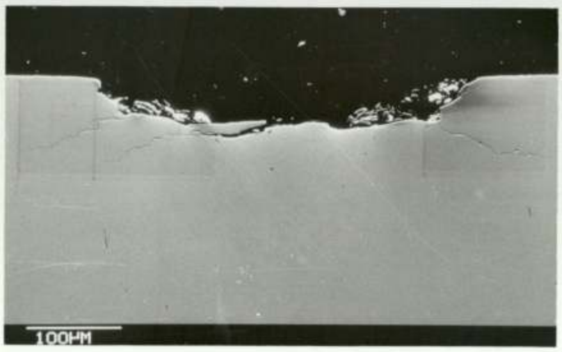

b) Transverse section (pit formed after 16·6 hours)

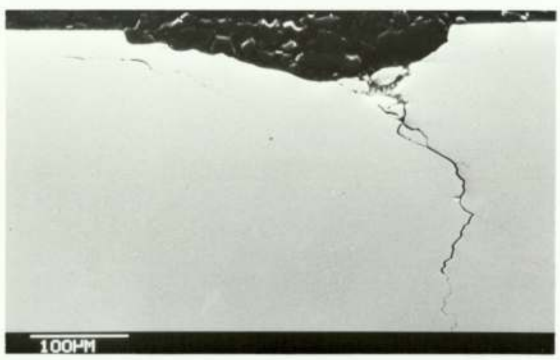

c) Longitudinal section (pit formed after 25·4 hours)

d) Longitudinal section (pit formed after 27·5 hours)

Figure 3·42. Typical cross sections of selected pits from the Unisteel experiment. (Run with test lubricant D)

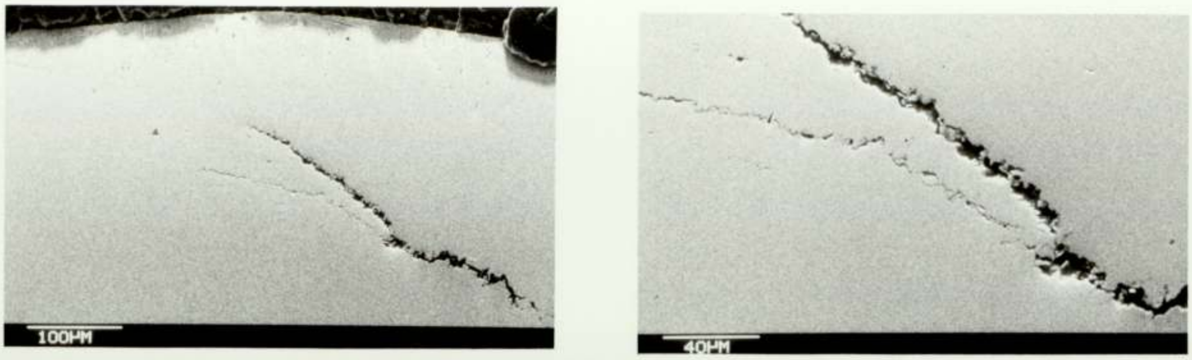

a) b)

Rolling direction: ←

Figure 3·43. Sectioned top ball from the Rolling Four Ball pitting test (after 36 minutes with test lubricant E).

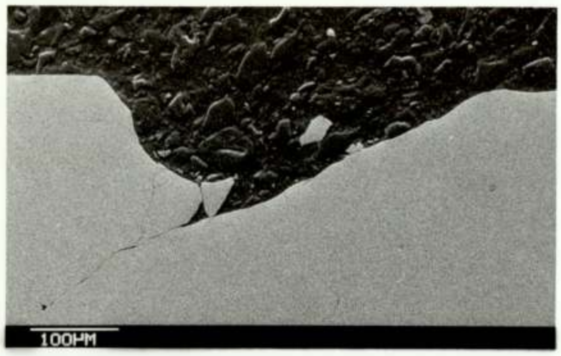

Lubrication region 3

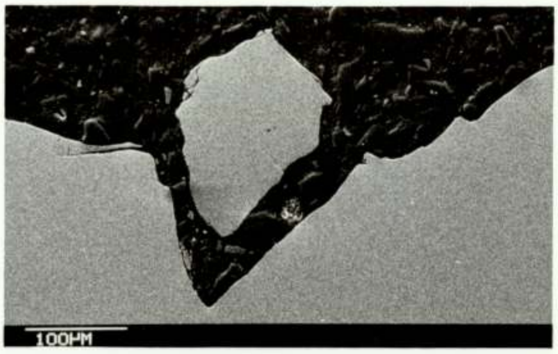

Lubrication region 4b

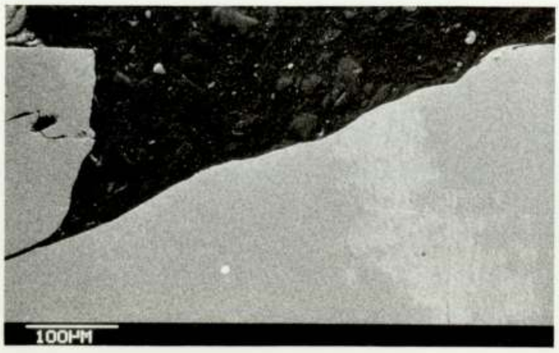

Lubrication region 6

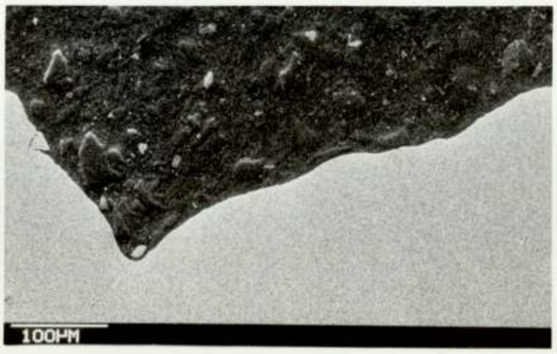

Lubrication region 8

Rolling direction: →

Figure 3·44. Typical cross sectioned pits run at the various lubrication regions with the antiwear additive.

according to Figure 2.11b). A crack of approximate length 0.6mm can be seen propagating in the path of an arc towards the centre of the ball and serves as an illustratioin, further emphasising the severe nature of the Rolling four-ball test. Such metallurgical sectioning has shown that cracks can propagate inwards to the centre of the ball, but not enough work has been carried out to reach any meaningful conclusions.

3.5.3. Amsler 2-disc Test Specimens

After each run the pitting discs were circumferentialy sectioned according to Figure 2.11c) to reveal subsurface damage and to investigate pit profiles. Figure 3.45 shows typical cross sections taken from the various lubrication regions investigated when run without the antiwear additive. All pit sections (Figure 3.45) have a characteristic triangular configuration and in general the cracks leading to the formation of pits appear at well defined angles of about 20 to 30° to the surface. Pit geometries measured directly from the Scanning electron microscope have been averaged at each lubrication region and are given in Table 3.7.

On inspection, it can be deduced that for experiments conducted at relatively thick film conditions (greater than 0.04μm - Lubrication Regions 6, 7 and 8) a tendency exists for crack penetration angles to be steeper than those obtained at thinner lubricant film conditions. No correlation between pit depth and fluid film thickness was obtained, although certain results taken at Lubrication Regions 2 and 4b would suggest that pits of a greater depth were formed at thinner film conditions.

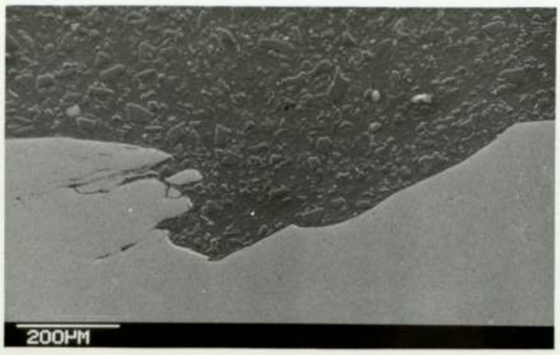

Lubrication region 2

Lubrication region 3

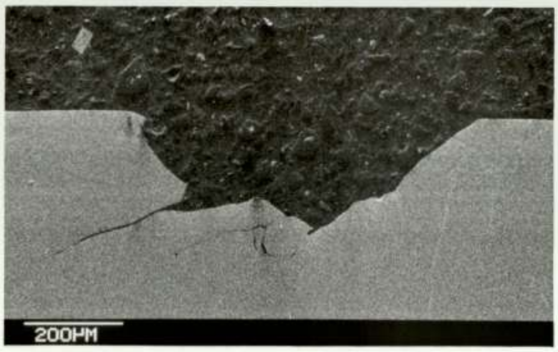

Lubrication region 4a

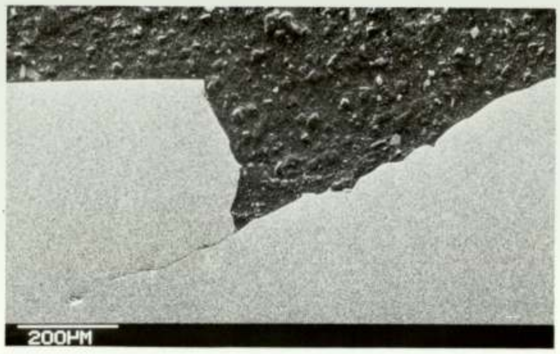

Lubrication region 4b

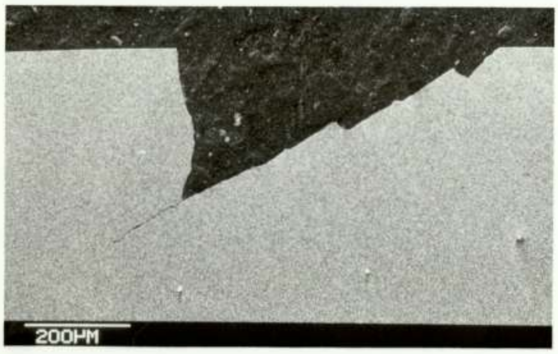

Lubrication region 5

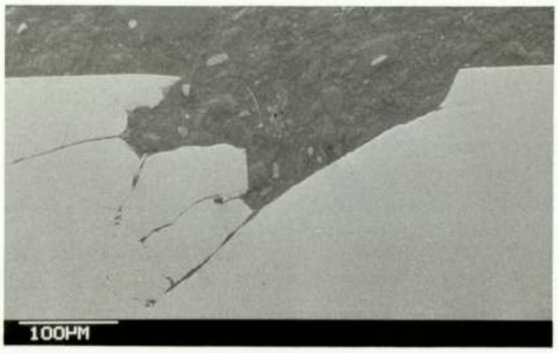

Lubrication region 6

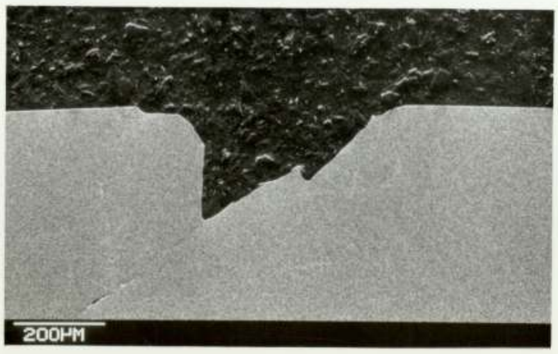

Lubrication region 7

Lubrication region 8

Rolling direction: ⟶

Figure 3·45. Typical cross sectioned pits run at the various lubrication regions without the antiwear additive.

Lubrication Region	Without Additive			With Additive		
	Depth(mm)	Angle(o)	S	Depth(mm)	Angle(o)	S
2	0.31	23	3.3	-	-	-
3	0.27	20	2.6	0.17	26	3.4
4a	0.22	18	3.4	-	-	-
4b	0.41	28	2.6	0.27	32	3.5
5	0.25	26	3.7	-	-	-
6	0.15	32	2.3	0.18	25	2.7
7	0.24	30	2.2	-	-	-
8	0.22	28	2.4	0.26	21	2.5

**Table 3.7. Pit depths and crack penetration angles.
S : Standard deviation.**

For experiments conducted using the antiwear additive pit profiles similar to those previously described were observed and are presented in Figure 3.44. It would appear that there is no relationship between pit depth or crack penetration angle with fluid film thickness.

To show the pit in perspective, Scanning electron micrographs were taken for selected pits run without the antiwear additive at Lubrication Regions 3 and 6, and are respectively given in Figures 3.46 and 3.47. Figure 3.46a) shows a well developed pit within the boundaries of the disc surface, the rolling direction being from right to left. Figure 3.46b) gives the same pit but at a higher magnification and reveals a difference in final surface finish between the internal sides of the pit. The triangular pit profile can also be seen with a smooth, gradual slope on the left hand side and a much steeper, rough appearance on the right hand

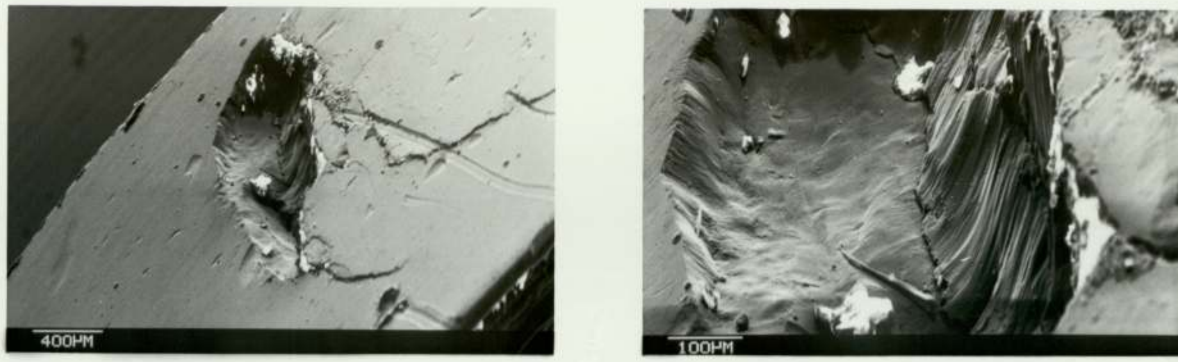

a) b)

Rolling direction: ⟵

Figure 3·46. Perspective view of a pit formed at lubrication region 3. (without additive)

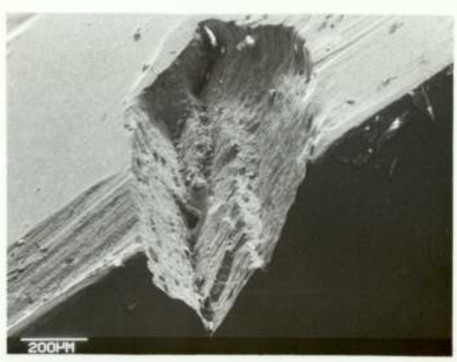

Rolling direction: ⟶

Figure 3·47. Cross sectioned view of a pit formed at lubrication region 6 (without additive).

side. The triangular configuration can best be observed with an unusually sectioned pit shown in Figure 3.47. The rolling direction in this micrograph is from left to right.

Circumferential sections taken from the non-pitted discs, run at boundary region 1, using test lubricants with and without the antiwear additive are respectively given in Figures 3.48b) and 3.48a). Both figures show subsurface damage in the form of cracks running almost parallel to the surface and within a depth of 20μm, although the degree of actual damage appears to be greater for discs run without the antiwear additive (Figure 3.48a)).

Circumferential sections taken from discs run in the hydrodynamic region 9, revealed that no subsurface damage was present.

Discs run with Test Lubricant B at Lubrication Region 3 were removed for sectioning after the formation of the first detectable crack, defined by Threshold Level 1 of the crack detector. Figure 3.49a) gives a typical surface view and Figure 3.49b) shows the sectioned view taken through the crack. At this stage, after 285,000 cycles, the crack was well established and was seen leading into the bulk of the material. Measurements show that the crack begins to level out at a subsurface depth of about 220μm and it is not unreasonable to assume that if the disc had been allowed to continue, a pit of similar depth would have resulted.

Figure 3.50 shows a probable subsurface initiated crack having not yet broken through the surface. Cracks at this particular stage in life were extremely rare and only found on discs especially sectioned to observe other Threshold

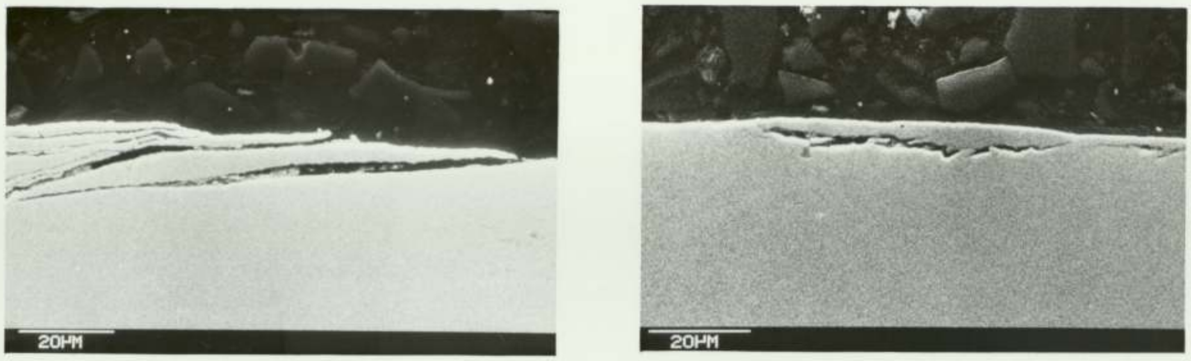

a) Without additive b) With additive

Rolling direction: →

Figure 3·48. Circumferential sections taken from the non-pitted discs run at lubrication region 1.

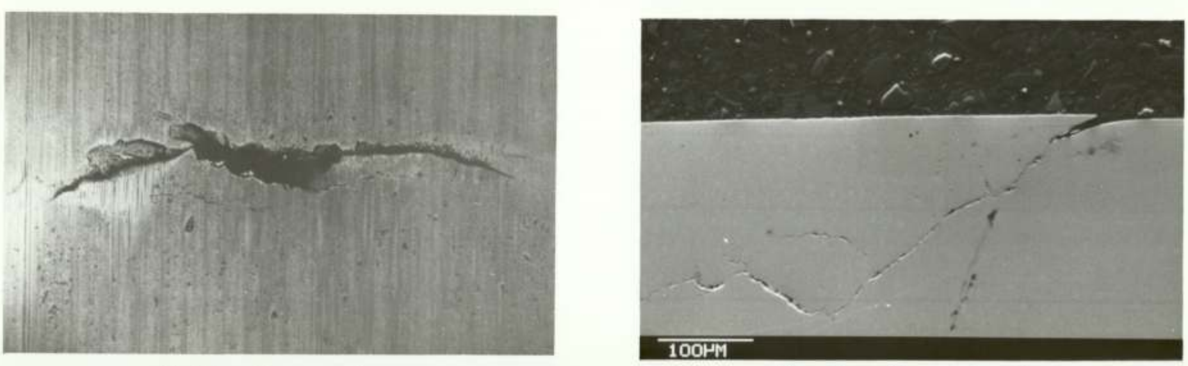

a) Surface view

Rolling direction: ↑

b) Sectioned view

Rolling direction: →

Figure 3·49. Threshold "1" crack obtained at lubrication region 3 (without additive)

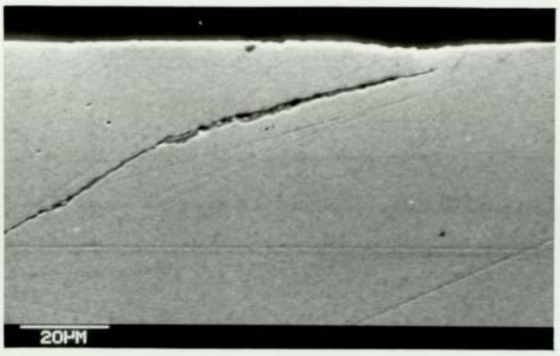

Rolling direction: ⟶

Figure 3·50. Subsurface initiated crack formed after 285,000 cycles obtained at lubrication region 3 (without additive).

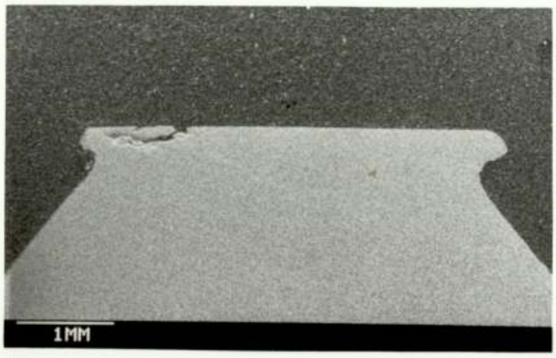

a)

b)

Figure 3·51 Section of disc surface taken after 288,000 cycles at lubrication region 1·1 (with additive).

Level 1 cracks. The crack is either propagating to, or from a depth of about 140μm, which is approximately the depth of maximum shear.

Figure 3.51a) shows a metallurgical section taken across the surface of the disc perpendicular to the rolling direction and shows the effect of surface contact pressure at boundary lubrication conditions. This disc was run under a load of 150kg for 288,000 cycles at a speed of 100rpm (Test Lubricant F, Lubrication Region 1.1). The calculated fluid film thickness was 0.0078μm. Plastic flow of metal has occurred on both sides of the track, increasing the track width from 3.4 to 4.4mm. Irregular shaped damage in the form of cracks can be seen to the left hand side of the disc and is shown at a greater magnification in Figure 3.51b). Pits formed under these conditions were very small and less well defined compared to those obtained at other lubrication regions.

3.6. Microhardness Measurements

Microhardness measurements were carried out on selected sectioned and polished test specimens taken from various lubrication regions. Each series consisted of determining the hardness of the metallographic cross-section at the surface and then every 20 to 25μm to a depth of 500μm. Microhardness values were then plotted as a function of depth as shown in the typical examples given in Figure 3.52. Most graphs were similar in profile, reaching a maximum hardness at some finite distance below the surface and diminishing towards the bulk hardness value at a subsurface depth greater than

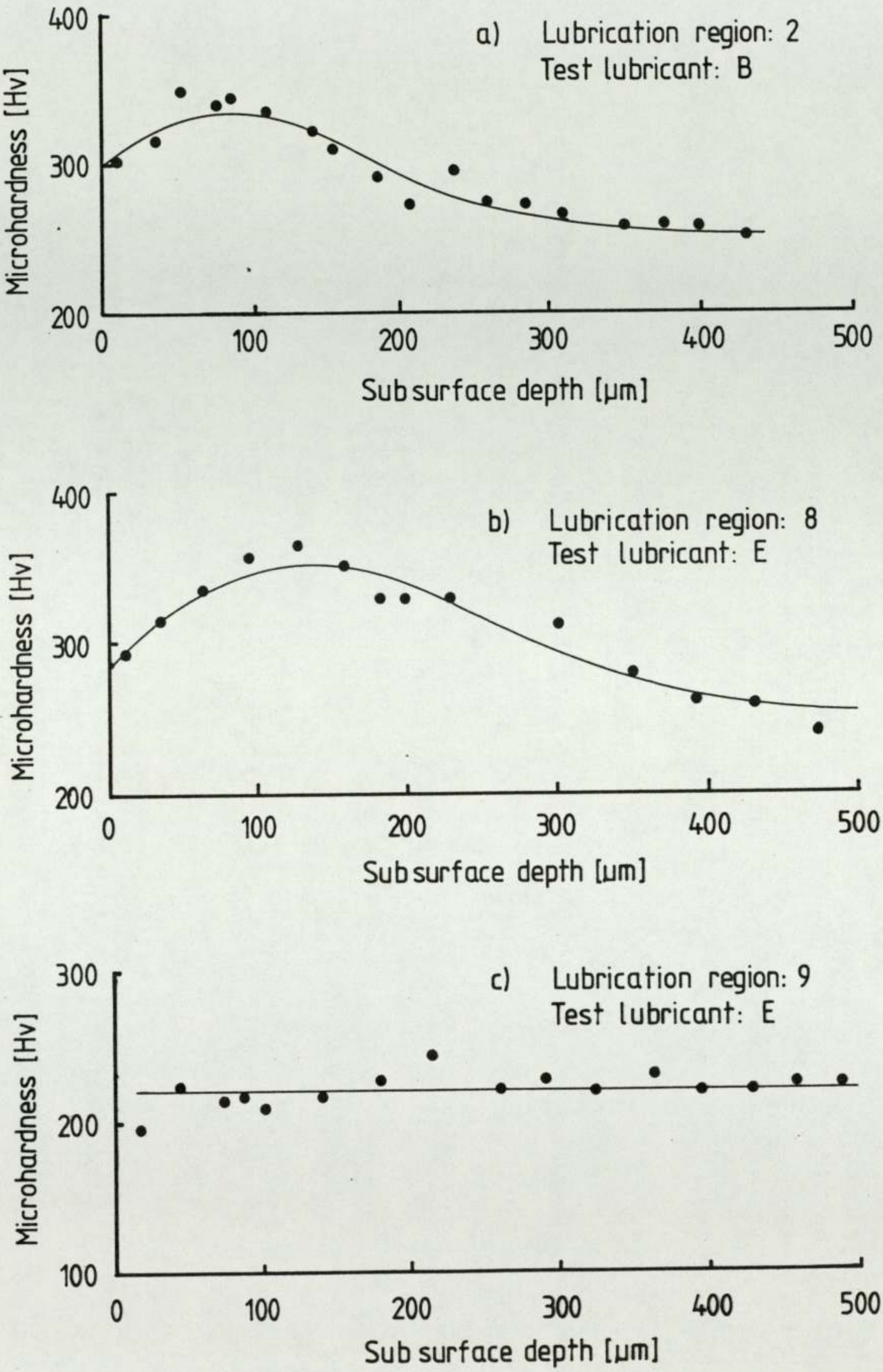

Figure 3·52. Typical examples of microhardness against subsurface depth for various lubrication regions.

500μm. Figure 3.52c) shows a typical profile obtained at hydrodynamic lubrication region 9. Here no maxima was observed and the hardness value remained constant with depth at a similar value to the bulk hardness. It was therefore necessary to define a maximum hardness and corresponding depth, and this is shown in Figure 3.53. Table 3.8 gives the average maximum hardness and depths for test specimens conducted at the various lubrication regions.

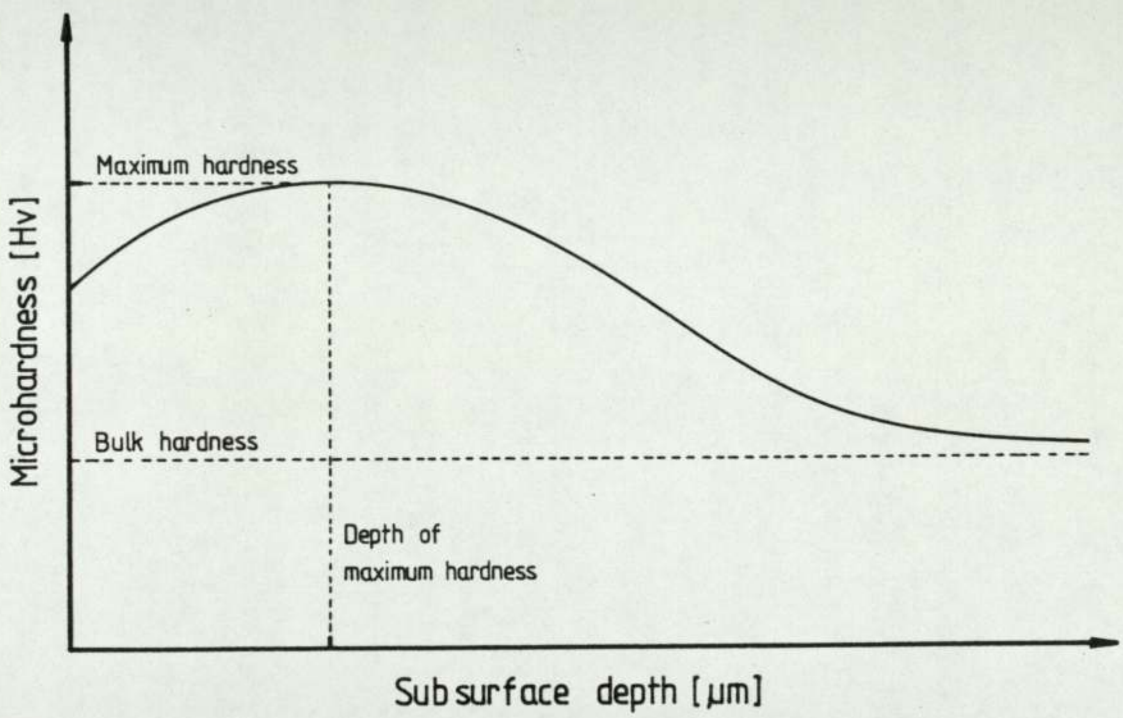

Figure 3·53. Defining the maximum microhardness and depth of maximum microhardness.

It can be seen that the maximum microhardness value obtained was about 100Hv greater than the bulk hardness of the steel and is fairly consistent throughout the lubrication regions. At Lubrication Regions 1, 2, 3, 6 and 8 the depth at which the maximum microhardness value was obtained increased with fluid film thickness but no respective correlation could be obtained for similar lubrication regions, when conducted with test lubricants containing the antiwear additive. The magnitude of the hardness values again remained fairly constant for the respective regions.

Lubrication Region	Without Additive		With Additive	
	Maximum Hardness (Hv)	Subsurface Depth (μm)	Maximum Hardness (Hv)	Subsurface Depth (μm)
1	342	66	-	-
2	338	88	222	140
3	329	100	330	123
6	330	140	290	110
8	330	144	322	158
9	220	Constant	-	-
1.1	-	-	376	92
2.1	-	-	396	180
2.2	-	-	394	164
2.3	-	-	384	160

Table 3.8. Maximum hardness and depths for pitting discs.

For experiments conducted with loads in excess of 90kg (Lubrication Regions 1.1, 2.1, 2.2 and 2.3) no relationship could be deduced although it is interesting to note that the magnitude of the hardness values is very much larger than the values obtained with the relatively lower load of 90kg. Maximum hardness is therefore dependant upon applied load.

3.7. AES Examination of Worn Pitting Disc Surfaces

Auger Electron Spectroscopy was employed to identify surface elements and chemical compositions of the pitting discs. A maximum of four discs were selected from each of the regions of lubrication and subsequently sectioned for examination. Auger traces were obtained for each disc surface during a total ion etching period of 240 minutes. Altogether nine Auger traces were obtained, the cumulative times of which are shown in section 2.11.4. Figures 3.54a) and 3.54b) show typical differentiated Auger spectra recorded after 1, 60, 180 and 240 minutes total etch, for disc surfaces run at Lubrication Region 4b with Test Lubricant B and F respectively.

Qualatative analysis showed that carbon, oxygen and iron were present at all etch times and are represented in Figures 3.54a) and 3.54b) by the respective Auger peaks occurring at 272, 503 and 703eV. Argon (215eV), used for ion etching, was detected after the first one minutes etch and the concentration remained fairly constant throughout further Auger traces. Chromium (529eV) was also detected, but only after a total etch period of about five minutes, and again remained fairly constant throughout subsequent Auger traces.

Quantitative information was extracted from the Auger spectra which allowed each element to be expressed as a percentage of all elements present. Percentage concentrations were calculated from the following equation:

$$\text{Concentration}(x) = \frac{E(x) \times S(x)}{\sum_{a=1}^{a=n} (E(xa) \times S(xa))} \times 100\% \qquad 3.15$$

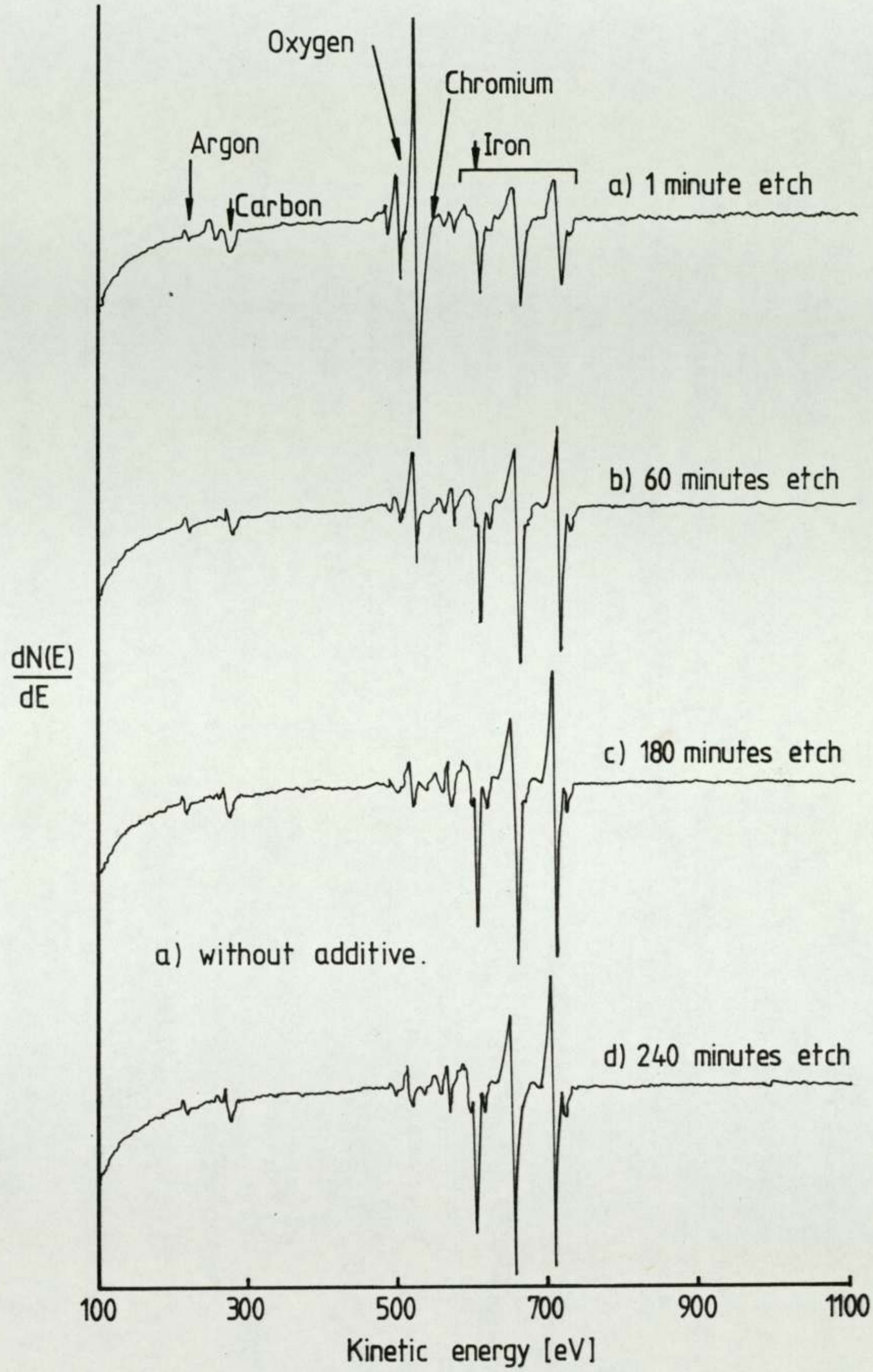

Figure 3·54. Differentiated Auger spectra taken from disc surfaces run at lubrication region 4b a) without the antiwear additive b) with antiwear additive (next diagram).

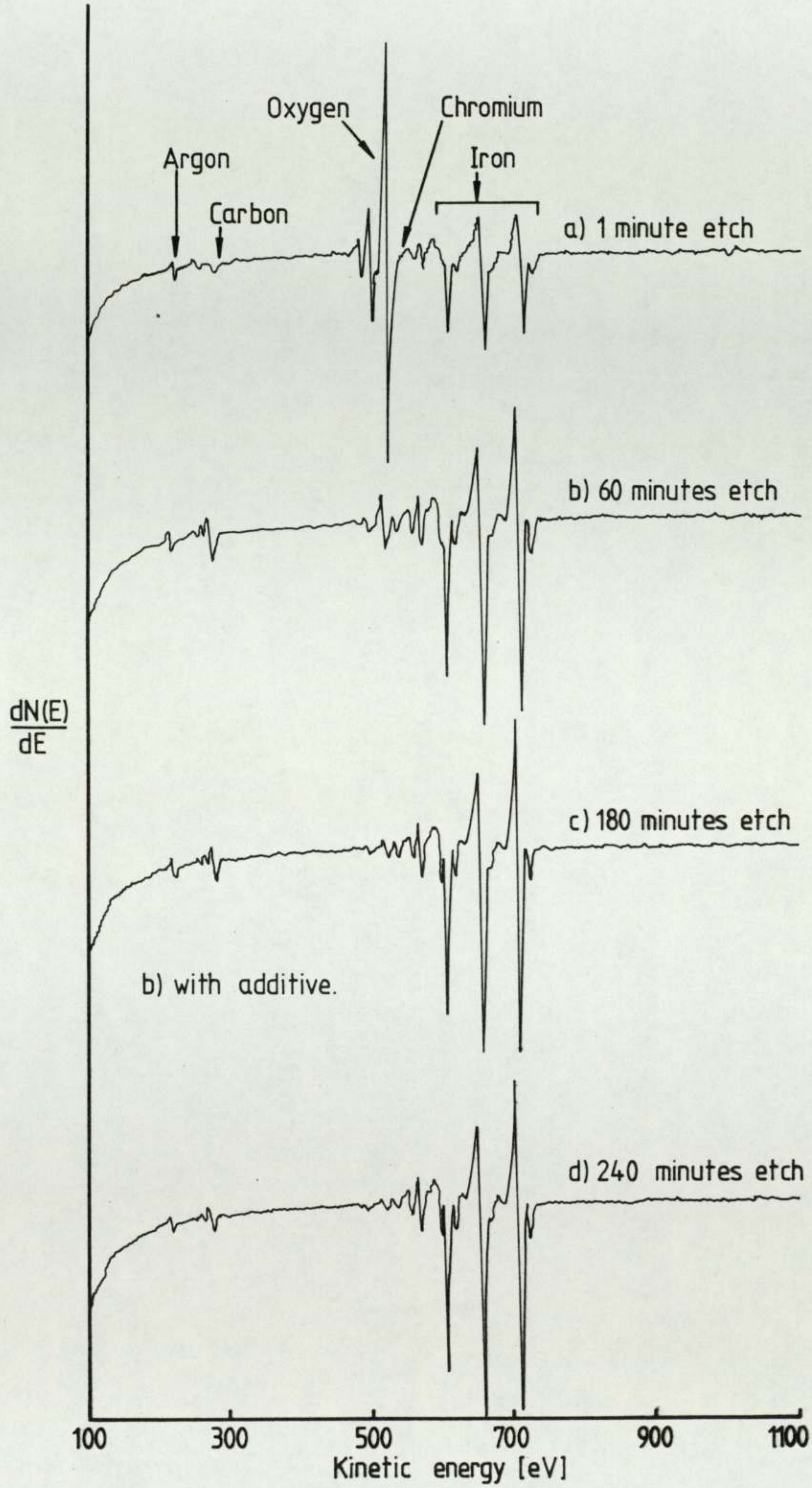
Oxygen
Chromium
Argon
Iron
Carbon
a) 1 minute etch
b) 60 minutes etch
dN(E)/dE
c) 180 minutes etch
b) with additive.
d) 240 minutes etch
100
300
500
700
900
1100
Kinetic energy [eV]

where $E(x)$ is the peak to peak height of element x,

$S(x)$ the sensitivity factor for element x (163),

n the number of elements present.

Figures 3.55 and 3.56 show the typical relationship between element concentration and total etch time, taken from discs run at various lubrication regions. It can be seen that both Argon and Chromium remain constant throughout the majority of the etch period, at about 1% and 2% respectively. Oxygen and Carbon tend to decrease with etch time, while Iron was observed to increase. From these graphs, the percentage concentration of Oxygen and Iron was extrapolated at etch periods of 0, 9, 25, 50, 75, 100 and 125 minutes. When more than one disc had been analysed, the respective concentrations were averaged at each depth.

The amount of Oxygen, taken as a percentage of the Iron oxide was calculated using the following equation:

$$\text{Oxygen in Iron oxide} = \frac{\%\text{Oxygen}}{(\%\text{Oxygen} + \%\text{Iron})} \times 100\% \qquad 3.16$$

and plotted against the above seven etch periods. Typical examples taken from various lubrication regions are shown in Figure 3.57.

All graphs show the anticipated reduction in Oxygen from about 65% at the surface, to a fairly constant value of 10%. The relative oxide thicknesses were estimated by noting the etch time at which the concentration leveled out. Oxide thickness values were measured in the units 'minutes etch' because it was impossible to relate accurately etch time with

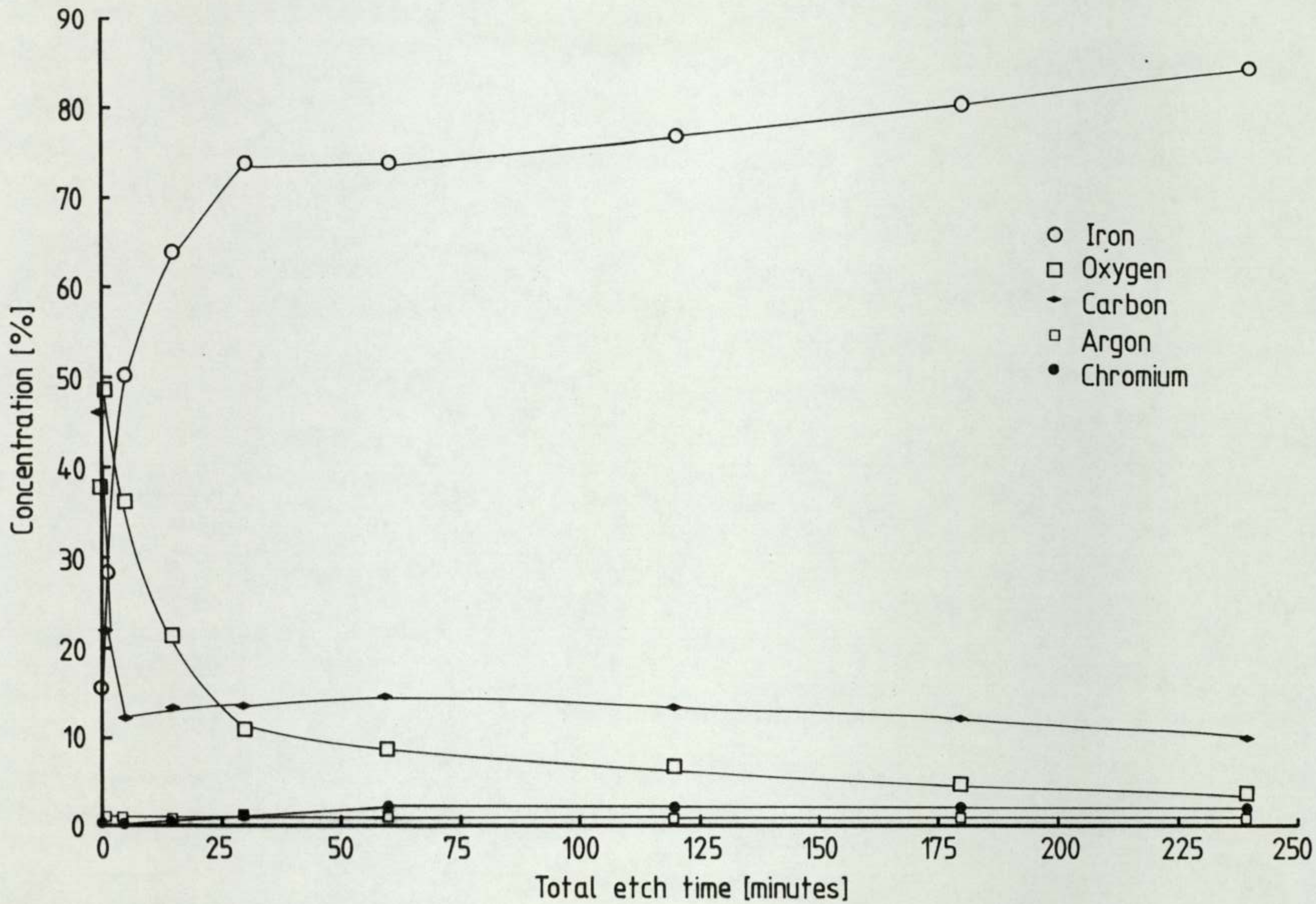

Figure 3·55a. Typical element concentration depth profile taken at lubrication region 3 without antiwear additive.

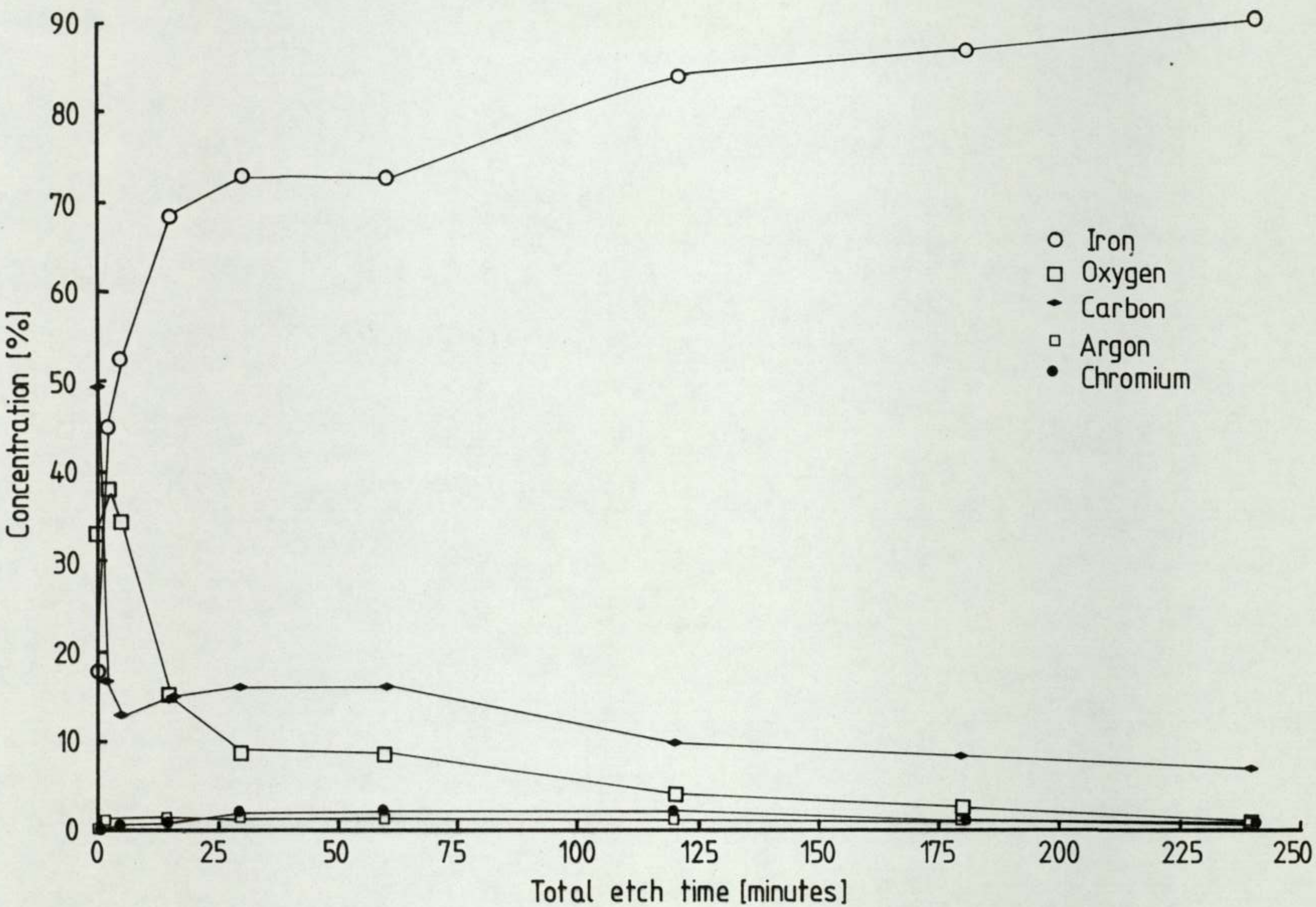

Figure 3·55b. Typical element concentration depth profile taken at lubrication region 3 with antiwear additive.

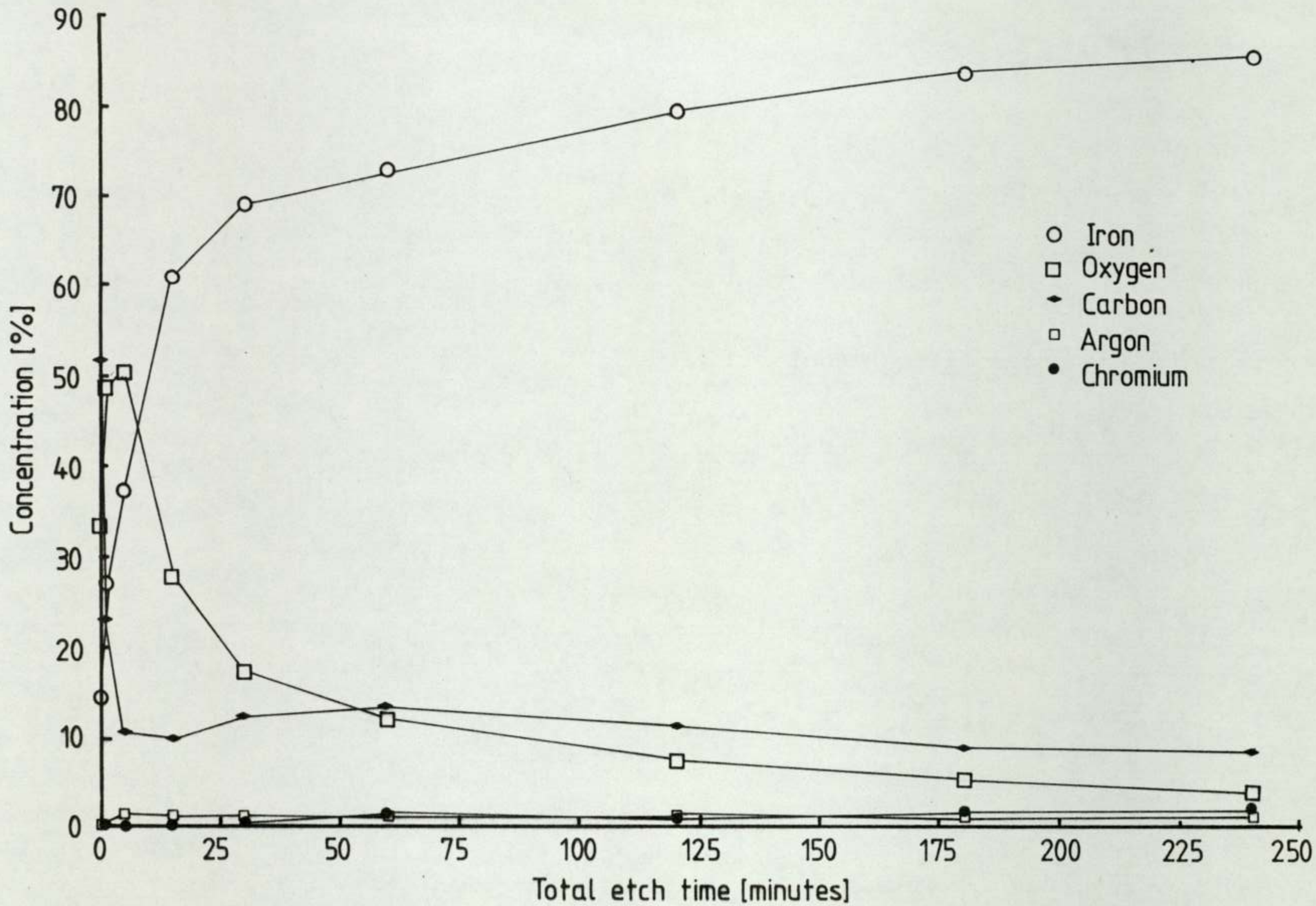

Figure 3·56a. Typical element concentration depth profile taken at lubrication region 8 without antiwear additive.

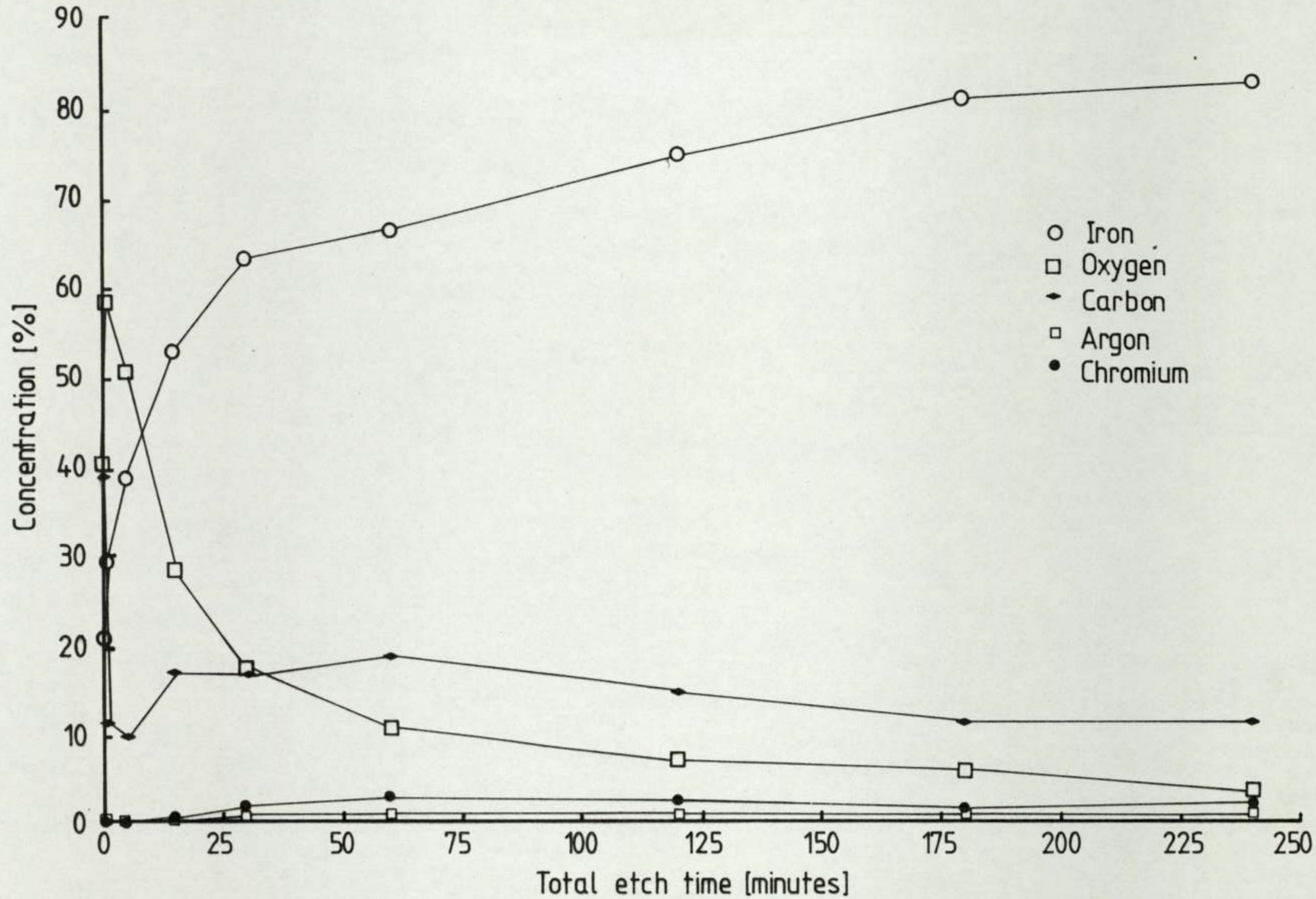

Figure 3·56b. Typical element concentration depth profile taken at lubrication region 8 with antiwear additive.

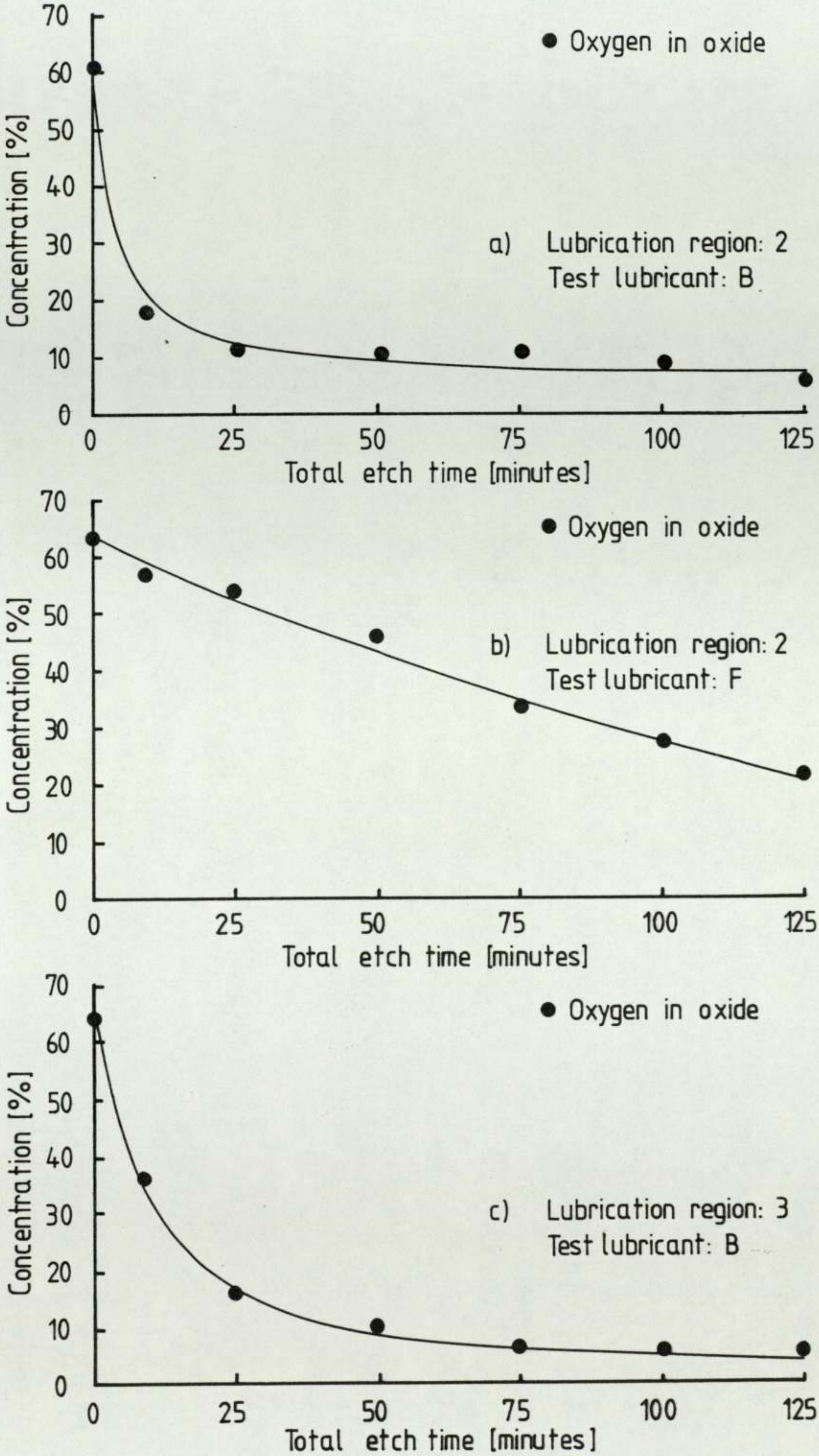

Figure 3·57. Typical oxygen-iron oxide concentrations against total etch time for various lubrication regions.

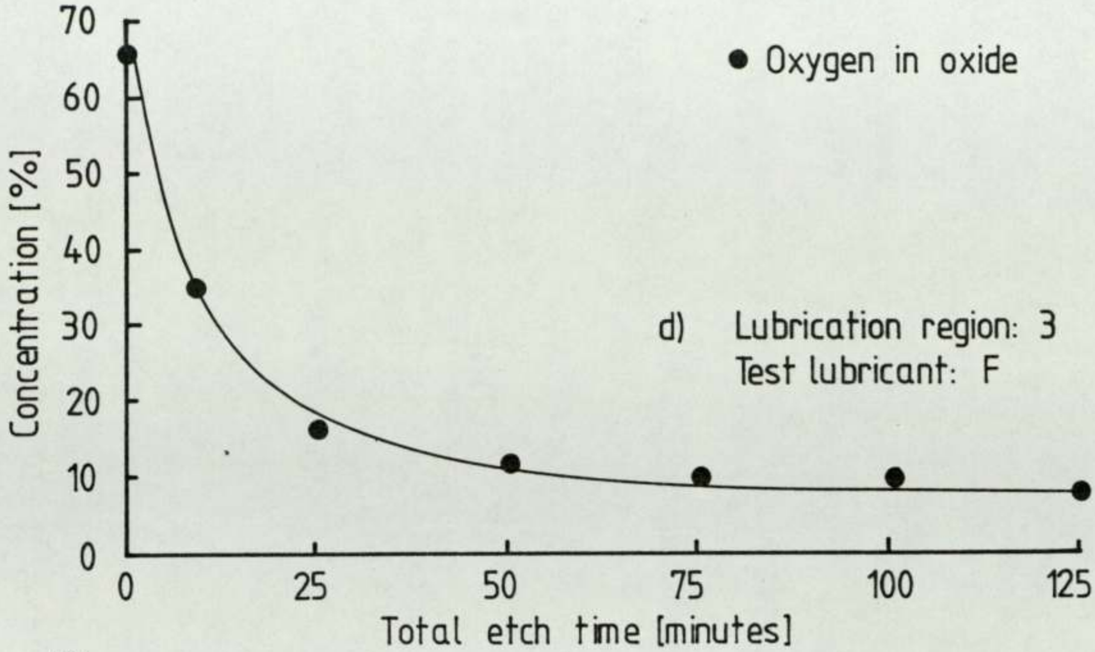

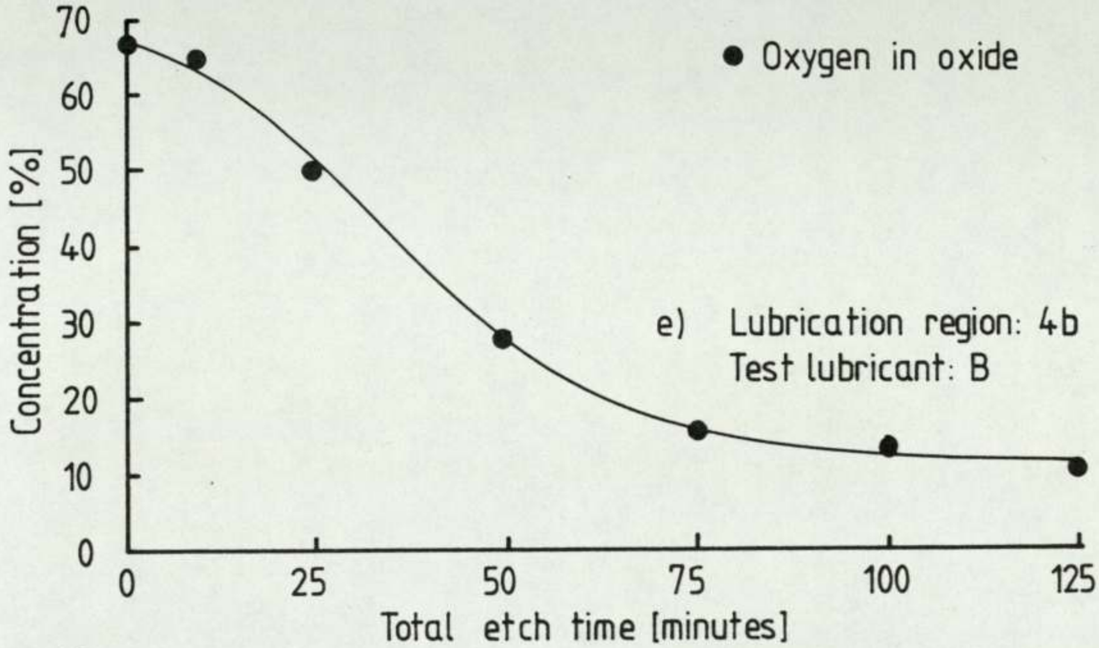

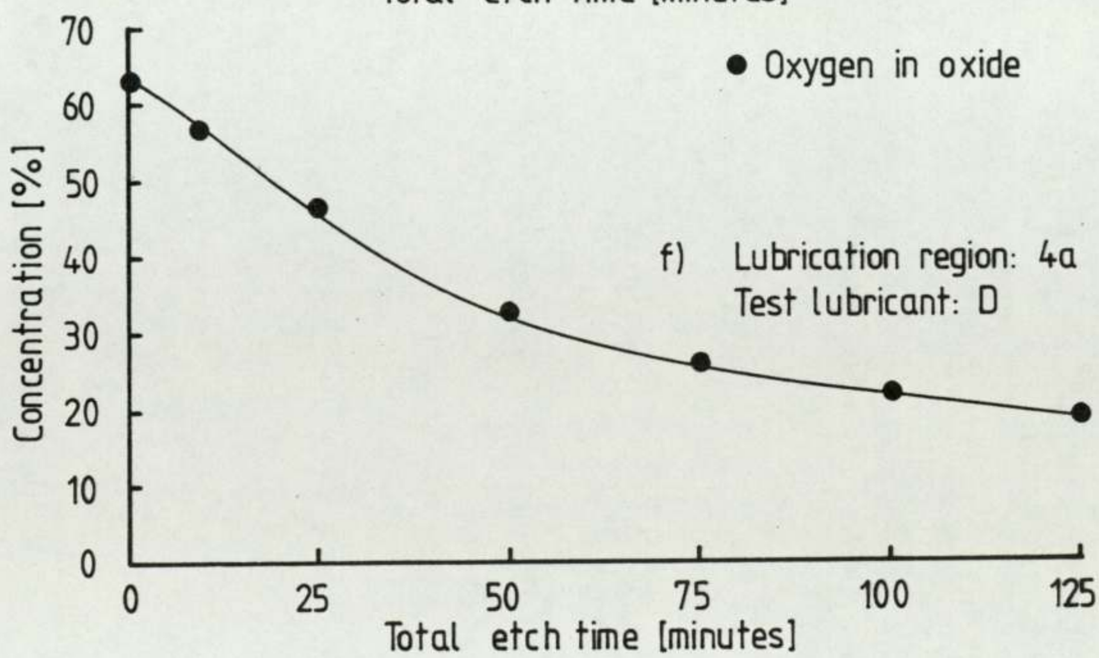

Figure 3·57(cont). Typical oxygen-iron oxide concentrations against total etch time for various lubrication regions.

depth, however, as an approximation one minutes etch represented a removal of 10nm of surface.

Table 3.9 gives a comparison between the various lubrication regions and oxide thickness for all test lubricants, together with the associated average pitting lives.

Lubrication Region	Without Additive		With Additive	
	Depth(mins)	Life(cycles)	Depth(mins)	Life(cycles)
1	10	Not pitted	-	-
1.1	-	-	100	185,879
2	60	470,802	>125	Not pitted
2.1	-	-	50	862,243
2.2	-	-	50	1,627,203
2.3	-	-	60	2,405,347
3	75	310,388	75	2,221,345
4a	120	363,346	-	-
4b	120	1,085,689	110	2,514,485
6	90	146,567	-	-
7	-	207,652	-	-
8	95	318,747	110	533,437
9	100	Not pitted	-	-

Table 3.9. Comparison of oxide depth with pitting life.

For test lubricants not containing the antiwear additive (and ignoring Lubrication Regions 4a and 4b) there appears to be an upward trend in oxide thickness with fluid film thickness as shown in Figure 3.58. The best fit line for this relationship is given by:

Oxide Depth(mins) = 48.8 log(Film thickness μm) + 150.2   3.17

with a correlation coefficient of 0.87.

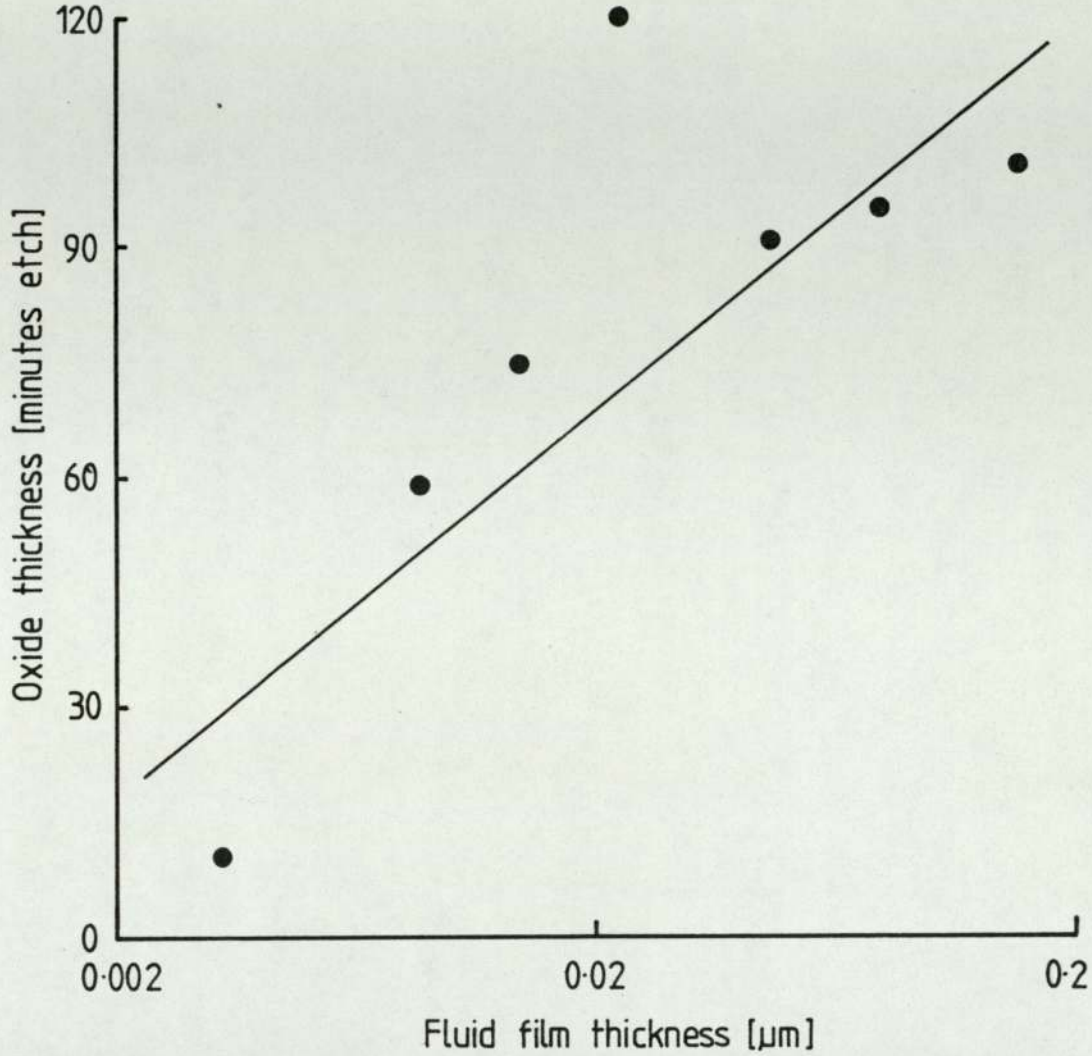

Figure 3·58. Oxide thickness against fluid film thickness for test lubricants not containing the antiwear additive.

This would be expected, since at boundary conditions of lubrication there was a lot more asperity interaction and hence wear. Oxide layers at hydrodynamic conditions of lubrication were about ten times as thick. At Lubrication Regions 4a and 4b (Figure 3.57e) and 3.57f)) there was a much greater oxide layer formed. In addition to this, there was an unusually high pitting life value for discs run at Lubrication Region 4b. It would seem probable that pitting life could be related to oxide thickness especially under mixed-elastohydrodynamic conditions of lubrication. It is interesting to note that both the oxide layers formed at Lubrication Region 4a and 4b are similar in thickness, the two lubrication regions being obtained by different combinations of speed and fluid viscosity.

At Lubrication Region 2 (Figures 3.57a) and 3.57b)) the effect of the antiwear additive increased oxide thickness from 60 to >125 minutes etch. This is important because it would suggest that pitting could be prevented by increasing the oxide layer above a certain thickness.

CHAPTER FOUR

DISCUSSION

4.1. Introduction

The aim of this chapter is to highlight and explain the phenomena associated with the pitting of steel in the presence of an aqueous lubricant. The following sections therefore discuss some of the mechanisms that could account for the observed behaviour of the fire resistant fluids.

The mechanisms proposed will be based upon the results and observations of Chapter Three together with supporting evidence from the literature. The discussion will centre on the results obtained from the disc machine and the early comparative data from the Unisteel and Rolling four-ball experiments will be reviewed.

To correlate the data it is necessary to divide the chapter into two sections. The first part consists mainly of a discussion of the data obtained whereas the latter part will be concerned with the mechanisms associated with pitting failure.

4.2. The Unisteel and Rolling Four-ball Results

Collectively, the results obtained from the Unisteel and Rolling four-ball experiments serve as a means by which the lubricating properties of the test lubricants can be compared. Previous authors have successfully used both the Unisteel (14) and Rolling four-ball (138) machines to evaluate different types of fire resistant fluid often by comparing the performance to that of a mineral oil. No previous work, however, has been reported in which these tests have been used to assess the relative performance of similar examples of the same type of fire resistant fluid differing only in viscosity and/or additive inclusion. As expected the two test methods produced considerable scatter. Weibull (71) statistics were used to analyse the data and, in essence, rank each lubricant.

Tables 3.1 and 3.2 show the beneficial effect of the antiwear additive. It is gratifying to note that both test machines were able to highlight the respective increases in life between fluids with and without the antiwear additive. It is also interesting to note that the effect of the additive was more pronounced at lower viscosities and hence at thin film lubrication conditions. This would imply that the antiwear additive used in the experiments functioned increasingly as lubrication conditions became more severe. The effect of increasing viscosity was also seen to increase life but only up to a certain value (Figure 3.2). It is thought that at this optimum viscosity near hydrodynamic conditions of lubrication are reached.

The effect of viscosity on fatigue life as obtained from the Rolling four-ball machine (Table 3.2) was more difficult to interpret. It appears that an optimum viscosity similar to the one experienced with the Unisteel machine could exist, although more work with fluids of different viscosity would be required to verify this.

Both machines suffer from the disadvantage that the load conditions encountered by the specimens are severe. This was more apparent, however, in the Rolling four-ball experiments where life values were determined in minutes.

Paradoxically, the high load may explain the unusually high life value obtained when the test was conducted with water (Test Lubricant A). A top ball from such a test is shown in Figure 3.27b). It can be seen that, due to the high pressure, the ball experienced excessive wear resulting in the enlarged (widened) wear track. This effectively reduces the contact pressure and hence increases the time taken for pitting to occur. A comparison of the maximum Hertzian pressures between the different test methods is given in Table 4.1.

Contact Machine Used (Test Method)	Maximum Hertzian Pressure (GPa)	Average Time Taken to Pit
Rolling four-ball (600kg)	7.69	11.5 mins
Rolling four-ball (500kg)	7.24	50 mins
Unisteel (334kg)	3.20	17.5 hours
Amsler 2-disc (90kg)	1.01	1 day

Table 4.1. Test methods and corresponding Hertzian pressures.

Included in Table 4.1 are the average times taken for the respective test specimens to fail when run with Test Lubricant E. These show how machine load conditions can seriously affect the duration of the test. Rolling four-ball tests conducted at 600kg load would be pointless since the magnitude of the life values make it virtually impossible to differentiate between different formulations of the same type of fluid.

From the preliminary results obtained from the Unisteel and Rolling four-ball machines it was clear that a more informative test method was required, giving information on wear rates, crack propagation rates and lubrication regions. For this reason a 2-disc machine was chosen for the main part of the work.

A direct comparison between the disc machine and the Unisteel or Rolling four-ball machines is difficult because of the different conditions under which the tests were conducted. These include maximum Hertzian pressure, material hardness and contact geometry.

4.3. Friction and Wear

The Stribeck curve (Figure 3.4) plotted for the 2-disc machine gives a useful visual representation of the various regimes of lubrication and enables experiments to be conducted in the mixed-elastohydrodynamic region where pitting is expected to occur. It should perhaps be more widely recognised by workers studying the wear and friction of surfaces under lubricated conditions that the plotting of this type of curve is essential in order to define fully the lubrication regimes prevailing under specific operating conditions.

The results and information obtained from the various monitoring techniques are therefore discussed in terms of the lubrication regimes which are in turn related to the degree of asperity interaction between the discs. Boundary lubrication represents significant asperity interaction whereas true hydrodynamic lubrication is representative of no asperity interaction.

Friction was monitored continuously at each lubrication regime as shown by the typical traces in Figure

3.6. Type A traces show the effects of friction (torque) for experiments run under boundary and hydrodynamic conditions of lubrication. For experiments conducted under boundary conditions of lubrication constant asperity interaction prevailed throughout the test, hence no reduction in friction was observed. Under less severe (hydrodynamic) conditions of lubrication no asperity interaction took place, thus the observed steady state of friction was due entirely to the shearing of the lubricant film.

Type B and C traces represent those experiments run in the mixed-elastohydrodynamic region and are best explained by considering friction in terms of contact changes. Near to boundary lubrication conditions (Type B) a large number of high asperities penetrate the thin lubricant film. The time taken to wear down the asperities to that of the film thickness is quite considerable as shown by the presence of the initial plateau. For near hydrodynamic conditions of lubrication (Type C) a small number of high asperities penetrate the thicker lubricant film. The time taken to wear these asperities is therefore shorter as shown by the immediate reduction in friction.

It is apparent that for all experiments conducted in the mixed-elastohydrodynamic lubrication regime a degree of surface modification has taken place which would appear to change the lubrication regions. However, it must be remembered that the lubrication regions for the system were based upon the parameters: viscosity, speed and load of which these remain constant throughout the duration of each test. Hence the regions of lubrication remain fixed even though friction decreased. Surface track width measurements taken before and after each run, however, showed that a certain amount of widening had occurred. Track widths increased by an average of 36%, 20% and 0.12% for experiments conducted under boundary, mixed-elastohydrodynamic and hydrodynamic conditions of lubrication respectively. Re-calculated fluid film thickness values showed only a slight increase in fluid film thickness and no over-lapping of lubrication regions occurred.

The Stribeck curve plotted for the system, therefore, is probably more representative of the final conditions of lubrication since the friction values were obtained from discs that had been initially surface modified ('run-in') and thus would not change significantly.

The wear graphs obtained by LVDT transducer show an initial region of rapid wear termed the "settle period" (Figure 3.9) followed by a gradual decrease in wear. The initial period is due to the higher asperities being worn, thus the presence of the settle period confirms the steady state friction mechanism discussed earlier.

As expected, no settle period was apparent in the wear rate traces obtained for experiments conducted under boundary conditions of lubrication. The steady increase in wear with time was due to continued asperity interaction through the thin lubricant film and was the highest observed in the programme. Under hydrodynamic conditions of lubrication an unexpected initial settle period was recorded which indicated that initial asperity penetration of the film had occurred. By considering the initial surface roughness of the discs and the thickness of the lubricant film it was inevitable that some interaction would take place, however, the wear rate leveled out and no further increase in wear was observed. Wear rates recorded under these conditions were in fact negligible.

The wear traces were quantified according to Figure 3.10 and calculated in terms of volume removed per unit distance of rotation using Equations 3.4 and 3.5.

Figure 3.11 shows a inverse linear correlation between wear rates for fluids without antiwear additive and the calculated film thickness. The calculations of film thickness are based on the assumption that surfaces are perfectly smooth and hence this parameter may be regarded as a measure of degree of asperity interaction. This concept should also be carried through to the interpretation of the D-ratio. If one takes this view then the inverse relationship:

Wear rate $\propto$ (Film thickness)$^{-1}$ might be expected since the degree of asperity interaction will increase with decrease in film thickness and this is important when considering the relationship between pitting life and the wear of surfaces (170).

The graphs of wear rate against film thickness determined by weight loss, shows a similar inverse relationship for the pitting disc (Figure 3.13 and Equation 3.9) except that the wear rates calculated by this method were slightly lower, only tending towards the LVDT calculated values at near boundary lubrication conditions (Figure 3.15).

Whereas the LVDT method measured the actual displacement of the pitting disc it must be remembered that the wear rates determined by weight loss took into account the weight of the disc before and after each run. Thus the final weight included the material lost due to pitting and to some degree, extensive cracking. One would therfore expect a higher wear rate than that calculated by LVDT transducer, however, considering the magnitude of the wear rate values and the nature of the investigation it was felt that this difference could be ignored. In addition to this the exponents of the respective wear rate Equations 3.6 and 3.9 were sufficiently close to warrant agreement thus confirming the inverse relationship between wear rate and fluid film thickness.

With the antiwear additive present it would appear that the exact inverse proportionality no longer applies and from LVDT measurements a slight reduction in the wear rate under thin film conditions has occurred. However, considering the scatter of results obtained from experiments conducted with and without the antiwear additive there is little significant difference between the two wear rate relationships. Thus the inverse proportionality relationship between wear rate and fluid film thickness can also be applied to those fluids containing the additive.

No relationship between wear rate calculated by weight loss and fluid film thickness could be obtained, although this might be expected if the pit geometries are considered. Since the wear rate is based on the amount of material lost due to pitting, the size of the pit will undoubtly influence the final wear rate value. The pits formed in the presence of the antiwear additive were of random configuration as can be seen in Tables 3.6 and 3.7 and hence could not be related to fluid film thickness. This may, therefore, account for the poor correlation between weight-loss calculated wear rates and fluid film thickness.

Although the wear rate of the driving disc was considered negligibly small compared to that of the pitting disc, it was interesting to note that the magnitude of the exponent was also very near unity (Figure 3.14 and Equation 3.10).

4.4. Pitting Life v Film Thickness

The life to first pit N, Figure 3.16a), initially shows the expected decrease with reduction in fluid film thickness and hence increase in degree of metallic contact, but for calculated fluid film thickness values below 0.04μm an increase in life is apparent. The graph in Figure 3.17, showing life to first pit (N) versus initial D-ratio, exhibits similar trends. However, for those experiments conducted at Lubrication Region 4b (speed: 400rpm, viscosity: $6\times10^{-3}Nsm^{-2}$, load: 90kg, film thickness: 0.0225μm) crack initiation and propagation rates were unsually low resulting in a marked increase in pitting life. In addition, the pits formed at this region were much larger than those observed at other lubrication regions and oxide layers were significantly thicker. The same phenomena were observed for trial experimental runs conducted at Lubrication Region 4b but with test lubricants not containing any rust inhibitor. While the reason for the beneficially slow cracking rates is still unclear the large pits observed are evidently the result of the larger period available for crack development

In the case of Figure 3.17 an alternative representation of the data is possible to give a classical log (life) versus log (D-ratio) straight line graph through all the points. The best straight line is then described by the equation:

$$\text{Log } N = -0.16 \text{ Log}(D) + 5.75 \qquad 4.1$$

with -0.44 correlation coefficient.

This compares with Equation 3.11 for points below a D-ratio of 22, however, from the evidence of wear rates, the pitting life results presented in Figure 3.16a) and correlation differences, this would be the wrong interpretation and Figure 3.17 showing an increase in life for D-ratios greater than 22 is a closer representation of the process occurring at the conjunction. This increase in life for D-ratios greater than 22 is strongly connected with the increase in wear rates with increased metallic contact in this region, although as will be shown, this is not the only factor affecting life. It is thus an interesting phenomenon, but of no engineering benefit since the high wear of components under these conditions would be quite unacceptable in practice.

To understand the mechanisms of pit formation and hence the results presented in Figures 3.16a) and 3.17, it is necessary to consider separately the process of crack initation and crack propagation.

4.4.1. Crack Initiation

Fatigue cracks which lead to pitting failure may be either surface or subsurface initiated (73). It is generally accepted that surface initation occurs under conditions of thin lubricant films (73) whereas subsurface initation, generally associated with case hardened materials (86) occurs under conditions of high contact stress and thick lubricant films (83).

From the detection of initial surface fatigue cracks in this study and considering the relatively poor lubricant used, it was concluded that fatigue cracks were formed due to asperity interaction at depths between 1 and 20μm (93). This mode is normally referred to as surface initation in order to distinguish it from true deep subsurface initation. A substantial amount of subsurface sectioning was undertaken and there was only one occasion on which there was any evidence of a possible wholly deep subsurface crack (Figure 3.50) and even in this case it is possible that healing of the surface aperture had taken place.

Another form of surface initation has been proposed by Tallian (172). Under conditions of near pure rolling, micropits (<2.5μm) generated by asperity interaction, were considered to be the initial point for crack propagation. A similar phenomenon has also been observed by Yamada (173), although it must be noted that these occurred under conditions of dry rolling and sliding of soft steel discs. Yamada (173) noted that after continual cycling the micropits eventually disappeared and gave rise to fine surface cracks orientated perpendicular to the rolling direction.

Such micropits were observed in the early part of this investigation when discs of equal hardness ($\approx$800 VPN) were employed, although, in this case the micropits formed did not lead to crack initiation. While no surface cracking was observed, it was interesting to note that micropitting occurred on both the pitting and driving discs when the maximum Hertzian pressure was increased to 3.7 GPa by reducing the track width of the slower disc to 0.5mm and increasing the load to 200kg.

Examination of sections of pitting discs run in the boundary lubrication regime revealed no evidence of micropit formation and confirmed the immediate subsurface initation mode of cracking. Figure 3.48 shows cracks running almost parallel to the surface at depths up to 20μm. These are very similar to those reported by Dawson (88) for discs run dry in rolling-sliding contact. Dawson found that subsequent introduction of a lubricant resulted in the formation of pits from propagation of these primary cracks at angles of between 10 and 30° to the surface, angles very close to those observed in this investigation (See Figures 3.44 and 3.45). This would suggest that initial cracks of the type shown in Figure 3.48 eventually break the surface and are responsible for pit formation in the mixed-elastohydrodynamic regime.

Contact fatigue conditions, numbers and frequency of asperity contacts are likely to be responsible for crack initation. Thus it is the initial surface condition which is the important determining factor in crack initation. This is confirmed by the relatively high correlation coefficient obtained for the life versus initial D-ratio graph (Figure 3.17), compared to the low correlation coefficient calculated for the life versus final D-ratio graph.

Figure 3.23 shows the effect of asperity interaction on crack initation. It can be seen that the rate at which new cracks are formed is much greater when high asperity interaction prevails (thinner lubricant film conditions). This is, perhaps, more readily observed by comparing the rate and magnitude of surface cracks formed in the mixed-elastohydrodynamic regime. The photomicrographs presented in Figures 3.28 to 3.32 depicting high asperity interaction, show considerably more crack development than those in Figures 3.33 to 3.35 (low asperity interaction). A similar trend was observed by plotting the final number of cracks against fluid film thickness as shown in Figure 3.24).

However, the above factors do not much influence subsequent propagation and pit formation as this will be shown to be strongly dependant upon the amount of fluid at the conjunction.

4.4.2. Crack propagation

After the formation of the initial crack the number of cycles required to pit does not follow the life trend, Figure 3.16, but increases steadily with decrease in fluid film thickness, Further, the values of this parameter are independent of whether the fluid contains the additive or not. These facts are important when considering pitting mechanisms. If after crack initation, propagation is dependant purely on contact fatigue conditions one would expect an increase in propagation rates (decrease in Np) as asperity contact increases with fall in fluid film thickness. The converse occurs! One would further expect a decrease in propagation rates (increase in Np) in the presence of an antiwear additive and this does not occur. The increase in Np with decrease in fluid film thickness might be related to the increase in wear rates, however, this is not likely since under near boundary conditions of lubrication wear is responsible for the removal of only 3μm of surface in the time taken for a pit of depth 310μm to form. The most likely explanation for the trend is that Np is related to the volume of fluid at the conjunction.

From the early work of Way (87) and later by Dawson (88),(92) it was evident that whilst crack initation under dry and lubricated conditions were similar, the propagation of such cracks to pitting failure required the presence of a lubricant. It was from these observations that Way (87) proposed the hydraulic wedge action of propagation whereby fluid is forced under hydraulic pressure into crack openings within the contact zone which leads to fatigue, however, in this investigation it is believed that the amount of fluid at the conjuction can influence the rate of crack propagation.

Under near hydrodynamic conditions of lubrication there is sufficient fluid available to promote fluid ingress into surface cracks and hence give rise to rapid crack propagation. This is indicated by the low value of Np obtained at this region.

Under near boundary lubrication there is a relatively small volume of fluid present (low fluid film thickness) to constantly sustain the hydraulic action of crack propagation. Thus under these conditions the number of cycles between crack initiation and pit formation increases, resulting in a low crack propagation rate.

Throughout this chapter results obtained from the various lubrication regions have been discussed in view of the lubricant film thickness and indirectly, the various regimes of lubrication by the Stribeck curve. Although no comparative work was carried out in this investigation between the water glycol based fire resistant fluids and say a mineral oil, it is well documented in the literature that the presence of water in any lubricant can considerably reduce the pitting life. The above considerations of crack development including hydraulic wedge considerations, will apply to fluids of different types. Some reasons why aqueous fluids are particularly prone to early crack formation are now given.

It has previously been shown that under less severe conditions of lubrication, the larger volumes of lubricant and hence water available can lead to rapid crack propagation. It is believed that two main processes could be occurring simultaneously, these being (i) chemical and (ii) mechanical interaction of the water with the crack.

Much of the work involving the chemical influence of water on crack and pit formation has been based on examining the effect of different additives on pitting life and generally, the majority of the adverse properties of water based fluids can be overcome by the additives available. However, because of the extremely small size of the water molecule compared to the lubricant and additive molecules, water can easily diffuse to the tip of the microcrack. Here, water undergoes decomposition by reactions with the newly created crack surface to produce atomic hydrogen, which readily diffuses into the metal ahead of the crack. Such a phenomenon is known as Hydrogen Embrittlement and can promote both crack propagation and crack branching (82).

The other process for crack propagation is mechanical, where according to Way (87) the fluid itself maintains the high compressive stresses necessary for crack growth, however, this latter effect can also be applied to mineral oils. A comparison between the physical properties of a mineral oil and water will now be made in order to establish some of the major differences which could explain the low performance ratings often associated with water.

It is well known that a high viscosity is required to maintain elastohydrodynamic lubrication. Mineral oils develop a high viscosity as a result of the high value of pressure viscosity coefficient. Water has a low pressure viscosity coefficient (178) and so offers little separation of surfaces under pressure. This will increase the crack initiation process and will result in the formation of more cracks.

It is possible that the low pressure viscosity coefficient increases propagation rates. This would arise because fluid at the mouth of the crack, instead of undergoing very high viscosity increase serving to isolate the growing crack tip from the high pressure pulse, maintains low viscosity readily transmitting pressure to the growing tip.

A second deficiency of water is its low compressibility or high rigidity. The high Hertzian pressures developed within the contact zone are easily transmitted as a series of stress waves to the propagating crack tip. Thus the hydraulic mode of propagation is accelerated due to the non-compressibility of the water. As a comparison, mineral oils are more compressible and so absorb shock.

Another property, although the effect may be small, is density. The high density of water means that more energy is transmitted per unit volume of fluid in the crack than with an equivalent volume of mineral oil.

Table 4.2 gives a comparison between the physical properties of mineral oil and water (178).

Property	Oil	Water
Pressure viscosity $(GPa)^{-1}$	≈ 20	≈ 0.5
Density kgm^{-3}	≈ 800	1000
Compressibility $(GPa)^{-1}$	≈ 0.5	≈ 0.4

Table 4.2. Some physical properties of mineral oil and water.

The poor lubrication associated with water based fire resistant fluids may therefore be attributed to four effects, these being (i) Hydrogen embrittlement, (ii) Pressure viscosity coefficient, (iii) Compressibility and (iv) Density.

4.4.3. Pit Formation

From the observations made during this investigation it was believed that a secondary mode of propagation during the latter part of pit formation was also operative. Figure 4.1 shows the various stages of pit formation immediately after the detection of the first crack and is based upon the evidence presented by both optical and scanning electron microscopy. Pit formation therefore proceeds as follows:

During the initial detection (the time taken to count 128 crack detector pulses) of the crack mouth a hairline crack propagates rapidly into the subsurface region of the disc.

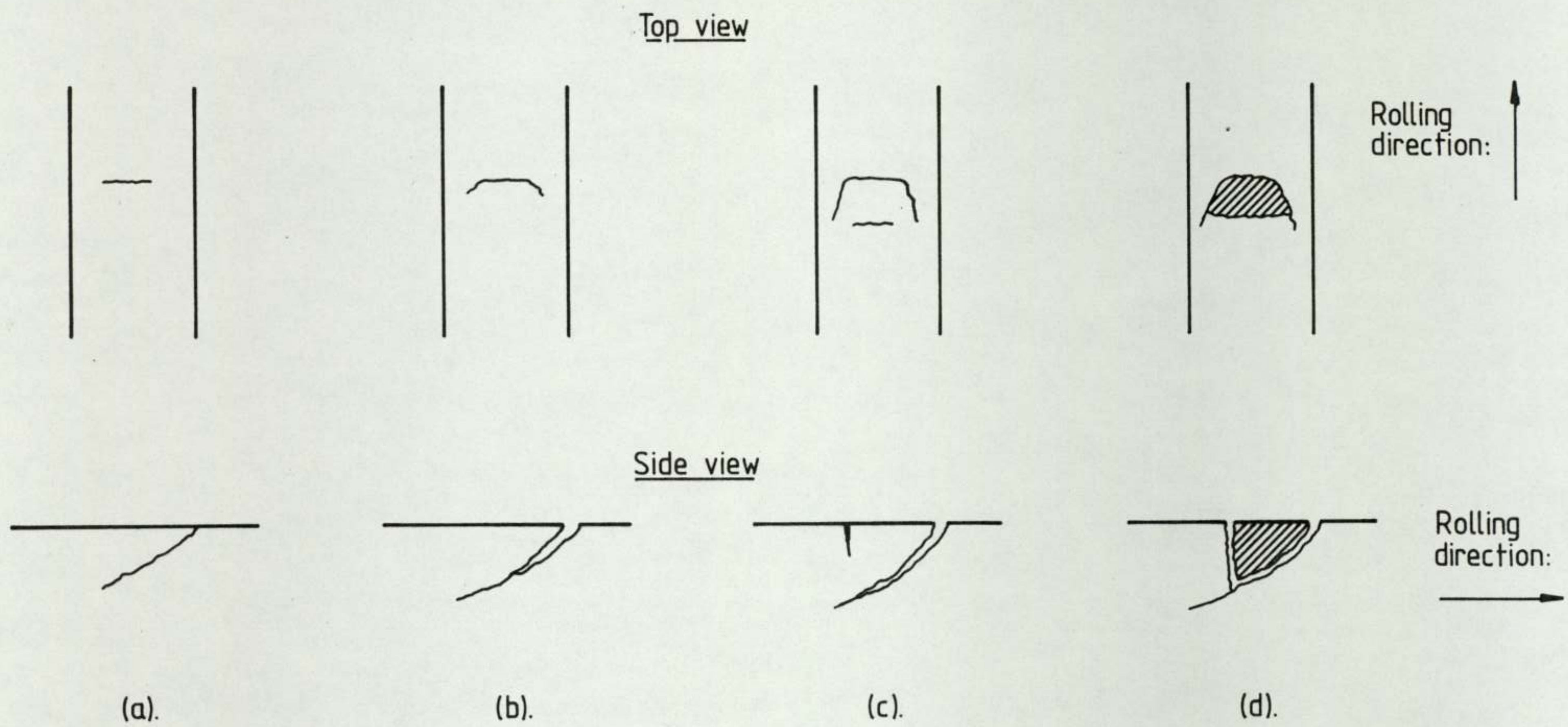

Figure 4·1. The different stages of pit formation.

Figure 3.49 shows that the angle of penetration is between 20 and 30° to the surface and is fairly well established at this point. It is not clear from the present study and indeed the literature, as to why such an angle should prevail although from measurements it appears that the angle increases with fluid film thickness. If the test is allowed to continue the crack mouth is subject to a series of compressive and tensile forces. For a fatigue crack to open in the first place Niemann et al (174) considered that the tensile surface stress ahead of the crack tip was responsible whereas Dawson (92) considered that the compressive stress was responsible. In this study where the driving disc is the faster, the crack mouth approaches the contact zone under tension and thus open and full of lubricant. As it passes through the contact zone, the lubricant becomes trapped and is subsequently forced to pursue the route of the hairline crack. On exit, the crack is under compression and lubricant is then forced back out. Cracks that reach the sides of the disc do not propagate further as it is believed that the hydraulic pressure of the lubricant is considerably reduced due to side leakage. Hence cracks under the conditions of these experiments propagate after the initial crack breaks the surface due to a cyclic pressure wedge created by fluid ingress (81). Wear will considerably influence crack initation, but will have little effect on propagation.

It must be remembered that the crack propagation times represent only about 10 to 20% of the total time taken to fail and were similar to those reported by Yamamoto (106). Thus the overall fatigue life is governed mainly by the crack initation process.

The measured pit depth tended to decrease with increase in fluid film thickness although it always exceeded the depth of maximum stress. It could therefore be considered that any subsurface hardening due to stress, had little or no effect on crack propagation. However the depth of maximum stress increased with thicker fluid film conditions. This may be expected if the early theoretical work (62),(63) is considered. It was shown that as traction between two rotating discs in contact decreased (approaching hydrodynamic conditions), the depth of maximum stress increased. Based upon the formulae given it can be shown (see Appendix 1) that good agreement is achieved between theoretical calculations and experimental measurements when the equilibrium friction is taken into account. For this system, the depth of maximum stress approaches the surface when the friction coefficient between the discs becomes greater than 0.24 (see Appendix II).

As the crack becomes enlarged unstable oscillations by the pit fragment brought about by repeated passage through the contact zone induce stress a short distance behind the crack mouth as indicated in Figure 4.1c). This eventually leads to the formation of a secondary fatigue crack as can be seen in Figures 3.29 to 3.32 and 3.34, however, its propagation is believed to be mainly controlled by the stress induced oscillations of the pit fragment, as its orientation is completely different to that of the initial crack.

This forceful effect was seen to explain the shear bands that were observed (Figure 3.46) around the rear halves of many of the pitting failures analysed. Thus the final failure mode was stress as opposed to fluid related.

At this point, mention must be given to the fact that pitting was only confined to the softer, slow moving disc. One reason for this is the velocity difference between the discs. Considering the 10% slip, any point on the pitting disc surface always saw more than one point on the driving disc surface as it passed through the contact zone. Thus the probability of crack initation on the softer pitting disc was far greater than that for the harder driving disc. In addition, plastic deformation (172),(175) and wear were more likely to have occurred on the softer disc and that the initation of surface cracks on the pitting disc was believed to be controlled by the initial surface roughness of the pitting disc itself. Indeed, Figure 3.17 shows the dependence on pitting life with initial combined surface roughness, the major variable component being the roughness of the softer disc. However, Onions and Archard (97) have obtained reasonable correlation between pitting life and the final combined surface roughness and believe that pitting is controlled by the roughness of the harder surface. Dawson (93) has reported that when there is a difference in hardness and surface finish between two discs, it is the surface finish of the harder disc which is predominant in determining the pitting life. In this investigation no correlation could be obtained between pitting life and final surface roughness, although the final surface roughness values of the pitting disc were similar to those values measured for the driving disc. From these considerations, it would be expected that a greater slip within the contact zone would reduce pitting life, however, Dawson (92) has shown that there was no difference in life between 0.1 and 4% slip. On the other hand MacPherson (176) has shown that life can be shortened when a slip of only 1% or less is introduced.

To determine whether or not speed was the governing factor for crack initation, a pair of discs were interchanged so that the harder disc became the slower moving disc. After continued cycling, pitting did not occur on either disc. On returning to the original machine conditions, crack initation and subsequent propagation resumed as normal. Thus before crack initation can occur in the mixed-elastohydrodynamic regime (and assuming a ready supply of lubricant) two conditions must be met. These are (i) the pitting disc must be softer than the driving disc and (ii) the speed of the pitting disc must be slower than the driving disc.

We are now in a position to explain the results presented in Figure 3.16. At thick fluid film conditions ($h > 0.04\mu m$) the infrequent asperity contacts lead to a low probability of crack formation, but when a crack does form it is not likely to be removed by wear and rapidly propagates due to the relatively large amount of fluid at the conjunction. Under these conditions crack propagation rates are greater than wear rates. As asperity contact increases with decrease in fluid film thickness ($h < 0.04\mu m$) cracks are formed more readily and in greater numbers but many are removed due to wear. Propagation also progresses more slowly due to the restricted amount of fluid present. Thus under these conditions an apparent increase in pitting life is observed but with unacceptably high wear rates.

4.5. The Effect of the Antiwear Additive

The effect of the antiwear additive was to increase life between two and seven times as shown in Figure 3.16b). The important difference between this graph and the one given in Figure 3.16a) is that pitting life increased only two fold at near hydrodynamic conditions whereas at near boundary conditions of lubrication a seven fold increase was observed. The additive therefore appears to work at all lubrication regions but more significantly at thin fluid film conditions.

The results presented in Figure 3.19 show that crack propagation is not influenced by the presence of the additive in the water glycol lubricant. This would suggest that it is ineffective in displacing water molecules at the crack tip and may simply be due to the relative size of the molecule. Hence the apparent increase in life over those lubricants not containing the antiwear additive must be governed by the time taken to initiate a crack. Crack initation, is in turn, controlled by the contact fatigue conditions and the number and frequency of asperity contacts. Since for comparison purposes the contact conditions remain the same it would seem likely that the role of the antiwear additive was to reduce effective asperity contact. This can be seen by comparing the low crack initation rates (Figure 3.23) and final number of crack locations (Figure 3.24) between those similar test lubricants with and without the antiwear additive. When the additive was used the respective initation rates and crack locations were reduced and the number of final crack locations remained constant throughout the mixed-elastohydrodynamic regime. The relative reduction in crack initation at thin film conditions together with the marked increase in pitting life under similar conditions can be explained by considering the nature of the antiwear additive.

Antiwear additives are polar materials having some electrical charge separation within their atomic structure and as such are attracted to metal oxide surfaces even when there is no asperity contact. Oxide layers have been shown to be present at all of the lubrication regions investigated (see Table 3.10). For each different concentration in solution there will be a value of "surface concentration" of the additive (at high solution concentrations there will be high surface concentrations). This represents an equilibrium state and if additive is removed by sliding contact, more will migrate to and cover the surface. The energy of the reaction is low and adsorption occurs at room temperature, thus the antiwear additive is mild in action and functions to reduce mild wear but only when metal remains covered by an oxide film. The lateral attraction bewteen the hydrocarbon chains of the additive provide an easily sheared film at the asperities and hence reduce subsurface damage with a significant reduction in crack initation.

Because the antiwear additive used was a fatty acid, and the rust inhibitor an alcohol, the question arises on whether acids (as their amine salts) or esters are the effective antiwear agents. Considering the esterification process and the nature of the lubricants it is more likely to be the fatty acid. This is because esters form from acid plus alcohol slowly and with difficulty because the equilibrium:

$$R - COOH \; + R'OH \; \underset{\text{Hydrolysis}}{\overset{\text{Esterification}}{\rightleftharpoons}} \; R - COOR' \; + H_2O \qquad 4.2$$

where $R = C_9H_{19}$ and $R' = N(CH_3)_2(CH_2)_2$
lies largely to the left (favouring acid) unless the water formed is removed continuously. Because of the high water content of the lubricants, ester formation is therefore very difficult. In addition to this acids and their amine salts have been shown by experiment (177) to be much better antiwear agents than esters and this is supported by the theoretical point that the ionic grouping is much more reactive at metal-oxide surfaces than the covalent grouping of esters.

At conditions of lubrication below a fluid film thickness of 0.04μm there is considerable asperity interaction and hence wear. The additive film reduces the probability of crack initation by dissapating much of the surface interaction stress in the additive film itself. There is therefore less stress available to initiate cracks and this is shown by the marked reduction in the crack initation rate for experiments conducted under these conditions of lubrication. However, when a crack does form it propagates slowly due to the relatively small quantity of fluid present at the conjuction. The slow rate of crack initation and propagation result in the very high pitting life values. In practice, despite the increased protection given by the antiwear additive the life of elastohydrodynamic contacts would be restricted by wear.

CHAPTER FIVE

CONCLUSIONS

The main conclusions that can be drawn from the work described in the thesis are as follows:

The pitting life of EN31 steel discs in rolling-sliding contact with 10% slip in the presence of water-glycol based fire resistant fluid was found to depend on the regimes of lubrication as defined by a Stribeck curve plotted for the system. This in turn can be related to the relative magnitude of the film thickness developed at the conjunction.

No pitting was found to occur at either extreme region of the curve, that is in the boundary and hydrodynamic lubrication regimes, although considerable surface distress and substantial subsurface cracking to a depth of 20μm was observed for the former of the two. Surfaces run under hydrodynamic conditions of lubrication were always smooth and damage free.

Pitting occurred throughout the mixed-elastohydrodynamic region with a minimum in pitting life recorded at a calculated film thickness of 0.04μm for fluids both with and without the addition of the decanoic acid antiwear additive. The apparent increase in pitting life at relatively thin film thickness was due to the high wear rates and high crack propagation times in this region.

Lives of components run in the presence of the antiwear additive were, however, greater by factors of two in the hydrodynamic regime and seven for the boundary regime.

Wear rates determined by both LVDT transducer and weight loss methods were inversely proportional to calculated film thickness for fluids without the antiwear additive and inversely dependant for fluids with additive, although direct proportionality was not observed in the latter case due to chemical modification of wear mechanisms.

Crack propagation times decreased with increase in film thickness, showing that propagation occurs more readily under thick film conditions. It was believed that the amount of fluid present at the conjunction was the controlling factor for crack propagation. These propagation times were unaffected by the presence of the antiwear additive. Thus while the additive undoubtly increased crack initation times it did not influence crack propagation and branching.

In the tests good inverse correlation was found between life to first pit and the D-ratio calculated from the combined initial surface roughness, but only for D-ratios up to a value of D = 22. Above this value an increase in life was observed. Very much poorer inverse correlation was found if D-ratios were calculated from combined final surface roughnesses. Thus it is the initial pitting disc condition which was the determining factor in crack initation and eventual pit formation.

The pits formed during this investigation were very similar in nature to those produced in the presence of mineral oils under similar conditions (154). Microhardness measurements showed that the depth of maximum hardness increased with increasing fluid film thickness confirming earlier theoretical work. No correlation could be obtained between pit depth and depth of maximum hardness, although surface damage increased towards boundary conditions of lubrication. Surface damage, however, remained constantly low when the additive was used. Optical microscopy showed that pit size (length and width) decreased at less severe conditions of lubrication, whereas for those discs run with the antiwear additive pit size remained uniform throughout the mixed-elastohydrodynamic lubrication regime.

Auger electron spectroscopy in conjunction with Argon ion depth profiling of pitting discs taken from the lubrication regions showed the presence of an oxide layer. The oxide layer appeared to increase in thickness with increasing fluid film thickness, although this was mainly due to the influence of asperity interaction and hence wear. Oxide layers were generally found to be thicker when the antiwear additive was employed.

It is suggested that the mechanism of pit formation is one of asperity contact induced crack initiation in the immediate subsurface region at depths of no more than 20μm. When these cracks break the surface they are further propagated by cyclic fluid ingress and hydraulic pressure. This leads to branching and eventually removal of material to form a pit.

CHAPTER SIX

SUGGESTIONS FOR FUTURE WORK

The usefulness and the potential of plotting a Stribeck curve for the Amsler 2-disc system has already been established. Further work should be aimed at studying other fire resistant fluids at each of the lubrication regions defined by the Stribeck curve. In addition, Lubrication Region 4b poses an interesting situation and hence should be further investigated. A much wider range of lubricant viscosities and speeds would therefore be needed in order to obtain a more comprehensive analysis of the regimes of lubrication. For completeness, the effect of load at the different lubrication regimes on pitting life could be studied.

Auger electron spectroscopy could be used to investigate the inside of pit profiles. Different surface elemental compositions might then be detected on both the leading and trailing sides of the pit. This would undoubtedly give rise to more information regarding pitting mechanisms for discs run in the presence of water based fire resistant fluids. Other techniques such as X-ray Photoelectron Spectroscopy (XPS) could be used to identify the chemical structure of surface films. The use of X-ray diffraction has shown the presence of different iron oxides in the lubricant. It would therefore be interesting to determine whether or not these iron oxides are present at other lubrication regimes.

The use of the magnetic monitoring technique has been shown to be a useful means by which the crack can be studied during its propagation stage. However, any further modification to this technique should be aimed at increasing the sensitivity in order that subsurface cracking in the immediate surface could be identified at a much earlier stage. The concept of full automation and subsequent computer analysis of the crack signal would be beneficial but would require a method for continuously recording the crack detector output signal. A relationship between crack length and perhaps signal height could then be established.

The angle of crack penetration as identified by metallurgical sectioning could be used as a basis for further study. To investigate this, changes in disc diameter, disc velocity difference (slip), load and hardness differences would have to be undertaken.

Although the Unisteel and Rolling four-ball method of analysis have been shown to be both reliable and effective in ranking the lubricating properties of fluids, it is felt that some metallurgical examination of the test pieces should be undertaken. The information gained from this analysis could then be used to identify other mechanisms associated with crack initiation and propagation.

APPENDIX I

The three principal stresses (P) at depth z for two discs in contact, under zero friction (pure rolling) can be expressed as (62):

$$Px = -2\sigma H(\ (1+(z/b)^2)^{0.5} - z/b\ ) \qquad A1$$

$$Py = -H(\ ((1+(z/b)^2)^{0.5} - z/b)^2/(1+z/b)^2\ ) \qquad A2$$

$$Pz = -H(\ 1/(1+(z/b)^2)^{0.5}\ ) \qquad A3$$

where H is the maximum Hertzian pressure, b is the half width and σ Poisson's ratio.

The shear stress (T) is given by:

$$T = 0.5(Pz - Py) \qquad A4$$

Substituting Equations A2 and A3 into Equation A4 gives:

$$T = H(\ ((z/b)/(1+(z/b)^2)^{0.5}) - 1\ ) \qquad A5$$

Differentiating T with respect to z gives:

$$dT/dz = 2R(1+R^2)^{-0.5} - 2R^3(1+R^2)^{-1.5} - 1 \qquad A6$$

where R = z/b

However the depth of maximum shear will occur when dT/dz = 0. It follows that:

$$2R(1+R^2)^{-0.5} = R^3(1+R^2)^{-1.5} + 1$$

$$2R = R^3(1+R^2)^{-1} + (1+R^2)^{0.5}$$

$$2R - R^3/(1+R^2) = (1+R^2)^{0.5}$$

$$(2R(1+R^2) - R^3)^2 = (1+R^2)^3$$

$$(R(2+R^2))^2 = (1+R^2)^3$$

$$\Rightarrow \qquad R^2(4+4R^2+R^4) = 1+3R^2+3R^4+R^6$$

$$\Rightarrow \qquad 4R^2 + 4R^4 + R^6 = 1 + 3R^2 + 3R^4 + R^6$$

$$\Rightarrow \qquad R^4+R^2-1 = 0$$

Solving for the quadratic:

$$R^2 = (-1\pm(5)^{0.5})/2$$

It follows that $R = (0.618)^{0.5}$ or $R = (-1.618)^{0.5}$, therefore $R = 0.786$.

However, $R = z/b$ so that the depth of maximum shear for the condition of pure rolling occurs at depth $z = 0.786b$.

The maximum shear stress (Tmax) is found on the substitution of $z/b = 0.786$ into Equations A2 and A3. It follows that: $Py = -0.186H$ and $Pz = -0.786H$, where H is the maximum Hertzian pressure. Subsituting these values into Equation A4 gives:

$$Tmax = 0.5(-0.786H - -0.186H) = 0.3H \qquad A7$$

The maximum shear stress under pure rolling conditions, occurring at a depth 0.786b, is therefore 0.3 of the maximum Hertzian pressure H.

The octahedral shear stress is given by:

$$OT = \tfrac{1}{3}(\ (Pz-Px)^2 + (Px-Py)^2 + (Py-Pz)^2\ )^{0.5} \qquad A8$$

The maximum octahedral shear stress is found on the substitution of $z/b = 0.786$ into Equations A1, A2 and A3 and the respective principal stress values (Px,Py,Pz) substituted into Equation A8:

$$OTmax = \tfrac{1}{3}(\ (-0.499H)^2 + (-0.101H)^2 + (0.600H)^2\ )^{0.5} = 0.26H$$

A value of 0.295 was assumed for Poisson's ratio. Thus the maximum octahedral shear stress, ocurring at a depth 0.786b, is 0.26 of the maximum Hertzian pressure.

APPENDIX II

According to Seely and Smith (62) the depth of maximum shearing stress between two discs in rotating contact decreases with the increase in traction between the discs.

The following is a listing of two computer programmes written for the Commadore PET personal computer based on the equations given by Seely and Smith. The first programme determines the maximum shearing stress at depths from 1μm to 150μm below the surface and within the contact zone.

The structure of the programme centres around three nested loops. The inner loop calculates the two main shearing stresses (T1 and T2) across the contact zone and stores the maximum values obtained. The middle loop repeats this procedure 150 times but on each occasion increases the depth condition by 1μm. The respective maximum shearing stress values taken at the different depths are then compared to yield two maximum shearing stresses. This whole procedure is then repeated by the outer loop for different friction conditions ranging from 0 to 0.5.

The second programme is very similar to the first programme except that it determines the shearing stress only at the surface of the disc and is based on the equations given by Smith and Liu (63).

By comparing all of the maximum shearing stresses obtained from both programmes a graph of friction against depth of maximum shear can be plotted, as shown in Figure A2.1.

Programme One - Subsurface shear calculations

```
10    OPEN 1,4
11    PRINT#1,"SUBSURFACE CALCULATION"
30    EM=200E9 : PR=0.295 : RD=0.02
40    PRINT#1,"THESE ARE FIXED:"
50    PRINT#1, : PRINT#1,
60    PRINT#1,"ELASTIC MODULUS     (PA):";EM
70    PRINT#1,"POISSONS RATIO      ----:";PR
80    PRINT#1,"RADIUS OF DISCS      (M):";RD
90    REM
100   REM D IS EQUIVALENT MODULUS
150   D=2*RD*((1-PR^2)/EM)
160   REM
180   INPUT"APPLIED LOAD          (KG)";AL
185   INPUT"TRACK WIDTH           (MM)";TW
186   REM
190   PRINT#1,"APPLIED LOAD          (KG)";AL
195   PRINT#1,"TRACK WIDTH           (MM)";TW
196   REM
197   REM B IS HERTZIAN HALF WIDTH
200   B=(2*AL*9.81*D)/(π*TW*0.001))^0.5
201   REM
202   REM OUTER LOOP TO CHANGE FRICTION (F)
205   FOR F=0 TO 0.5 STEP 0.05
206   REM
207   REM THESE VARIABLES WILL HOLD BOTH MAXIMUM
208   REM SHEARING STRESSES AND CORRESPONDING DEPTHS
209   M3P=0 : M4P=0 : S5T=1 : S6T=1
210   REM
211   PRINT#1,"FRICTION = ";F
212   REM
213   REM MIDDLE LOOP TO CHANGE DEPTH (Z IN METRES)
214   FOR V=1 TO 150 STEP 1
215   Z=V*1E-6
216   REM
217   REM THESE VARIABLES WILL HOLD THE MAXIMUM
218   REM SHEAR STRESS WITHIN THE CONTACT ZONE
219   M1P=0 : M2P=0
300   REM
350   REM INNER LOOP TO CHANGE POSITION IN THE
400   REM CONTACT ZONE
500   FORI=-0.4 TO 1.1 STEP 0.1
510   X=I*B
550   M=((B+X)^2+Z^2)^0.5
560   N=((B-X)^2+Z^2)^0.5
574   D1=π*(M+N)/(M*N*(2*M*N+2*X^2+2*Z^2-2*B^2)^0.5
575   D2=π*(M-N)/(M*N*(2*M*N+2*X^2+2*Z^2-2*B^2)^0.5
600   DZ=-B/(π*D)*(Z*(B*D1-X*D2)+F*Z^2*D2)
670   T1=Z*((B^2+2*Z^2+2*X^2)*D1/B-2*π/B-3*X*D2)
680    T2=F*((2*X^2-2*B^2-3*Z^2)*D2+2*π*X/B+2*(B^2-X^2-Z^2)*X*D1/B
690   DX=-B/(π*D)*(T1+T2)
720   T3=Z*((B^2+X^2+Z^2)*D1/B-π/B-2*X*D2)
730   T4=F*((X^2-B^2-Z^2)*D2+π*X/B+(B^2-X^2-Z^2)*X*D1/B)
740   DY=-2*PR*B/(π*D)*(T3+T4)
770   T5=F*((B^2+2*X^2+2*Z^2)*Z*D1/B-2*π*Z/B-3*X*Z*D2)
780   TZX=-B/(π*D)*(Z^2*D2+T5)
```

```
810  H=DY
820  G=(DZ+DX)/2+0.5*((DZ-DX)^2+4*TZX^2)^0.5
830  J=(DZ+DX)/2-0.5*((DZ-DX)^2+4*TZX^2)^0.5
900  REM
908  REM T1M AND T2M ARE THE MAXIMUM SHEAR STRESSES
910  T1M=-0.5*(J-H)
920  T2M=-0.5*(J-G)
930  REM
935  REM THIS DETERMINES THE MAXIMUM SHEAR STRESS
936  REM WITHIN THE CONTACT ZONE
960  IF T1M>M1P THEN MIP=T1M
970  IF T2M>M2P THEN M2P=T2M
980  NEXT I
990  REM
1000 REM THIS DETERMINES THE DEPTH OF MAXIMUM SHEAR
1100 IF M1P>M3P THEN M3P=M1P : S5T=V
1150 IF M2P>M4P THEN M4P=M2P : S6T=V
1200 NEXT V
1300 REM
1350 REM THIS PRINTS THE DEPTHS AND MAGNITUDES
1355 REM OF THE TWO MAIN MAXIMUM SHEAR STRESSES
1400 PRINT#1,
1450 PRINT#1,"MAXIMUM T1    (PA):";M3P
1500 PRINT#1,"DEPTH OF T1   ( M):";S5T
1525 REM
1550 PRINT#1,"MAXIMUM T2    (PA):";M4P
1600 PRINT#1,"DEPTH OF T2   ( M):";S6T
1700 PRINT#1,
1800 REM
1900 NEXT F
```

Programme Two - Surface shear calculation

```
10   OPEN 1,4
11   PRINT#1,"SURFACE CALCULATION"
30   EM=200E9 : PR=0.295 : RD=0.02
40   PRINT#1,"THESE ARE FIXED:"
50   PRINT#1, : PRINT#1,
60   PRINT#1,"ELASTIC MODULUS    (PA):";EM
70   PRINT#1,"POISSONS RATIO     ----:";PR
80   PRINT#1,"RADIUS OF DISCS     (M):";RD
90   REM
100  REM D IS EQUIVALENT MODULUS
150  D=2*RD*((1-PR^2)/EM)
160  REM
180  INPUT"APPLIED LOAD          (KG)";AL
185  INPUT"TRACK WIDTH           (MM)";TW
186  REM
190  PRINT#1,"APPLIED LOAD          (KG)";AL
195  PRINT#1,"TRACK WIDTH           (MM)";TW
196  REM
197  REM B IS HERTZIAN HALF WIDTH
200  B=(2*AL*9.81*D)/(π*TW*0.001))^0.5
```

```
202  REM OUTER LOOP TO CHANGE FRICTION (F)
205  FOR F=0 TO 0.5 STEP 0.05
206  REM
207  REM THESE VARIABLES WILL HOLD BOTH MAXIMUM
208  REM SHEARING STRESSES
209  M3P=0 : M4P=0
210  REM
211  PRINT#1,"FRICTION = ";F
212  REM
217  REM THESE VARIABLES WILL HOLD THE MAXIMUM
218  REM SHEAR STRESS WITHIN THE CONTACT ZONE
219  M1P=0 : M2P=0
300  REM
350  REM INNER LOOP TO CHANGE POSITION IN THE
400  REM CONTACT ZONE
500  FORI=-0.4 TO 1.1 STEP 0.1
510  X=I*B
550  M=((B+X)^2+Z^2)^0.5
560  N=((B-X)^2+Z^2)^0.5
620  IFX>=B THEN 700
630  IFX<=-B THEN 750
650  DX=-B/D*((1-X^2/B^2)^0.5+2*F*X/B)
660  DY=-PR*B/D*(2*(1-X^2/B^2)^0.5+2*F*X/B)
670  DZ=-B/D*(1-X^2/B^2)^0.5
680  TZX=-F*B/D*(1-X^2/B^2)^0.5
680  GOTO 780
685  REM
700  DX=-2*F*B/D*(X/B-(X^2/B^2-1)^0.5)
710  DY=-PR*B/D*F*2*(X/B-(X^2/B^2-1)^0.5)
720  DZ=0
725  TZX=0
730  GOTO 780
740  REM
750  DX=-2*F*B/D*(X/B+(X^2/B^2-1)^0.5)
760  DY=-PR*B/D*F*2*(X/B+(X^2/B^2-1)^0.5)
770  DZ=0
775  TZX=0
776  REM
780  H=DY
820  G=(DZ+DX)/2+0.5*((DZ-DX)^2+4*TZX^2)^0.5
830  J=(DZ+DX)/2-0.5*((DZ-DX)^2+4*TZX^2)^0.5
900  REM
908  REM T1M AND T2M ARE THE MAXIMUM SHEAR STRESSES
909  REM AT THE SURFACE
910  T1M=-0.5*(J-H)
920  T2M=-0.5*(J-G)
930  REM
935  REM THIS DETERMINES THE MAXIMUM SHEAR STRESS
936  REM AT THE SURFACE WITHIN THE CONTACT ZONE
960  IF T1M>M1P THEN MIP=T1M
970  IF T2M>M2P THEN M2P=T2M
980  NEXT I
1000 REM
1350 REM THIS PRINTS THE MAGNITUDES OF THE TWO MAIN
1375 REM MAXIMUM SHEAR STRESSES AT THE SURFACE
1400 PRINT#1,
```

```
1450 PRINT#1,"MAXIMUM T1   (PA):";M1P
1500 PRINT#1,
1550 PRINT#1,"MAXIMUM T2   (PA):";M2P
1700 PRINT#1,
1800 REM
1900 NEXT F
```

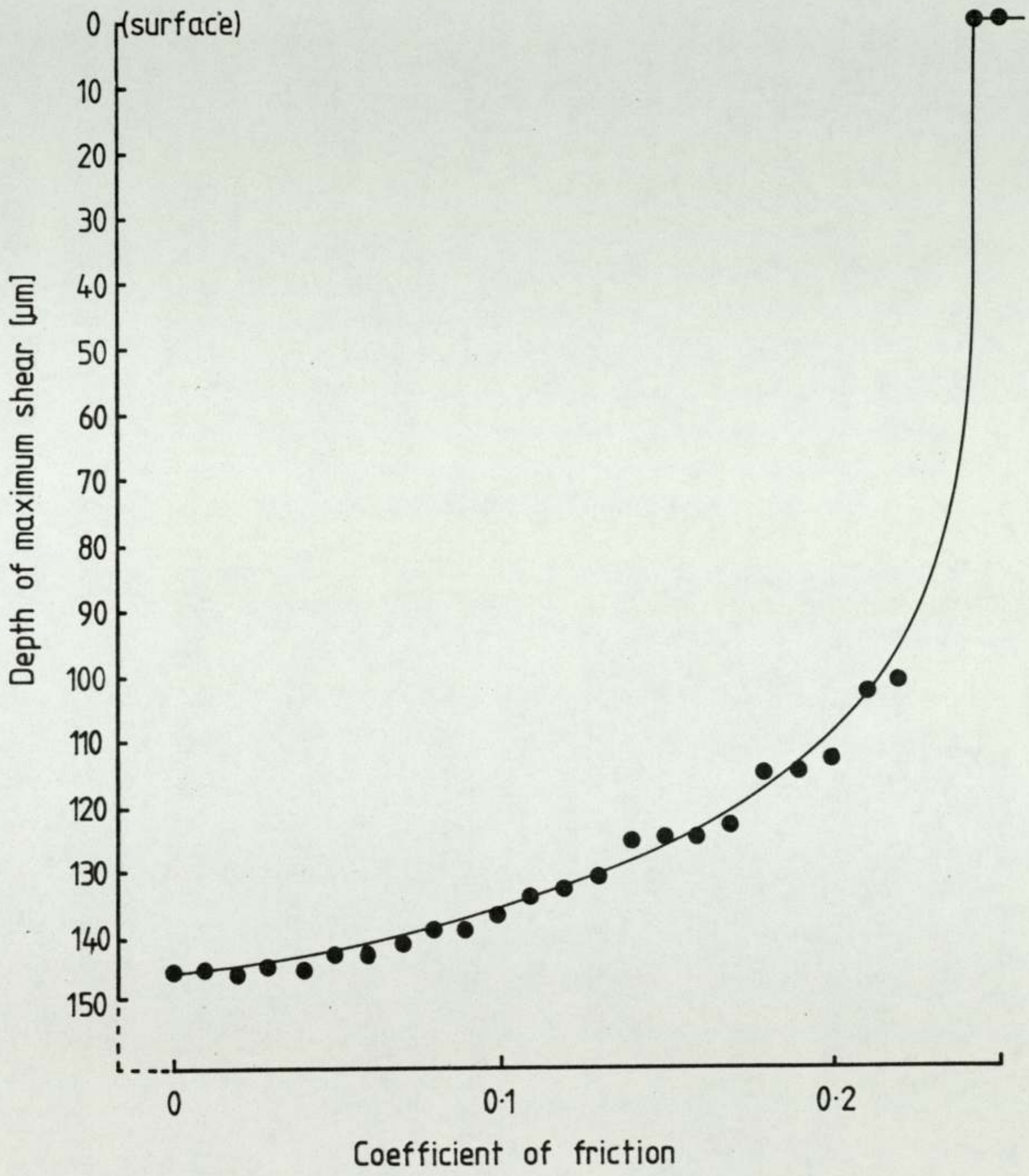

Figure A2·1. Friction against depth of maximum shear.

REFERENCES

1. Ellis E.G. Industrial applications of hydraulic mechanisms. Fundamentals of lubrication. Scientific Publications (GB) Ltd., 103-109, 1968.
2. Hampson D.F and Harper W.Y. Hydraulic transmissions. Lubrication in Practice. Edited by Evans G.G. Macmillan Press and Esso petroleum co., 57-65, 1972.
3. Warring R.H. Water as a hydraulic fluid. Hydraulic fluids and engineering applications. Trade and Technical Press Ltd., 96-102, 1961.
4. Taylor R. and Wang Y.Y. Lubrication regimes and tribological properties of fire-resistant hydraulic fluids. ASLE. Lub. Engr., 40, 1, 44-50, 1985.
5. Maxwell J.F., Schwartz S.E. and Viel D.J. Flow characteristics of hydraulic fluids of different viscosities II. Flow in pumps : Internal leakage and loss efficiency. ASLE. Trans., 24, 2, 224-231, 1981.
6. Maxwell J.F., Schwartz S.E. and Viel D.J. Flow characteristics of hydraulic fluids of different viscosities I. Flow in pumps : A transition from laminar to turbulent flow. ASLE. Trans., 24, 2, 215-223, 1981.
7. Whirl S.F. and Knight R.G. Fire resistant turbine lubricating fluids. ASLE. Lub. Engr., 26, 164-170, 1970.
8. Myers M.B. Fire resistant hydraulic fluids. Their application in British mines. Colliery Guardian., 796-808, 1977.

9. Law D.A. The development and testing of an advanced water-in-oil emulsion for underground mine service. ASLE. Lub. Engr., 37, 2, 82-90, 1981.

10. Knight G.C. The assessment of the suitability of hydrostatic pumps and motors for use with fire resistant fluids. Rolling Contact Fatigue - Performance Testing of Lubricants. Lond. Edited by Tourret R. and Wright E. Heyden and Sons Ltd. For IP., 193-215, 1977.

11. Hobbs R.A. and Mullett G.W. Effect of some hydraulic fluid lubricants on the fatigue lives of roller bearings. Proc. I. Mech. Engr., 183, Pt3P, 21-27, 1968-1969.

12. Cordiano H.V., Cochran E.P. and Wolfe R.J. Effect of combustion resistant hydraulic fluids on ball bearing fatigue life. ASME-ASLE. Lub. Conf., 55, lub 21, 989-996, 1955.

13. Cordiano H.V., Cochran E.P. and Wolfe R.J. A study of combustion resistant hydraulic fluids as ball bearing lubricants. ASLE. Lub. Engr., 261-266, 1956.

14. Kenny P. and Yardley E.D. The use of Unisteel rolling contact fatigue machines to compare the lubricating properties of fire resistant fluids. Wear, 20, 105-121, 1972.

15. Hobbs R.A. Fatigue lives of ball bearings lubricated with oils and fire resistant fluids. Elastohydrodynamic Lubrication. I. Mech. Engr. Symp., 1-4, 1972.

16. Knight G.C. Water Hydraulics : Application of water-based fluids to hydraulic systems. Trib. Int., 105-107, 1977.

17. Wan G.T.Y., Kenny P. and Spikes H.A. Elastohydrodynamic properties of water-based fire-resistant hydraulic fluids. Trib. Int., 17, 6, 309-315, 1984.

18. Levesque A., McCabe M., Piotrowski J. and Webber F. Improved synthetic coolants using a modified poly-alkylene glycol. ASLE. Lub. Engr., 40, 11, 664-666, 1984.

19. Bowden F.B. and Tabor D. Friction - An Introduction to Tribology. Anchor Press / Doubleday NY. 1973.

20. Stribeck R. Characteristics of plain roller bearings. Zeit. V.D.I. 46, 134-148, 1432-1438, 1463-1470, 1902.

21. Rein S.W. Viscosity - I. Lubrication, 64, 1, 1-12, 1978.

22. Tower B. First report on friction experiments. Proc. I. Mech. Engrs., 632-659, 1883 and 29-35, 1884. Also: Second report on friction experiments. Proc. I. Mech. Engrs., 58-70, 1885.

23. Reynolds O. On the theory of lubrication and its applications to Mr. Beauchamp Towers' experiments, including an experimental determination of the viscosity of olive oil. Phill. Trans. 177, 1, 157-234, 1886.

24. Hertz H. On the contact of elastic solids. Misc. Papers, CH5, 146-162, 1896.

25. Timoshenko S. and Goddier J.N. Theory of Elasticity. 2nd Ed., McGraw Hill Co., 382 and 375, 1951.

26. Greenwood J.A., Johnson K.L. and Matsubara E. A surface roughness parameter in Hertz. contact. Wear, 100, 47-57, 1984.

27. Barus C. Isothermals, Isopiestics and Isometrics relative to viscosity. Am. J. Sci., 45, 3, 87-96, 1893.

28. Chu P.S. and Cameron A. Pressure viscosity characteristics of lubricating oils. J. Inst. Pet., 48, 461, 147-155, 1962.

29. Roelands C.J., Vlugter J.C. and Waterman H.I. The viscosity - temperature - pressure relationship of lubricating oils and its correlation with chemical constitution. ASME Trans. J. Basic. Engr., 85, 601-610, 1963.

30. Johnston W.G. A method to calculate the pressure-viscosity coefficient from bulk properties of lubricants. ASLE. Trans., 24, 2, 232-238, 1980.

31. Wright W.A. Prediction of bulk moduli and pressure - volume - temperature data for petroleum oils. ASLE. Trans., 10, 349-356, 1967.

32. Grubin A.N. and Vinogradova I.E. Central Scientific Research Institute for Technology and Mechanical Engineering. Book No. 30 (Moscow). DSIR., Lond., Translation No. 337, 1949.

33. Terrill R.M. On Grubin's formula in elastohydrodynamic lubrication theory. Wear, 92, 67-78, 1983.

34. Dowson D. and Higginson G.R. A numerical solution to the elastohydrodynamic problem. J. Mech. Engr. Sci., 1, 1, 6-15, 1959.

35. Wedeven L.D. What is EHD? ASLE. Lub. Engr., 31, 6, 291-296, 1975.

36. Dowson D. and Higginson G.R. The effect of material properties on the lubrication of elastic rollers. J. Mech. Engr. Sci., 2, 3, 188-194, 1960.

37. Dowson D. and Higginson G.R. New roller-bearing lubrication formula. Engr., 192, 158-159, 1961.

38. Dowson D., Higginson G.R. and Whitaker A.V. Elasto-hydrodynamic lubrication : A survey of isothermal solutions. J. Mech. Engr. Sci., 4, 2, 121-126, 1962.

39. Hamrock B.J. and Jacobson B.O. Elastohydrodynamic lubrication of line contacts. ASLE. Trans., 27, 4, 275-287, 1984.

40. Cheng H.S. and Sternlicht B. A numerical solution for the pressure, temperature and film thickness between two infinitely long, lubricated rolling and sliding cylinders, under heavy loads. ASME. J. Basic. Engr., 87, 3, 695-707, 1965.

41. Dowson D. and Whitaker A.V. A numerical solution of the elastohydrodynamic problem of rolling and sliding contacts lubricated by a Newtonian fluid. Proc. I. Mech. Engrs., 180, Pt3B, 57-71, 1965-1966.

42. Trachman E.G. and Cheng H.S. Traction in elstohydro-dynamic line contacts for two synthesised hydrocarbon fluids. ASLE. Trans., 17, 4, 271-279, 1974.

43. Krause H. and Poll G. The influence of tangential tractions at the surface on the stresses in contacting bodies during rolling - sliding contact. Wear, 88, 221-232, 1983.

44. Crook A.W. Developments in elastohydrodynamic lubrication. J. Inst. Pet., 49, 478, 295-304, 1963.

45. Jackson A. A simple EHL film thickness equation for rolling element bearings. ASLE. Trans., 24, 2, 147-158, 1979

46. Cheng H.S. A numerical solution of the EHD film thickness in an elliptical contact. ASME. J. Lub. Tech., 92, 1, 155-162, 1970.

47. Sibley L.B. and Orcutt F.K. Elastohydrodynamic lubrication of rolling - contact surfaces. ASLE. Trans., 4, 234-249, 1961.

48. Dyson A., Naylor H. and Wilson A.R. The measurement of oil - film thickness in elastohydrodynamic contacts. Proc. I. Mech. Engrs., 180, Pt3B, 119-134, 1965-1966.

49. Dyson A. and Wilson A.R. Film thickness in elastohydrodynamic lubrication by silicone fluids. Proc. I. Mech. Engrs., 180, Pt3K, 3, 97-112, 1965-1966.

50. Archard J.F. and Cowking E.W. Elastohydrodynamic lubrication at point contacts. Proc. I. Mech. Engrs., 180, Pt3B, 47-56, 1965-1966.

51. Cameron A. and Gohar R. Theoretical and experimental studies of the oil film in lubricated point contacts. Proc. Roy. Soc., 291A, 520-536, 1966.

52. Machinery Handbook. Industrial Press Inc., NY. 21st Ed., 2384-3390, 1979.

53. Christensen H. Nature of metallic contact in mixed lubrication. Proc. I. Mech. Engrs., 180, Pt3B, 147-157, 1965-1966.

54. Furey M.J. Metallic contact and friction between sliding surfaces. ASLE. Trans., 4, 1-11, 1961.

55. Tallian T.E., McCool J.J. and Sibely L.B. Partial elastohydrodynamic lubrication in rolling contact. Proc. I. Mech. Engrs., 180, Pt3B, 169-183, 1965-1966.

56. Hardy W.B. and Doubleday I. Boundary lubrication - The paraffin series. Proc. Roy. Soc., A100, 550-574, 1921-1922.

57. Perry D.M., Moran P.J. and Robinson G.M. Three dimensional surface metrology of magnetic recording materials through direct-phase-detecting microscopic interferometry. J. Instn. Elec. Rad. Engrs., 55, 4, 145-150, 1985.

58. LeMar R. Proper maintenance practicies for fire - resistant hydraulic fluid systems. ASLE. Lub. Engr., 32, 10, 539-541, 1976.

59. Wilson A.C.M. Fire-resistant fluids for general hydraulic and steam turbine systems. Proc. I. Mech. Engrs., 182, Pt1, 5, 1967-1968.

60. Snyder C.E., Krawetz A.A and Tovrog T. Determination of the flammability characteristics of aerospace hydraulic fluids. ASLE. Lub. Engr., 37, 12, 705-714, 1980.

61. Hoffmann N.M. Hydraulic fluid of 95 percent water? ASLE. Lub. Engr., 35, 2, 65-71, 1979.

62. Seely F.B. and Smith J.O. Advanced Mechanics of Materials. John Willey and Sons. 2nd Ed., 342-378, 1953.

63. Smith J.O and Liu C.K. Stresses due to tangential and normal loads on an elastic solid with application to some contact stress problems. ASME. A13, 52, 157-166, 1953.

64. Dowson D., Higginson G.R. and Whitaker B.A. Stress distribution in lubricated rolling contacts. I. Mech. Engrs. Fatigue in Rolling Contact., 66, 6, 66-75, 1963.

65. Czyzewski T. Changes in the stress field in the elasto-hydrodynamic contact zone due to some operating factors and their role in the rolling contact fatigue of cylinderical surfaces. Wear, 31, 119-140, 1975.

66. Merwin M.S. and Johnson K.L. An analysis of plastic deformation in rolling contact. Proc. I. Mech. Engrs., 177, 25, 676-690, 1963.

67. Crook A.W. Simulated gear-tooth contacts : Some experiments upon their lubrication and subsurface deformations. Proc. I. Mech. Engrs., 171, 187-214, 1957.

68. Hamilton G.M. Plastic flow in rollers loaded above the yield point. Proc. I. Mech. Engrs. 177, 667-675, 1963.

69. Johnson L.G. The Statistical Treatment of Fatigue Experiments. Elsevier publishing Co., 1-47, 1964.

70. Lieblein J. and Zelen M. Statistical investigation of the fatigue life of deep-grooved ball bearings. J. Res. Nat. Bur. Stn., 57, 5, 273-315, 1956.

71. Weibull W. A statistical distribution function of wide applicability. ASME. J. App. Mech., A6, 51, 293-297, 1951.

72. Hills D.A. and Ashelby D.W. The initation of wear cracks. Wear, 70, 365-371, 1981.

73. Littmann W.E. and Widner R.L. Propagation of contact fatigue from surface and subsurface origins. ASME. J. Basic. Engr., 88, 624-636, 1966.

74. Griffith A.A. Phenomenon of rupture and flaws in solids. Phil. Trans. Roy. Soc., 221A, 163-198, 1920.

75. Pook L.P. Analysis and application of fatigue crack growth data. I. Mech. Engrs. J. Strain. Anal., 10, 4, 242-250, 1975.

76. Keer L.M., Bryant M.D and Haritos G.K. Subsurface and surface cracking due to Hertzian contact. ASME. J. Lub. Tech., 101, 347-351, 1982.

77. Corten H.T. and Park F.R. Fracture. Int. Sci. Tech., March, 24-36, 1963.

78. Clark W.G. Fracture mechanics in fatigue. Exp. Mech., 11, 421-428, 1971.

79. Polk C.J., Murphy W.R. and Rowe C.N. Determining fatigue crack propagation rates in lubricating environments through the application of a fracture mechanics technique. ASLE. Trans., 18, 4, 290-298, 1975.

80. Littmann W.E., Widner R.L., Wolf J.O. and Stover J.D. The role of lubrication in propagation of contact fatigue cracks. ASME. J. Lub. Tech., 90, 89-100, 1968.

81. Michau B., Berthe D. and Godet M. Observations of oil pressure effects in surface crack development. Trib. Int., 7, 119-122, 1974.

82. Rowe C.N. and Armstrong E.L. Lubricant effects in rolling contact fatigue. ASLE. Lub. Engr., 38, 1, 23-30, 39-40, 1982.

83. Littmann W.E. The mechanism of contact fatigue. Interdisciplinary approach to the lubrication of concentrated contacts. NASA., SP 237, 309-377, 1970.

84. McKelvey R.E and Moyer C.A. The relationship between critical maximum compressive stress and fatigue life under rolling contact. I. Mech. Engrs., 1-10, 1963.

85. Gustafson J.H. High temperature oil evaluation in full scale bearing fatigue tests. ASLE. Lub. Engr., 20, 2, 65-68, 1964.

86. Pederson R. and Rice S.L. How to select proper case depth for carburised and hardened gears. SAE. J., 68, 34-38, 1960.

87. Way S. Pitting due to rolling contact. J. Appl. Mech., 2, A49-A58, 1935.

88. Dawson P.H. Rolling contact fatigue crack initation in a 0.3 per cent carbon steel. Proc. I. Mech. Engrs., 183, Ptl, 4, 75-83, 1968-1969.

89. Miki H. and Kobayashi S. Pitting failure of annealed carbon steel under rolling contact. Wear, 67, 1-13, 1981.

90. Martin J.A. and Eberhardt A.D. Identification of potential failure nuclei in rolling contact fatigue. ASME. J. Basic. Engr., 89, 932-942, 1967.

91. Ciftan M. and Saibel E. The effect of zeta potential on pitting. Wear of Materials, 653-658, 1979.

92. Dawson P.H. The pitting of lubricated gear teeth and rollers. Pwr. Trms., 30, 208-217, 1961.

93. Dawson P.H. Effect of metallic contact on the pitting of lubricated rolling surfaces. J. Mech. Engr. Sci., 4, 1, 16-21, 1962.

94. Dawson P.H. Present position in the series of tests on the pitting of lubricated rolling surfaces. Proc. I. Mech. Engrs., 180, Pt3B, 224, 1965-1966.

95. Dawson P.H. The effect of sliding on rolling contact pitting. J. Mech. Engr. Sci., 23, 6, 289-294, 1981.

96. Harris T.A. Roller Bearing Analysis. John Wiley and Sons. NY., 1966.

97. Onions R.A. and Archard J.F. Pitting of gears and discs. Proc. I. Mech. Engrs., 188, 673-682, 1975.

98. Tallian T.E. On competing failure modes in rolling contact. ASLE. Trans., 10, 418-439, 1967.

99. Skurka J.C. Elastohydrodynamic lubrication of roller bearings. ASME. J. Lub. Tech., 92, 281-291, 1970.

100. Martin J. B. and Cameron A. Effect of oil on the pitting of rollers. J. Mech. Engr. Sci., 3, 148-152, 1961.

101. Niemann G., Rettig H. and Botsch H. The effect of different lubricants on the pitting resistance of gears. Proc. I. Mech. Engrs., Pt3D, 179, 192-200, 1964-1965.

102. Bartz W.J. and Kruger V. Test method for evaluating the influence of lubricants and lubricant additives on fatigue failure of heat treated and case-hardened spur gears. Rolling Contact Fatigue - Performance Testing of Lubricants. Edited by Tourret R. and Wright E.P. Heyden and sons Ltd. for IP, 161-182, 1977.

103. Soda N. and Yamamoto T. Effect of tangential traction and roughness on crack initation/propagation during rolling contact. ASLE. Trans., 25, 2, 198-206, 1982.

104. Polk C.J. and Rowe C.N. Crack growth rate : Its measurement and a controlling factor in rolling contact fatigue. ASLE. Trans., 19, 1, 23-32, 1976.

105. Keer L.M. and Bryant M.D. A pitting model for rolling contact fatigue. ASME. J. Lub. Tech., 105, 198-205, 1983.

106. Yamamoto T. Crack growth in lubricated rollers. Solid Contact and Lubrication. Edited by Cheng H.S. and Keer L.M. ASME/AMD., 39, 223-236, 1980.

107. Yoshimura H., Rubin C.A. and Hahn G.T. A technique for studying crack growth under repeated rolling contact. Wear, 95, 29-34, 1984.

108. Eisenstadt R. and Fuller W.D. Generation of crack propagation data on notched rotating beam specimens by means of an interrupted stressing technique. ASME. J. Basic. Engr., 92, 183-189, 1970.

109. Phillips M.R. and Quinn T.F.J. The effect of surface roughness and lubricant film thickness on the contact fatigue life of steel surfaces lubricated with a sulphur-phosphorus type of extreme pressure additive. Wear, 51, 11-24, 1978.

110. Rowson D.M. and Wu Y.L. The effect of the additive chemistry of elemental sulphur on the contact fatigue life of steel EN31 discs. Wear, 70, 373-381, 1981.

111. Kelley B.W. Lubrication of concentrated contacts - The practical problem. Interdisciplinary approach to the lubrication of concentrated contacts. NASA., SP 237, 1970.

112. Littmann W.E., Kelley B.W., Anderson W.J., Fein R.S., Klaus E.E., Sibley L.B. and Winer W.O. Chemical effects of lubrication in contact fatigue. Part III : Load-life exponent, life scatter and overall analysis. ASME. J. Lub. Tech., 98, 308-315, 1976.

113. Rounds F.G. Some effects of additives on rolling contact fatigue. ASLE. Trans., 10, 243-254, 1967.

114. Cann P., Spikes A. and Cameron A. Thick film formation by zinc dialkyldithiophosphates. ASLE Trans., 26, 1, 48-52, 1983.

115. Scott D. Study of the effect of lubrication on pitting failure of balls. Proc. Conf. on lubrication and wear. I. Mech. Engrs., 58, 463-468, 1957.

116. Mould R.W. and Silver H.B. A study of the effect of acids on the fatigue life of EN31 steel balls. Wear, 37, 333-343, 1976.

117. Rounds F.G. Effects of base oil viscosity and type on bearing ball fatigue. ASLE. Trans., 5, 172-182, 1962.

118. Rounds F.G. Influence of steel composition on additive performance. ASLE. Trans., 15, 1, 54-66, 1972.

119. Cantley R.E. The effect of water lubricating oil on bearing fatigue life. ASLE. Trans., 20, 3, 244-248, 1977.

120. Grunberg L and Scott D. The acceleration of pitting failure by water in the lubricant. J. Inst. Pet., 44, 419, 406-410, 1958.

121. Schatzberg P. and Felsen I.M. Effects of water and oxygen during rolling-contact lubrication. Wear, 12, 331-342, 1968.

122. Schatzberg P. and Felsen I.M. Influence of water on fatigue failure location and surface alteration during rolling-contact lubrication. J. Lub. Tech., 91, 301-307, 1969.

123. Felsen I.M., McQuaid R.W. and Marzani J.A. Effect of seawater on the fatigue life and failure distribution of flood-lubricated angular contact ball bearings. ASLE. Trans., 15, 1, 8-17, 1972.

124. Mantel E.R., Robinson G.H. and Thompson R.F. Influence of atmospheric moisture on fatigue of hardened steel. Met. Engr. Quart., 1, 3, 57-61, 1961.

125. Vaessen G.H.G. and De Gee A.W.J. Influence of water vapour on the wear of lightly loaded contacts. Wear, 18, 325-332, 1971.

126. Beagley T.M. and Pritchard C. Wheel/rail adhesion - The overriding influence of water. Wear, 35, 299-313, 1975.

127. Grunberg L., Jamieson D.T. and Scott D. Hydrogen penetration in water-accelerated fatigue of rolling surfaces. Phill. Mag., 8, 1553-1568, 1963.

128. Ciruna J.A. and Szieleit H.J. The effect of hydrogen on the rolling contact fatigue life of AISI 52100 and 400C steel balls. Wear, 24, 107-118, 1973.

129. Ray D., Vincent B., Coquillet B., Guirandenq P., Chene J. and Aucouturier M. Hydrogen embrittlement of a stainless ball bearing steel. Wear, 65, 103-111, 1980.

130. Grunberg L. and Scott D. The effect of additives on the water induced pitting of ball bearings. J. Inst. Pet., 46, 440, 259-266, 1960.

131. Grunberg L. The formation of hydrogen peroxide on fresh metal surfaces. Proc. Roy. Soc., B66, 153-161, 1953.

132. Schatzberg P. Inhibition of water-accelerated rolling contact fatigue. ASME. J. Lub. Tech., 93, 231-233, 1971.

133. Scott D. Further data on the efect of additives on the water-accelerated pitting of ball bearings. J. Inst. Pet., 48, 457, 24-25, 1962.

134. Murphy W.R., Polk C.J. and Rowe C.N. Effect of lubricant additives on water-accelerated fatigue. ASLE. Trans., 21, 63-70, 1978.

135. Hother-Lushington S. Water lubricated bearings. Trib. Int., 9, 257-260, 1976.

136. Borowski J.L. The use of invert emulsion hydraulic fluid in a steel slab caster. ASLE. Lub. Engr., 36, 11, 652-656, 1980.

137. Scott W. The influence of fire resistant hydraulic fluids on system and component design. Wear, 56, 105-121, 1979.

138. Scott D. and Blackwell J. NEL Rolling contact tests - accelerated simulation tests for lubricants and materials for rolling elements. Wear, 17, 323-333, 1971.

139. Scott D. The effect of material properties, lubricant and environment on rolling contact fatigue. I. Mech. Engrs. Fatigue in Rolling Contact, 10, 103-115, 1963.

140. Zaretsky E.V., Parker R.J. and Anderson W.J. Component hardness differences and their effect on bearing fatigue. ASME. J. Lub. Tech., 89, 47-62, 1967.

141. Yardley E.D., Kenny P. and Sutcliffe D.A. The use of rolling-fatigue test methods over a range of loading conditions to assess the performance of fire-resistant fluids. Wear, 28, 29-47, 1974.

142. AHEM. Guidlines for derating the life of ball bearings when used with fire resistant fluids. AHEM Ltd., Lond., S5865, January 1977.

143. Dalmaz G. and Godet M. Film thickness and effective viscosity of some fire resistant fluids in sliding point contacts. ASME. J. Lub. Tech., 100, 304-308, 1978.

144. Hamaguchi H., Spikes H.A. and Cameron A. Elastohydrodynamic properties of water-in-oil emulsions. Wear, 43, 17-24, 1977.

145. Wan G.T.Y. and Spikes H.A. The elastohydrodynamic lubricating properties of water-polyglycol fire-resistant fluids. ASLE. Trans., 27, 4, 366-372, 1984.

146. Syniuta W.D. and Corrow C.J. A scanning electron microscope fractographic study of rolling contact fatigue. Wear, 15, 187-199, 1970.

147. O'Brien J.L. and King A.H. Electron microscopy of stress-induced structural alterations near inclusions in bearing steels. ASME. J. Basic. Engr., 88, 568-572, 1966.

148. Calabrese S.J., Ling F.F. and Murray S.F. Dynamic wear tests in the SEM. ASLE. Trans., 26, 4, 455-465, 1983.

149. Takagi R. Effect of oxide film on the friction of 52100 steel in vacuum. ASLE. Trans., 13, 2, 87-98, 1970.

150. Phillips M.R., Dewey M., Hall D.D., Quinn T.F.J. and Southworth H.N. The application of Auger electron spectroscopy to tribology. Vacuum, 26, 10/11, 451-456, 1976.

151. Pepper S.V. Auger analysis of films formed on metals in sliding contact with halogenated polymers. J. Appl. Phys., 45, 7, 2947-2956, 1974.

152. Quinn T.F.J. Physical techniques for examining surfaces. Trib. Int., 3, 198-205, 1970.

153. March C.N. The evaluation of fire-resistant fluids using the Unisteel rolling contact fatigue machine. Rolling Contact Fatigue - Performance Testing of Lubricants. Lond. Edited by Tourret R. and Wright E. Heyden and Sons Ltd. For IP., 217-230, 1977.

154. Phillips M.R. PhD Thesis. The University of Aston in Birmingham, 1979.

155. Fowle T.I. Lubrication for fluid film and Hertzian contact conditions. Proc. I. Mech. Engrs., 182, Pt3A, 568-584, 1968.

156. Phillips M.R. and Chapman C.J. A magnetic method for detecting the onset of surface contact fatigue. Wear, 49, 265-272, 1978.

157. IP 305/79 Tentative. The assessment of lubricants by measurement of their effect on the rolling fatigue resistance of bearing steel using the Unisteel machine. IP standards for petroleum and its products Part I : Methods for analysis and testing. Heyden and Sons for IP, Lond., 2, 1982.

158. IP 300/79. Rolling contact fatigue tests for fluids in a modified four-ball machine. IP standards for petroleum and its products Part I : Methods for analysis and testing. Heyden and Sons for IP, Lond., 2, 1982.

159. Torrance A.A. The metallography of worn surfaces and some theories of wear. Wear, 50, 169-182, 1978.

160. Electron microscopy and micro-analysis of crystalline materials. Edited by Belk J.A. Applied Science Publishers Ltd., 1-16, 99-120, 1979.

161. Auger P. On the compound photoelectric effect. J. Phys. Radium, 6, 205-208, 1925.

162. A perspective on the analysis of surfaces and interfaces. Practical surface analysis by Auger and X-ray photoelectron spectroscopy. Edited by Briggs D. and Seah M.P. John Wiley and Sons, 1-16, 1983.

163. Handbook of Auger spectroscopy. Physical Electronics Division, 11-15, 1976.

164. Woolfson M.M. X-ray crystallography. Cambridge University Press, 130-134, 1970.

165. Klug H.P. and Alexander L.E. X-ray diffraction procedures (for polycrystalline and amorphous materials). John Wiley and Sons, 2nd Ed., 175-222, 1974.

166. Weibull W. The phenomenon of rupture in solids. Ingeniors Ve Tenskaps Akademiens Handlingar, Stockholm, Vols 151-160, 5-55, 1939-1941.

167. Weibull W. A statistical representation of fatigue failure in solids. Trans. Roy. I. Tech., Stockholm, 27, 311-326, 1949.

168. Galvin G.D. and Naylor H. Effect of lubricants on the fatigue of steel and other metals. Proc. I. Mech. Engrs., 179, Pt3J, 56-70, 1964-1965.

169. Powder diffraction file search manual (inorganic). Published by JCPDS (USA) 1979.

170. Private communication, T.F.J. Quinn, Georgia Institute of Technology, Georgia, Atlanta, USA.

171. Poole W. and Sullivan J.L. The role of aluminium segregation in the wear of aluminium/bronze-steel interfaces under conditions of boundary lubrication. ASLE. Trans., 23, 4, 401-408, 1980.

172. Tallian T.E. The theory of partial elastohydrodynamic contacts. Wear, 21, 49-102, 1972.

173. Yamada T. Rolling wear characteristics of annealed carbon steel under dry contact conditions. Wear, 51, 279-288, 1978.

174. Niemann G., Rettig H. and Botsch H. The effect of different lubricants on the pitting resistance of gears. Proc. I. Mech. Engrs., 179, Pt3D, 192-201, 1964-1965.

175. Johnson K.L., Greenwood J.A and Poon S.Y. A simple theory of asperity contact in elastohydrodynamic lubrication. Wear, 19, 91-108, 1972.

176. MacPherson P.B. Pitting of hardened steels under traction. Rolling Contact Fatigue - Performance Testing of Lubricants. Edited by Tourret R. and Wright E.P. Heyden and sons Ltd. for IP, 127-136, 1977.

177. Private communication, S.G. Rudston, BP Research Centre, Sunbury-on-Thames, Middlesex.

178. Woodger G.B. Progress towards the introduction of HWBF hydraulic fluids. Automotive Manufacturing update '81 Conf., Mech. Engr. Publications Ltd., C278/81, 33, 1981.

Abbreviations used in the references:

AHEM. : The Association of Hydraulic Equipment Manufacturers.

Am. J. Sci. : American Journal of Science.

ASLE. : American Society of Lubricantion Engineers.

ASLE. Lub. Engr. : Lubrication Engineering.

ASLE. Trans. : Transactions.

ASME. : American Society of Mechanicl Engineers.

ASME. J. App. Mech. : Journal of Applied Mechanics.

ASME. J. Basic. Engr. : Journal of Basic Engineering.

ASME. J. Lub. Tech. : Journal of Lubrication Technology.

ASME-ASLE. Lub. Conf. : Lubrication Conference.

DSIR. : Department of Scientific and Industrial Research.

Engr. : Engineering.

Exp. Mech. : Experimental Mechanics.

I. Mech. Engrs. : Institute of Mechanical Engineers.

Int. Sci. Tech. : International Science and Technology.

IP. : Institute of Physics.

J. Appl. Mech. : Journal of Applied Mechanics.

J. Appl. Phys. : Journal of Applied Physics.

J. Inst. Pet. : Journal of the Institute of Petroleum.

J. Instn. Elec. Rad. Engrs. : Journal of the Institution of Electronic and Radio Engineers.

J. Mech. Engr. Sci. : Journal Mechanical Engineering Science.

J. Phys. Radium. : Journal of Physics Radium.

J. Res. Nat. Bur. Stn. : Journal of Research of the National Bureau of Standards.

J. Strain. Anal. : Journal of Strain Analysis.

Met. Engr. Quart. : Metals Engineering Quartely.

NASA. : National Aeronautics and Space Administration.

Phill. Mag. : Phillisophical Magazine.

Phill. Trans. : Phillisophical Transactions of the Royal Society of London.

Pwr. Trms. : Power Transmission.

Proc. I. Mech. Engr. : Proceedings of the Institute of Mechanical Engineers.

Proc. Roy. Soc. : Proceedings of the Royal Society.

SAE. J. : The Society of Automotive Engineers Journal.

Trans. Roy. I. Tech. : Transactions of the Royal Institute of Technology.

Trib. Int. : Tribology International.

Zeit. VDI. : Zeitschrift Verein Deutscher Ingenieure.

PUBLICATIONS

PREPRINT NO. 84-LC-3C-4
ASLE PREPRINT

The Pitting and Cracking of SAE 52100 Steel in Rolling/ Sliding Contact in the Presence of an Aqueous Lubricant©

J. L. SULLIVAN and M. R. MIDDLETON
University of Aston
Gosta Green, Birmingham, England

The use of aqueous lubricants is well established in applications where their fire-resistant properties are of prime importance. A major disadvantage of the use of such fluids, however, is their relatively poor performance in high-stress rolling-contact bearings where components suffer fatigue cracking and pitting at an earlier stage than with mineral oils.

In this investigation, factors affecting the cracking and pitting of SAE 52100 steel in the presence of a water-glycol-based fluid have been studied using an Amsler two-disk machine. A Stribeck curve was plotted and has shown that pitting damage is dependent on the region of the curve in which the system is operated, pitting life being a minimum in mixed-elastohydrodynamic lubrication.

Good correlation was found betwen pitting life and specific film thickness λ above $\lambda = 0.05$. Below this value, inverse correlation was observed.

Finally, a mechanism for crack initiation, propagation, and subsequent pitting in aqueous fluids is proposed.

INTRODUCTION

In certain industries, the use of mineral-based lubricating oils is not possible due to the risk of ignition, hence fire-resistant fluids have been developed to replace them. The four major classes of fire-resistant fluid are oil-in-water emulsions, water-in-oil invert emulsions, synthetic fluids, and water-glycol-based fluids. All these fluids are not necessarily completely fire resistant and some may burn under certain conditions, particularly if mixed with some other combustible material such as coal dust. The fluids which exhibit the most pronounced fire resistance are the water-glycol-based solutions and, for this reason, they are potentially the most attractive. Unfortunately they are also the poorest lubricants (*1*), (*2*). Although many of the problems associated with sliding wear and corrosion have been solved by the inclusion of additives (*3*), these fluids still perform badly in rolling-contact bearings where steel elements suffer fatigue cracking and pitting at a much earlier stage than with conventional mineral oil lubrication (*4*), (*5*). It is thus of great commerical interest to study the factors affecting the pitting failure of steels in the presence of water-glycol fluids in order to facilitate the design of systems and the definition of operating conditions to obtain reasonable life expectancy with optimum fire resistance.

Presented as an American Society of Lubrication Engineers paper at the ASLE/ASME Lubrication Conference in San Diego, California, October 22–24, 1984
Final manuscript approved July 10, 1984

It would be impossible to fully instrument in-service machinery, hence for a fundamental investigation accelerated tests must be devised. A number of test machines have been used in such investigations; for example, Scott and Blackwell (*6*) have used a rolling 4-ball machine and Kenny and Yardley (*1*) the Unisteel Machine, but in these, together with a number of other ball-bearing test machines used by other workers, full instrumentation cannot easily be achieved. A better approach is to employ a two-disk configuration of the type used in the pioneering work by Way (*7*) on pitting failure. With this configuration, it is possible to continuously monitor wear and friction and to identify cracks and study their progress to form pits. Thus, a two-disk machine was chosen for our experiments and with the results, together with extensive surface and subsurface examination, it is hoped that the mechanism of pitting failure can be identified.

EXPERIMENTAL

Experiments were conducted using an Amsler test machine where two 40-mm diameter disks were loaded against each other circumferentially and rotated independently with a 10 percent slip between the upper "pitting" disk and the lower "driving" disk. The pitting disk was the slower moving surface. A diagramatic representation of this cofiguration is shown in Fig. 1. Speed could be varied between 20 and 400 rpm and load (by means of a variable compression spring) between 200 and 2000 N.

This load variation gave maximum Hertzian stresses between 0.47 and 1.5 GPa. The fire-resistant fluid was pumped to the conjunction at a rate of 0.24 $\ell.\text{min}^{-1}$ and recirculated through a glass wool filter to remove debris. Table 1 gives the composition and viscosities of the three fluids used.

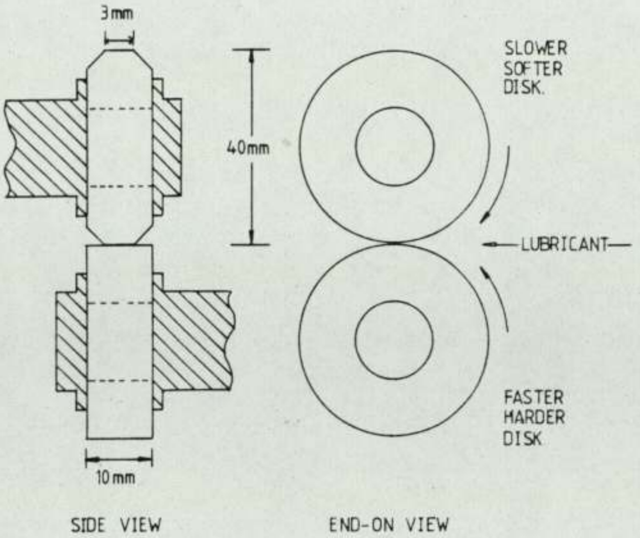

Fig. 1—Schematic diagram of the disk configuration

The SAE 52100 steel disks were of hardness 750 and 250 VPN for the driving and pitting disk, respectively. Hardness differences of this magnitude are required (*8*) if pitting is to occur in a reasonable time period. The driving disks had a surface roughness of 0.07 μm cℓa and the majority of pitting disks a roughness of 0.25 μm cℓa, however, for investigations on the effects of surface roughness on pitting life, roughnesses between 0.05 and 0.5 μm cℓa were used.

Friction was measured using a load dynamometer. Wear was continuously monitored by means of an LVDT distance transducer located on the top disk housing. This gave a measure of relative displacement between the disks, but since wear on the harder disk was found to be negligible, it is reasonable to assume that displacement is due to pitting disk wear.

In order to investigate the formation of cracks and pits during disk motion, a magnetic crack detector similar to that developed by Phillips and Chapman (*9*) was used. The amplitude of the voltage output from the detector gave a measure of the magnitude of surface and subsurface irregularities. This output was displayed as a function of disk circumferential distance on an oscilloscope trace. The size of the first detectable crack varied with orientation, but was generally about 1 mm long by 0.025 mm wide. The test machine could be automatically stopped at any preset output amplitude, in order to monitor the progress of individual cracks and examine surfaces at all stages of damage. Total surface damage could be quantified by use of a frequency counter at the detector output.

One object of the investigation was to examine pitting failure relative to different lubrication regimes. It is, therefore, essential to define these regimes for our system and this is best done by generating a Stribeck curve, where coefficient of friction, μ, is plotted against the dimensionless parameter $\frac{\text{viscosity }(\eta)\quad\text{speed }(s)}{\text{contact pressure }(p)}$ sometimes called the "bearing number." To do this, new ultrasonically cleaned disks were run-in for a period of 24 hours in one of the fluids prior to any measurement. Friction was then recorded for a number of values of $\frac{\eta s}{p}$, determined mainly by change in speed. It was not possible to cover the whole range from boundary to hydrodynamic lubrication with a single-viscosity fluid, hence fluids with three different viscosities were used and the above procedure repeated for each of the other viscosities. The difference in fluid viscosity was due entirely to differing ratios of polyalkylene glycol (thickener) to propylene glycol and hence there should be no additional surface chemical effects associated with fluid change in this or any subsequent experiment. The resultant single Stribeck curve, of classical shape clearly indicating boundary, mixed-elastohydrodynamic, and hydrodynamic lubrication régimes, is shown in Fig. 2.

Eight regions of lubrication, designated A to H in Fig. 2, were selected for further investigation and Table 2 gives the operating conditioins for each regime.

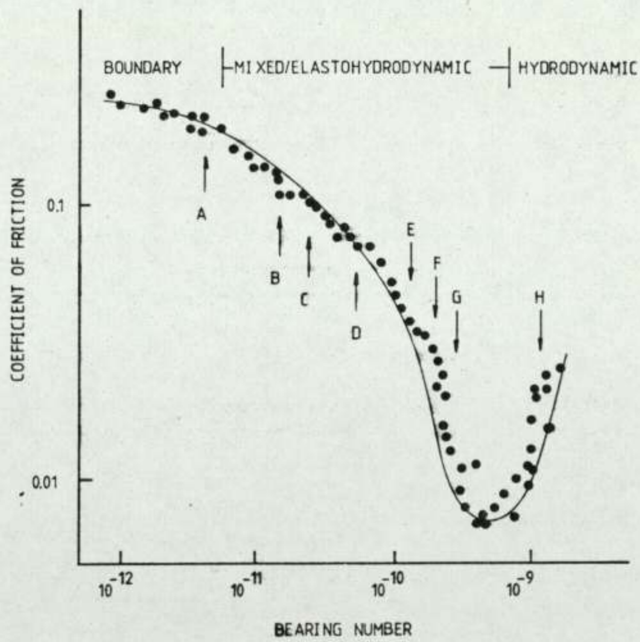

Fig. 2—The Stribeck curve

TABLE 1—COMPOSITION AND VISCOSITIES OF TEST FLUIDS					
FLUID	DEIONIZED WATER	PROPYLENE GLYCOL	2-DIMETHYLAMINO ETHANOL RUST INHIBITOR	POLYALKYLENE GLYCOL THICKENER	VISCOSITY Nsm^{-2}
A	43	55.75	1.25	0	6×10^{-3}
B	43	41.75	1.25	14	23.5×10^{-3}
C	43	22.75	1.25	33	70.3×10^{-3}

TABLE 2—TEST CONDITIONS USED FOR DETAILED INVESTIGATION OF WEAR BEHAVIOR OF HYDRAULIC FLUIDS

REGION	BEARING NUMBER $\frac{\eta s}{p}$	SPEED rpm	LOAD N	FLUID VISCOSITY $\times 10^{-3}$ Nsm^{-2}	MEAN CONTACT PRESSURE GPa
A	3.8×10^{-12}	30	900	6.0	0.8
B	1.3×10^{-11}	100	900	6.0	0.8
C	2.5×10^{-11}	200	900	6.0	0.8
D	5.3×10^{-11}	100	900	23.5	0.8
D	5.5×10^{-11}	400	900	6.0	0.8
E	1.5×10^{-10}	100	900	70.2	0.8
F	2.1×10^{-10}	400	900	23.5	0.8
G	3.1×10^{-10}	200	900	70.2	0.8
H	1.3×10^{-9}	400	200	70.2	0.4

In each region, the test machine was automatically stopped at the first detectable crack and the surface examined before the run was allowed to continue. Detector trip-out levels were progressively increased and surfaces examined in order to follow the growth of individual cracks to the formation of a pit. The runs were terminated at the appearance of the first pit, the number of revolutions noted and the disks removed for examination and sectioning. Up to 20 experiments were conducted at each region.

To investigate the effects of surface roughness and film thickness, two regions were chosen for further examination. In these tests, composite roughnesses were varied from 0.07 to 0.29 μm. The specific film thickness or Lambda function factor λ (*10*) defined as:

$$\left[\frac{\text{elastohydrodynamic film thickness}}{\text{composite relative roughness}}\right]$$

was plotted as a function of life to first pit, N. The film thickness was plotted using the Dowson-Higginson equation (*11*).

EXPERIMENTAL RESULTS

Wear rates for experiments conducted in regions A to H are shown as a function of bearing number, $\left(\frac{\eta s}{p}\right)$, in Fig. 3. The superscripts against each point on this and the next graph show the average number of detectable cracks at the appearance of the first pit. The graph shows that both wear rate and surface damage decrease with increase in bearing number. From the graph, the wear rate is described by the equation

$$w = 3.24 \times 10^{-20} \left(\frac{\eta s}{p}\right)^{-0.76}$$

Figure 4 shows the variation in "life at first pit" (expressed in number of contact cycles, N) with bearing number. The graph shows a minima in life at a value of $\left(\frac{\eta s}{p}\right)$ of about 1×10^{-10}.

Figure 5 showing the variation in life with λ (calculated for initial surface roughnesses) indicates similar trends, with the expected increase in N with λ only occurring after a value of $\lambda = 0.05$, when the best fit line gives a relationship of

$$\log_{10} N = 0.42 \log_{10} \lambda + 5.91$$

with 0.77 correlation coefficient. Below $\lambda = 0.05$ an inverse correlation exists. A curve plotted for λ calculated from final surface roughnesses showed similar variations, but with a greater scatter of points. The best fit line for this graph is described by the equation

$$\log_{10} N = 0.20 \log_{10} \lambda + 5.70$$

with a correlation coefficient of only 0.31.

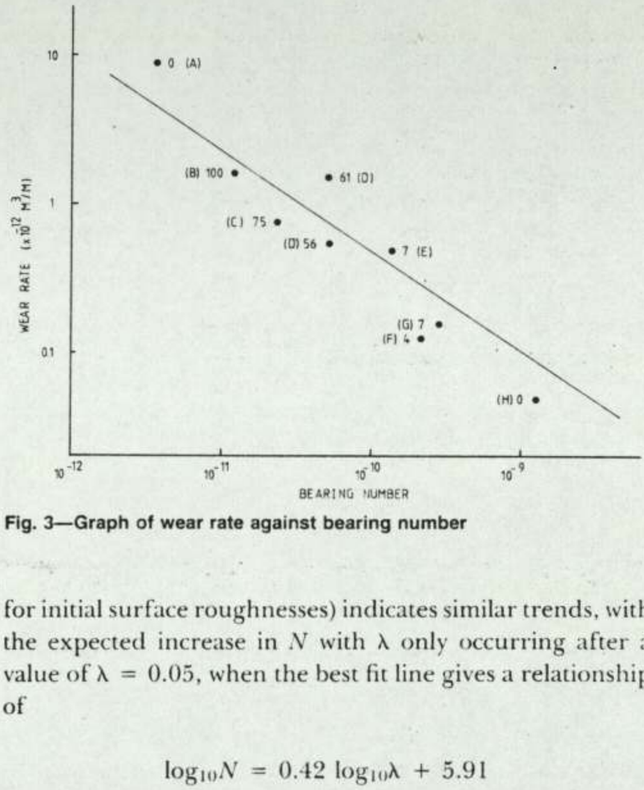

Fig. 3—Graph of wear rate against bearing number

To study the development of surface cracks into pits, optical photomicrographs were recorded for disks stopped at various stages of crack propogation. Such a series, with corresponding crack detector traces for region C, is shown in Fig. 6. The figure shows that the initial crack grows in both length and depth and that new cracks appear and grow throughout the run. Disk surfaces run in regions B and D were of similar appearance with extensive surface cracking. The extent of the damage was greater in region B than in

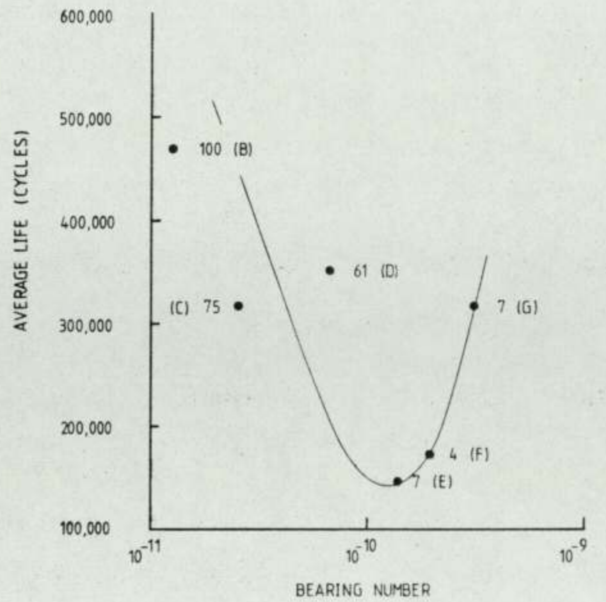

Fig. 4—Graph of average life to first pit against bearing number

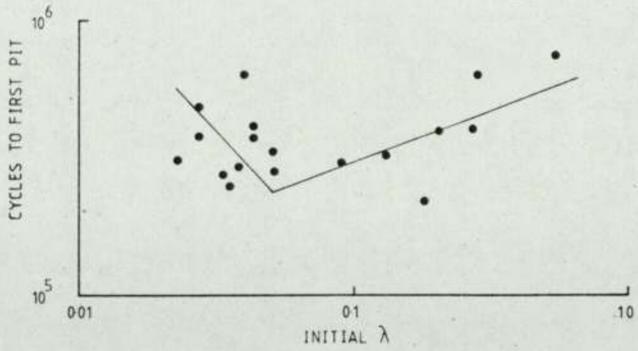

Fig. 5—Graph of cycles to first pit against initial lambda factor

C and less in region D than in C. In all regions, the high wear rates ensured that all cracks did not necessarily progress to form pits.

Tests conducted in regions E, F, and G yielded very few additional cracks before a pit was formed and, in general, each initial crack formed a pit. Figure 7(a) and (b) show surfaces from regions E and G, respectively, together with corresponding detector traces after the formation of the first pit. The detector traces show few perturbations compared with the previous figure. The times between crack initiation and pit formation were much lower in region G than in other regions and crack propogation rates in general appear to be inversely dependent on bearing number.

Pitting did not occur either in the boundary region A or for thick film lubrication, region F, although tests were run for three times the number of cycles in any of the other regions. Surfaces from the boundary region were rough and the corresponding detector traces indicated many small shallow cracks, Fig. 8(a). In contrast, Fig. 8(b) shows surfaces from the hydrodynamic region to be smooth with correspondingly smooth detector traces indicating no cracks present.

Figure 9 shows typical cross sections taken from various regions investigated. The shallow cracks formed in the boundary region, Fig. 9(a), are quite different to the cracks

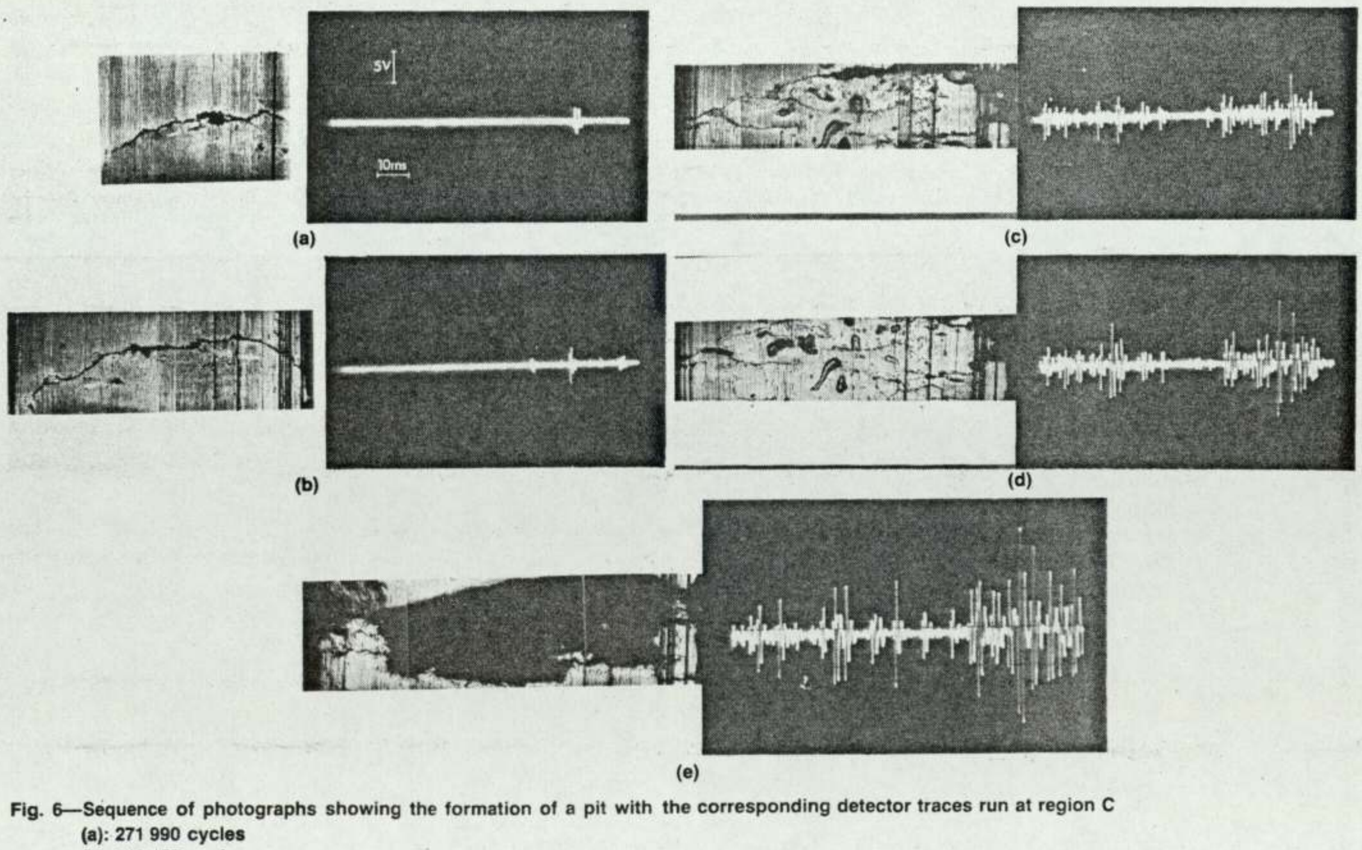

Fig. 6—Sequence of photographs showing the formation of a pit with the corresponding detector traces run at region C

(a): 271 990 cycles
(b): 312 157 cycles
(c): 359 234 cycles
(d): 368 961 cycles
(e): 378 235 cycles

↑ DIRECTION OF MOTION

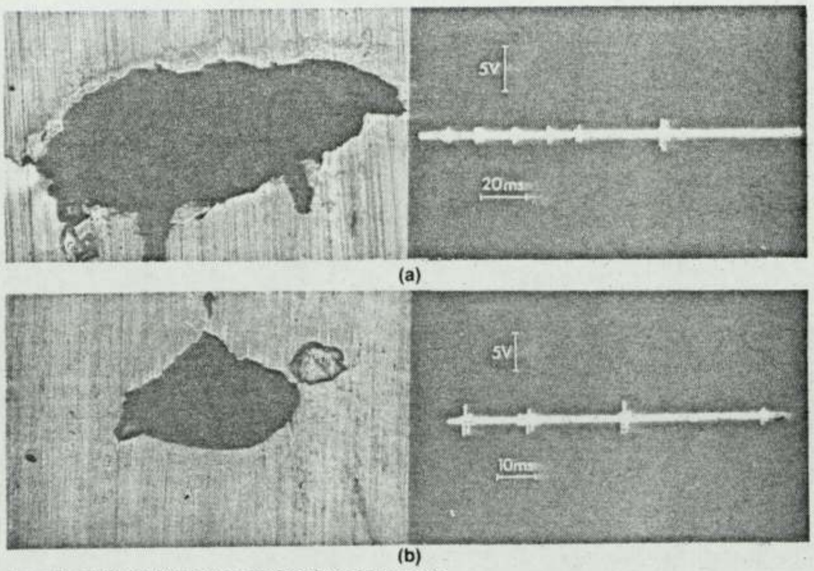

Fig. 7—Final pits formed at regions E and G with their respective detector traces.
(a): region E
(b): region G

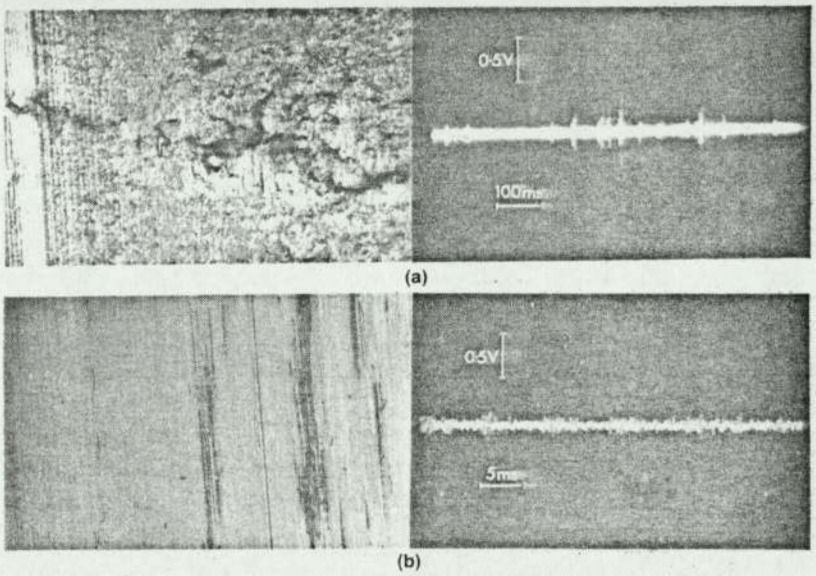

Fig. 8—General surface view of the nonpitted surfaces after running at regions A and H with the corresponding detector traces.
(a): region A
(b): region H

and pits formed in other regions shown in the lower magnification photomicrographs 9(b), (c), and (d), where cracks leading to pits form at well-defined angles of between 20° and 30° to the surface. The depth and size of the pits decreased with increase in bearing number.

DISCUSSION

The Stribeck curve, Fig. 2, gave a useful representation of the various regimes of lubrication and this enabled the authors to concentrate their efforts in the mixed-elastohydrodynamic lubrication regime.

The graph of wear rate versus bearing number, Fig. 3, shows a fall in wear rate of almost three orders of magnitude between region A and region H. This result is to be expected since asperity/asperity interaction also decreases with increase in bearing number. From the graph, wear rate was found to vary as $(\eta s)^{-0.76}$, since contact pressure, p, was kept constant at 0.8 GPa throughout the tests in regions A to G. It is interesting to note that from the equations for minimum elastohydrodynamic film thickness for line contact (*11*), thickness, h, depends on the product $(\eta_o U)^{0.7}\alpha^{0.6}$, where η_o in absolute viscosity at the working temperature of the fluid, U the mean surface velocity (directly related to S) and α the pressure coefficient of viscosity. For point contact, Archard and Cowking (*12*) have shown that h depends on $(\alpha\, \eta_o U)^{0.74}$. It is a matter of conjecture whether ultimate film breakdown and asperity contact conditions are governed by gross film thicknesses, determined from line contact conditions for our disks or microfilms due to the essentially point-contact conditions prevailing at the asperity junction. However, the modulus of the exponent in our wear relationship is sufficiently close to those in the film thickness equations to strongly suggest that wear rate is

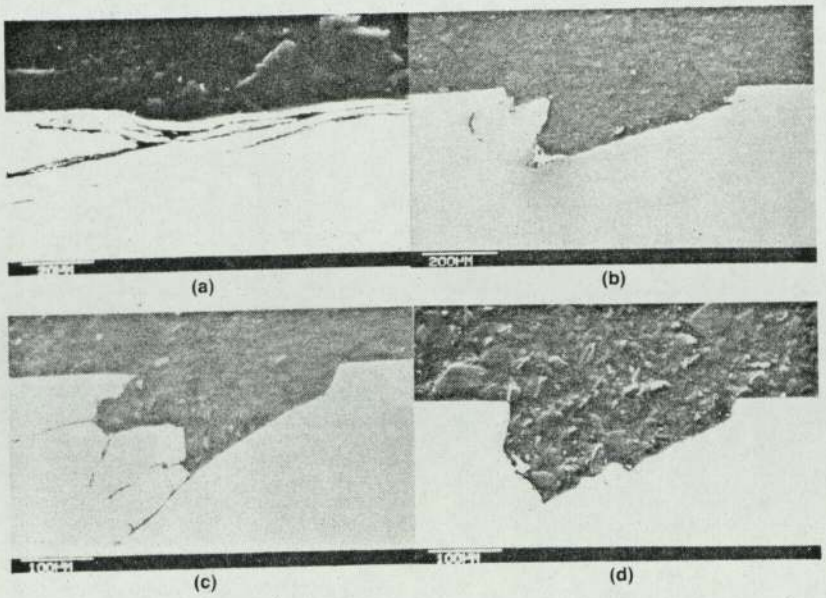

Fig. 9—Cross sections of the disks taken at the various regions
(a): region A
(b): region C
(c): region E
(d): region G
DIRECTION OF MOTION →

inversely proportional to film thickness. Hence, the relationship $\omega \propto \frac{1}{h}$ is important when considering the relation between pitting life and surface wear.

Figures 4 and 5 show an apparent increase in life below specific values of bearing number and λ, both of which are directly related to film thickness. This increase in life is connected to the increase in wear rate with increased metallic contact in these regions. It is thus an interesting phenomenon, but of no engineering benefit since the high wear rate of components under these conditions would be quite unacceptable in practice. Similar effects have been observed in mineral oils at values of λ four times less than those in our investigation (*8*).

Considering the mechanisms of crack initiation propagation and eventual pit formation, it is well known that cracks may be either surface or subsurface initiated (*13*). For a system like ours where a relatively poor lubricant is used, cracks are most probably initiated in the immediate subsurface region at depths between 1 and 20 μm due to asperity-asperity interaction. We have carried out a substantial amount of subsurface sectioning and on only one occasion was there any evidence of an isolated deep subsurface crack. Sections of disks run in the boundary region, 9(a), show cracks almost parallel to the surface and within a depth of about 20 μm. These are very similar to those reported by Dawson (*14*) for disk surfaces run in dry rolling/sliding contact, Dawson found that subsequent introduction of a lubricant resulted in formation of pits from propagation of primary cracks at angles between 10° and 30° to the surface. Further, both the shape and size of the pits formed in this investigation, Figs. 6 and 7, are similar to those observed using the same test configuration with a similar steel, but mineral-oil-based lubricants. It is thus proposed that the mechanism of pit formation for the water-glycol fluid is similar to that for mineral oils under similar conditions. Cracks are initiated close to the surface due to asperity interaction (*15*), break through the surface and propagate due to a pressure wedge created by fluid ingress (*16*). Cyclic stressing leads to further propagation and branching until a pit is formed. Correlation coefficients of 0.77 and 0.31 for life versus λ calculated for initial and final composite roughnesses, respectively, indicate that it is the initial surface condition which is the important rate determining factor in crack initiation.

The results suggest that crack propagation rates are inversely dependent on film thickness. Thus with thick elastohydrodynamic films, the infrequent asperity contacts lead to a low probability of crack formation, but when a crack does occur, it progresses fairly rapidly to form a pit. As asperity contact increases with decrease in film thickness, cracks are formed more readily and in greater numbers, but the propagation rate is relatively low and the higher wear rates ensure that many cracks are removed before they can form pits. Even the smallest concentration of water in mineral oil has a detrimental effect and super-saturated lubricants considerably reduce lives (*17*). Hence, in the thicker film regions where more water is forced into the cracks, propagation rates are higher due to two effects. One is mechanical, where a greater volume of fluid is more likely to maintain the high compressive stress necessary for rapid crack growth. The other chemical, where, according to Scott (*18*), water-produced hydrogen diffuses into highly stressed surfaces ahead of microcracks resulting in hydrogen embrittlement.

For boundary lubrication, cracks never developed into pits. The high wear rate results in surface removal at a greater rate than crack propagation, but also there is insufficient fluid at the conjunction to enter the cracks and maintain the hydraulic pressure necessary to promote crack propagation.

In the hydrodynamic region, little asperity contact takes place and the surfaces, Fig. 8(b), show no evidence of cracking or other damage even when run for three times the number of cycles in any other test. The surfaces in this region were thus effectively separated by the fluid, removing the possibility of asperity contact initiated cracking and hence preventing pitting.

CONCLUSIONS

The pitting life of SAE 52100 steel disks in rolling contact with 10 percent slip in the presence of water-glycol fire-resistant fluid was found to depend on the regimes of lubrication as defined by a Stribeck curve plotted for the system. Pitting did not occur at either extreme region of the curve, that is for boundary or for thick-film lubrication, although considerable surface distress was observed for the former of the two. Pitting occurred throughout the mixed-elastohydrodynamic regime between bearing numbers 1.7×10^{-12} and 1.3×10^{-10} with a minimum of pitting life observed at a bearing number of 1×10^{-10}. This minimum may be explained in terms of a balance between degree of asperity contact, wear, and volume of fluid present at the conjunction.

In the tests, a good correlation was found between life to first pit and λ, calculated from the composite initial surface roughness, above a value of $\lambda = 0.05$. Below this value, an inverse correlation was observed.

Pits formed during this investigation were very similar to those produced in mineral oils under similar conditions. It is suggested that the mechanism of formation is one of asperity-contact-induced crack initiation in the immediate subsurface region at depths of no more than 20 μm. When the cracks break the surface, they are propagated by cyclic fluid ingress and hydraulic pressure. This leads to branching and eventual removal of material to form a pit. The life to first pit depends on the rate of fluid-controlled crack propagation compared with the rate of removal of surface material.

ACKNOWLEDGMENTS

One of the authors, M. R. Middleton, would like to thank BP Research Ltd. and The Science and Engineering Research Council for financial support during this project.

REFERENCES

(*1*) Kenny, P. and Yardley, E. D., "The Use of Unisteel Rolling Fatigue Machines to Compare the Lubrication Properties of Fire Resistant Fluids," *Wear*, **20**, pp 105–121 (1972).

(*2*) Knight, G. C., "Water Hydraulics—Applications of Water Based Fluids to Hydraulic Systems," *Tribology Intl.*, **10**, pp 105–107 (1977).

(*3*) Knight, G. C., "The Assessment of the Suitability of Hydrostatic Pumps and Motors for Use with Fire Resistant Fluids," *Rolling Contact Fatigue—Performance Testing of Lubricants*, London, edited by Tourret and Wright, published Heyden & Sons Ltd for IP, pp 193–215 (1977).

(*4*) Cantley, R. E., "The Effect of Water in Lubricant Oil on Bearing Fatigue Life," *ASLE Trans.*, **20**, 3, pp 244–248 (1977).

(*5*) Hobbs, R. A. and Mullett, G. W., "Effect of Some Hydraulic Fluid Lubricants on the Fatigue Lives of Roller Bearings," *Proc. I. Mech. E.*, **183**, pt 3P, pp 23–29 (1968–69).

(*6*) Scott, D. and Blackwell, J., "NEL Rolling Contact Tests—Accelerated Simulation Tests for Lubricants and Materials for Rolling Elements," *Wear*, **17**, pp 323–333 (1971).

(*7*) Ways, S., "Pitting Due to Rolling Contact," *J. Appl. Mech.*, **2**, A49–A58 (1935).

(*8*) Phillips, M. R. and Quinn, T. F. J., "The Effects of Surface Roughness and Lubricant Film Thickness on the Contact Fatigue Life of Steel Lubricated with a Sulphur-Phosphorus Type Extreme Pressure Additive," *Wear*, **51**, pp 11–24 (1978).

(*9*) Phillips, M. R. and Chapman, C. J. S., "A Magnetic Method for Detecting the Onset of Surface Fatigue," *Wear*, **49**, pp 265–272 (1978).

(*10*) Harris, T. A., *Rolling Bearing Analysis*, John Wiley and Sons Inc., NY (1966).

(*11*) Dowson, D. and Higginson, G. R., *Elastohydrodynamic Lubrication*, Pergamon Press, London (1966).

(*12*) Archard, J. F. and Cowking, E. W., "Elastohydrodynamic Lubrication at Point Contacts," *Proc. Inst. Mech. Eng.*, **180**, pp 47–56 (1966).

(*13*) Littman, W. E. and Widner, R. L., "Propagation of Contact Fatigue from Surface and Subsurface Origins," *Trans. ASME J. Basic Eng.*, **88**, pp 624–636 (1966).

(*14*) Dawson, P. H., "Rolling Contact Fatigue Crack Initiation in 0.3% Carbon Steel," *Proc. Inst. Mech. Eng.*, **183**, pp 75–83 (1968).

(*15*) Dawson, P. H., "The Effect of Metallic Contact on the Pitting of Lubricated Rolling Surfaces," *J. Mech. Eng. Sci.*, **4**, pp 16–21 (1962).

(*16*) Michan, B., Berthe, D. and Godet, M., "Observations of Oil Pressure Effects in Surface Crack Development," *Tribology Intl.*, **1**, pp 119–122 (1974).

(*17*) Armstrong, E. L., Leonardi, S. J., Murphy, W. R., and Wooding, P. S., "Evaluation of Water-Accelerated Bearing Fatigue in Oil-Lubricated Ball Bearings," *Lubr. Eng.*, **34**, 1, pp 15–21 (1978).

(*18*) Scott, D., "The Effect of Material Properties, Lubricant and Environment on Rolling Contact Fatigue," *Proc. Symp. Fatigue in Rolling Contact, I. Mech. E.*, pp 103–115 (1963).

DISCUSSION

T. F. J. QUINN (Member, ASLE)
Georgia Institute of Technology
Atlanta, Georgia 30332

The authors are to be congratulated on their meticulous attention to establishing the appropriate regime of lubrication for water-glycol and SAE 52100 steel. Figure 2, the Stribeck Curve, is one of the best such curves I have seen. I was especially impressed with the strong inverse correlation between wear rate and bearing number, and I would agree with the authors in their conclusion that wear rate is inversely proportional to film thickness. Although possibly expected, this relationship has not been so convincingly established before.

It is also to the authors' credit that they have been able to show that water-glycol acts very similarly to mineral oil as far as pitting is concerned, although I am a little perturbed by their suggestion that there is an inverse relationship between "cycles to first pit" and the "initial λ" (for λ less than 0.05). This seems to imply that, for very thin films, the life to first pit is greater than for thicker films. In the work carried out by Phillips and myself (*A1*) using mineral oils, we showed that for D ($= 1/\lambda$) less than about 16 (i.e., $\lambda > 0.06$) there was an increase in "cycles to first pit" with decreasing D (increasing λ) which agress with what the authors have found for the water-glycols. None of our results related to $D > 20$ (i.e., $\lambda < 0.05$). Would the authors please comment on their results for pitting at $\lambda < 0.05$, since it seems (to me) that this is the region where their usually good results show some instability.

REFERENCE

(*A1*) Phillips, M. R. and Quinn, T. F. J., "The Effect of Surface Roughness and Lubricant Film Thickness on the Contact Fatigue Life of Steel

Surfaces Lubricated with a Sulphur-Phosphorus Type of Extreme Pressure Additive," *Wear*, **51** pp 11–24 (1978).

DISCUSSION

ANDREW JACKSON (Member, ASLE)
Mobil Oil Corporation
Princeton, New Jersey 08540

The viscosity values given in Table 1 and Table 2 would be more meaningful with associated temperatures. It would also be worthwhile knowing the pressure viscosity coefficient values used for the three test fluids.

AUTHORS' CLOSURE

The authors wish to thank Dr. Quinn and Dr. Jackson for their comments.

In reply to Dr. Quinn, the results do indeed show that for very thin films in regions of mixed-elastohydrodynamic lubricaton close to the boundary region, pitting lives can be greater than for thicker film lubrication for these poor aqueous lubrications. The reason for this result is that as effective fluid film support tends to zero in the boundary region, the rate of wear increases such that the rate of surface removal becomes comparable with and eventually greater than the rate of crack propogation. Thus, although the rate of crack initiation is greater in the thin film region, due to increased asperity interaction, the majority of the cracks formed will be worn away before progressing to a pit. This apparent increase is, however, of no engineering value since wear rates under these conditions are unacceptably high.

In reply to Dr. Jackson, all viscosity values were measured at 32°C, the mean working temperature of the fluid during the experiments. Pressure viscosity coefficients were not measured, but values were taken from Fowle (*C1*).

REFERENCE

(*C1*) Fowle, . . "Lubrication for Fluid Film and Hertzian Contact Conditions," *Proc. I. Mech. E.*, **182,** 3A, pp 568–584 (1968).

Paper VI(iv)

The effect of water based fire resistant lubricants on the pitting of steel

J. L. Sullivan and M. Middleton

In many industries lubrication by mineral oils is not possible due to the risk of ignition and fire resistant fluids have, therefore, been developed as a substitute. A major disadvantage of the use of such fluids is that they perform poorly when used in rolling contact bearings, the steel elements of which suffer premature fatigue pitting and cracking compared with similar components run in mineral oil.

In this investigation factors affecting the fatigue damage of steel surfaces in rolling-sliding contact in the presence of a water-glycol based fire resistant fluid have been studied using an Amsler two disc machine. It has been shown that pitting life depends on the relative magnitude of the fluid film thickness and that a minimum in pitting life occurs in the mixed-elastohydrodynamic region. Mechanisms for crack initiation, propagation and subsequent pit formation in aqueous lubricants are proposed.

1 INTRODUCTION

The use of fire resistant lubricants may be expected to grow in applications where their ability to resist ignition, resist flame propagation and to self extinguish is considered to be more important than their ultimate lubricating properties.

Lubrication by any of the four major types of fire resistant fluids namely, oil in water emuslions, water in oil invert emulsions, synthetic fluids and water glycol solutions results in significant reduction in bearing lives compared with systems lubricated with mineral oils (1). The inclusion of suitable additives (2) solves some problems, but the fluids still perform poorly in rolling contact bearings, where steel elements suffer cracking and pitting at a much earlier stage than with mineral oil lubrication. It is unfortunate that the water glycol based fluids, which exhibit the most pronounced fire resistance and are hence potentially the most attractive, are also the poorest performers in this respect (3,4). It is thus of great commercial interest to study the factors affecting the pitting failure of steels in the presence of water-glycol fluids in order that systems and fluids might be developed to reduce pitting and increase life.

Of necessity accelerated tests must be used for such an investigation. Various ball bearing based fatigue test machines have been used in such investigations, for example rolling 4 - ball (5) and Unisteel machines (3), and have proved reliable in comparisons of fluid performances. They all suffer, however, from the disadvantage that continuous monitoring of wear, friction and crack initiation and propagation is not possible and examinations of wear processes and of crack and pit formation must be of a forensic nature. A better method is to use a two disc configuration similar to that employed by Way (6), where the above parameters may be recorded continuously. For this reason this configuration was chosen for our investigation and experiments were conducted in the presence of water-glycol fluids of varying viscosity, both with and without the addition of an anti-wear agent. From the results gained it is hoped that the mechanism of pitting failure in this important range of lubricants can be identified.

2 EXPERIMENTAL PROCEDURES

Experiments were conducted using an Amsler two disc machine where two 40 mm diameter SAE52100 steel discs were circumferentially loaded and rotated independently with 10% slip. The faster 'driving' discs were of hardness 750 V.P.N. and the slower discs of hardness 250 V.P.N. Surface roughnesses averaged 0.07 μm c.l.a. and 0.25 μm c.l.a. respectively. Pitting only occurred at the surfaces of the slower discs. The load, applied through a variable compression spring, was kept constant at 900 N giving a maximum Hertzian stress of 1.01 GPa. Speed was varied between 20 and 400 r.p.m. All specimens were thoroughly cleaned and degreased before each test. Figure 1 shows a schematic diagram of the test configuration.

The test fluids consisted of 43% by weight deionized water, 1.25% 2-dimethylamino ethanol rust inhibitor and the remainder a mixture of propylene glycol and polyalkylene glycol, the relative proportions of which determined fluid viscosity. This gave a viscosity range between 6×10^{-3} and 70.3×10^{-3} Nsm^{-2}. In a second series of tests 0.8% decanoic acid anti wear agent was added to similar fluids. The fluids were pumped to the conjunction at a rate of $0.24 \, lm^{-1}$ and recirculated through a fine glass wool filter.

Friction was measured using a load dynamometer. Wear was continuously monitored by means of an LVDT distance transducer located on the top disc housing. A magnetic crack detector similar to that described by Phillips and Chapman (7) was used to investigate the formation of cracks and pits during disc motion. The amplitude of the voltage output from the detector gave a measure of the magnitude of surface and sub-surface irregularities. This output was displayed as a function of disc circumferential distance on an oscilloscope trace. The size of the first detectable crack varied with orientation, but was generally about 1 mm long by 0.025 mm wide. The test machine could be automatically stopped at any pre-set output amplitude, in order to monitor the progress of individual cracks and examine surfaces at all stages of damage and total surface damage could be quantified by use of a frequency counter at the detector output.

Prior to any long term tests a Stribeck curve was plotted for our system, in order to fully define the lubrication regimes, and this is shown in figure 2. In order to construct the curve, discs were initially run for a period of 24 hours in a fluid of a certain viscosity and friction measurements were made at a series of values of the dimensionless parameter

$$\frac{\text{viscosity}\,(\eta) \times \text{angular velocity}\,(s)}{\text{contact pressure}}$$

sometimes called the bearing number B. B was altered for any one viscosity fluid by changing the angular speed of the discs. In order to cover the range from boundary to hydrodynamic lubrication, fluid of a number of different viscosities was used and the procedure repeated for each viscosity value. A number of regions defined by the curve and determined by alteration of speed and viscosity at constant load were chosen for further long term fatigue tests. In each region the test machine was run until automatically stopped at the first detectable crack. Photomicrographs of the resultant damage were then recorded before the experiment was allowed to continue with an increased detector trip-out threshold level. In this way crack progress was monitored. The experiments were terminated at the appearance of the first pit when the number of cycles was noted. Wear and friction were monitored continuously throughout each run. Up to 20 experiments were conducted at each selected point.

3 RESULTS

Wear rates for the fluids both with and without the addition of anti-wear agent are shown as a function of calculated elastohydrodynamic (e.h.l) film thickness h, calculated using the Dowson-Higginson Equation (8), in figure 3. Variation with bearing number is also indicated in this figure. The numbers next to each point in this and the following graph show the average number of detectable cracks at the appearance of the first pit. From the graphs wear rates, $w\,(m^3m^{-1})$, in the mixed - e.h.l. regime are described by the equation

$$w = 1.6 \times 10^{-20}\,(h)^{-1}$$

for fluid without additive, and

$$w = 8.57 \times 10^{-18}\,(h)^{-0.65}$$

for fluid containing the anti-wear agent

Figure 4 shows the variation in the life N (number of cycles) to first pit shown as a function of calculated film thickness and bearing number for both fluid with and without additive. Both curves exhibit a minimum life in the centre of the mixed-e.h.l. region defined by the Stribeck curve. The graphs clearly indicate that the addition of the anti-wear agent results in a significant increase in the mean recorded life to first pit throughout the mixed-e.h.l. region. There is a further significant reduction in surface damage under more severe conditions in the presence of this additive.

Figure 5 shows the number of cycles N_p between the first detectable crack and its progression to form a pit, again as a function of calculated e.h.l. film thickness and of bearing number. In contrast to the previous two figures there appears to be little difference in this parameter whether the additive is present or not as all points lie about a line described by the equation

$$N_p = 7.33\,(h)^{-\frac{1}{2}}$$

It is also interesting to note that N_p does not follow the variation of life to first pit N with film thickness and that no minima in the value of N_p occurs.

The pitting process was studied by taking a series of sequential photomicrographs of the surface at various stages in the discs life. Such a series is shown in figure 6 together with associated detector traces for experiments conducted at a bearing number of 1.5×10^{-10} (0.0475 m calculated film thickness) in a fluid without additive. This series is typical of test runs in the fluid without additive for bearing numbers greater than about 10^{-10}, that is in regions tending towards thick film lubrication and for all test runs for the fluid with additive. The test runs yielded few additional cracks and in general each initial crack progressed to form a pit. In contrast figure 7 shows a series for a region tending towards the boundary regime where there is extensive surface cracking and where each initial crack did not necessarily progress to form a pit.

Figure 8 shows typical cross sections. The shallow cracks formed under boundary lubrication, figure 8(a) are quite different to the cracks and pits formed in other regions, a typical example of which is shown in 8(b), where initial cracks appear at well defined angles of between 20 and 30° to the surface. Depth and size of pits decreased with increase in film thickness for fluids without additive, but remained at constant size when the additive was present. Pitting did not occur in either the boundary region or for hydrodynamic lubrication. Figure 9 shows, however, that the surfaces were completely different, the former were very rough with many small shallow cracks, the latter smooth with little sign of surface distress.

4 DISCUSSION

Figure 3 shows a direct inverse correlation between wear rates for fluid without additive and the calculated film thickness. This relationship might be expected since the degree of asperity interaction will increase with decrease in film thickness. The increase in wear rates of almost three orders of magnitude in this mixed region will, however, substantially affect the pitting process. With the additive present the inverse proportionallity no longer applies since chemical interaction will now influence wear mechanisms. It is interesting to note that the additive appears to be pro-wear under less severe conditions, only beginning to exhibit its anti-wear effect in the mixed region tending towards boundary lubrication. Pro-wear effects have been observed for organic acid additives in quite different systems (9).

Figure 4 shows an apparent increase in pitting life below specific values of h. This increase is related to the increase in wear at small relative e.h.l. thicknesses and although interesting is of no engineering benefit since the high wear of components under these conditions would be unacceptable in practice. The figure does, however, show the benefit of using an anti-wear agent, since lives are increased by between 2 and 7 times.

After the formation of the initial crack the number of cycles required to pit does not follow the life trend, figure 4, but increases steadily with decrease in film thickness, figure 5. Further the values of this parameter are independent of whether the fluid contains an additive or not. These facts are important when considering pitting mechanisms. If, after crack initiation, propagation is dependent purely on contact fatigue conditions one would expect an increase in propagation rates (a decrease in N_p) as asperity contact increases with fall in film thickness. The converse occurs. One would further expect a decrease in propagation rates (and an increase in N_p) in the presence of an anti-wear additive and this does not occur. The increase in N_p with decrease in h might be related to the increase in wear rates, but this is not likely since under the most severe conditions wear is responsible for the removal of only 13μm of surface in the time taken for a pit of depth 400μm to form. The most likely explanation for the trend is that N_p is related to the volume of fluid at the conjunction, rapid propagation occurring with a greater volume.

To understand the mechanisms of pit formation we must consider separately the processes of crack initiation and crack propagation and branching. Cracks may be either surface or subsurface initiated (10) and in a system like ours, where a poor lubricant is used, it is likely that cracks are formed due to asperity interaction at depths between 1 and 20 μm (11). Sections of discs run in the boundary region, figure 8(a), confirm this and show cracks running almost parallel to the surface at depths up to 20μm. These cracks are very similar to those reported by Dawson (12) for discs run dry in rolling-sliding contact. Dawson found that subsequent introduction of a lubricant resulted in the formation of pits from propagation of these primary cracks at angles of between 10 and 30° to the surface, angles very close to those observed in our investigation. This suggests that initial cracks, of the type shown in figure 8(a), eventually break the surface and are responsible for pit formation in the mixed - e.h.l. regime.

Contact fatigue conditions, numbers and frequency of asperity contacts are likely to be responsible for crack initiation, but the results shown in figure 6 suggest that these factors do not much influence subsequent propagation and pit formation and that this is likely to be strongly dependent on the amount of fluid at the conjunction. Hence cracks, under the conditions of our experiments, propagate after the initial crack breaks the surface due to a cyclic pressure wedge created by fluid ingress (13). Wear will considerably influence crack initiation, but will have little effect on propagation.

With thick e.h.l. films the infrequent asperity contacts lead to a low probability of crack formation, but when a crack forms it is not likely to be removed by wear and rapidly propagates due to the relatively large amount of fluid at the conjunction. As asperity contact increases with decrease in film thickness cracks are formed more readily and in greater numbers, but many are removed due to wear. Propagation also progresses more slowly due to the restricted amount of fluid present. Thus under these conditions an apparent increase in pitting life is observed, but with unacceptably high wear rates. Considering the inverse relationship between crack propagation and film thickness for this system, it is known that water in any lubricant considerably reduces pitting life, the effect increasing with concentration (14). In the thicker film regions, where more water is forced into the cracks propagation rates are higher due to two effects. One is mechanical due to the greater volume of fluid maintaining the high compressive stresses necessary for rapid growth. The other chemical where, according to Rowe and Armstrong (15) water produced hydrogen diffuses into the highly stressed surfaces ahead of micro-cracks resulting in hydrogen embrittlement.

The anti-wear agent is likely to provide an easily sheared film at the asperities and thus reduce sub-surface damage with subsequent reduction in crack initiation rate. The fact that propagation is not influenced by the presence of the additive would suggest that it is ineffective in displacing water molecules at the crack tip. This may simply be due to the relative size of the molecule.

For boundary lubrication cracks are formed in the immediate sub-surface region, but do not develop into pits. High wear undoubtedly results in surface removal, but more important than this is the fact that there is insufficient fluid at the conjunction to maintain the hydraulic pressure necessary for crack propagation. For hydrodynamic lubrication the surfaces are effectively separated by the fluid removing the possibility of asperity contact initiated crack formation and hence preventing pitting.

5 CONCLUSIONS

The pitting life of SAE 52100 steel in the presence of water-glycol based lubricants was found to depend on the relative magnitude of the film thickness developed at the conjucntion between two discs in rolling-sliding contact. For mixed - elastohydrodynamic lubrication a minimum in pitting life was found to occur at a calculated film thickness of about 0.038 μm (bearing number of 1×10^{-10}) for fluids both with and without the addition of a decanoic acid anti-wear agent. Lives of components run in the presence of the additive were, however, greater by factors of between two and seven times. The apparent increase in pitting life at small film thickness was due to the high wear rates in these regions. Wear rates were inversely proportional to calculated film thickness for fluids without additive and inversely dependent for fluids with additive, although direct proportionality was not observed in this latter case due to chemical modification of wear mechansisms

Crack propagation times decreased with increase in film thickness, suggesting that propagation occurs more readily in thick film conditions. These propagation times were unaffected by the presence of the anti-wear additive. Thus, while the additive undoubtedly increased crack initiation times it did not influence crack propagation and branching.

Pitting did not occur in boundary lubrication, although considerable surface distress was observed and substantial sub-surface cracking to a depth of about 20 μm, neither did it occur in hydrodynamic lubrication where surfaces were always smooth and damage free.

6 ACKNOWLEDGEMENTS

The authors would like to thank B.P.Research and SERC for their support of this work.

APPENDIX

References

(1) HOBBS, R.A. and MULLETT, G.W. 'Effect of some hydraulic fluid lubricants on the fatigue lives of roller bearings', Proc. I. Mech. E. 1968-69, 183 pt 3P, 23-29

(2) KNIGHT, G.C. 'The assessment of the suitability of hydrostatic pumps and motors for use with fire resistant fluids.' Rolling contact fatigue - performance testing of lubricants, London, edited by Tourret and Wright, published Heyden & Sons Ltd for IP, 1977, 193-215

(3) KENNY, P and YARDLEY, E.D. 'The use of Unisteel rolling fatigue machines to compare the lubrication properties of fire resistant fluids.' Wear 20, 1972, 105-121

(4) KNIGHT, G.C. 'Water hydraulics - applications of water based fluids to hydraulic systems.' Tribology International, 1977, 105-107

(5) SCOTT, D. and BLACKWELL, J. 'NEL rolling contact tests - accelerated simulation tests for lubricants and materials for rolling elements' Wear 17, 1971, 323-333

(6) WAYS, S. 'Pitting due to rolling contact', J. Appl. Mech. 2, 1935, A49-A58.

(7) PHILLIPS, M.R. and CHAPMAN, C.J.S. 'A magnetic method for detecting the onset of surface fatigue', Wear 49, 1978, 265-272

(8) DOWSON, D. and HIGGINSON, G.R. 'Elastohydrodynamic lubrication', Pergamon Press, London, 1966

(9) POOLE, W. and SULLIVAN, J.L. 'The role of aluminium segration in the wear of aluminium bronze/ steel interfaces under condition of boundary lubrication', ASLE Trans. 23, 1980, 401-409

(10) LITMAN, W.E. and WIDNER, R.L. 'Propagation of contact fatigue from surface and subsurface origins', Trans. ASME. Journal of Basic Engineering, 88, 1966, 624-636

(11) DAWSON, P.H. 'The effect of metallic contact on the pitting of lubricated rolling surfaces', J. Mech. Eng. Sci. 4, 1962, 16-21

(12) DAWSON, P.H. 'Rolling contact fatigue crack initiation in 0.3% carbon steel', Proc. Inst. Mech. Eng. 183, 1968, 75-83

(13) MICHAN, B., BERTHE, D. and GODET, M. 'Observations of oil pressure effects in surface crack development', Tribology International, 1974, 119-122

(14) ARMSTRONG, E.L., LEONARDI, S.J., MURPHY, W.R. and WOODING, P.S. 'Evaluation of water-accelerated bearing fatigue in oil lubricated ball bearings', Lub. Eng. 34,1, 1978, 15-21

(15) ROWE, C.N. and ARMSTRONG, E.L. 'Lubricant effects in rolling contact fatigue', ASLE Journal of Lubrication Engineering, 38, 1982, 23-40

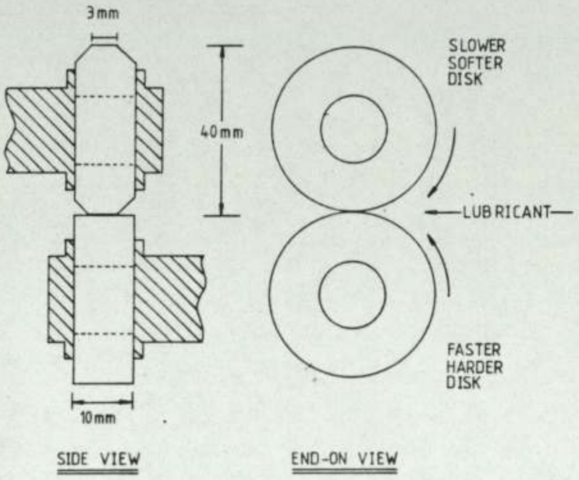

Fig. 1. Schematic diagram of the disc configuration

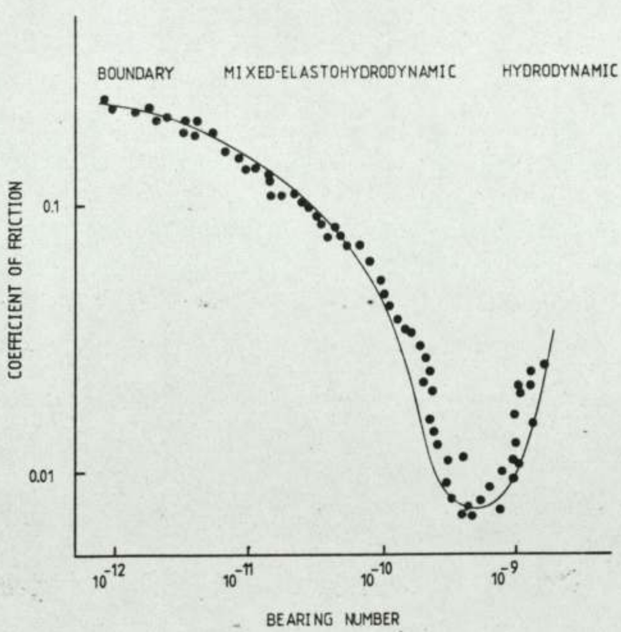

Fig. 2. The Stribeck curve

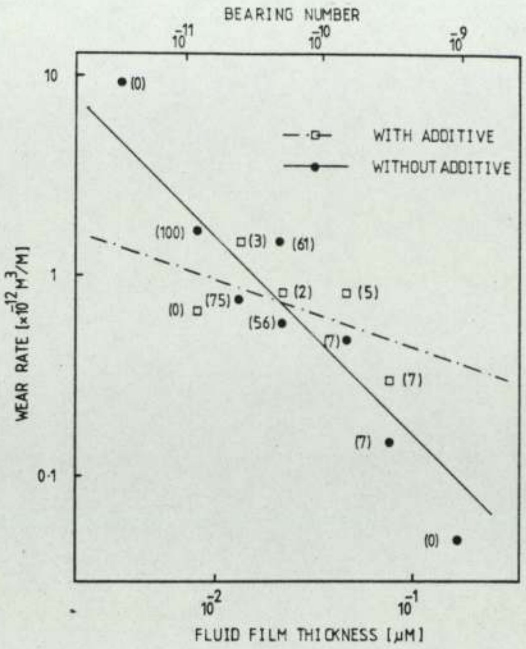

Fig. 3. Wear rate *vs* fluid film thickness

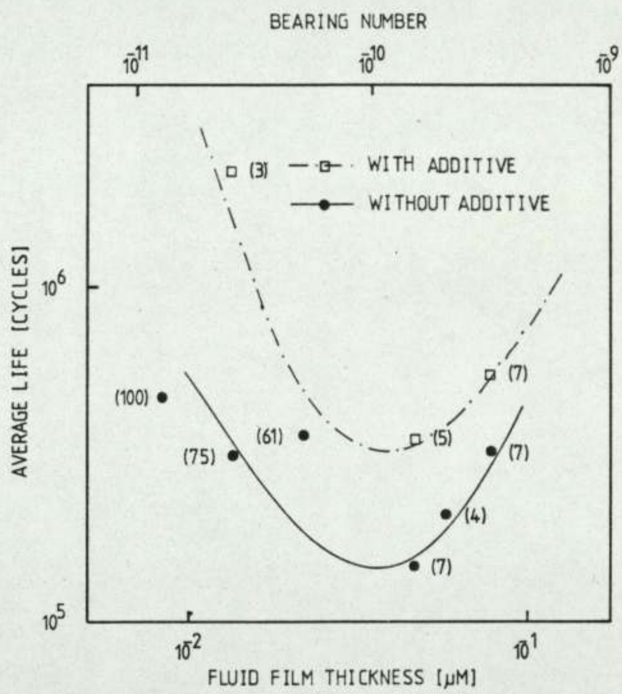

Fig. 4. Average life to first pit *vs* fluid film thickness

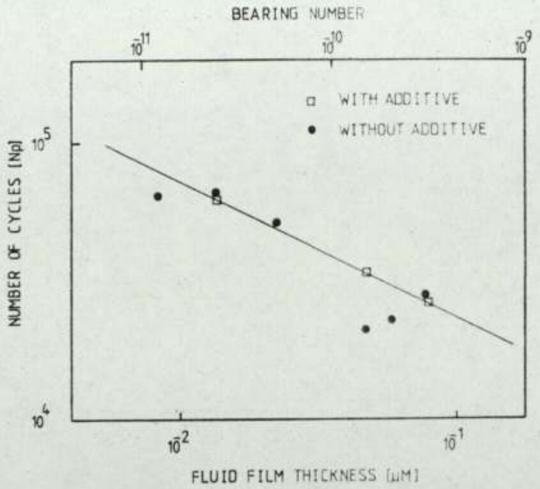

Fig. 5. Number of cycles taken between first crack and pit formation (N_p) against fluid film thickness

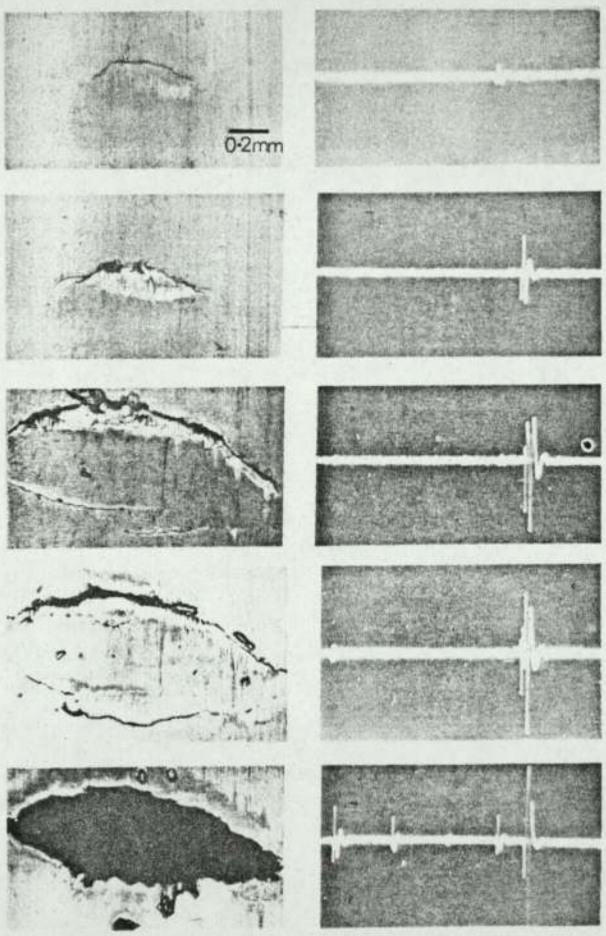

Fig. 6. Sequence of photographs showing the formation of a pit with the corresponding detector signals run near the hydrodynamic regime:
(a, top) 143,852 cycles
(b) 146,088 cycles
(c) 154,419 cycles
(d) 160,722 cycles
(e) 172,343 cycles

↑ direction of motion

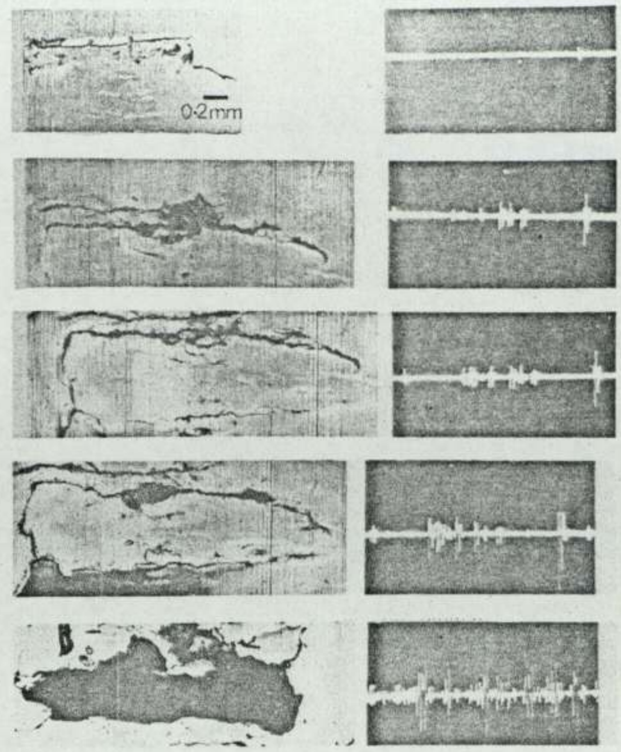

Fig. 7. Sequence of photographs showing the formation of a pit with the corresponding detector signals run near the boundary regime:
(a, top) 246,975 cycles
(b) 274,851 cycles
(c) 275,955 cycles
(d) 282,709 cycles
(e) 295,289 cycles

↑ direction of motion

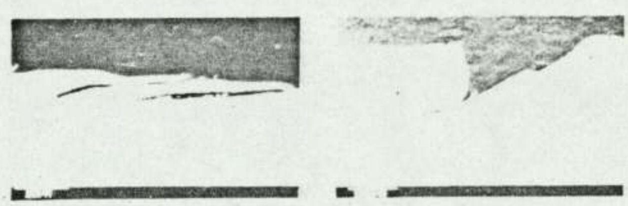

Fig. 8. Cross sections of the disks run at various lubrication regimes:
(a, left) Boundary lubrication
(b) Mixed/Elastohydrodynamic lubrication
Rolling direction ⟶

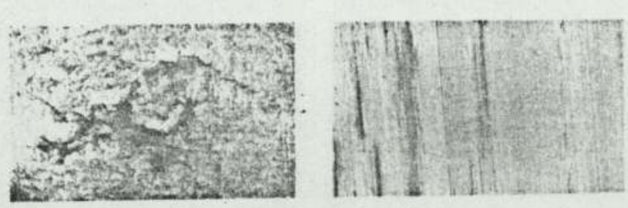

Fig. 9. Surface view of the non-pitted surfaces after running at the two extreme regimes of lubrication
(a, left) Boundary lubrication
(b) Hydrodynamic lubrication

↑ direction of motion